NIST GCR 99-770

MIXING AND RADIATION PROPERTIES OF BUOYANT LUMINOUS FLAME ENVIRONMENTS: II. STRUCTURE AND OPTICAL PROPERTIES OF SOOT

S.S. Krishnan, T.L. Farias, J.-S. Wu,
Ü.Ö. Köylü and G.M. Faeth

University of Michigan
Department of Aerospace Engineering
Ann Arbor, MI 48109-2140

United States Department of Commerce
Technology Administration
National Institute of Standards and Technology

NIST GCR 99-770

MIXING AND RADIATION PROPERTIES OF BUOYANT LUMINOUS FLAME ENVIRONMENTS: II. STRUCTURE AND OPTICAL PROPERTIES OF SOOT

Prepared for
U.S. Department of Commerce
Building and Fire Research Laboratory
National Institute of Standards and Technology
Gaithersburg, MD 20899

By
S.S. Krishnan, T.L. Farias, J.-S. Wu,
Ü.Ö. Köylü and G.M. Faeth

University of Michigan
Department of Aerospace Engineering
Ann Arbor, MI 48109-2140

Final Report

October 1998
Issued March 1999

Notice:

This report was prepared for the Laboratory for Building and Fire Research of the National Engineering Laboratory, National Institute of Standards and Technology, under Grant number 60NANB4D1696. The statements and conclusions contained in this report are those of the authors and do not necessarily reflect the views of the National Institute of Standards and Technology or the Laboratory for Building and Fire Research.

Report No. GDL/GMF-98-02

MIXING AND RADIATION PROPERTIES OF BUOYANT LUMINOUS FLAME ENVIRONMENTS: II. STRUCTURE AND OPTICAL PROPERTIES OF SOOT

S.S. Krishnan, T.L. Farias, J.-S. Wu, Ü.Ö. Köylü and G.M. Faeth
Department of Aerospace Engineering
The University of Michigan
Ann Arbor, Michigan 48109-2140

Prepared for:

U.S. Department of Commerce
National Institute of Standards and Technology
(formerly National Bureau of Standards)
Laboratory for Building and Fire Research
Washington, D.C. 20234

Final Report
Grant No. 60NANB4D1696
H.R. Baum, NIST Scientific Officer

October 1998

MIXING AND RADIATION PROPERTIES OF BUOYANT LUMINOUS FLAME ENVIRONMENTS: II. STRUCTURE AND OPTICAL PROPERTIES OF SOOT

Abstract

An investigation of the structure and optical properties of soot is described, motivated by the need to develop nonintrusive methods for measuring soot properties and to estimate the continuum radiation properties of soot for flame environments. The study included evaluation of Rayleigh-Debye-Gans/polydisperse-fractal-aggregate (RDG-PFA) approximate scattering theory for the optical properties of soot aggregates, the determination of the structure and fractal properties of soot that are needed to make predictions with RDG-PFA theory, and the use of RDG-PFA theory to measure the refractive index and related optical properties of soot. Measured soot optical properties were in good agreement with the predictions of RDG-PFA theory over a broad test range, as follows: soot from both the fuel-rich and fuel-lean regions of buoyant diffusion flames, wavelengths of 350-800 nm, primary particle size parameters as large as 0.46, and soot formed in diffusion flames burning in air for a variety of gaseous and liquid hydrocarbon fuels (acetylene, ethylene, propylene, butadiene, benzene, cyclohexane, toluene and n-heptane). Evaluation of the structure and fractal properties of soot was carried out for a similar range of wavelengths and soot properties showing that soot aggregate fractal properties are relatively independent of flame conditions, yielding a fractal dimension of 1.82 and a fractal prefactor of 8.5, with experimental uncertainties (95% confidence) of 0.08 and 0.5, respectively. The research also yields some helpful relationships between actual and projected soot aggregate properties. Evaluation of the refractive index properties of soot was limited to soot emitted from buoyant turbulent diffusion flames in the long residence time regime (where soot properties are independent of position in the overfire region and characteristic residence time) for the same range of wavelengths and fuels as before. Major findings concerning soot refractive index and related properties are as folows: dimensionless extinction coefficients were relatively independent of fuel type and wavelength and agreed with results from earlier studies within experimental uncertainties; in agreement with recent studies, there was no evidence of a resonance condition in the near uv for soot, similar to graphite; the refractive index functions relevant to absorption and emission, E(m), were relatively independent of fuel type and wavelength and agreed with earlier work for wavelengths greater than 400 nm; and the refractive index functions relevant to scattering, F(m), were also relatively independent of fuel type but increased faster with increasing wavelength than observed during earlier studies.

Acknowledgments

This research was supported by the U.S. Department of Commerce, National Institute of Standards and Technology (formerly National Bureau of Standards), Grant No. 60NANB4D1696, with H. R. Baum of the Laboratory for Building and Fire Research serving as Scientific Officer.

Table of Contents

	Page
Abstract	iv
Acknowledgments	v
List of Tables	vii
List of Figures	viii
Nomenclature	ix
1. Introduction	1
2. Absorption and Scattering Properties of Soot	3
2.1 Introduction	3
2.2 Experimental Methods	5
2.3 Theoretical Methods	5
2.4 Results and Discussion	7
2.5 Conclusions	14
3. Fractal and Projected Structure Properties of Soot	14
3.1 Introduction	14
3.2 Numerically-Simulated Aggregates	15
3.3 Flame-Generated Aggregates	16
3.4 Conclusions	19
4. Refractive Index Properties of Soot	20
4.1 Introduction	20
4.2 Experimental Methods	21
4.3 Theoretical Methods	23
4.4 Results and Discussion	24
4.5 Conclusions	41
References	41
Appendix A: Köylü and Faeth (1994b)	46
Appendix B: Farias, et al. (1995a)	56
Appendix C: Faeth and Köylü (1995)	65
Appendix D: Köylü et al. (1995)	89
Appendix E: Köylü and Faeth (1996)	102
Appendix F: Wu et al. (1997)	111

List of Tables

Table		Page
1	Summary of publications.....	1
2	Test conditions in measurements of the optical properties of soot emitted from buoyant turbulent diffusion flames at long residence times.....	25
3	Physical and fractal properties of soot emitted from buoyant turbulent diffusion flames at long residence times.....	26

List of Figures

Figure	Caption	Page
1	TEM photograph of the soot aggregate emitted from an ethylene/air flame. From Urban et al. (1999).	8
2	Measured and predicted angular soot scattering patterns for underfire soot in an ethylene/air diffusion flame. From Köylü and Faeth (1994b).	10
3	Measured and predicted angular soot scattering patterns for underfire soot in an acetylene/air diffusion flame. From Köylü and Faeth (1994b).	11
4	Projected images of typical aggregates used for the computational evaluation of RDG-PFA theory. From Farias et al. (1995a).	12
5	Normalized scattering patterns for fractal aggregates of various size, computed using ICP and RDG-PFA methods ($D_f = 1.75$, $k_f = 8.0$, $\lambda = 514.5$, nm, $m = 1.57 + 0.57i$ and $x_p = 0.4$). From Farias et al. (1995a).	13
6	Number of primary particles as a function of projected area ratio for simulated soot aggregates. From Köylü et al. (1995).	17
7	Ratio of actual to projected radius of gyration as a function of simulated soot aggregates. From Köylü et al. (1995).	18
8	Dimensionless extinction coefficient as a function of fuel type and wavelength for soot emitted from buoyant turbulent diffusion flames.	28
9	Dimensionless extinction coefficients for soot as a function of wavelength.	29
10	Typical Rayleigh scattering pattern for calibrating absolute soot scattering levels.	30
11	Measured and predicted angular soot scattering patterns for soot emitted from buoyant turbulent diffusion flames (toluene at 351.2 nm).	32
12	Volumetric vv cross section as a function of the modulus of the scattering vector for soot emitted for buoyant turbulent diffusion flames.	33
13	Fractal dimensions as a function of fuel type and wavelength for soot emitted from buoyant turbulent diffusion flames.	34
14	E(m) as a function of fuel type and wavelength for soot emitted from buoyant turbulent diffusion flames.	36
15	E(m) for soot as a function of wavelength.	37
16	F(m) as a function of type and wavelength for soot emitted from buoyant turbulent diffusion flames.	39
17	F(m) for soot as a function of wavelength.	40

Nomenclature

A_a	=	projected area of an aggregate
A_p	=	projected area of a primary particle
C	=	optical cross section
d_p	=	primary particle diameter
D_f	=	mass fractal dimension
$E(m)$	=	refractive index function = $\mathrm{Im}((m^2-1)/(m^2+2))$
f_v	=	soot volume fraction
$f(q\,R_g)$	=	aggregate form factor
$F(m)$	=	refractive index function = $\lvert(m^2-1)/(m^2+2)\rvert^2$
$g(\lambda,R_g,D_f)$	=	aggregate total scattering factor
i	=	$(-1)^{1/2}$
I	=	light intensity
k	=	wave number = $2\pi/\lambda$
k_a	=	projected area constant
k_e	=	dimensionless extinction coefficient
k_{eR}	=	k_e at Rayleigh scattering limit
k_f	=	fractal prefactor
L	=	light path length
m	=	soot refractive index = $n+i\kappa$
n	=	real part of soot refractive index
n_p	=	mean number of primary particles per unit volume
N	=	number of primary particles per aggregate
q	=	modulus of scattering vectdor = $2k\sin(\theta/2)$
Q	=	volumetric optical cross section
R_g	=	radius of gyration of an aggregate
x_p	=	primary particle size parameter = $\pi d_p/\lambda$
α	=	projected area exponent
θ	=	angle of scattering from forward direction
κ	=	imaginary part of refractive index of soot
λ	=	wavelength of radiation

ρ_s	=	density of soot
ρ_{sa}	=	ratio of scattering to absorption cross sections
ρ_v	=	depolarization ratio

Subscripts

a	=	absorption
e	=	extinction
h	=	horizontal polarization
ij	=	incident (i) and scattered (j) polarization directions
s	=	total scattering
v	=	vertical polarization

Superscripts

a	=	aggregate property
p	=	primary particle property
$(\bar{\ })$	=	mean value over a polydisperse aggregate population

1. Introduction

An investigation of the structure and optical properties of soot is described in this report. The findings of this research have applications to the development of nonintrusive methods for measuring soot properties and to estimating the continuum radiation properties of soot in flame environments.

The investigation was motivated by the observation that there is a strong correlation between carbon monoxide and soot emissions from buoyant turbulent diffusion flames (Köylü et al., 1991; Köylü and Faeth, 1991) while continuum radiation from soot dominates the radiation processes of practical fires (Köylü and Faeth, 1993). Understanding the optical properties of soot is crucial for a better understanding of both these problems: soot concentrations and structure generally are measured using nonintrusive laser-based methods that require knowledge about soot optical properties in order to correctly interpret the measurements while soot optical properties are a controlling factor in the continuum radiation properties of flames. Past work has shown that soot structure properties could be approximated by mass fractal aggregates of spherical primary particles, where the primary particles were nearly monodisperse at given flame conditions, while the number of primary particles per aggregate varied widely at each flame condition, in agreement with earlier work (Köylü and Faeth, 1992). The use of the Rayleigh-Debye-Gans(RDG) approximation, while approximating soot aggregates as polydisperse mass fractal objects (PFA), was shown to be acceptable for soot emitted from large buoyant turbulent diffusion flames in the long residence time regime, where soot in the fuel-lean portions of the flame is independent of position in the overfire region and flame residence time (Köylü and Faeth, 1994a). These results showed that there were several limitations concerning soot optical properties, as follows: important fractal properties of soot aggregates needed by RDG theory were not known very well; relationships between actual soot structure properties and easily observed projected soot structure properties were not known; evaluation of RDG theory was limited to the large angle (power-law) scattering regime due to the large size of soot aggregates emitted from large buoyant turbulent diffusion flames; and existing information about the refractive index properties of soot, and how they vary with fuel type, was very limited. Thus, the objectives of this phase of the present investigation was to help fill these gaps in the literature.

The present investigation considered the following three aspects of soot optical properties, in turn: the absorption and scattering properties of soot, the fractal and projected structure properties of soot, and the refractive index properties of soot. The present discussion of the research is brief, more details about the investigation can be found in the articles, papers, reports and theses describing aspects of the investigation that are summarized in Table 1 and cited in the list of references. Finally, key references are included in the appendices of this report, e.g., Köylü and Faeth (1994b), Farias et al. (1995a), Faeth and Köylü (1995), Köylü et al. (1995), Köylü and Faeth (1996) and Wu et al. (1997), in appendices A-F, respectively.

Table 1. Summary of Publications

Archival Publications (articles and book chapters):

Wu, J.-S., Krishnan, S.S., and Faeth, G.M. (1997) Refractive Indices at Visible Wavelengths of Soot Emitted from Buoyant Turbulent Diffusion Flames. J. Heat Trans. 119, 230-237.

Faeth, G. M. (1997) Combustion Fluid Dynamics (Tools and Methods). Proceedings of the Workshop on Fuels with Improved Fire Safety, National Academy Press, Washington, DC, pp. 81-96.

Faeth, G.M. and Köylü, Ü.Ö. (1996) Structure and Optical Properties of Flame-Generated Soot. *Transport Phenomena in Combustion* (S.H. Chen, ed.), Taylor & Francis, Washington, DC, Vol. 1, pp. 19-44.

Farias, T.L., Carvalho, M.G., Köylü, Ü.Ö. and Faeth, G.M. (1996) Total Scattering and Absorption Cross Sections of Carbonaceous Soot Particles. Symp. Rad. Transfer (M.P. Mengüc, ed.), Begell House, Inc., New York, pp. 296-308.

Köylü, Ü.Ö. and Faeth, G.M. (1996) Spectral Extinction Coefficients of Soot Aggregates from Turbulent Diffusion Flames. J. Heat Trans. 118, 415-421.

Farias, T.L., Carvalho, M.G., Köylü, Ü.Ö. and Faeth, G.M. (1995) Computational Evaluation of Approximate Rayleigh-Debye-Gans/Fractal-Aggregate Theory for the Absorption and Scattering Properties of Soot. J. Heat Trans. 117, 152-159.

Faeth, G. M. and Köylü, Ü.Ö. (1995) Soot Morphology and Optical Properties in Nonpremixed Turbulent Flame Environments. Combust. Sci. Tech. 108, 207-229.

Köylü, Ü.Ö., Faeth, G.M., Farias, T.L. and Carvalho, M.G. (1995) Fractal and Projected Structure Properties of Soot Aggregates. Combust. Flame 100, 621-633.

Farias, T.L., Carvalho, M.G., Köylü, Ü.Ö. and Faeth, G.M. (1995)Light Scattering from Soot Aggregates with Radially Inhomogeneous Primary Particles. Int. J. Heat and Technology 13, 27-47.

Köylü, Ü.Ö., and Faeth, G.M. (1994) Optical Properties of Soot in Buoyant Laminar Diffusion Flames. J. Heat Trans. 116, 971-979.

Köylü, Ü.Ö., and Faeth, G.M. (1994) Optical Properties of Soot in Buoyant Laminar Diffusion Flames. J. Heat Trans. 116, 971-979.

Papers:

Krishnan, S.S., Lin, K.-C. and Faeth, G.M. (1999) Scattering and Extinction Properties of Overfire Soot in Large Buoyant Turbulent Diffusion Flames. Proc. Natl. Heat Trans. Conf., Albuquerque, NM, submitted.

Faeth, G.M. (1999) The Structure, Optical and Radiative Properties of Soot in Flame Environments: A Review. Proceedings of the 5th ASME/JSME Joint Thermal Engineering Conference, San Diego, CA, in press.

Krishnan, S.S., Lin, K.-C., Wu, J.-S. and Faeth, G.M. (1998) Optical Properties in the Visible of Soot Emitted from Turbulent Pool Fires. Proceedings of Annual Conference on Fire Research, NIST, Gaithersburg, MD, in press.

Wu, J.-S., Krishnan, S.S., Lin, K.-C. and Faeth, G.M. (1997) Measurements of the Optical Properties of Soot Emitted from Buoyant Turbulent Diffusion Flames at Long Residence Times. Proceedings of Spring Technical Meeting, Canadian Section of the Combustion Institute, Halifax, pp. 1-6 to 1-10.

Krishnan, S.S., Lin, K.-C., Wu, J.-S. and Faeth, G.M. (1999) Optical Properties in the Visible of Soot Emitted from Turbulent Pool Fires. Proceedings of the ASME Winter Annual Meeting, ASME, New York, HTD-352-2, 39-48.

Wu, J.-S., Krishnan, S.S. and Faeth, G.M. (1996) Refractive Indices at Visible Wavelengths of Soot Emitted from Buoyant Turbulent Diffusion Flames, Proceedings of National Heat Transfer Conference, Houston, TX.

Köylü, Ü.Ö. and Faeth, G.M. (1995) Spectral Extinction Coefficients of Soot Aggregates from Turbulent Diffusion Flames. Proceedings of the Fall Technical Meeting, Eastern Section of the Combustion Institute, Pittsburgh, PA, pp. 211-214.

Reports and Theses:

Dai, Z., Krishnan, S.S., Lin, K.-C., Sangras, R., Wu, J.-S. and Faeth, G.M. (1996) Mixing and Radiation Properties of Buoyant Luminous Flame Environments. Report No. GDL/GMF-96-01, The University of Michigan, Ann Arbor.

Dai, Z., Krishnan, S.S., Lin, K.-C., Sangras, R., Wu, J.-S. and Faeth, G.M. (1995) Mixing and Radiation Properties of Buoyant Luminous Flame Environments. Report No. GDL/GMF-95-02, The University of Michigan, Ann Arbor.

Farias, T.L. (1997) Evaluation of Light Scattering Theories for Fractal Aggregates. Ph.D. Thesis, Mechanical Engineering Department, Instituto Superior Técnico, Lisbon, Portugal.

---

2. Absorption and Scattering Properties of Plumes

2.1 Introduction

Both predictions of continuum radiation from flames, and nonintrusive laser-based measurements of soot structure and concentrations, require an understanding of the optical properties of soot. Soot optical properties are a challenging problem, however due to the complexities of soot structure. In particular, soot consists of small spherical primary particles that collected into open structured aggregates having a broad distribution of sizes, see Jullien and Botet (1987) and references cited therein. Thus, although the individual primary particles generally are small enough to satisfy the Rayleigh scattering approximation, even early work showed that soot aggregates generally exhibited neither simple Rayleigh nor Mie scattering behavior (Erickson et al., 1964; Dalzell et al., 1969). As a result, improved methods have been sought based on the Rayleigh-Debye-Gans scattering approximation while treating the aggregates as polydisperse collections of mass-fractal objects (denoted the RDG-PFA scattering approximation in the following), see Jullien and Botet (1987), Martin and Hurd (1987), Dobbins and Megaridis (1991) and Köylü and Faeth (1994a). The objective of the present investigation was to conduct an evaluation of RDG-PFA theory in two ways, as follows: (1) by measuring both the structure and scattering properties of soot found in the fuel-rich (underfire) region of buoyant laminar jet diffusion flames, and (2) to complete theoretical evaluation, based on computations using a more exact theory for populations of mass-fractal aggregates having prescribed properties.

Although RDG-PFA theories have been available for some time, and have been used to interpret soot scattering properties and to infer soot aggregate structure properties from scattering measurements (Dobbins and Megaridis, 1993; Sorensen et al., 1992a,b),

evaluation of the method has only just begun. Köylü and Faeth (1993) discuss early attempts to evaluate various approximations of soot scattering properties using more exact solutions for simulated aggregates. Unfortunately, computational limitations have prevented definitive results in the past for the relatively large soot aggregates often encountered in practice. An alternative approach involves direct experimental evaluation by measuring the soot structure properties need for RDG-PFA scattering predictions and comparing these predictions with measured scattering properties for the same soot population. Köylü and Faeth (1994a) carried out a study along these lines for the large soot aggregates found in the overfire region of buoyant turbulent diffusion flames at long characteristic residence times. It was found that the RDG-PFA predictions were in reasonably good agreement with measurements of scattering and extinction properties over the wavelength range 514.5-1152 nm. However, these overfire soot aggregates were too large for practical scattering measurements in the small-angle (Guinier) regime where use of the RDG scattering approximation is least reliable (Nelson, 1989a,b; Köylü and Faeth, 1993), in order to complete a thorough evaluation of the approximation theory. Thus, one specific objective of the present investigation was to extend the work of Köylü and Faeth (1994a) in order to consider soot aggregates in the fuel-rich (underfire) region of buoyant laminar jet diffusion flames, where smaller aggregate sizes provide greater access to the Guinier regime as well as the transition regime between the Guinier and the power-law (large-angle) regimes.

Although the experiments extended evaluation of RDG-PFA theory farther into the Guinier regime, some deficiencies in the evaluation remained. In particular, establishing the performance of scattering predictions at small angles critically depends upon accurately measuring both scattering properties at small angles and the higher moments of the aggregate size distribution function (e.g., $\overline{N}^2$) that dominate scattering predictions at small angles — both of which are very difficult. This is unfortunate because multiple-scattering effects that could compromise the use of RDG-PFA theory are most significant in the Guinier regime (Nelson, 1989a). Theoretical computations offer a way to circumvent the difficulties of experimental evaluation of RDG-PFA theory at small angles; unfortunately, existing computer simulations of the optical properties of soot also do not provide an adequate basis for evaluating RDG-PFA scattering theory. In particular, they either involve fundamentally accurate solutions for small non-fractal aggregates where effects of multiple and self-induced scattering are small, or approximate solutions having uncertain accuracy for the large soot aggregates of interest for practical flames (Köylü and Faeth, 1993). Additionally, existing computations have been limited to relatively small samples of both orientations of given aggregates and aggregate configurations, raising questions about the statistical significance of the results (Köylü and Faeth, 1993). Thus, a second objective of the present work was to undertake a theoretical evaluation of RDG-PFA theory, emphasizing the Guinier regime. This evaluation was based on computations using the ICP approach of Iskander et al. (1989), which provides a more exact treatment of aggregate scattering in the Guinier regime than RDG-PFA theory, by including effects of multiple and self-induced scattering. Problems of defining the higher moments of the size distribution functions of polydisperse aggregates during experiments were avoided by using numerical simulations to generate aggregates having prescribed sizes and mass-fractal properties.

In the following, experimental and theoretical methods are described first. The results are then discussed before summarizing conclusions. The following description of the study is brief, more details can be found in Köylü and Faeth (1994b), Farias et al. (1995a,b,1996) and Faeth and Köylü (1995,1996); for convenience Köylü and Faeth (1994a), Farias et al. (1995a) and Faeth and Köylü (1995); appear in appendices A, B and C.

2.2 Experimental Methods

The measurements to evaluate RDG-PFA theory were carried out in laminar ethylene and acetylene/air diffusion flames, which are representative of lightly and heavily sooting materials (Köylü and Faeth, 1992). Soot structure was measured using thermophoretical sampling and analysis by transmission electron microscopy (TEM) to find primary particle diameters, distributions of the number of primary particle per aggregate and aggregate mass fractal dimensions. Soot optical property measurements included differential scattering cross sections for various polarizations of incident and scattered light (vv, hh, vh and hv), total scattering cross sections and the albedo at 514.5 nm. Predictions of scattering properties were based on the measured structure properties considering RDG-PFA scattering following Dobbins and Megaridis (1993) and Köylü and Faeth (1994). The features of this formulation will be briefly described next.

2.3 Theoretical Methods

RDG-PFA Scattering Theory. Predictions of soot optical properties were based on methods described by Jullien and Botet (1987), Martin and Hurd (1987) and Dobbins and Megaridis (1991) for a single aggregate. However, attention was focused on the treatment of Köylü and Faeth (1994a) for polydisperse aggregate populations. It involves use of the RDG scattering approximation so that effects of multiple- and self-scattering are ignored, the electric field of each particle is assumed to be the same as the incident field, and differences of the phase shift of scattered light from various points within a particular primary particle are neglected. The RDG scattering approximation requires that both $|m-1| << 1$ and $2x_p|m-1| << 1$ (Bohren and Huffman, 1983), which is questionable due to the relatively large refractive indices of soot Köylü and Faeth (1994a). Recent computational studies also suggest significant effects of multiple scattering for soot aggregates, see Köylü and Faeth (1994a) and references cited therein. Thus, use of RDG theory only can be justified by its capabilities to treat measured soot properties or by comparison with the results of more exact theory.

The major assumptions with respect to aggregate structure are as follows (Köylü and Faeth, 1994a): spherical primary particles having constant diameters, primary particles do not overlap but just touch one another, uniform refractive indices, and the aggregates are mass fractal-like objects. The mass fractal approximation implies the following relationship between the number of particles in an aggregate and its radius of gyration (Jullien and Botet (1987):

$$N = k_f(R_g / d_p)^{D_f} \tag{1}$$

Based on past measurements for both overfire and underfire soot, $k_f = 8.1$ was used during present work (Köylü and Faeth, 1994a). The assumptions of nearly constant diameter primary particles and mass fractal-like behavior are justified by the present soot structure measurements, as discussed later while the remaining assumptions are typical of past work, see Köylü and Faeth (1994a). One change from the approach of Köylü and Faeth (1994a), however, was that the measured aggregate size distribution was used directly in the computations, to avoid potential errors due to empirical fits of the distribution.

Only the main results of RDG-PFA scattering theory will be summarized in the following, see Köylü and Faeth (1994a) for the complete formulation. The treatment begins with the scattering cross sections for a single fractal aggregate under the RDG approximation:

$$C_{vv}^{a}(\theta) = C_{hh}^{a}(\theta)/\cos^2\theta = N^2 C_{vv}^{p} f(q\,R_g) \tag{2}$$

where C_{vv}^{p} is the scattering cross section of a primary particle under the Rayleigh scattering approximation. The form factor, $f(q\,R_g)$, in equation (2) is expressed as follows (Jullien and Botet, 1987; Martin and Hurd,1987):

$$f(q\,R_g) = \exp(-(q\,R_g)^2/3), \quad \text{Guinier regime} \tag{3}$$

$$f(q\,R_g) = (q\,R_g)^{-D_f}, \quad \text{power-law regime} \tag{4}$$

where the boundary between the small q (Guinier) regime and the power-law regime $(qR_g)^2 = 3D_f/2$, is chosen to match the value and derivative of $f(q\,R_g)$ where the regimes meet, following Dobbins and Megaridis (1993). The total scattering cross section then becomes:

$$C_s^{a} = N^2 C_s^{p} g(\lambda, R_g, D_f) \tag{5}$$

where $g(\lambda,R_g,D_f)$ takes on different forms if the power-law regime is reached for $\theta \leq 180°$ or not, see Köylü and Faeth (1994a) for these expressions.

The mean optical cross sections of populations of randomly oriented polydisperse aggregates (polydisperse aggregates) are found by integrating over all aggregate sizes, as follows:

$$\overline{C}_j^{a} = \int_{N=1}^{\infty} C_j^{a}(N)p(N)dN; \quad j = pp,s,a \tag{6}$$

where p(N) is the measured size distribution of the aggregate population. In general, equation (6) must be integrated numerically when scattering extends over both the Guinier and power-law regimes. However, simple closed form expressions are possible when all the aggregates are either in the Guinier ($p(N) << 1$ for $N \geq N_c$) or power-law ($p(N) << 1$ for $N \leq N_c$) regimes, where

$$N_c = k_f(3D_f/(2q^2 d_p^2))^{D_f/2} \tag{7}$$

This yields (Köylü and Faeth, 1994a):

$$\overline{C}_{vv}^{a}(\theta) = \overline{N}^2 C_{vv}^{p} \exp(-q^2 \overline{R}_{gG}^{2}/3), \quad \text{Guinier regime} \tag{8}$$

$$\overline{C}_{vv}^{a}(\theta) = \overline{N}^2 C_{vv}^{p} (q^2 \overline{R}_{gL})^{-D_f}, \quad \text{power-law regime} \tag{9}$$

The mean-squared radius of gyration in the limiting expressions of equations (8) and (9) is found as a N^2 weighted average in the Guinier regime, and as fractal dimension-weighted average in the power-law regime, as summarized by Köylü and Faeth (1994a). The general expression for the total scattering cross section of the polydisperse aggregate population is

$$\overline{C}_s^{a} = \overline{C}_a^{p} \int_{N=1}^{\infty} N^2 g(\lambda, R_g, D_f)p(N)dN \tag{10}$$

which must be numerically integrated in both scattering regimes. The absorption cross section of the polydisperse aggregate population is evaluated quite simply for RDG-PFA scattering, as follows:

$$\overline{C}_a^{\,a} = \overline{N} C_a^{\,p} \tag{11}$$

ICP Scattering Theory. Ku and Shim (1992) review theories of aggregate optical properties more accurate than the RDG approximation and conclude that the ICP formulation of Iskander et al. (1989) was superior to the rest; therefore, this approach was adopted for the present calculations. Later work by Lou and Charalampopoulos (1994) suggested that the IEFS formulation was superior to ICP because it formally satisfies the optical theorem at all conditions while ICP only approximates this restriction. Extensive comparisons between ICP and IEFS were carried out for present conditions, however, and showed that differences between these two approaches were comparable to numerical accuracy, 2% (Farias, 1997). Thus, only ICP results will be considered in the following.

The soot aggregate structure approximations of the ICP and RDG-PFA calculations were the same. In addition, each primary particle constituted an ICP computational cell, which implies that individual primary particles satisfy the Rayleigh scattering approximation, i.e., the internal electrical fields of primary particles are assumed to be uniform. This approximation is reasonable because errors are less than 10% for cross sections and near-forward scattering when $x_p < 0.8\ |m^2 + 5)/(2m^2 + 1)|$, taking individual primary particles to be ICP computational cells (Ku and Shim, 1992). The refractive index factor in this expression is roughly unity for soot, so that present calculations satisfied the criterion with a significant margin for $x_p \leq 0.4$. The complete ICP formation and description of the numerical calculations for ICP predictions can be found in Farias (1997) and Farias et al. (1995a).

Aggregates used in ICP calculations were numerically simulated. The approach sought to create populations of aggregates by cluster/cluster aggregation, following Jullien and Botet (1987). The process started with individual and pairs of primary particles which then were attached to each other randomly, assuming uniform distributions of the point and orientation of attachment but rejecting configurations where primary particles intersected. This procedure was continued in order to form progressively larger aggregates, but with the additional restriction that the aggregates should have $1.7 < D_f < 1.8$ and k_f ca. 8 for $N > 8$. It was observed that D_f fell naturally in the range 1.6-1.9 for $N > 48$ during these simulations; therefore, few cluster/cluster combinations were rejected for inappropriate fractal properties when larger aggregates were constructed. Similarly, for D_f in the range 1.7-1.8, the value of k_f fell naturally near $k_f = 8.0$ for statistically significant populations of aggregates.

2.4 Results and Discussion

Evaluation Based on Experiments. The general appearance of the soot aggregates in the present test flames is illustrated by the TEM photograph appearing in Fig. 1. Present results are qualitatively similar to other TEM observations of soot at fuel-rich conditions in laminar diffusion flames (Dobbins and Megaridis, 1987). In particular, the soot consists of open (rather than compact) structures of aggregated primary particles that have nearly constant diameters. The aggregates exhibit a broad range of sizes, with the largest aggregates having maximum dimensions on the order of 1 μm. This yields aggregate optical size parameters, based on the maximum aggregate dimension, greater than 5, which

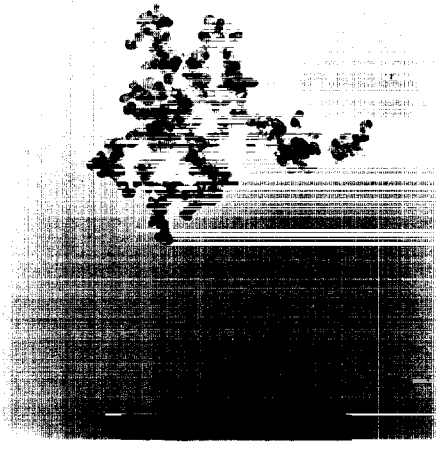

Figure 1 TEM photograph of the soot aggregate emitted from an ethylene/air flame. From Urban et al. (1999).

implies significant potential for departure from Rayleigh scattering behavior. Such behavior was confirmed by aggregate scattering measurements to be discussed subsequently.

Measured and predicted angular scattering patterns of ethylene and acetylene soot are illustrated in Figs. 2 and 3, respectively. These results are for the lowest position in the ethylene flame and the highest position in the acetylene flame, which spans the range of soot aggregate sizes. Similar to Köylü and Faeth (1994a), the formulation for $\overline{C}_{hh}^{a}(\theta)$ was modified from an approach based on equation (2) in order to account for observed depolarization phenomena. This was done analogous to Rayleigh scattering theory as follows (Rudder and Bach, 1968):

$$\overline{C}_{hh}^{a}(\theta) = C_{vv}^{a}(\theta)[(1 - \overline{\rho}_{v}^{a})\cos^2\theta + \overline{\rho}_{v}^{a}] \tag{12}$$

The corresponding estimates of hv and vh scattering cross sections are:

$$\overline{C}_{hv}^{a} = \overline{C}_{vh}^{a} = \overline{C}_{vv}^{a}(90°)\overline{\rho}_{v}^{a} \tag{13}$$

Present results for $\overline{C}_{hh}^{a}(\theta), \overline{C}_{hv}^{a}$ and $\overline{C}_{vh}^{a}$ are in qualitative agreement with earlier findings for the much larger overfire soot aggregates (Köylü and Faeth, 1994a); equation (12) is in excellent agreement with measured values of $\overline{C}_{hh}^{a}(\theta)$ while equation (13) is effective except for the forward-scattering direction where the measured values show a steady increase as the forward scattering direction is approached. This latter increase of the hv and vh scattering cross sections as θ becomes small is expected, however, due to the strong forward scattering of soot aggregates. Fortunately, vh and hv scattering levels are small and have little effect on total scattering estimates for most conditions of interest so that this deficiency of equation (13) is not very important.

Evaluation Based on Computations. Projected images of typical aggregates constructed using the present simulation for the ICP computations are illustrated in Fig. 4 for N = 16, 64 and 256. The appearance of the aggregates varies considerably with the direction of projection, and from aggregate to aggregate within a population of given size. Nevertheless, the simulated aggregates are qualitatively similar to both past experimental observations of soot aggregates (Dalzell et al., 1970; Jullien and Botet, 1987; Köylü and Faeth, 1993) and other numerical simulations of soot aggregates (Jullien and Botet, 1987; Mountain and Mulholland, 1988; Nelson, 1989a,b). Combined with their prescribed fractal properties, this suggests that the present simulated aggregate populations are reasonably representative of the structure of the soot aggregates found in flame environments.

Normalized differential scattering patterns found from both the ICP and RDG-PFA theories are illustrated in Fig. 5. The results are normalized so that effects of aggregate size are highlighted. A relatively large value of the primary particle size parameter, $x_p = 0.4$, is also used in order to emphasize RDG-PFA performance near the upper limit of its practical use. The hh scattering cross sections have been corrected as just described in connection with Fig. 4. After correcting hh scattering cross sections in this manner, the agreement between RDG-PFA and ICP predictions is within numerical uncertainties throughout the Guinier regime (roughly $\theta < 20$, and 90 deg for N = 256, 64 and 16, respectively). As discussed by Farias et al. (1995a), ICP predictions underestimate scattering levels at larger angles due to truncation errors at large x_p. In contrast, extensive past evaluations have shown that RDG-PFA theory is effective for soot in the large-angle (power-law) scattering regime (Köylü and Faeth, 1994a,b). Thus, the discrepancies seen at large angles in Fig. 5

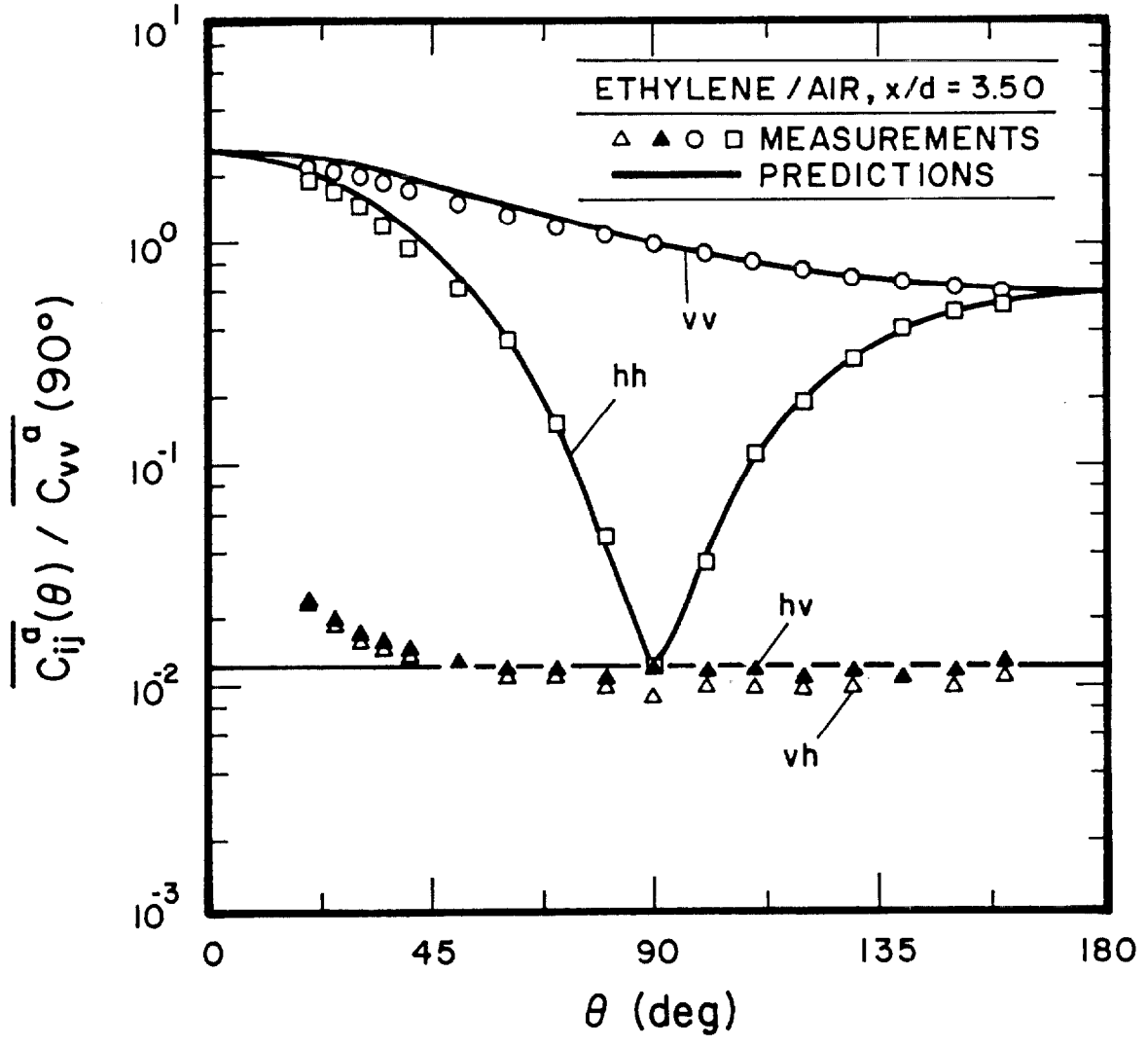

Figure 2 Measured and predicted angular soot scattering patterns for underfire soot in an ethylene/air diffusion flame. From Köylü and Faeth (1994b).

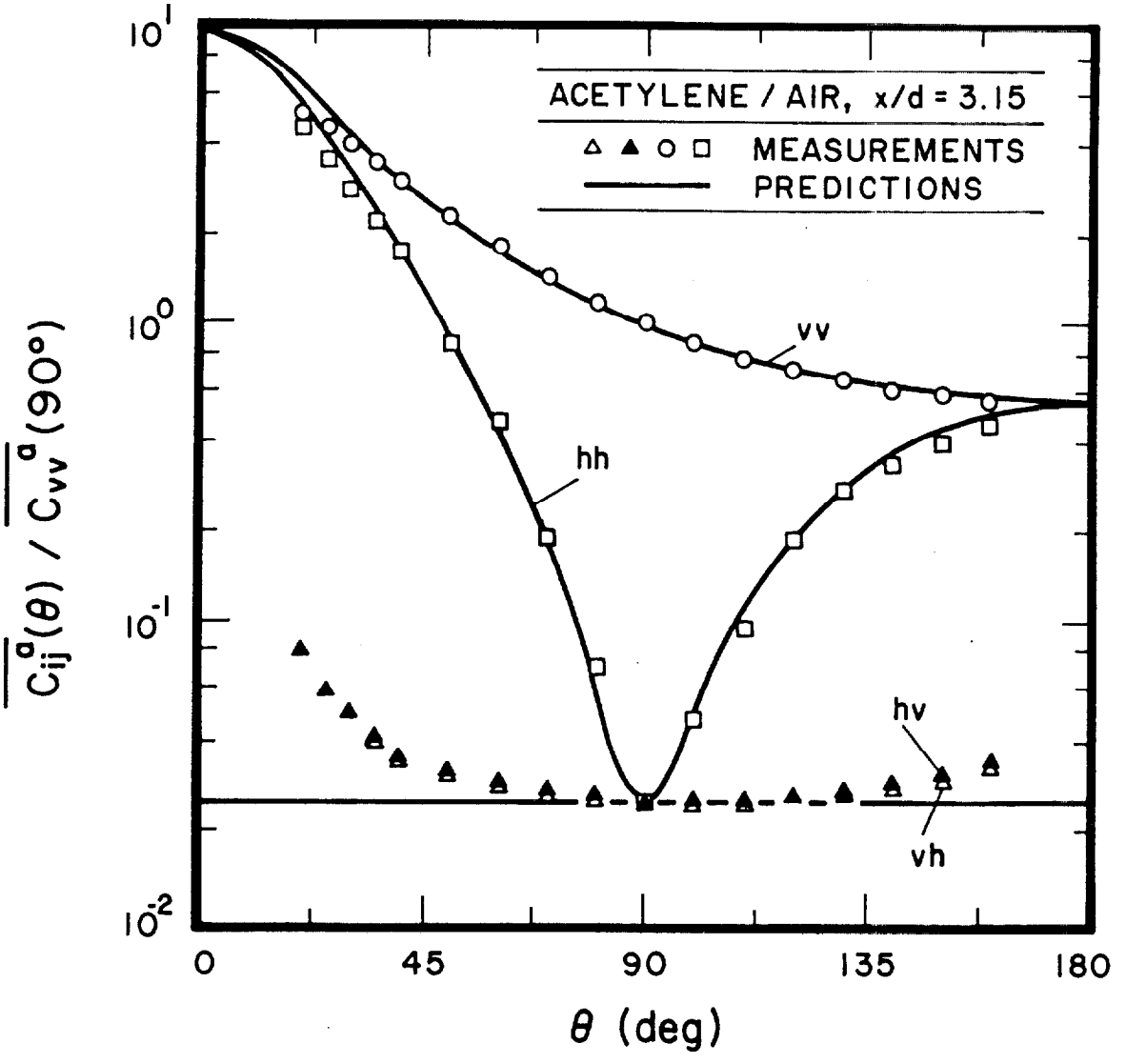

Figure 3 Measured and predicted angular soot scattering patterns for underfire soot in an acetylene/air diffusion flame. From Köylü and Faeth (1994b).

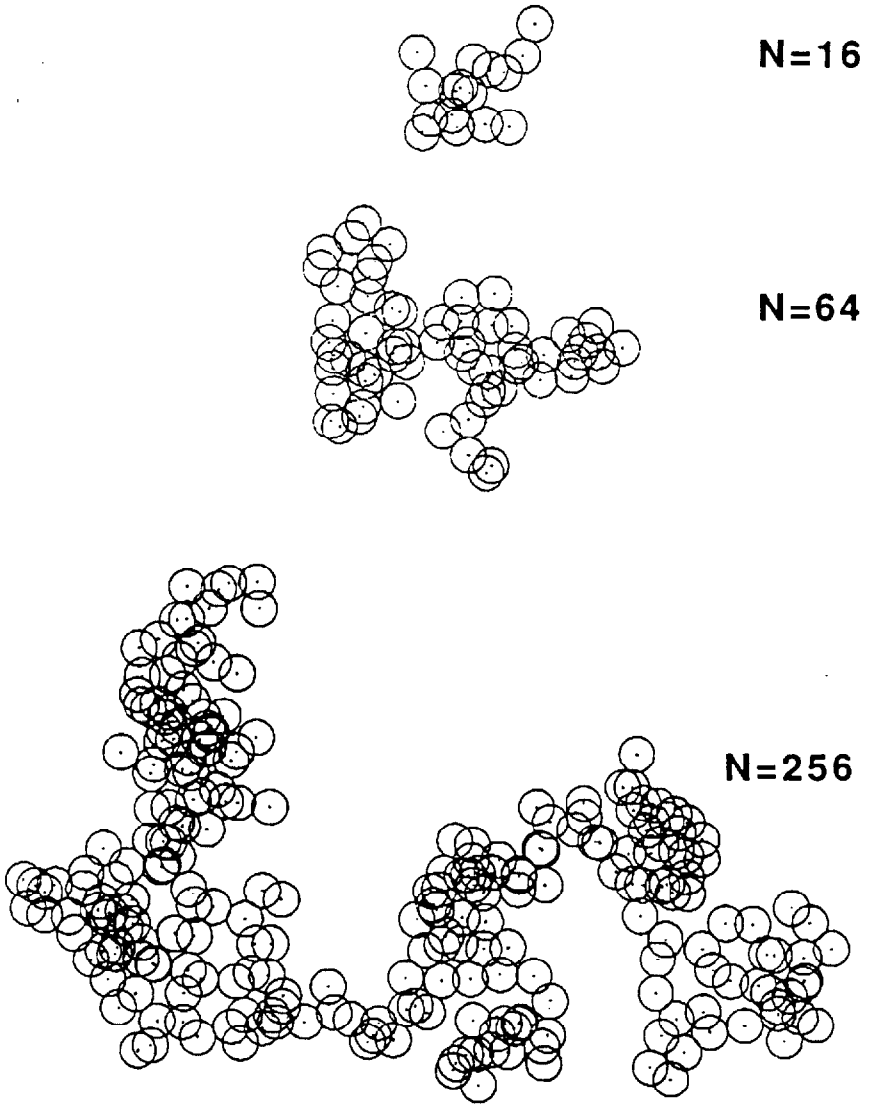

Figure 4 Projected images of typical aggregates used for the computational evaluation of RDG-PFA theory. From Farias et al. (1995a).

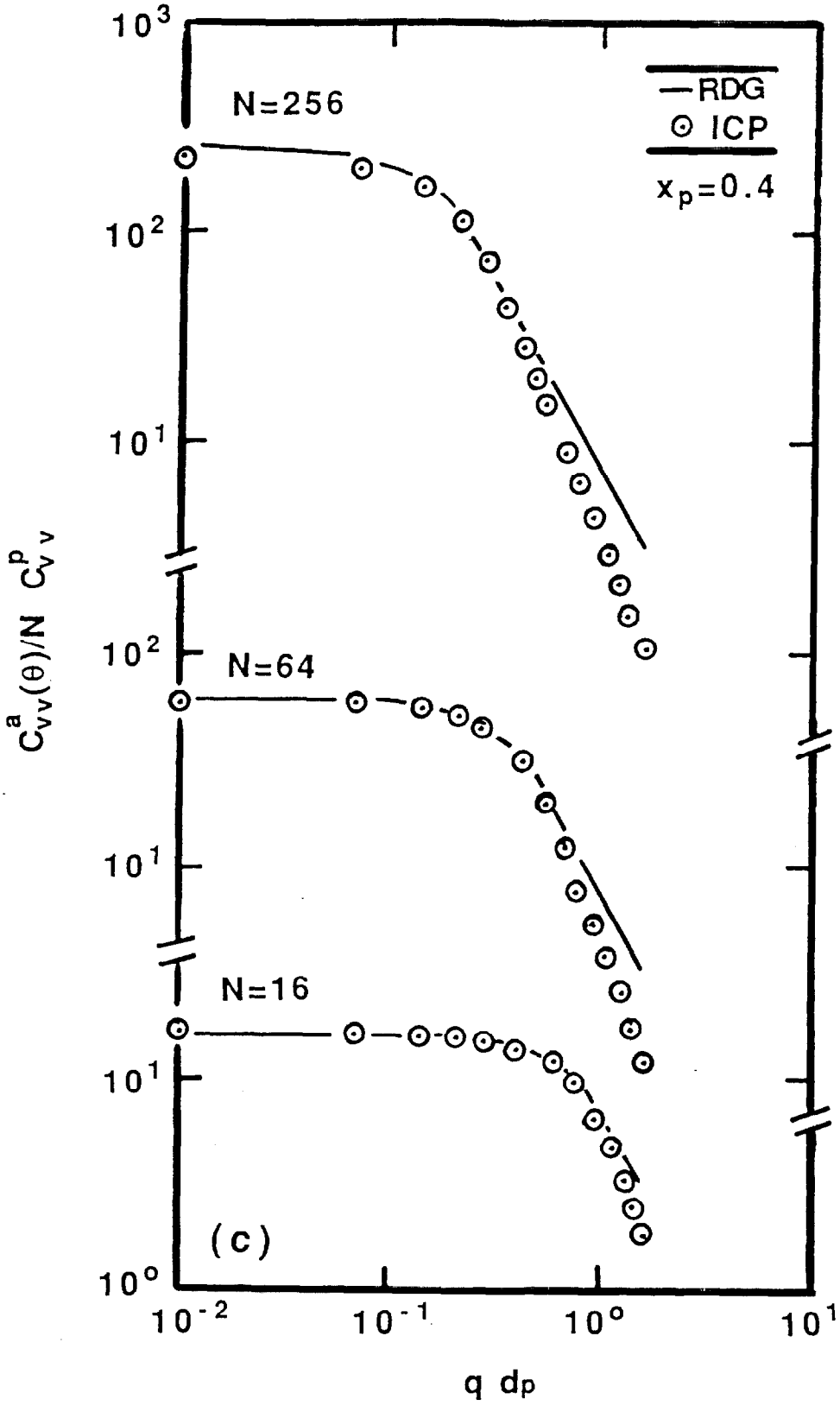

Figure 5 Normalized scattering patterns for fractal aggregates of various size, computed using ICP and RDG-PFA methods (D_f = 1.75, k_f = 8.0, λ = 514.5, nm, m = 1.57 + 0.57i and x_p = 0.4). From Farias et al. (1995a).

are due to problems with ICP, not with the RDG-PFA approximations. Köylü and Faeth (1994ab).

2.5 Conclusions

1. The approximate RDG-PFA scattering theory was in good agreement with measurements of soot in the fuel-rich region of diffusion flames, confirming earlier evaluations for soot in the fuel-lean region of diffusion flames due to Köylü and Faeth (1994a).

2. The approximate RDG-PFA scattering theory was in good agreement with more exact calculations using the ICP algorithm in the Guinier regime, which implies overall successful evaluation of RDG-PFA theory for soot for both the Guinier and large-angle (power-law) regimes for primary particle size parameters less than 0.42.

3. Present ICP calculations were not satisfactory in the large angle regime based on evaluations using Mie scattering predictions, discussed by Farias et al. (1995a), as well as evaluations based on well-established RDG-PFA predictions for soot aggregates in the power-law regime. This difficulty is attributed to excessive truncation errors of the ICP algorithm when $q\ d_p$ is large.

4. Finally, variations of the refractive index and fractal properties of soot over the test range, typical of current uncertainties about these properties, yielded far greater variations of optical cross sections than uncertainties concerning RDG-PFA predictions. Thus, current uncertainties about the refractive index and fractal properties of soot are the main limitation concerning estimates of optical properties of soot at the present time.

3. Fractal and Projected Structure Properties of Soot

3.1 Introduction

The reasonably successful evaluation of the RDG-PFA scattering theory for soot aggregates provides potential for resolving long-standing problems of the accurate determination of the refractive indices of soot, as well as for developing methods of solving the inverse problem so that soot structure properties can be found nonintrusively from scattering measurements (Köylü and Faeth, 1993, 1994a,b; Sorensen et al., 1992a,b). Both these objectives, however, are inhibited by limitations about the fractal and polydisperse properties of practical soot aggregates in flames. In particular, RDG theory requires values of R_g as a function of N but this determination is inhibited by current uncertainties concerning D_f and more particularly k_f (Köylü and Faeth, 1993). Additionally, information about k_f requires analysis of actual three-dimensional soot aggregates, which can be facilitated by the availability of relationships between the projected and the actual properties of soot aggregates. Unfortunately, currently available information along these lines is rather limited. In particular, evaluation of relationships between projected and true three-dimensional properties of soot aggregates have only involved small aggregate samples and a few flame conditions (Martin and Hurd, 1987; Samson et al., 1987; Köylü and Faeth, 1992).

In view of current limitations about the structure and optical properties of soot aggregates, the objective of this phase of the investigation was to study soot structure in order to define soot optical and fractal properties, as well as the relationships between actual and projected soot images. This work involved direct evaluation of the relationships

between the number of primary particles and the projected image of an aggregate, the relationships between the radius of gyration of an aggregate and properties of its projected image, and the values of the mass fractal dimensions and prefactors of soot in flame environments. The new information was developed by considering both numerically simulated and experimentally measured soot aggregates. The numerical simulations to create soot aggregates were based on cluster-cluster aggregation along the lines of Jullien and Botet (1987), Mountain and Mulholland (1988) and Farias et al. (1995a). The experimental soot aggregates were obtained from two sources, as follows: the large soot aggregates found in the fuel-lean region of buoyant turbulent diffusion flames in the long residence time regime, where soot structure is independent of flame position and residence time (Köylü and Faeth, 1991, 1992, 1994a; Sivathanu and Faeth, 1990); and soot aggregates in both the fuel-rich and fuel-lean regions of laminar jet diffusion flames (Sunderland et al., 1995). Taken together, the experimental soot properties involve a variety of fuels — acetylene, ethylene, propylene, and propane — burning in air within diffusion flames.

The discussion begins with consideration of numerically simulated soot aggregates in order to establish relationships between actual and projected soot aggregate properties. Measured soot aggregate properties are then considered, emphasizing soot fractal properties. The present description of the study is brief, more details can be found in Farias et al. (1995a), Farias (1997) and Köylü et al. (1995).

3.2 Numerically-Simulated Aggregates

Aggregate Simulation. A large sample of simulated soot aggregates was required for present work, with D_f in the range 1.7-1.8 and k_f of roughly 8.0 to correspond to experimental observations of the fractal properties of soot aggregates (Köylü and Faeth, 1992, 1994a,b). The necessary simulations were carried out using the approach of Farias et al. (1995a) and Farias (1997) that was already discussed in Section 2.

Using the approach of Farias et al. (1995a), it was found that D_f fell naturally in the range 1.6-1.9 for $N > 48$ so that few samples were rejected for inappropriate fractal properties. Similarly, for D_f of 1.7-1.8, the value of k_f fell naturally near $k_f = 8.0$ for statistically significant populations of aggregates. Naturally, these numerically simulated aggregates were not useful for investigating aggregate fractal properties because their fractal properties had been prescribed. Nevertheless, these objects were useful for investigating relationships between projected and actual aggregate properties because the simulated aggregates were very similar to actual aggregates while their known geometry vastly simplified determinations of actual and projected aggregate properties.

The population of simulated aggregates involved N in the range 20-1000 considering 20 aggregate sizes. Results for each aggregate size were averaged over different aggregates to yield a total sample of 400 aggregates. In order to fix ideas, a primary particle diameter of 50 nm was used for the simulations, which is typical of soot aggregates for heavily sooting materials (Köylü and Faeth, 1992). Present results are normalized by d_p or A_p, however, and such normalized results are independent of d_p at least for d_p less than 60 nm (Köylü and Faeth, 1994a,b). Typical aggregates using the present simulation method are illustrated in Fig. 4. These objects appear similar to existing observations of soot and combined with their prescribed fractal properties, they should be reasonably representative of the structure of soot aggregates found in flames.

Results and Discussion. The first property studied using the numerically simulated aggregates was the relationship between the number of primary particles in an aggregate and the projected area of the aggregate. Several workers have suggested the following

relationship between the projected area of a soot aggregate, A_a, and N (Samson et al., 1987; Megaridis and Dobbins, 1989, 1990; Köylü and Faeth, 1992):

$$N = k_a(A_a/A_p)^{\alpha} \tag{14}$$

where α is an empirical projected area exponent and k_a is a constant normally taken to be unity. Results for the present simulated aggregates, based on random projections of aggregates, are plotted according to equation (14) in Fig. 6. The power-law correlation of equation (14) is seen to provide an excellent fit of the data. The least-squares fit values of the correlation of equation (14) are $\alpha = 1.09$ and $k_a = 1.15$ with standard deviations of 0.002 and 0.01, respectively. The value of α is in reasonably agreement with earlier assessments, although the present values of k_a exceeds the value of unity used in earlier work (Samson et al., 1987; Megaridis and Dobbins, 1989, 1990; Köylü and Faeth, 1992). Further consideration of these differences will be undertaken when the experimental results are discussed.

The radius of gyration is an important aggregate property because it directly affects scattering properties computed using RDG theory. Thus, the simulated aggregates were used to compare actual values of the radius of gyration with values found from projected images of the aggregates. These results are illustrated in Fig. 7 where $R_g(3D)/R_g(2D)$ is plotted as a function of N for N in the range 20-1000. Remarkably, the ratio of the actual to projected radius of gyration is essentially independent of N and has the values of 1.24 with a standard deviation less than 0.01, i.e.:

$$R_g(3D) = 1.24R_g(2D) \tag{15}$$

Thus, equations (14) and (15) provide convenient relationships between the properties of projected images of aggregates, and the values of N and R_g needed to assess the fractal properties of aggregates that are defined in equation (1).

Other relationships between the projected shapes of soot aggregates and the fractal dimension and radius of gyration of actual aggregates were also developed, using the simulated aggregates, see Köylü et al. (1995) for these findings.

3.3 Flame-Generated Aggregates

Experimental Methods. Soot structure was observed using flame generated aggregates collected by thermophoretic sampling. Sampling procedures were based on the methods of Dobbins and Megaridis (1987,1991) with specific techniques identical to past work in this laboratory (Köylü and Faeth, 1992). Sampling times were controlled so that soot aggregates covered no more than 10% of the TEM grid in order to avoid overlapping aggregates on the grid. The time of transit of the grids to and from the sampling location through the flame environments was less than 5% of the sampling time so that soot on the grid was representative of the sampling location. This effect is not of any consequence for the soot sampled in the fuel-lean region of buoyant turbulent diffusion flames, however, because the properties of this soot are independent of position in any event (Köylü and Faeth, 1992). For present conditions, primary particle diameters were less than 60 nm, which implies that primary particle dimensions are smaller than the mean free path for all sampling conditions, so that the thermophoretic velocities of individual primary particles are identical. In addition, Rosner et al. (1991) have shown that the thermophoretic velocities of aggregates and individual primary particles agree within 20%, even when the

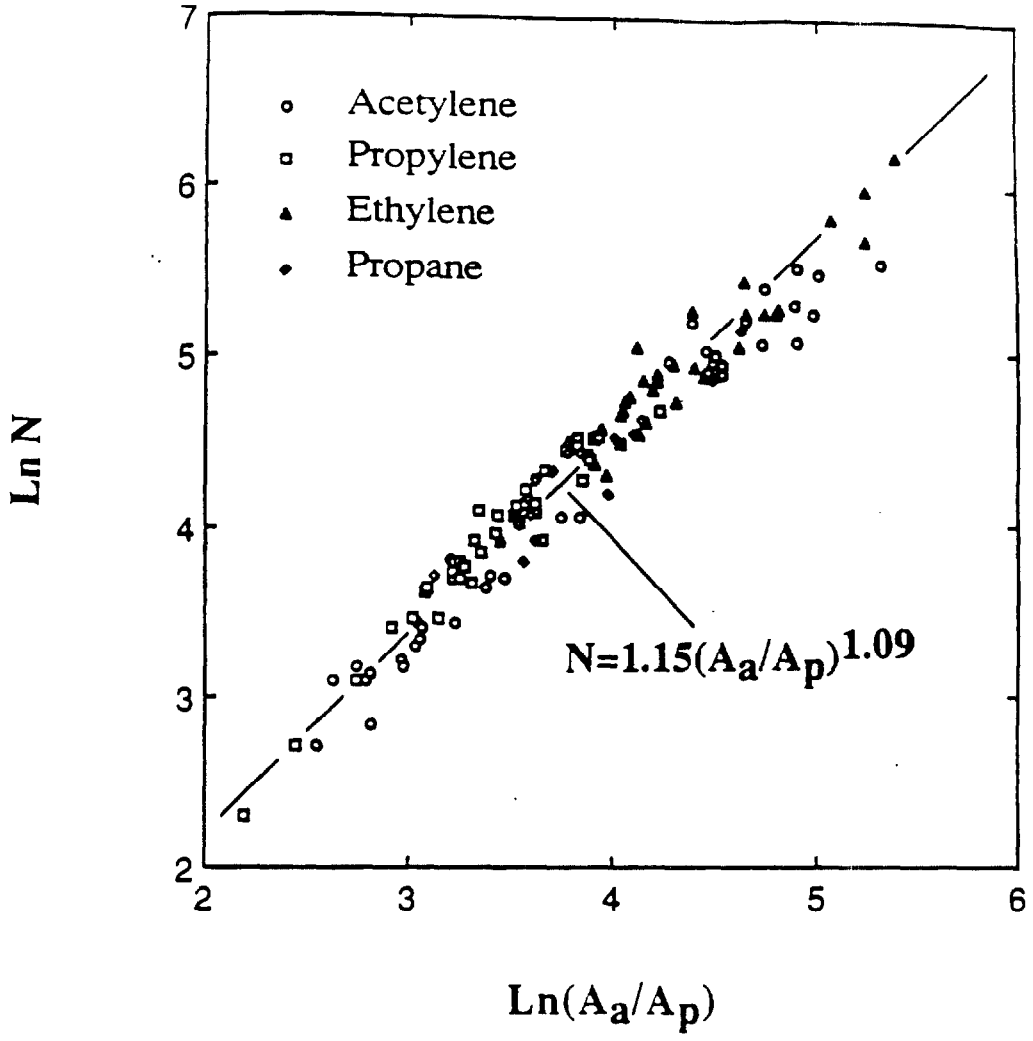

Figure 6 Number of primary particles as a function of projected area ratio for simulated soot aggregates. From Köylü et al. (1995).

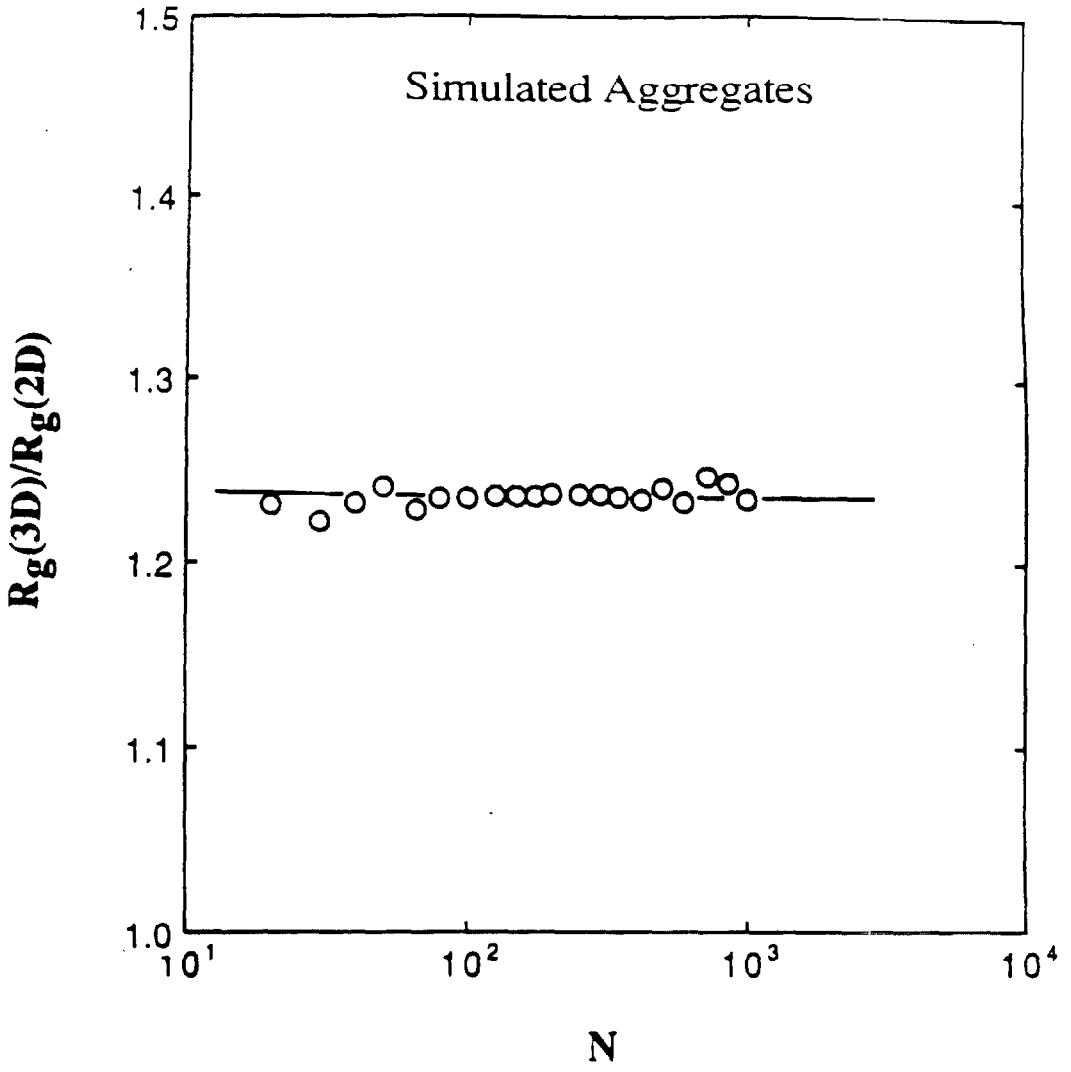

Figure 7 Ratio of actual to projected radius of gyration as a function of simulated soot aggregates. From Köylü et al. (1995).

aggregates are larger than mean free path lengths. Thus, effects of intrinsic bias with respect to aggregate size for the present thermophoretic sampling technique are small.

Results and Discussion: Turbulent Flames. The turbulent flame measurements involved soot emitted from buoyant turbulent diffusion flames in the long residence time regime. Specific measurements considered acetylene, ethylene, propylene and propane fueled flames burning in still air. The measurements involved a total of 127 aggregates containing 10-500 particles per aggregate.

These measurements were used to find the relationship between the number of primary particles in an aggregate and its projected area on a TEM image. These results were qualitatively similar to the results for simulated aggregates illustrated in Fig. 6. The resulting values of α and k_a in equation (14) were 1.09 and 1.15 with standard deviations of 0.02 and 0.18 respectively. These values are essentially the same as the results found for the simulated particles, within statistical significance.

The major effort during this phase of the investigation was the determination of the fractal prefactor, k_f, from measurements of soot fractal properties. The methodology of these measurements involved use of TEM stereopair images and other images at various projection angles to obtain three-dimensional primary particle positions. The results yielded $k_f = 8.5$ with an uncertainty (95% confidence) of 0.5 and a fractal dimension, $D_f = 1.8$ with a corresponding uncertainty of 0.08 (Köylü et al., 1995).

Results and Discussion: Laminar Flames. The final experimental results involved the fractal dimensions of soot in both the fuel-rich and fuel-lean regions of laminar diffusion flames. The most important finding in this case was that $D_f = 1.78$ with a standard deviation of 0.01. This value is comparable to the results for large buoyant turbulent diffusion flames and supports the conclusion that the fractal properties of soot are relatively universal.

3.4 Conclusions

Study of the structure of soot aggregates obtained from numerical simulations using cluster-cluster aggregation, measured properties of soot aggregates from the fuel-lean region of buoyant turbulent diffusion flames at long residence times, and measured properties of soot aggregates from both the fuel-rich and fuel-lean regions of weakly buoyant laminar jet diffusion flames, yielded the following major conclusions:

1. In contrast to primary particle diameters and aggregate size, which vary considerably depending on flame conditions and fuel type, both the fractal properties, and the relationships between actual and projected soot aggregate structure properties, appear to be durable properties of soot that are relatively independent of fuel type and flame condition.

2. The best estimates of the fractal properties of soot aggregates based on present measurements yield $D_f = 1.82$ and $k_f = 8.5$ with experimental uncertainties (95% confidence) of 0.08 and 0.5, respectively. These results agree within experimental uncertainties with earlier determinations from sampling and TEM measurements, see Samson et al. (1987), Megaridis and Dobbins (1990) and Köylü and Faeth (1994a,b).

3. Both computer simulations and experimental measurements indicated that it is possible to characterize soot aggregate structure properties from projected images

yielding $k_a = 1.15$, $\alpha = 1.09$ and $R_g(3D)/R_g(2D) = 1.24$, with standard deviations of these properties of 0.01, 0.002 and 0.01, respectively. The value of α is in good agreement with earlier estimates of this property, see Tien and Lee (1982), Megaridis and Dobbins (1989, 1990) and Köylü and Faeth (1992). In contrast, the present value of k_a is significantly larger than earlier estimates of unity for this parameter.

4.Refractive Index Properties of Soot

4.1 Introduction

Information about the structure and optical properties of soot is needed in order to develop reliable nonintrusive (optical) measurements of soot properties and estimates of continuum radiation due to soot in flame environments. Some information about the optical properties of soot is known, as already discussed: it consists of nearly monodisperse spherical primary particles that collect into mass fractal aggregates having broad size distributions, primary particle diameters and aggregate sizes vary widely but soot fractal properties (fractal dimensions and fractal prefactors) appear to be relatively universal, soot optical properties in the visible and infrared (for primary particle size parameters up to 0.42) can be approximated reasonably well by Rayleigh-Debye-Gans scattering from polydisperse mass fractal aggregates (called RDG-PFA theory), and current estimates of soot optical properties in flame environments are mainly limited by excessive uncertainties about soot refractive indices. Motivated by these observations, the objective of the present investigation was to experimentally determine soot optical properties at visible wavelengths, emphasizing soot refractive indices.

Earlier studies of soot refractive indices in the visible are briefly reviewed in the following; more details can be found in Chang and Charalampopoulos (1992), Charalampopoulos (1992), Lee and Tien (1980), Tien and Lee (1982), Viskanta and Mengüc (1987), and references cited therein. The earliest determinations of soot refractive indices involved *ex situ* reflectivity measurements of compressed soot samples (Dalzell and Sarofim, 1969; Felske et al., 1984); these results were questioned, however, due to potential changes of soot properties caused by sample collection and compression as well as potential effects of surface irregularities on measured reflectance properties (Charalampopoulos, 1992; Felske et al., 1984; Tien and Lee, 1982). As a result, subsequent work emphasized *in situ* measurements of extinction and scattering (Chang and Charalampopoulos, 1990; Charalampopoulos, 1992; Habib and Vervisch, 1988; Lee and Tien, 1980; Vaglieco et al., 1990); unfortunately, these studies also involved a number of deficiencies as follows: soot structure generally was not characterized adequately; Rayleigh and Mie scattering approximations were used to interpret the measurements that have not proven to be very effective for soot aggregates; and questionable approximations, involving either Drude-Lorentz dispersion models or Kramers-Krönig causality relationships, had to be adopted so that soot refractive indices could be found from the measurements (Dobbins and Megaridis, 1991; Faeth and Köylü, 1995, and Köylü and Faeth, 1994a,b 1996).

In view of these considerations, the present experimental study of soot refractive indices and related optical properties was undertaken, considering soot emitted from buoyant turbulent diffusion flames in the long residence time regime where soot properties are relatively independent of position in the fuel-lean (overfire) region and residence time. The approach to find optical properties involved *ex situ* measurements of soot physical and structure properties, gravimetric measurements of soot volume fractions, and *in situ* measurements of soot extinction and scattering properties. Then , after checking that RDG-PFA theory was acceptable, this theory was used to find the fractal dimensions, refractive

indices and dimensionless extinction coefficients of the soot. Present measurements were carried out at visible wavelengths (350-630 nm) because this wavelength range is important for nonintrusive (optical) measurements of soot properties and is accessible for *in situ* optical techniques due to reasonably large soot scattering levels.

In the following, experimental and theoretical methods are described first. Results are then discussed before summarizing conclusions. A preliminary report of the study appears in Wu et al. (1997) where soot emitted from several gas-fueled flames is considered. The following discussion will cover soot from both gas and liquid-fueled flames. The present discussion is brief: more details can be found in Köylü and Faeth (1996) and Wu et al. (1997) which appears in Appendices E and F.

4.2 Experimental Methods

Apparatus. The apparatus id described by Köylü and Faeth (1994a). Combustion was in still air within a large enclosure to control room disturbances. Gas- and liquid-fueled burners injecting fuel gases vertically upward, were used to yield strongly-buoyant turbulent diffusion flames. Soot properties were measured by collecting the combustion products in a hood and a 152 mm dia. sampling duct (which were heated to prevent thermophoretic deposition of soot on their surfaces) that discharged into the main exhaust hood of the flame apparatus. Measurements showed that mixing within the collection system was sufficient to yield uniform properties (soot concentrations, gas concentrations and temperatures) across the exit of the sampling duct where measurements were made. Note that using a collection system in this way does not affect soot structure and optical properties because soot properties are relatively independent of position in the overfire region and residence time within the long residence time regime (Köylü and Faeth, 1994a).

A water-cooled burner having a diameter of 50 mm was used for the gas-fueled flames, see Sivathanu and Faeth (1990) for a description of this arrangement. Uncooled burners having diameters of 51 and 102 mm were used for the liquid-fueled flames. The liquid fuel flow rate was adjusted for these flames to attain steady pool fires with the liquid surface somewhat below the burner exit.

Sampling Measurements. Aside from routine sampling measurements of gas temperatures and compositions at the measuring location, sampling measurements included soot structure, density, composition and gravimetric volume fractions. Soot structure was found by thermophoretic sampling and analysis using transmission electron microscopy (TEM), following (Köylü and Faeth (1992).. The sampling surfaces were the carbon-supported copper grids used to hold TEM specimens (3 mm dia., 200 mesh copper grids supported by a 20 nm thick elemental carbon film, SPI Supplies, Philadelphia, part no. 3520C). When sampling, the grids were parallel to the flow direction (vertical) at the flow axis. The grids were mounted on a double-acting pneumatic probe with sampling times measured using a pair of light-intercepting sensors and controlled so that soot aggregates covered less than 10% of the grid surface in order to avoid overlapping aggregates on the grid. Effects of aggregate size on sampling bias for the present soot aggregates are discussed by Köylü and Faeth, 1992) and Köylü et al. (1995): approximating aggregates by equivalent spheres suggests sampling velocity variations less than 20% over the size range of 95% of the aggregates; similarly allowing for the branched structure of the aggregates following Rosner et al. (1991) also suggests sampling velocity variations less than 20% over the aggregate size range. The samples were observed using a JEOL 2000 FX analytical electron microscope system with a 1 nm edge-to-edge resolution. Latex spheres having a diameter of 91 nm (5.8 nm standard deviation) were used to calibrate the TEM measurements. Samples of 400 primary particles selected from more than 50 aggregates, were used to find the mean value of d_p with an experimental uncertainties (95%

confidence) less than 2%. These measurements also established that primary particles were reasonably monodisperse, i.e., standard deviations were typically 17-21% of mean values of d_p.

Soot densities were found by thermophoretic sampling at the axis of the measuring location, using a finned water-cooled metal plate. Soot was periodically scraped from the plane until a sample weighing roughly 500 mg was obtained. The samples were then compressed into pellets to facilitate density measurements using helium pycnometry with a 1000 mm^3 cell (Micrometrics, Inc., Norcross, GA). Experimental uncertainties (95% confidence) of density measurements were estimated to be less than 1%. The composition of a portion of the overfire soot was known from Köylü (1992); therefore, these measurements were not repeated.

Gravimetric soot volume fractions were measured along the optical path through the soot following Choi et al. (1995). This involved sampling the flow and determining the volumes of soot and gas collected. A 13 mm inside diameter water-cooled probe, aligned with the flow direction, was used for sampling. The probe was connected to a modified filter holder that could accommodate a 47 mm diameter filter (Gelman Product 2220, in-line). The filter was connected to a vacuum pump through a flowmeter and valve. The flowmeter had a manometer at its inlet and was calibrated over the required range of inlet pressures and flow rates using a wet test meter. Soot samples were collected for a timed period using two filters (Gelman Part No. 66143, 200 nm, TF200, PTFE membrane filter), one filter in the filter holder and the second filter to mechanically collect soot from the sampling line and filter assembly. The mass of sampled soot was found by weighing the filters before and after sampling using an electronic balance. Then, given the density of the soot, the mass of soot collected, the volume of gas collected, and gas temperatures at the sampling and volume measuring conditions, the gravimetric soot volume fraction can be calculated in a straightforward manner. Times of sampling for these measurements were adjusted to achieve experimental uncertainties (95% confidence) less than 6%. The exhaust flow was nearly uniform so that sampling rates varying 4:1 around estimated isokinetic sampling rates had negligible effect on the measurements.

Optical Measurements. Scattering and extinction properties of the soot aggregates were found using the same general arrangement as Köylü and Faeth (1994ab). Light sources used for measurements at various wave lengths were as follows: 351.2, 457.9, 488.0 and 514.5 nm using an argon-ion laser (4 W Coherent Innova model 90-4); and 405.0 nm using a mercury lamp and a 10 nm bandwidth filter (100 W, Oriel model 6333); and 632.8 nm using a He-Ne laser (28 mW, Jodon Model HN10G1R). The incident beams were passed through a polarization rotator and a mechanical chopper before being focused on the axis of the sampling duct using a 1000 mm focal length lens. The collecting optics for scattering measurements were mounted on a turntable surrounding the exhaust duct so that scattering angles of 5-160 deg could be considered. The collecting optics consisted of an 85 mm focal length lens (having a collection angle of 0.7 msr), dichroic sheet polarizer filters (1 nm bandwidth), neutral density filters (to control the dynamic range), and a photodetector. The extinction measurements employed similar, but rigidly mounted, collecting optics. As noted earlier, concentrations of soot were nearly constant along the optical path for extinction measurements; nevertheless, gravimetric measurements along the optical path allowed correction of the extinction measurements to conditions at the axis where all other measurements were made. An optical system housing and darkroom conditions in the laboratory were used to control optical noise from ambient lighting. The output of the photodetectors was passed through lock-in amplifiers prior to sampling and storage using a laboratory computer.

The angular light scattering system was calibrated by measuring Rayleigh scattering from propane gas. After correcting for the reciprocal sin θ effect caused by the geometry of the measuring volume, the vv and hh differential cross sections agreed with Rayleigh scattering predictions with 5% for $20 \leq \theta \geq 160$ deg. Then, absolute volumetric differential scattering cross sections of soot were found from ratios of the detector signal for soot and propane, after accounting for signal attenuation in the optical path, based on the Rayleigh scattering properties of propane from Rudder and Bach (1968) and Dyer (1979). Total volumetric scattering cross sections were found by integrating volumetric differential scattering cross sections over the whole spherical surface; this required extrapolation to reach $\theta = 0$ and 180 deg but the effect of these extrapolations were small due to the relatively small solid angles involved. The optical arrangement for the extinction measurements was designed as discussed by Manickavasagam and Mengüc (1993) so that uncertainties due to forward scattering were less than 1% over the present test range. The experimental uncertainties (95% confidence) of the angular and total light scattering measurements were comparable and are estimated to be less than 10%, dominated by calibration uncertainties, finite sampling times, the finite aperture of the collection system and the angular uncertainty of the collecting optics; the corresponding uncertainties of total extinction and absorption cross sections are smaller, less than 5%, due to reduced effects of calibration uncertainties.

4.3 Theoretical Methods

Analysis of the scattering measurements to find soot optical properties was based on RDG-PFA theory. The main assumptions of RDG-PFA theory are as follows: individual primary particles satisfy the Rayleigh scattering approximation, soot aggregates satisfy the Rayleigh-Debye-Gans (RDG) scattering approximation, primary particles are spherical and monodisperse, primary particles just touch one another, the number of primary particles per aggregate satisfies a log-normal probability distribution function and the aggregates are mass fractal-like objects that satisfy equation (1). These approximations have problem to be satisfactory during past evaluations for a variety of conditions (Köylü and Faeth, 1992, 1994a,b); nevertheless, they still were evaluated using present measurements before the theory was used to find soot optical properties.

The first step of the present calculations involved the determination of the mean number of primary particles per unit volume at the measurement location from the gravimetric measurements of soot volume fraction and the TEM measurements of primary particle diameter, as follows:

$$n_p = 6f_v/(\pi d_p^3) \tag{16}$$

Then, noting that $\overline{Q}_a^a = \overline{Q}_e^a - \overline{Q}_s^a$, so that $\overline{Q}_a^a$ can be found from present measurements of $\overline{Q}_e^a$ and $\overline{Q}_s^a$, the refractive index functions, E(m) and F(m) can be computed as follows:

$$E(m) = k^2 \overline{Q}_a^a/(4\pi x_p^3 n_p) \tag{17}$$

$$F(m) = k^2(qd_p)^{D_f}\, \overline{Q}_{vv}^a(qd_p)/(k_f x_p^6 n_p) \tag{18}$$

where qd_p must be large enough so that scattering is in the large-angle (power-law) regime where equation (18) is appropriate. This requirement was established by noting the

behavior of scattering at the limiting conditions of small-angle (Guinier) and large-angle (power-law) scattering, as follows:

$$\overline{Q}_{vv}^{a}(qd_p)/Q_{vv}^{p} = (\overline{N}^2/\overline{N})\exp(-q^2\overline{R}_g^2/3), \quad \text{Guinier regime} \tag{19}$$

$$\overline{Q}_{vv}^{a}(qd_p)/Q_{vv}^{p} = k_f(qd_p)^{-D_f}, \text{ power-law regime} \tag{20}$$

where the expression for $\overline{R}_g^2$ in the Guinier regime can be found in Köylü and Faeth, 1994a) while the value of $k_f = 8.5$ was adopted from the determination of Köylü et al. (1995). The volumetric primary particle Rayleigh scattering cross section used to normalize equations (19) and (20) is given by:

$$\overline{Q}_{vv}^{p} = n_p x_p^6 F(m)/k^2 \tag{21}$$

It is evident that $\overline{Q}_{vv}^{a}(qd_p)/Q_{vvp}$ provides a simple determination of soot fractal dimensions because D_f is the slope of this function in the power-law regime. Finally, E(m) and F(m) provide two nonlinear algebraic equations that can be solved to find the real and imaginary parts of the soot refractive indices.

The dimensionless extinction coefficient is a useful optical property that provides a simple relationship between extinction and soot volume fractions (Dobbins et al., 1994; Choi et al., 1995). This parameter was found for present test conditions by noting that properties were constant along the optical path used for extinction measurements, which implies (Choi et al., 1995):

$$k_{eR} = k_e(1+\rho_{sa}) = -\lambda \ln(I/I_o)/(Lf_v). \tag{22}$$

4.4 Results and Discussion

Test Conditions. Flame properties for the present experiments are summarized in Table 2. The flames involved both gaseous (acetylene, ethylene, propylene and butadiene) and liquid (benzene, cyclohexane, toluene and n-heptane) hydrocarbon fuels. Burner diameters were in the range 50-102 mm. Heat release rates were in the range 1700-6580 W. Finally, characteristic residence times were in the range 254-333 ms, which places all these flames in the long residence time regime where soot properties in the overfire region are independent of both position and residence time (Sivathanu and Faeth, 1990; Köylü and Faeth, 1992).

Soot properties for the present experiments are summarized in Table 3. Primary particle diameters are in the range 32-51 nm; this implies values of x_p in the range 0.16-0.46. Fractal dimensions will be discussed later but their variation with fuel type and wavelength is small over the present test range with a mean value of $D_f = 1.79$ and a standard deviation of 0.01. The mean number of primary particles per aggregate was not measured for butadiene and cyclohexane but was in the range 260-552 for the rest of the fuels. The compositions of acetylene and propylene soot measured by Köylü and Faeth, 1994a) are listed in the table: carbon dominates the soot mass with small contributions of hydrogen, oxygen and nitrogen. Finally, the density of the present acetylene, propylene and ethylene soot was 1870, 1850 and 1930 kg/m^3 from Wu et al. (1997); this variation is not large so that a mean value of soot density of 1880 kg/m^3 was used during present work.

Table 2. Test conditions for measurements of the optical properties of soot emitted from buoyant turbulent diffusion flames at long residence times

Fuel	Formula	Phase[a]	Burner Dia. (mm)	Heat Rate (W)	Char. Res. Time (ms)[b]
Acetylene	C_2H_2	g	50	6160	329
Ethylene	C_2H_4	g	50	5140	317
Propylene	C_3H_6	g	50	6580	333
Butadiene	C_4H_6	g	50	1700	254
Benzene	C_6H_6	f	51	3400	292
Cyclohexane	C_6H_{12}	f	102	5000	315
Toluene	C_7H_8	f	51	2500	274
n-Heptane	C_7H_{16}	f	102	4100	303

[a]The symbols g and f denote gas and liquid, respectively.
[b]Computed from the correlation of Sivathanu and Faeth (1990) for buoyant turbulent diffusion flames.

Table 3 Physical and fractal properties of soot emitted from buoyant turbulent diffusion flames at long residence times.[a]

Fuel	d_p(nm)	D_f	$\overline{N}$	C/H	C/O	C/N
Acetylene	47	1.79	417	16.8	107.0	295
Ethylene	32	1.80	467	---	---	---
Propylene	41	1.79	400	17.0	57.6	411
Butadiene	42	1.79	---	---	---	---
Benzene	50	1.77	552	---	---	---
Cyclohexane	37	1.81	---	---	---	---
Toluene	51	1.79	526	---	---	---
n-Heptane	35	1.79	260	---	---	---

[a]Soot at these conditions is independent of position in the overfire region and residence time (Köylü and Faeth, 1992). Fractal prefactor of 8.5 taken from Köylü et al. (1996).

Dimensionless Extinction Coefficients. Present measurements of dimensionless extinction coefficients, k_{eR}, are plotted as a function of fuel type and wavelength in Fig. 8. The present mean value of k_{eR}, averaged over all wavelengths and fuels is 8.4 with a standard deviation of 1.2; this average is marked on the plots as a dashed line. There is a tendency for overfire soot from acetylene and n-heptane-fueled flames to be somewhat lower and higher than the rest, respectively, however, these variations are not statistically significant. Thus, it is concluded that the k_{eR} are independent of both fuel type and wavelength for present results.

Values of k_{eR} averaged over all the fuels are plotted as a function of wavelength in Fig. 9. Other measurements of k_{eR} are also illustrated on the plot for comparison with the present measurements. This includes values of k_{eR} in the range 8.1-9.4 reported by Dobbins et al. (1994) for crude oil, and a mean value of $k_{eR} = 8.6$ with a standard deviation of 0.5 reported by Choi et al. (1995) for acetylene. Clearly, the results from all three sources are in excellent agreement. In contrast, the earlier measurements of Wu et al. (1997) for overfire soot from acetylene-, propylene-, ethylene- and propane-fueled flames in the long residence time regime yielded a much smaller value of the mean $k_{eR} = 5.1$ with a standard deviation of 0.5, although their observations of small effects of fuel type and wavelength were similar to the present study. The reasons for these differences could not be established during the present study and the findings of Wu et al. (1997) could not be repeated. Thus, the results of Wu et al. (1997) are judged to be wrong and will not be considered any further in the following.

It is interesting that in spite of the relatively strong variation of absorption and scattering cross sections with wavelength of fractal aggregates under the RDG approximation, values of k_{eR} remain relatively constant in the visible. For example, under the present assumptions, the primary particles satisfy the Rayleigh scattering approximation, yielding the following expressions for their optical properties (Bohren and Huffman, 1983):

$$C_a^p = 4\pi x_p^3 E(m)/k^2 \tag{23}$$

$$C_s^p = 8\pi x_p^6 F(m)/(3k^2) \tag{24}$$

$$C_{vv}^p = x_p^6 F(m)/k^2 \tag{25}$$

which implies $C_a^p \sim 1/\lambda$ and $C_s^p \sim C_{vv}^p \sim 1/\lambda^4$. RDG-PFA scattering from aggregates of primary particles is somewhat modified from the behavior of individual primary particles but the general trend toward increasing optical cross sections with decreasing wavelength is similar. Thus, the fact that a property like k_{eR} remains relatively independent of wavelength over the present test range requires compensating reductions of the refractive index functions, E(m) and F(m), with decreasing wavelength. Results considered subsequently will show that this is the case.

Scattering Patterns. RDG-PFA scattering theory was evaluated in order to justify the present approach to find soot refractive indices. A first concern was effective measurements of Rayleigh scattering from gaseous propane because these results were needed to calibrate the absolute scattering measurements from soot in the large angle (power-law) regime that were used to find E(m) and F(m) as discussed earlier. A typical evaluation of this type is illustrated in Fig. 10. This involves scattering from propane at a wavelength of 351.2 nm. The measurements of vv and hh optical cross sections are compared with predictions using the Rayleigh scattering approximation as discussed

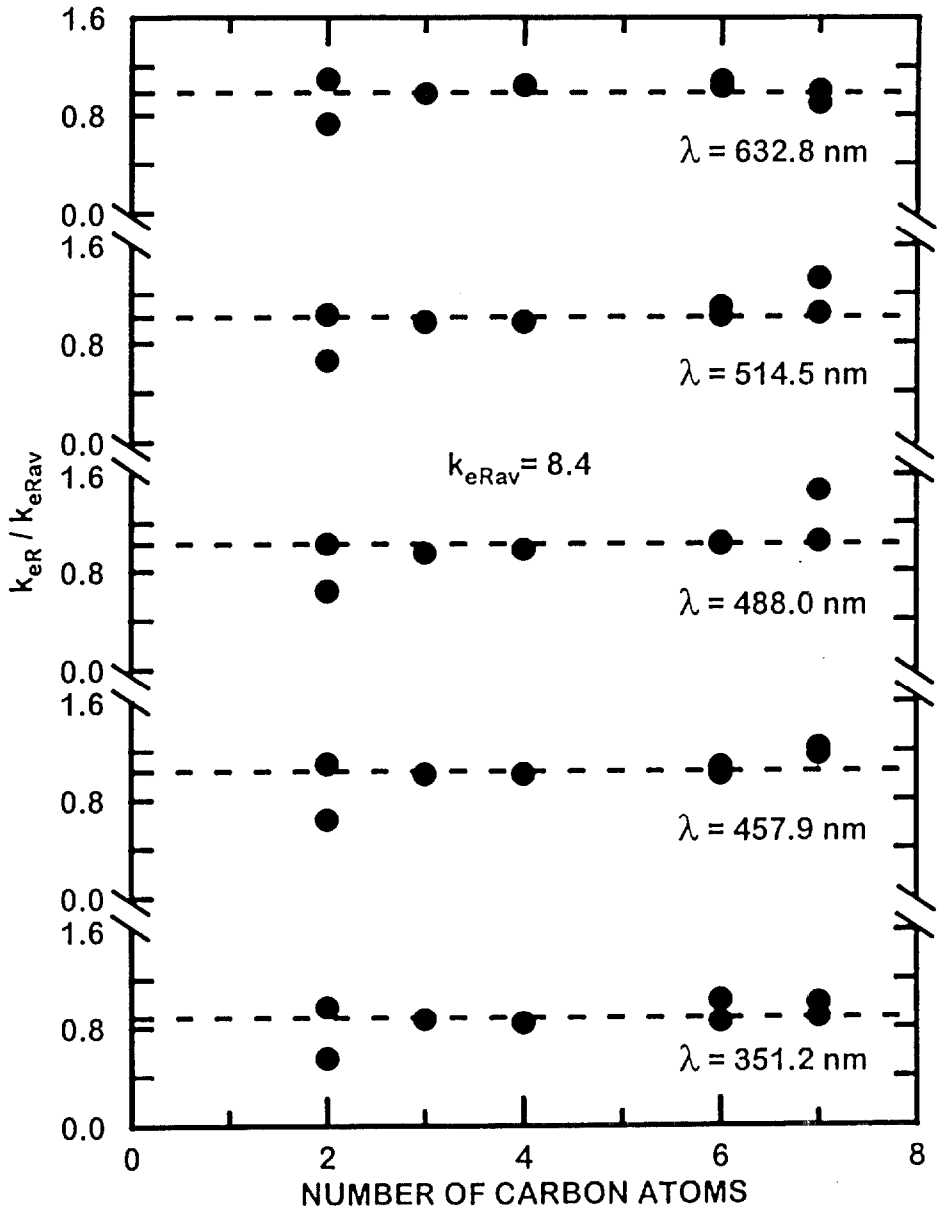

Figure 8 Dimensionless extinction coefficient as a function of fuel type and wavelength for soot emitted from buoyant turbulent diffusion flames.

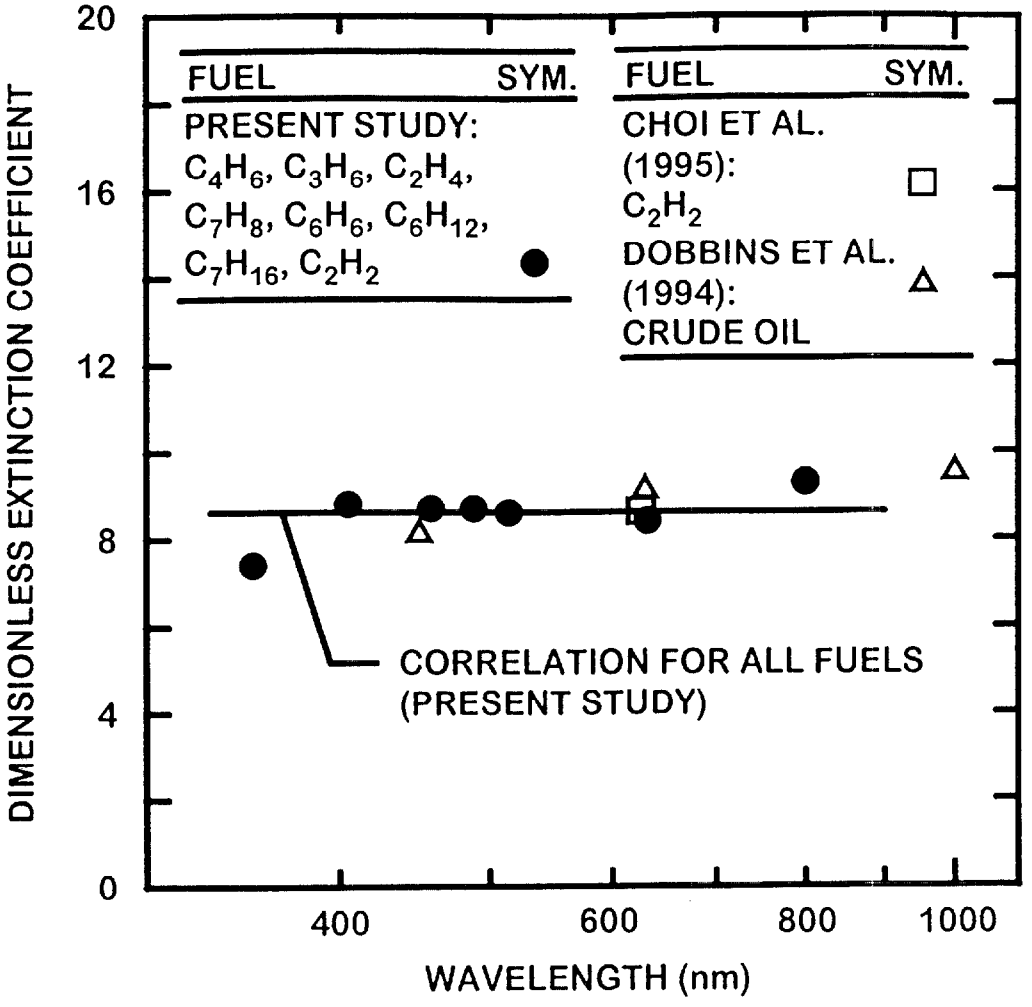

Figure 9 Dimensionless extinction coefficients for soot as a function of wavelength.

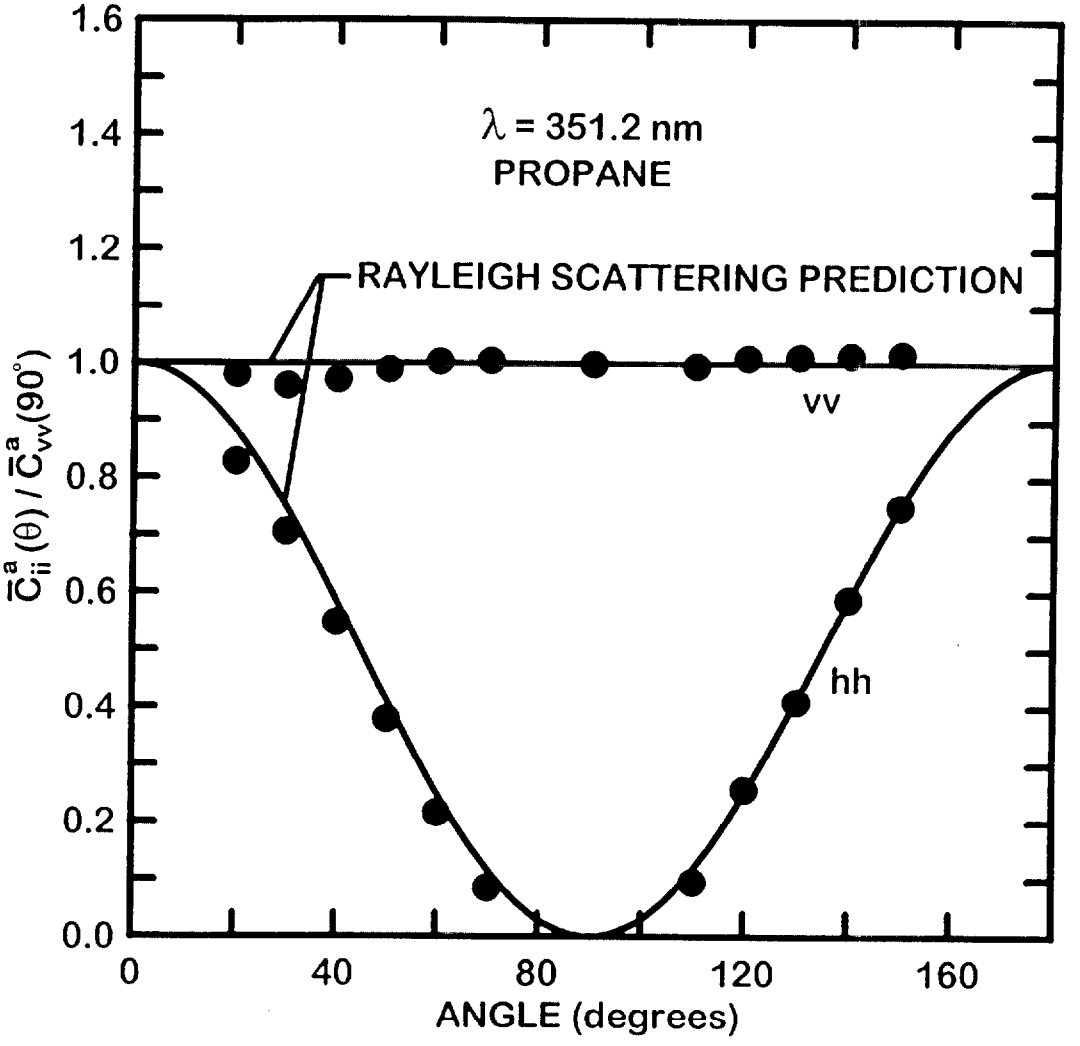

Figure 10 Typical Rayleigh scattering pattern for calibrating absolute soot scattering levels.

earlier. The comparison between measurements and predictions is excellent providing confidence in the present calibration procedure.

The next evaluation concerned predicted and measured scattering patterns in order to justify use of RDG-PFA scattering theory to find soot refractive index properties. The smallest wavelengths of the test range were a particular concern because values of x_p become large at these conditions which raises questions about the RDG scattering approximations (Faeth and Köylü, 1995). Thus, measured and predicted scattering patterns at the worst-case condition for the present test range (toluene soot at 351.2 nm which yields $x_p = 0.46$) are illustrated in Fig. 11. The hh scattering pattern on this plot has been corrected by introducing a depolarization ratio, ρ_v, as discussed in connection with equations (12) and (13). The resulting predictions and measurements are seen to be in excellent agreement, justifying the use of RDG-PFA scattering theory over the present test range. The scattering pattern of Fig. 11 exhibits strong scattering at small values of θ in the Guinier regime which is not typical of Rayleigh scattering where the scattering cross section in the vv direction is independent of scattering angle as illustrated in Fig. 10. In addition, scattering from soot is not well approximated by Mie scattering for an equivalent sphere as shown by Köylü and Faeth (1994a,b); this occurs because soot has a rather open structure (see Fig. 1) as indicated by its fractal dimension which is less than 2.0 (which is the fractal dimension value that separates Mie-type scatterers having large solidity from open-structure scatterers like soot). Finally, the present evaluation of the RDG-PFA theory seems satisfactory; therefore, the next step in finding refraction index properties is to establish that present measurements properly extend to the large angle regime and that the present soot is properly represented as a mass fractal object. These issues are considered next.

Fractal Properties. Evaluating whether present measurements properly reach the power-law regime, so that equation (10) can be used to find refractive indices, and exploiting these conditions to find fractal dimensions, can best be done by plotting $\overline{Q}_{vv}^{a}(qd_p)/Q_{vv}^{p}$ as a function of the modulus of the scattering vector, qd_p, as suggested by equation (20). These results are illustrated for the four gaseous fuels at a wavelength of 632.8 nm in Fig. 12, however, behavior for other fuels and wavelengths is similar. The results shown in the figure include the measurements and predictions over the available ranges of qd_p, as well as the extrapolation of power-law behavior based on equation (18). As before, the substantial departure of scattering properties from Rayleigh scattering behavior (where $\overline{Q}_{vv}^{a}(qd_p)/Q_{vv}^{p}$ would be independent of qd_p) is evident, with forward scattering 100-1000 times larger than back scattering for the present large soot aggregates. The measurements also clearly provide the extended power-law regime where scattering properties are represented by equation (18), e.g., roughly $qd_p > 0.1$, that is needed for the current *in situ* method to find soot refractive indices.

The measurements of $\overline{Q}_{vv}^{a}(qd_p)/Q_{vv}^{p}$ in the power-law regime were used to compute fractal dimensions. Based on equation (20), it is clear that the slope of the dashed-line plots of Fig. 12 is the fractal dimension. These slopes were obtained and are plotted as a function of fuel type and wavelength in Fig. 13. The average value is $D_f = 1.79$, with a standard deviation of 0.01, and this value is shown on the plots for comparison with the present measurements. It is clear that effects of fuel type on D_f are negligible. In addition, D_f is also independent of wavelength over the present test range as required by both proper fractal behavior and RDG-PFA theory.

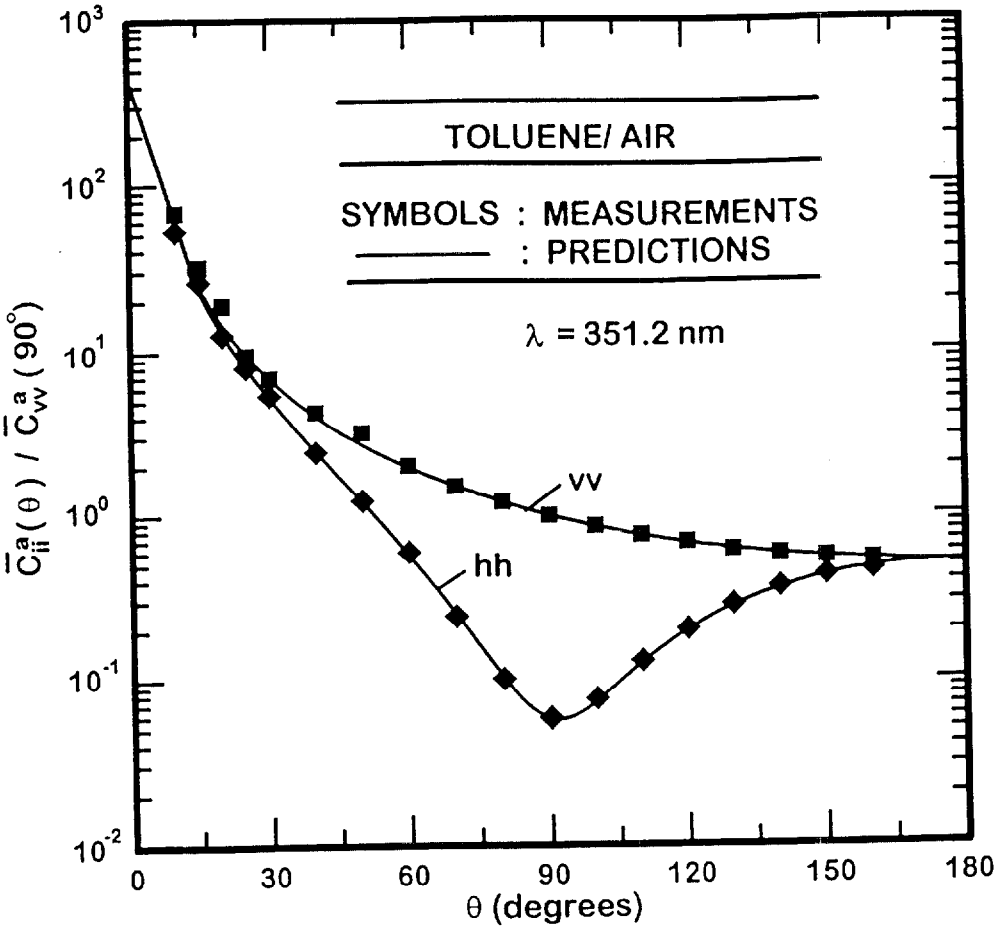

Figure 11 Measured and predicted angular soot scattering patterns for soot emitted from buoyant turbulent diffusion flames (toluene at 351.2 nm).

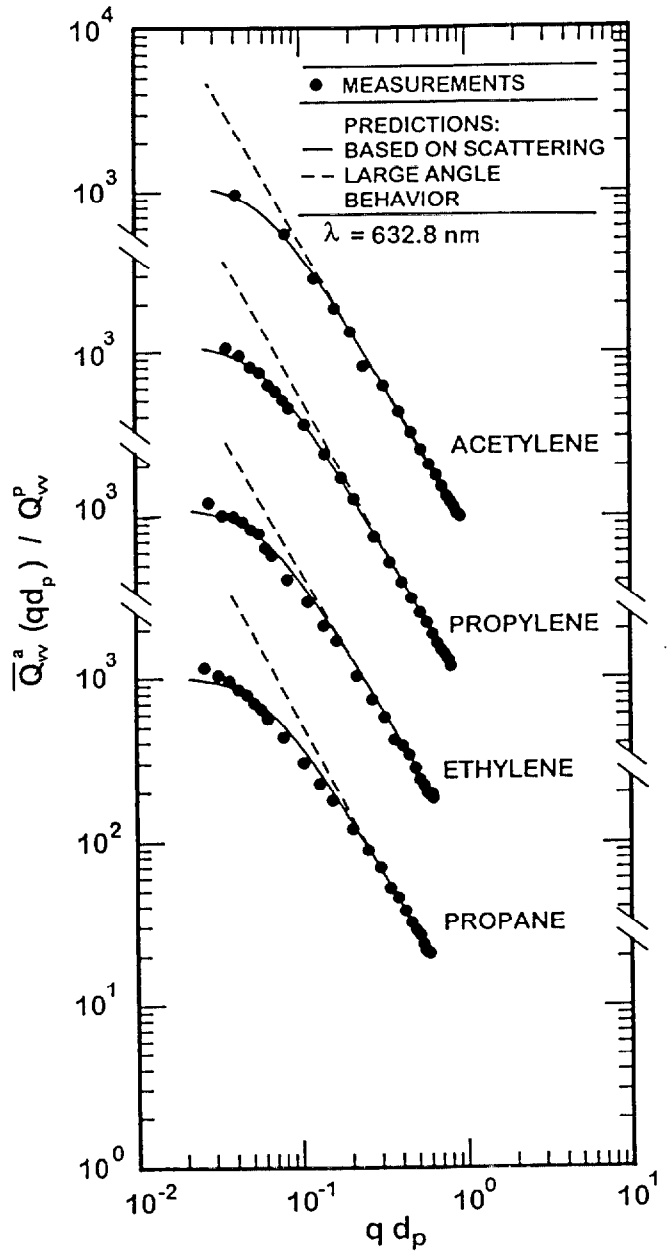

Figure 12 Volumetric vv cross section as a function of the modulus of the scattering vector for soot emitted for buoyant turbulent diffusion flames.

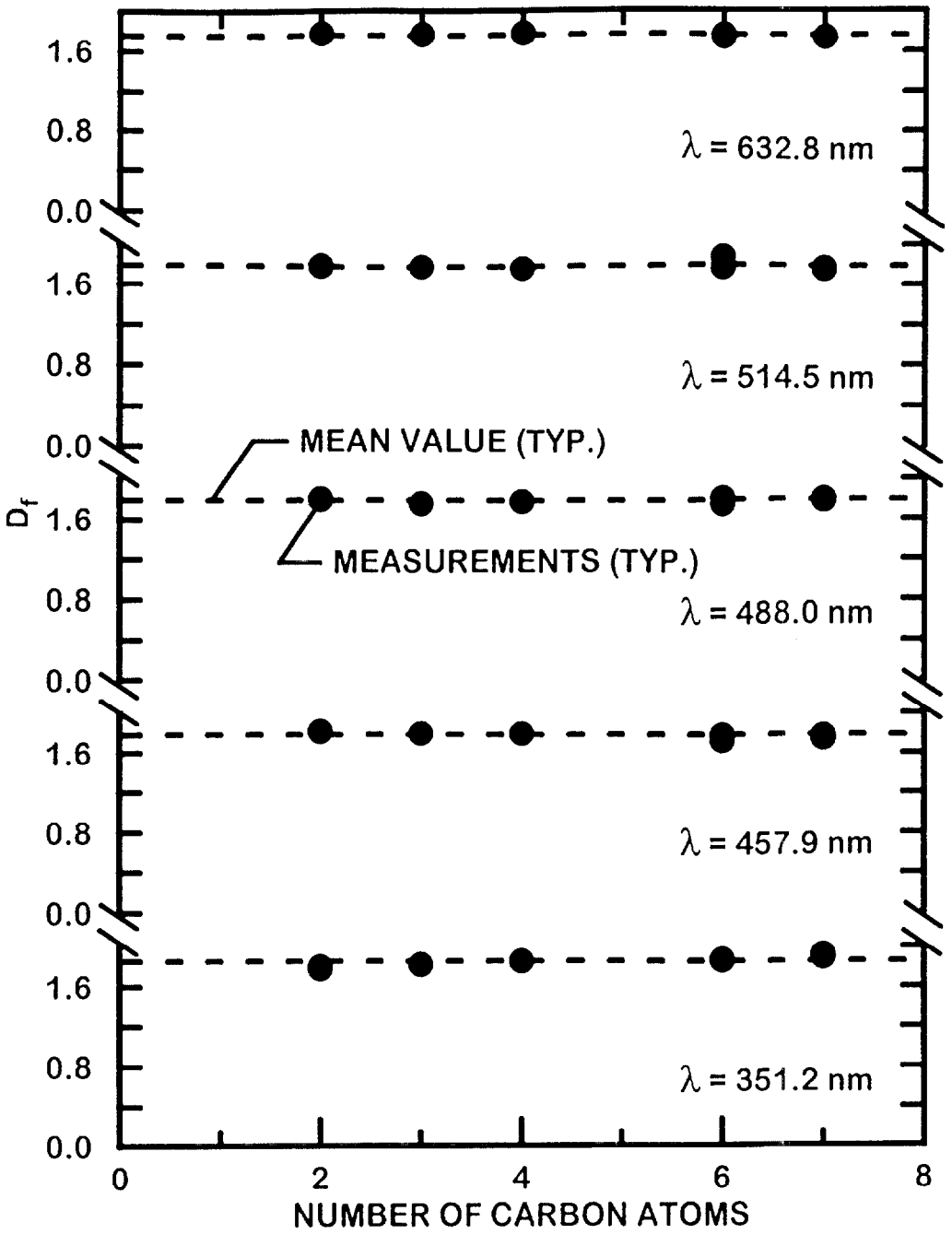

Figure 13 Fractal dimensions as a function of fuel type and wavelength for soot emitted from buoyant turbulent diffusion flames.

The final values of D_f have been averaged over wavelength for each fuel and are summarized in Table 3. Thus, the necessary fractal properties and performance of RDG-PFA theory have been established so that refractive index properties can now be addressed.

Refractive Index Function E(m). The refractive index function E(m) was evaluated next due to its importance for radiation absorption and emission. As discussed earlier, E(m) was found from equation (17), based on present measurements of volumetric extinction and total scattering cross sections, the gravimetric measurements of the volume fraction of soot and the TEM measurements of primary particle diameters.

The resulting values of E(m) are plotted as a function of fuel type and wavelength in Fig. 14. Combining all factors, the experimental uncertainties of the E(m) are less than 20 percent, with the largest uncertainties encountered at a wavelength of 632.8 nm where combined uncertainties due to laser power and scattering levels were larger than the rest (which particularly affected calibration of absolute scattering levels based on Rayleigh scattering from propane). Mean values of E(m), averaged over all the fuels, are also shown on the plots for each wavelength. Effects of fuel type on these plots are within experimental uncertainties and it is concluded that E(m) is independent of fuel type over the present test range.

Given the results of Fig. 14, present results were used in conjunction with earlier laser extinction measurements of Köylü and Faeth (1996) to obtain estimates of E(m) over a somewhat broader range of wavelengths. This was done by matching the values of E(m) for the two data sets at 514.5 nm and extrapolating present measurements of ρ_{sa} to cover the range 200-1000 nm. These calculations were completed for acetylene, propylene and ethylene soot which were the only fuels considered during both studies.

The results for E(m), including the present measurements and the results extended from Köylü and Faeth (1996), are plotted in Fig. 15 as a function of wavelength. The agreement between the present results and the results extended from Köylü and Faeth (1996) is excellent over the range of conditions where they overlap. The present values of E(m) also progressively increase with increasing wavelength and do not suggest an approach to a resonance condition in the near uv for soot, based on the behavior of graphite, that has been used to reduce refractive index measurements by some workers, e.g., Chang and Charalampopoulos (1990) and Lee and Tien (1980). As noted earlier, increasing E(m) with increasing wavelength over the present test range is not unexpected because this behavior is needed to explain why k_{eR} is relatively independent of wavelength in the visible.

Several earlier measurements of E(m) are illustrated in Fig. 15 for comparison with the present measurements. These measurements include the classical *ex situ* reflectometry measurements for soot in the fuel-lean region of acetylene and propane/air diffusion flames due to Dalzell and Sarofim (1969), the *ex situ* measurements for soot in the fuel-lean regions of acetylene/air and propane/air diffusion flames due to Batten (1985), the *in situ* measurements for soot in the fuel-lean region of plexiglass/air diffusion flames due to Lee and Tien (1980), the *in situ* measurements for soot in the post-flame region of fuel-rich premixed propane/air flames due to Chang and Charalampopoulos (1990), and the *in situ* measurements for soot in the post-flame region of fuel-rich premixed ethylene/air flames due to Vaglieco et al. (1990). It should be noted that the *ex situ* measurements of Dalzell and Sarofim (1969) have been criticized by Lee and Tien (1980) for potential problems of soot property changes due to soot collection and sample preparation, and by Felske et al. (1984) for potential problems of diffuse scattering for reflectometry measurements due to surface roughness. On the other hand, the measurements of Lee and Tien (1980), Batten

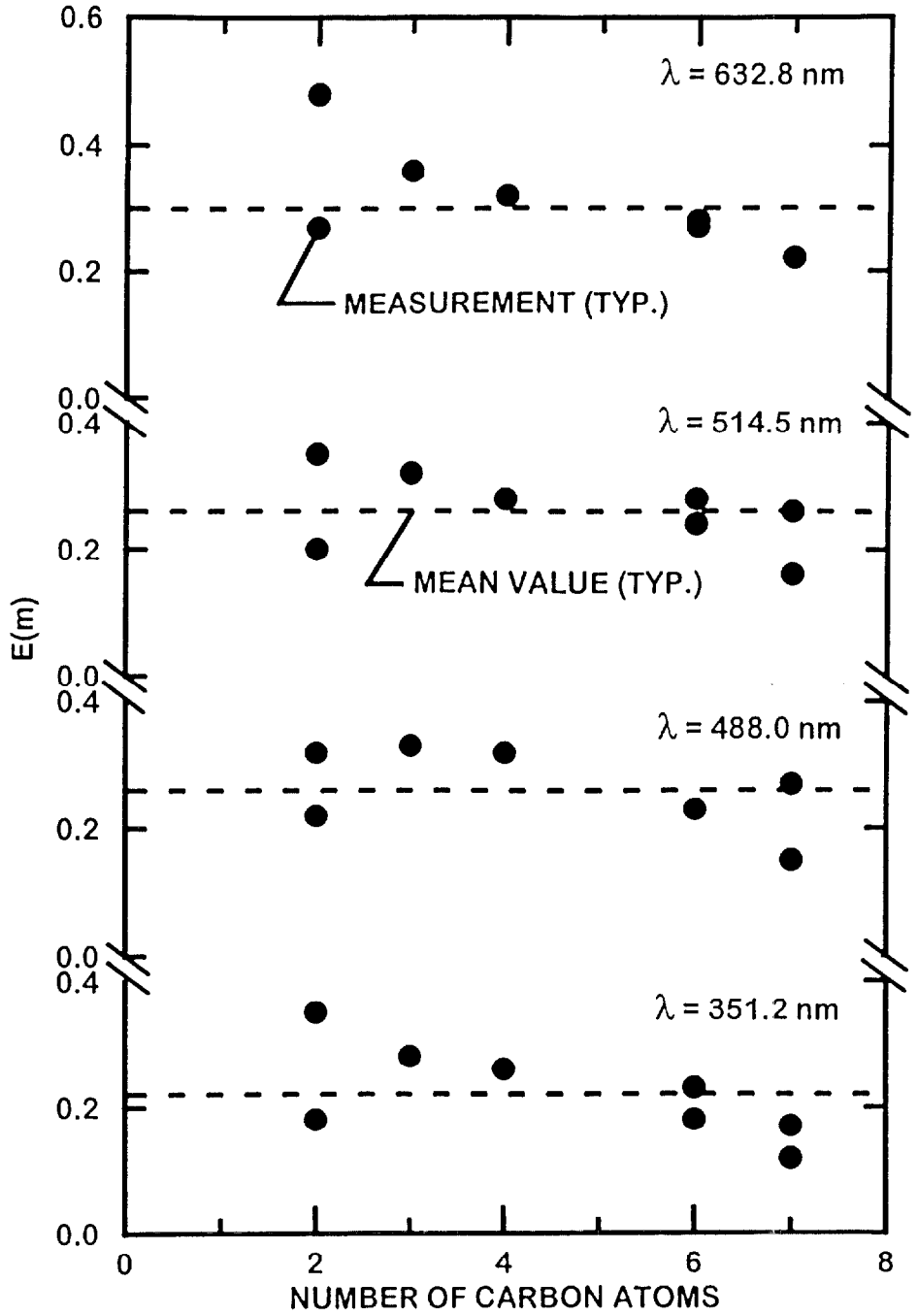

Figure 14 E(m) as a function of fuel type and wavelength for soot emitted from buoyant turbulent diffusion flames.

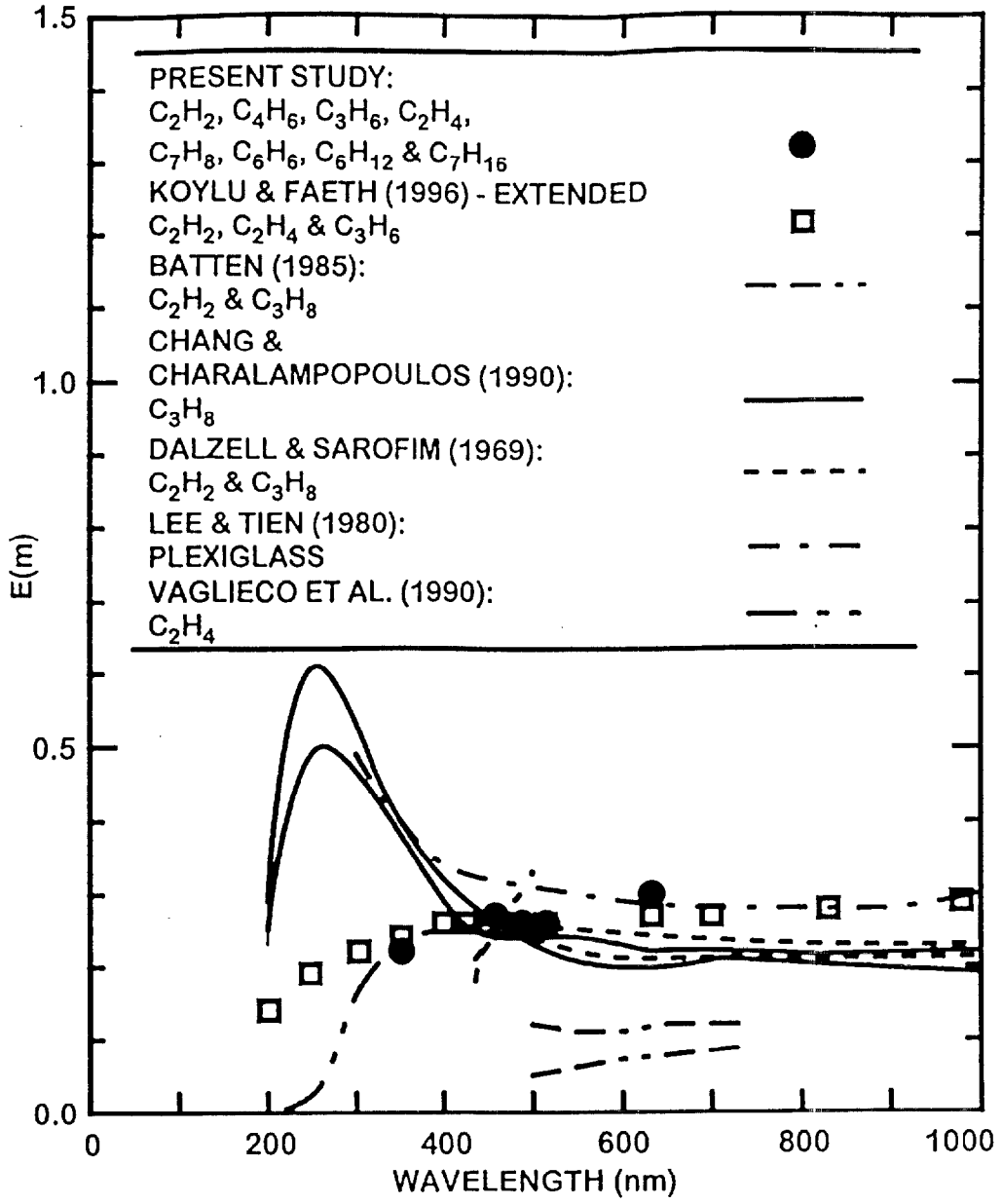

Figure 15 E(m) for soot as a function of wavelength.

(1985), Chang and Charalampopoulos (1990) and Vaglieco et al. (1990) can be criticized as noted earlier, because they all involve questionable models for the optical properties of soot, some involve questionable soot transport properties in cases where dynamic scattering measurements are used to estimate soot aggregate properties, and some involve questionable approximations associated with either Drude-Lorentz dispersion models or Kramers-Krönig causality relationships used to close the procedure to find soot refractive indices. Finally, Chang and Charalampopoulos (1990) observe variations of soot refractive indices with increasing residence time in the post-flame region of premixed flames, attributed to an effect of soot aging (or annealing) in a high temperature environment, so that their results are indicated by a band.

Present measurements agree reasonably well with the results of Dalzell and Sarofim (1969) for wavelengths of 400-550 nm and then transition toward the measurements of Lee and Tien (1980) at long wavelengths. In view of experimental uncertainties, the results of all three of these studies are in reasonable agreement for wavelengths larger than 400 nm. Notably, the combined measurements in this region involves soot from a broad range of fuel types. At shorter wavelengths, present measurements follow Vaglieco et al. (1990) for a time but do not approach zero as rapidly with decreasing wavelength. The results of Batten (1985) are very different from the rest for reasons that are not known. Finally, the present variation of E(m) with wavelength is qualitatively similar to the results of Wu et al. (1997) although the magnitudes differ somewhat due to the problems with these earlier measurements discussed in connection with the dimensionless extinction coefficient results. Naturally, this progressive reduction of E(m) with decreasing wavelength suggests problems for some past determinations of soot refractive indices where the presence of resonance conditions is assumed, by analogy with graphite, when either Drude-Lorentz dispersion relations or Kramers-Krönig causality relationships were developed.

Refractive Index Function F(m). Final measurements involved the refractive index function F(m), due to its importance for soot scattering. As discussed earlier, F(m) was found from equation (18), based on present measurements of absolute vv cross sections in the large angle regime, present gravimetric measurements of soot volume fraction, TEM measurements of primary particle diameter, present measurements of the fractal dimensions, and values of the fractal prefactor from Köylü et al. (1995).

The resulting values of F(m) are plotted as a function of fuel type and wavelength in Fig. 16. Increased uncertainties about calibrations of absolute scattering measurements and the value of k_f, increased the uncertainties of F(m) compared to E(m). Thus, the uncertainties (95% confidence) of F(m) are less than 30%, with the largest uncertainties at 632.8 nm, as before. Mean values, averaged over all the fuels, are also shown on the plots for each wavelength. Effects of fuel type on these plots do not exhibit any consistent trends and are comparable to experimental uncertainties; therefore, it is concluded that F(m) is independent of fuel type over the present test range.

The present mean values of F(m) are plotted as a function of wavelength in Fig. 17. It was not possible to develop an estimate of F(m) from Köylü and Faeth (1996), however, earlier measurements from the other investigations discussed in connection with Fig. 16 are plotted in Fig. 17 as well. Present measurements agree with the other studies, except Batten (1985), for the wavelength range 400-550 nm. On the other hand, present measurements increase more rapidly with increasing wavelength than seen before. An exception is the qualitative trends of F(m) observed by Wu et al. (1997) although the magnitudes of F(m) differ from the present results due to the problems discussed in connection with the measurements of k_{eR}. Finally, a rapid increase of F(m) with wavelength, as seen in the

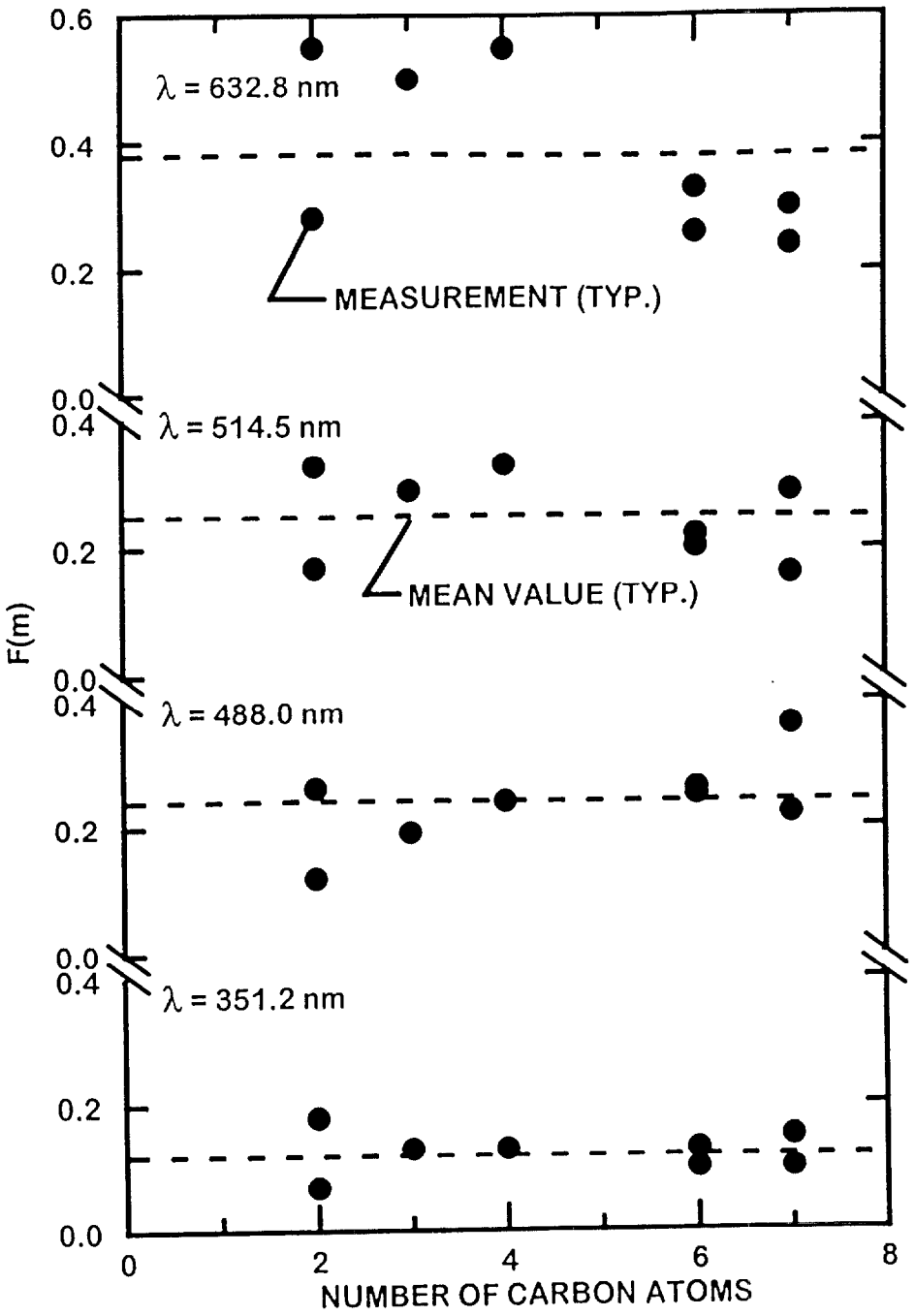

Figure 16 F(m) as a function of type and wavelength for soot emitted from buoyant turbulent diffusion flames

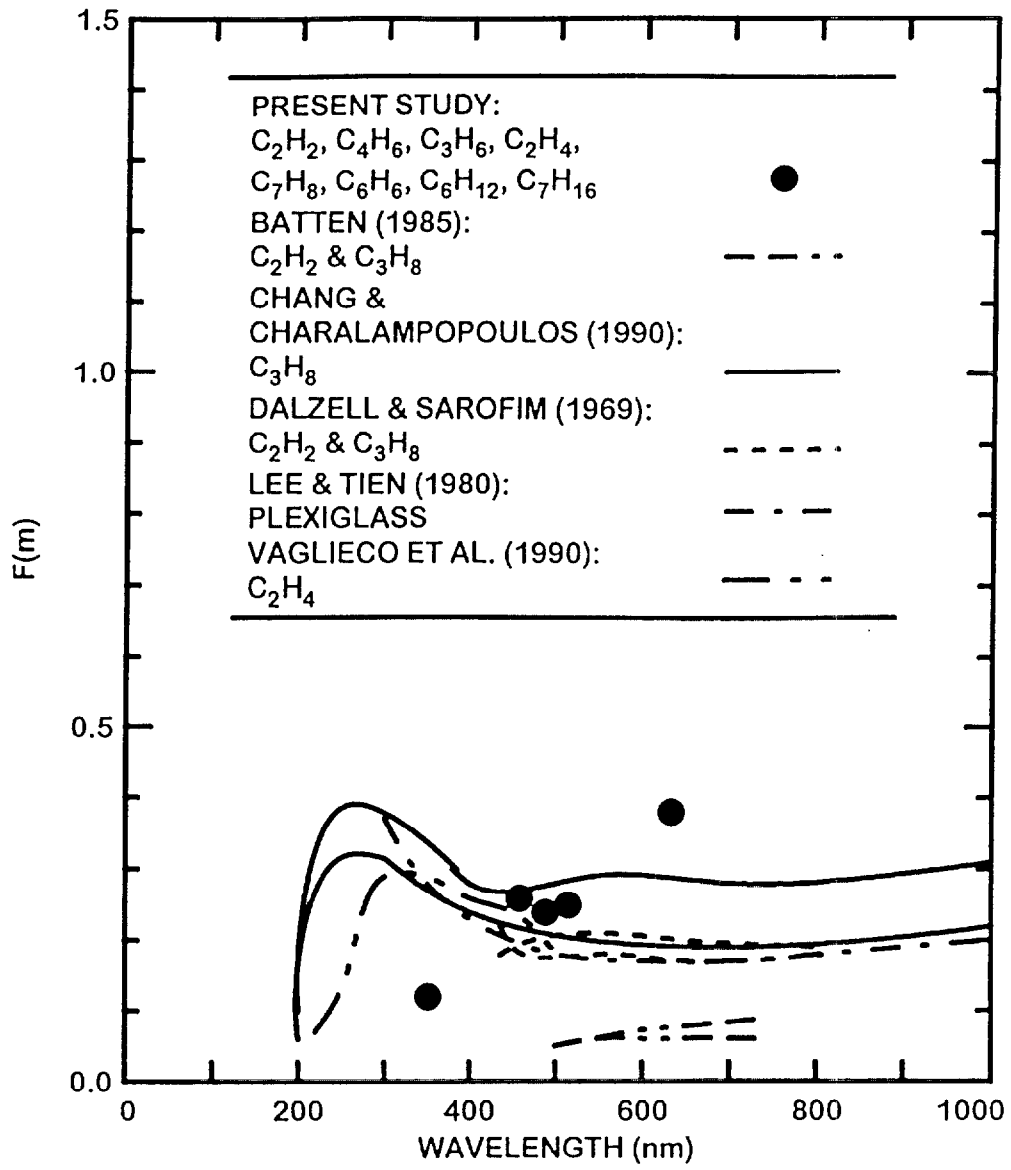

Figure 17 F(m) for soot as a function of wavelength.

present measurements, helps explain why k_{eR} is relatively independent of wavelength as discussed earlier.

4.5 Conclusions

Observations of soot optical properties were undertaken for wavelengths of 351.2-632.8 nm considering soot in the overfire region of buoyant turbulent diffusion flames in the long residence time regime where overfire soot becomes independent of position and residence time. A variety of gaseous and liquid hydrocarbon fuels (acetylene, ethylene, propylene, butadiene, benzene, cyclohexane, toluene and n-heptane) were burned in still air. Major conclusions of the study are as follows:

1. The approximate RDG-PFA scattering theory agreed with present measurements within experimental uncertainties; this represents a severe test of the approximate theory because present measurements reached primary particle size parameters large a 0.46, which are the largest values considered thus far.

2. Present fractal dimensions were independent of fuel type and wavelength and yielded an average value of 1.79 with a standard deviation of 0.01 which is in excellent agreement with the earlier measurements of Köylü and Faeth (1994a) for similar soot and other measurements for a variety of conditions (Faeth and Köylü 1995,1996). This suggests that the fractal dimensions of soot are relatively universal.

3. Present dimensionless extinction coefficients were independent of fuel type and wavelength and agreed with earlier measurements of Dobbins et al. (1994) and Choi et al. (1995). This resolves discrepancies between the earlier studies and the findings of Wu et al. (1997) although the reasons for these discrepancies have not been identified.

4. Present values of E(m) were relatively independent of fuel type and agreed with the extended results of Köylü and Faeth (1996) in the region where they overlapped, and the earlier results of Dalzell and Sarofim (1969), Lee and Tien (1980) and Chang and Charalampopoulos (1990) for wavelengths greater than 400 nm.

5. Present values of F(m) were relatively independent of fuel type and agreed with the studies of Dalzell and Sarofim (1969), Lee and Tien (1980) and Chang and Charalampopoulos (1990) for wavelengths of 400-550 nm. Otherwise, present values of F(m) increased more rapidly with increasing wavelength than observed before, although such behavior is consistent with k_{eR} being relatively independent of wavelength as observed during the present study.

References

Batten, C.E. (1985) Spectral Optical Constants of Soots from Polarized Angular Reflectance Measurements. Appl. Optics, Vol. 24, pp. 1193-1199.

Berry, M. V., and Percival, I. C. (1986) Optics of Fractal Clusters Such as Smoke. Optica Acta, Vol. 33, pp. 577-591.

Bohren, C.F., and Huffman, D.R. (1983) *Absorption and Scattering of Light by Small Particles*, Wiley, New York, pp. 69-81.

Chang, H.Y., and Charalampopoulos, T. T. (1990) Determination of the Wavelength Dependence of Refractive Indices of Flame Soot, Proc. R. Soc. London A, Vol. 430, pp. 577-591.

Charalampopoulis, T.T. (1992) Morphology and Dynamics of Agglomerated Particles in Combustion Systems Using Light Scattering Techniques, Prog. Energy Combust. Sci. Vol. 18, pp. 13-45.

Choi, M.Y., Hamins, A., Mulholland, G.W., and Kashiwagi, T. (1994) Simultaneous Optical Measurement of Soot Volume Fraction and Temperature. Combust. Flame, Vol. 99, pp. 174-186.

Choi, M.Y., Mulholland, G.W., Hamins, A., and Kashiwagi, T. (1995) Comparisons of the Soot Volume Fraction Using Gravimetric and Light Extinction Techniques, Combust. Flame, Vol. 102, pp. 161-169.

Dalzell, W.H., and Sarofim, A.F. (1969) Optical Constants of Soot and Their Application to Heat Flux Calculations, J. Heat Trans., Vol. 91, pp. 100-104.

Dalzell, W.H., Williams, G.C., and Hottel, H.C. (1970) A Light Scattering Method for Soot Concentration Measurements, Combust. Flame, Vol. 14, pp. 161-170.

Dobbins, R.A., and Megaridis, C.M. (1987) Morphology of Flame-Generated Soot as Determined by Thermophoretic Sampling, Langmuir, Vol. 3, pp. 254-259.

Dobbins, R.A., and Megaridis, C.M. (1991) Absorption and Scattering of Light by Polydisperse Aggregates, Appl. Optics, Vol. 30, pp. 4747-4754.

Dobbins, R.A., Mulholland, G.W., and Bryner, N.P. (1993) Comparison of a Fractal Smoke Optics Model with Light Extinction Measurements. Atmospheric Environment, Vol. 28, pp. 889-897.

Dyer, T.M. (1979) Rayleigh Scattering Measurements of Time-Resolved Concentration in a Turbulent Propane Jet, AIAA J., Vol. 17, pp. 912-914.

Erickson, W.D., Williams, G.C., and Hottel, H.C. (1964) Light Scattering Measurements of Soot in a Benzene-Air Flame, Combust. Flame, Vol. 8, pp. 127-132.

Faeth, G. M., and Köylü, Ü.Ö. (1995) Soot Morphology and Optical Properties in Nonpremixed Turbulent Flame Environments, Combust. Sci. Tech., Vol. 108, pp. 207-229.

Faeth, G.M., and Köylü, Ü.Ö., (1996) Structure and Optical Properties of Flame-Generated Soot. *Transport Phenomena on Combustion* (S.H. Chan, ed.), Taylor & Francis, Washington, DC, Vol. 1, pp. 19-44.

Farias, T.L., Carvalho, M.G., Köylü, Ü.Ö., and Faeth, G.M. (1995a) Computational Evaluation of Approximate Rayleigh-Debye-Gans/Fractal-Aggregate Theory for the Absorption and Scattering Properties of Soot, J. Heat Trans., Vol. 117, pp. 152-159.

Farias, T.L., Carvalho, M.G., Köylü, Ü.Ö., and Faeth, G.M. (1995b) Light Scattering from Soot Aggregates with Radially Inhomogeneous Primary Particles, Int. J. Heat and Technology, Vol. 13, pp. 27-47.

Farias, T.L., Carvalho, M.G., Köylü, Ü.Ö., and Faeth, G.M. (1996) Total Scattering and Absorption Cross Sections of Carbonaceous Soot Particles, *International Symposium on Radiative Heat Transfer* (M.P. Mengüc, ed.), Begell House, Inc., New York. pp. 296-308.

Felske, J.D., Charalampopoulos, T.T., and Hura, H. (1984) Determination of the Refractive Indices of Soot Particles from the Reflectivities of Compressed Soot Pellets, Combust. Sci. Tech., Vol. 37, pp. 263-284.

Habib, Z.G., and Vervisch, P. (1988) On the Refractive Index of Soot at Flame Temperature, Combust. Sci. Tech., Vol. 59, pp. 261-274.

Iskander, M.F., Chen, H.Y., and Penner, J.E. (1989) Optical Scattering and Absorption by Branched Chains of Aerosols, Appl. Optics,, Vol. 28, pp. 3083-3091.

Jullien, R., and Botet, R. (1987) *Aggregation and Fractal Aggregates*, World Scientific Publishing Co., Singapore, pp. 45-60.

Köylü, Ü.Ö., and Faeth, G.M. (1991) Carbon Monoxide and Soot Emissions from Liquid-Fueled Buoyant Turbulent Diffusion Flames, Combust. Flame, Vol. 87, pp. 61-76.

Köylü, Ü.Ö., and Faeth, G.M. (1992) Structure of Overfire Soot in Buoyant Turbulent Diffusion Flames at Long Residence Times, Combust. Flame, Vol. 89, pp. 140-156.

Köylü, Ü.Ö., and Faeth, G.M. (1993) Radiative Properties of Flame-Generated Soot. J. Heat Trans., Vol. 111, pp. 409-417.

Köylü, Ü.Ö., and Faeth, G.M. (1994a) Optical Properties of Overfire Soot in Buoyant Turbulent Diffusion Flames at Long Residence Times, J. Heat Trans., Vol. 116, pp. 152-159

Köylü, Ü.Ö., and Faeth, G.M. (1994b) Optical Properties of Soot in Buoyant Laminar Diffusion Flames. J. Heat Trans., Vol. 116, pp. 971-979.

Köylü, Ü.Ö., and Faeth, G.M. (1996) Spectral Extinction Coefficients of Soot Aggregates from Turbulent Diffusion Flames, J. Heat Trans., Vol. 118, pp. 415-421.

Köylü, Ü.Ö., Sivathanu, Y., and Faeth, G.M. (1991) Carbon Monoxide Emissions from Buoyant Turbulent Diffusion Flames. *Third International Symposium on Fire Safety Science*, Elsevier, London, 625-634.

Köylü, Ü.Ö., Faeth, G.M., Farias, T.L., and Carvalho, M.G. (1995) Fractal and Projected Structure Properties of Soot Aggregates, Combust. Flame, Vol. 100, pp. 621-633.

Krishnan, S.S., Lin, K.-C., Wu, J.-S., and Faeth, G.M. (1997) Optical Properties in the Visible of Soot Emitted from Turbulent Pool Fires, Proceedings of the 1997 ASME Winter Annual Meeting, New York, HTD Vol 352-2, pp. 39-84.

Krishnan, S.S., Lin, K.-C., and Faeth, G.M. (1999) Scattering and Extinction Properties of Overfire Soot in Large Buoyant Turbulent Diffusion Flames, Proceedings of the National Heat Transfer Conference, Albuquerque, NM, submitted.

Ku, J.C., and Felski, J.D. (1986) Determination of Refractive Indices of Mie Scatterers from Kramers-Kronig analysis of Spectral Extinction Data. J. Opt. Soc. Am., Vol. 3, pp. 617-623.

Ku, J.C., and Shim, K.-H.(1992) A Comparison of Solutions for Light Scattering and Absorption by Agglomerated or Arbitrarily-Shaped Particles, J. Quant. Spect. and Rad. Trans., Vol. 47, pp. 201-220.

Lee, S.C., and Tien, C.L. (1980) Optical Constants of Soot in Hydrocarbon Flames, *Eighteenth Symposium (International) on Combustion,* The Combustion Institute, Pittsburgh, PA, pp. 1159-1166.

Lee, S.C., and Tien, C.L. (1983) Effect of Soot Shape on Soot Radiation, J. Quant. Spectrosc. Radiat. Transfer, Vol. 29, pp. 259-265.

Lou, W., and Charalampopoulos, T.T. (1994) On the Electromagnetic Scattering and Absorption of Agglomerated Small Spherical Particles, J. Phys. D: Appl. Phys., Vol. 27, pp. 2258-2270.

Martin, J.E., and Hurd, A.J. (1987) Scattering from Fractals, J. Appl. Cryst., Vol. 20, pp. 61-78.

Medalia, A.I., and Heckman, F.A. (1969) Morphology of Aggregates — II. Size and Shape Factors of Carbon Black Aggregates from Electron Microscopy, Carbon, Vol. 7, pp. 567-582.

Megaridis, C.M., and Dobbins, R.A. (1989) Comparison of Soot Growth and Oxidation in Smoking and Nonsmoking Ethylene Diffusion Flames, Combust. Sci. Tech., Vol. 66, pp. 1-16.

Megaridis, C.M., and Dobbins, R.A. (1990) Morphological Description of Flame-Generated Materials, Combust. Sci. Tech., Vol. 71, pp. 95-109.

Mountain, R.D., and Mulholland, G.W. (1988) Light Scattering from Simulated Smoke Agglomerates, Langmuir, Vol. 4, pp. 1321-1326.

Mulholland, G.W., Samson, R.J., Mountain, R.D., and Ernst, M.H. (1988) Cluster Size Distribution for Free Molecular Aggregation, J. Energy Fuels, Vol. 2, pp. 481-486.

Nelson, J. (1989a) Test of a Mean Field Theory for the Optics of Fractal Clusters, J. Modern Optics, Vol. 36, pp. 1031-1057.

Nelson, J., (1989b) Fracticality of Sooty Smoke: Implications for the Severity of Nuclear Winter, Nature, Vol. 339, pp. 611-613.

Rosner, D.E., Mackowski, D.W., and Garcia-Ybarra, P. (1991) Size- and Structure-Insensitivity of the Thermophoretic Transport of Aggregated 'Soot' Particles in Gases, Combust. Sci. Tech., Vol. 80, pp. 87-101.

Rudder, R.R., and Bach, D. R. (1968) Rayleigh Scattering of Ruby-Laser Light by Neutral Gases, J. Opt. Soc. Amer., Vol. 58, pp. 1260-1266.

Samson, R. J., Mulholland, G. W., and Gentry, J. W. (1987) Structural Analysis of Soot Agglomerates, Langmuir, Vol. 3, pp. 272-281.

Sivathanu, Y.R., and Faeth, G.M. (1990) Soot Volume Fractions in the Overfire Region of Turbulent Diffusion Flames, Combust. Flame , Vol. 81, pp. 133-149.

Sorensen, C.M., Cai, J., and Lu, N. (1992) Test of Static Structure Factors for Describing Light Scattering from Fractal Soot Aggregates, Langmuir, Vol. 8, pp. 2064-2069.

Sorensen, C.M., Cai, J., and Lu, N. (1992) Light-Scattering Measurements of Monomer Size, Monomers per Aggregate, and Fractal Dimension for Soot Aggregates in Flames, Applied Optics, Vol. 31, pp. 6547-6557.

Stagg, B.J., and Charalampoulos, T.T. (1990) Method to Minimize the Effects of Polarizer Leakage on Reflectivity Measurements, Appl. Optics, Vol. 29, pp. 4638-4645.

Stagg, B.J., and Charalampoulos, T.T. (1991) Surface-Roughness Effects on the Determination of Optical Properties of Materials by the Reflection Method. Appl. Optics, Vol. 30, pp. 4113-4118.

Stagg, B.J., and Charalampoulos, T.T. (1993) Refractive Indices of Pyrolytic Graphite, Amorphous Carbon, and Flame Soot in the Temperature Range 25° to 600° C., Combust. Flame, Vol. 94, pp. 381-396.

Sunderland, P.B., Köylü, Ü.Ö., and Faeth, G.M., (1995) Soot Formation in Weakly Buoyant Acetylene-Fueled Laminar Jet Diffusion Flames Burning in Air, Combust. Flame, Vol. 100, pp. 310-322.

Tien, C. L., and Lee, S. C. (1982) Flame Radiation, Prog. Energy Combust. Sci., Vol. 8, pp. 41-59.

Vaglieco, B.M., Beretta, F., and D'Alessio, A. (1990) In Situ Evaluation of the Soot Refractive Index in the UV-Visible from the Measurements of Scattering and Extinction Coefficients in Rich Flames, Combust. Flame, Vol. 79, pp. 259-271.

Viskanta, R., and Mengüc, M.P. (1987) Radiation Heat Transfer in Combustion Systems, Prog. Energy Combust. Sci., Vol. 13, pp. 97-160.

Wu, J.-S., Krishnan, S.S., and Faeth, G.M. (1997) Refractive Indices at Visible Wavelengths of Soot Emitted from Buoyant Turbulent Diffusion Flames, J. Heat Trans., Vol. 119, pp. 230-237.

Appendix A: Köylü and Faeth (1994b)

Optical Properties of Soot in Buoyant Laminar Diffusion Flames

Ü. Ö. Köylü
Research Fellow.

G. M. Faeth
Professor.
Fellow ASME

Department of Aerospace Engineering,
The University of Michigan,
Ann Arbor, MI 48109-2118

The structure and optical properties of soot were studied in the fuel-rich (underfire) region of buoyant laminar diffusion flames of ethylene and acetylene burning in coflowing air. The objective was to evaluate scattering predictions based on the Rayleigh–Debye–Gans (RDG) approximation for polydisperse fractal aggregates of spherical primary soot particles having constant diameters, for conditions where the Guinier (small angle) regime, and the transition between the Guinier and the power-law (large-angle) regimes, were dominant, in order to supplement earlier work for conditions where the power-law regime was dominant. Soot structure was measured using thermophoretic sampling and analysis by transmission electron microscopy (TEM) to yield primary particle diameters, distributions of the number of primary particles per aggregate, and the aggregate mass fractal dimensions. Soot optical property measurements included vv, hh, hv, and vh differential scattering cross sections, total scattering cross sections, and the albedo at 514.5 nm, as well as several soot structure parameters inferred from these measurements using the approximate theory. The approximate RDG theory generally provided an acceptable basis to treat the optical properties of the present soot aggregates over a range of conditions spanning the Guinier and power-law regimes. Other scattering approximations were less satisfactory with performance progressively becoming less satisfactory in the order: RDG polydisperse fractal aggregate scattering using a single mean squared radius of gyration (from the Guinier regime), Mie scattering for an equivalent sphere, and Rayleigh scattering—the last underestimating differential scattering levels by a factor of roughly 100 for the present test conditions.

Introduction

Both predictions of continuum radiation from flames, and nonintrusive laser-based measurements of soot structure and concentrations, require an understanding of the optical properties of soot. Soot optical properties are a challenging problem, however, due to the complexities of soot structure. In particular, soot consists of small spherical primary particles that collect into open structured aggregates having a broad distribution of sizes; see Jullien and Botet (1987) and references cited therein. Thus, although the individual primary particles generally are small enough to satisfy the Rayleigh scattering approximation, even early work showed that soot aggregates usually exhibited neither simple Rayleigh nor Mie scattering behavior (Erickson et al., 1964; Dalzell et al., 1970; Wersborg et al., 1972; Magnussen, 1974). As a result, improved methods have been sought based on the Rayleigh–Debye–Gans (RDG) scattering approximation while treating the aggregates as polydisperse collections of mass fractal objects (denoted the RDG-PFA scattering approximation in the following); see Jullien and Botet (1987), Martin and Hurd (1987), Dobbins and Megaridis (1991), and Köylü and Faeth (1994). The objective of the present investigation was to conduct an evaluation of RDG-PFA theory by measuring both the structure and scattering properties of soot found in the fuel-rich (underfire) region of buoyant laminar jet diffusion flames.

Although RDG-PFA theories have been available for some time, and have been used to interpret soot scattering properties and to infer soot aggregate structure properties from scattering measurements (Dobbins et al., 1990; Puri et al., 1993; Sorensen et al., 1992), evaluation of the method has only just begun. Köylü and Faeth (1993) discuss recent attempts to evaluate various approximations of soot scattering properties using more exact solutions for simulated aggregates. Unfortunately, computational limitations have prevented definitive results for the relatively large soot aggregates often encountered in practice. An alternative approach involves direct experimental evaluation by measuring the soot structure properties needed for RDG-PFA scattering predictions and comparing these predictions with measured scattering properties for the same soot population. Köylü and Faeth (1994) recently carried out a study along these lines for the large soot aggregates found in the overfire region of buoyant turbulent diffusion flames at long characteristic flame residence times. It was found that the RDG-PFA predictions were in reasonably good agreement with measurements of scattering and extinction properties over the wavelength range 514.5–1152 nm. However, these overfire soot aggregates were too large for practical scattering measurements in the small-angle (Guinier) regime where use of the RDG scattering approximation is least reliable (Nelson, 1989; Köylü and Faeth, 1993), in order to complete a thorough evaluation of the approximate theory. Thus, the specific objective of the present investigation was to extend the work of Köylü and Faeth (1994) in order to consider soot aggregates in the fuel-rich (underfire) region of buoyant laminar diffusion flames, where smaller aggregate sizes provide greater access to the Guinier regime as well as the transition regime between the Guinier and the power-law (large-angle) regimes.

Present measurements were carried out in ethylene and acetylene/air flames, which are representative of lightly and heavily sooting materials (Köylü and Faeth, 1992). Soot structure was measured using thermophoretic sampling and analysis by transmission electron microscopy (TEM), to find primary particle diameters, distributions of the number of primary particles per aggregate, and aggregate mass fractal dimensions. Soot optical property measurements included differential scattering cross sections for various polarizations of incident and scattered light (vv,

Contributed by the Heat Transfer Division and presented at the ASME Winter Annual Meeting, New Orleans, Louisiana, November 28–December 3, 1993. Manuscript received by the Heat Transfer Division May 1993; revision received December 1993. Keywords: Combustion, Fire/Flames, Radiation. Associate Technical Editor: W. L. Grosshandler.

hh, vh, and hv), total scattering cross sections, and the albedo at 514.5 nm. Predictions of scattering properties were based on the measured structure properties, considering several scattering approximations, as follows: Rayleigh scattering, Mie scattering for an equivalent sphere, RDG-PFA scattering following Dobbins and Megaridis (1991), and RDG-PFA scattering following Köylü and Faeth (1994).

The paper begins with descriptions of experimental and theoretical methods. Results are then considered, treating soot structure properties and evaluation of soot scattering approximations in turn.

Experimental Methods

Apparatus. The test apparatus consisted of a round coflowing laminar jet diffusion flame burner, directed vertically upward, having nearly the same port dimensions as the arrangement used by Santoro et al. (1983) and Dobbins and Megaridis (1987). The burner involved fuel flowing from a center tube, having an inside diameter of 14.3 mm and a wall thickness of 0.9 mm, with air flowing from a concentric outer tube, having an inside diameter of 102 mm. Both flows passed through a 50 mm deep bed of 2-mm-dia stainless steel balls, a 10 mm gap, and a 25 mm long honeycomb (1 mm hexagonal cells). The downstream end of the honeycomb was flush with the exit of the fuel and air tubes. The burner could be traversed in three directions (5 μm positioning accuracy in the two horizontal directions and 0.5 mm positioning accuracy in the vertical direction) in order to accommodate rigidly mounted instrumentation.

Fuel gases were stored in commercial cylinders under pressure. Air was obtained by filtering the laboratory air supply. Both gas flows were controlled by metering valves and measured using rotameters. The rotameters were calibrated using a wet test meter.

The flames were shielded because they were easily disturbed by drafts. The primary shield was a screen (0.3 mm wire diameter, 200 wires/m, square mesh) wrapped around the outside of the air tube and extending 300 mm from the burner exit. Slits in the screen provided access for sampling and scattering measurements. Additional flow shielding, as well as reduced background light levels, was provided by a black cloth enclosure having a diameter of 1 m that surrounded the entire apparatus.

Soot Structure Measurements. The structure of soot was measured by thermophoretic sampling and analysis using TEM,

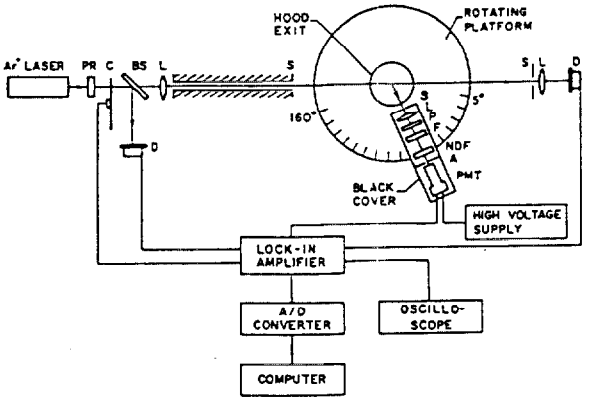

Fig. 1 Sketch of the light scattering apparatus: A = detector aperture, BS = beam splitter, C = chopper, D = laser power detector, F = laser-line filter, L = lens, NDF = neutral-density filter, P = polarizer, PMT = photomultiplier detector, PR = polarization rotator, and S = variable aperture

similar to Dobbins and Megaridis (1987) and Köylü and Faeth (1992). The sampling surfaces were the carbon-supported copper grids used to hold TEM specimens (3 mm diameter, 200 mesh copper grids supported by a 20 nm thick elemental carbon film, SPI Supplies, Philadelphia, part No. 3520C). The grids were aligned in the vertical direction, parallel to the mean flow direction at the axis. The grids were mounted on a 1 × 4 × 15 mm metal strip using double-backed adhesive which was mounted in turn on a retractable probe. The probe was stored in a cylinder located outside the screen shield, with roughly a 50 mm stroke to reach the flame axis. A double-acting pneumatic cylinder rapidly drove the probe out of the storage cylinder to the sampling position and returned it again to the cylinder when sampling was complete. Sampling times were measured using a pair of light-interrupting sensors. Sampling times were controlled so that soot aggregates covered no more than 10 percent of the surface of the TEM grid in order to avoid overlapping aggregates on the grid. This required 18–30 ms sampling times with 2–3 ms traveling times of the grid through the flame to the axis where measurements were made. Thus, residence times of the grid in

Nomenclature

A = albedo
C = optical cross section
d = diameter of fuel port
d_p = primary particle diameter
D_f = mass fractal dimension
D_{30} = aggregate volume mean diameter, Eq. (14)
$E(m)$ = refractive index function $= \mathrm{Im}((m^2-1)/(m^2+2))$
$f(qR_g)$ = aggregate form factor, Eq. (2)
$F(m)$ = refractive index function $= |(m^2-1)/(m^2+2)|^2$
$g(\lambda, R_g, D_f)$ = aggregate total scattering factor, Eq. (5)
i = $(-1)^{1/2}$
k_f = fractal prefactor, Eq. (1)
m = refractive index of soot $= n + i\kappa$
n = real part of refractive index of soot
n_a = mean number of aggregates per unit volume
n_p = mean number of primary particles per unit volume
N = number of primary particles per aggregate
N_c = aggregate size for onset of power-law regime, Eq. (7)
$p(N)$ = probability density function of aggregate size
q = modulus of scattering vector $= (4\pi/\lambda)\sin(\theta/2)$
Q = volumetric optical cross section
R_g = radius of gyration of an aggregate
$\bar{R}^2_{gG}$ = mean square radius of gyration for the Guinier regime, Eq. (10)
$\bar{R}^2_{gL}$ = mean square radius of gyration for the power-law regime, Eq. (11)
x_p = primary particle optical size parameter $= \pi d_p/\lambda$
θ = angle of scattering from forward direction
κ = imaginary part of refractive index of soot
λ = wavelength of radiation
ρ_v = depolarization ratio
σ_N = standard deviation of N
σ_p = standard deviation of d_p

Subscripts

a = absorption
h = horizontal polarization
ij = incident (i) and scattered (j) polarization direction
s = total scattering
v = vertical polarization

Superscripts

a = aggregate property
p = primary particle property
$\bar{(\ )}$ = mean value over a polydisperse aggregate population

the soot layer were only 3–5 percent of residence times at desired conditions along the flame axis so that contamination of the samples from the soot layer was small.

The principles of thermophoretic sampling are discussed elsewhere (Dobbins and Megaridis, 1987; Köylü and Faeth, 1992; Rosner et al., 1991). For present conditions, primary particle diameters are smaller than the mean free path so that the thermophoretic velocities of individual particles are the same. In addition, Rosner et al. (1991) have shown that the thermophoretic velocities of aggregates are the same as individual primary particles, even when the aggregates are larger than mean free path lengths. Thus, there is no intrinsic bias with respect to aggregate size for the thermophoretic sampling technique.

The samples were observed using a JEOL 2000 FX analytical electron microscope system with a 1 nm edge-to-edge resolution. Latex spheres having a diameter of 91 nm (with a standard deviation of 5.8 nm) were used to calibrate the TEM measurements. The details of the TEM measurements, and the software used to analyze the images, are discussed by Köylü and Faeth (1992). Experimental uncertainties of soot structure parameters are considered when these measurements are discussed. All measurements were repeatable within the stated uncertainties.

Soot Scattering Measurements. The arrangement for soot scattering measurements was similar to Köylü and Faeth (1994), except for changes in optics to improve the spatial resolution so that underfire conditions could be treated. A sketch of the arrangement appears in Fig. 1. An argon-ion laser having an optical power of 1700 mW at 514.5 nm was used for the scattering measurements. The incident laser beam was passed through a polarization rotator and a mechanical chopper (operating at 1250 Hz) before being focused at the axis of the flame using a 350 mm focal length lens. This yielded a waist diameter of 150 μm and a confocal length of roughly 140 mm. The collecting optics were mounted on a turntable surrounding the burner so that scattering angles, θ = 20–160 deg, could be considered. The collecting optics consisted of an 85 mm focal length lens, a dichroic sheet polarizer, a laser line filter (1 nm bandwidth) and a cooled photomultiplier. The lens aperture defined a solid collection angle of 0.7 msr with a 0.4 mm long sampling volume at θ = 90 deg, which increased to roughly 1.2 mm at θ = 20 and 160 deg. Neutral-density filters were used in the optical path to control the dynamic range of detection. The detector output passed through a lock-in amplifier and was stored on a computer, sampling at 500 Hz for 10 s and averaging five sampling intervals to achieve a repeatability within 10 percent.

The angular light scattering system was calibrated by measuring Rayleigh scattering from nitrogen gas. After correction for the reciprocal sin θ dependence of the scattering volume, the vv and hh differential cross sections were within 5 percent of Rayleigh scattering predictions for θ of 20–160 deg. Absolute volumetric differential scattering cross sections of soot were found from ratios of the detector signal for soot and nitrogen, after accounting for signal attenuation in the optical path, based on the nitrogen optical properties of Rudder and Bach (1968). Total volumetric scattering cross sections were found by integrating the volumetric differential scattering cross sections over the whole spherical surface. This required extrapolation of the measurements to reach θ = 0 and 180 deg; however, uncertainties caused by the extrapolations were small due to the relatively slow variation of scattering properties near the forward and backward directions and the relatively small solid angles involved.

The laser power was monitored continuously and did not fluctuate. The dark current of the photomultiplier also did not vary with time and was small, e.g., roughly 1 percent of the vh and hv scattering signals. Effects of fluorescence from the reactive soot-containing mixture at fuel-rich conditions in the test flame are more difficult to evaluate but are not thought to be large. In particular, fluorescence contributions are the same for all scattering signals; therefore, they can be no larger than the vh and hv scattering signals, which are only on the order of 10^{-2} of the main scattering signals of interest, e.g., $\bar{C}^a_{vv}(\theta)$. Additionally, values of $\bar{\rho}^a_v$ for the present underfire soot were comparable to values measured by Köylü and Faeth (1994) for overfire soot, where fuel-lean conditions and substantial dilution imply negligible effects of fluorescence. Thus, it is suspected that effects of fluorescence were small even for vh and hv scattering measurements, although quantitative evaluation of effects of fluorescence on optical measurements of soot properties at fuel-rich conditions clearly merits further attention. Based on these considerations, the overall experimental uncertainties (95 percent confidence) of the angular (excluding depolarization ratios and $\bar{C}^a_{hh}(\theta)$ near 90 deg) and the total light scattering measurements were comparable and were estimated to be less than 20 percent, dominated by finite sampling times, the finite aperture of the detector, and the angular uncertainty of the collecting optics.

Test Conditions. Measurements were limited to soot found along the axis of the fuel-rich region of the ethylene and acetylene/air flames summarized in Table 1. The ethylene/air flame was nonsooting while the acetylene/air flame was soot emitting. Two heights above the burner exit were considered for each of the flames: 50 and 70 mm for the ethylene/air flame and 30 and 45 mm for the acetylene/air flame. These conditions provide access to both the Guinier and power-law regimes while involving a reasonable range of soot aggregate structure properties.

Theoretical Methods

Present RDG-PFA Scattering Theory. Predictions of soot optical properties were based on methods described by Jullien and Botet (1987), Martin and Hurd (1987), and Dobbins and Megaridis (1991) for a single aggregate. However, attention was focused on the treatment of Köylü and Faeth (1994) for polydisperse aggregate populations. This involves use of the RDG scattering approximation so that effects of multiple- and self-scattering are ignored, the electric field of each particle is assumed to be the same as the incident field, and differences of the phase shift of scattered light from various points within a particular primary particle are neglected. The RDG scattering approximation requires that both $|m - 1| \ll 1$ and $2x_p|m - 1| \ll 1$ (Kerker, 1969; van de Hulst, 1957; Bohren and Huffman, 1983), which is questionable due to the relatively large refractive indices of soot (Köylü and Faeth, 1993). Recent computational studies also suggest significant effects of multiple scattering for soot aggregates, see Köylü and Faeth (1993) and references cited therein. Thus, use of RDG theory only can be justified by its capabilities to treat measured soot properties, which is considered during the present investigation.

The major assumptions with respect to aggregate structure are as follows (Köylü and Faeth, 1994): spherical primary particles having constant diameters, primary particles do not overlap but just touch one another, uniform refractive indices, and the aggregates are mass fractal-like objects. The mass fractal approximation implies the following relationship between the number of particles in an aggregate and its radius of gyration (Jullien and Botet, 1987):

Table 1 Summary of test flames*

Fuel	Ethylene/Air	Acetylene/Air
Fuel mass flow rate (mg/s)	5.0	4.0
Air mass flow rate (mg/s)	400	400
Condition	nonsooting	sooting
Flame height (mm)	83	55

*Coflowing buoyant laminar jet burner with fuel and air port diameters of 14.3 and 102 mm at atmospheric pressure, 99 ± 0.5 kPa.

$$N = k_f(R_f/d_p)^{D_f} \quad (1)$$

Based on past measurements for both overfire and underfire soot, $k_f = 8.1$ was used during present work (Köylü and Faeth, 1994; Puri et al., 1993). The assumptions of nearly constant diameter primary particles and mass fractal-like behavior are justified by the present soot structure measurements, as discussed later, while the remaining assumptions are typical of past work; see Köylü and Faeth (1993) and references cited therein. One change from the approach of Köylü and Faeth (1994), however, was that the measured aggregate size distribution was used directly in the computations, to avoid potential errors due to empirical fits of the distribution.

Only the main results of the RDG-PFA scattering theory will be summarized in the following; see Köylü and Faeth (1994) for the complete formulation. The treatment begins with the scattering cross sections for a single fractal aggregate under the RDG approximation:

$$C_w^a(\theta) = C_{hh}^a(\theta)/\cos^2\theta = N^2 C_w^p f(qR_g) \quad (2)$$

where C_w^p is the scattering cross section of a primary particle under the Rayleigh scattering approximation. The form factor, $f(qR_g)$, in Eq. (2) is expressed as follows (Freltoft et al., 1986; Jullien and Botet, 1987; Lin et al., 1989; Martin and Hurd, 1987):

$$f(qR_g) = \exp(-(qR_g)^2/3), \quad \text{Guinier regime} \quad (3)$$

$$f(qR_g) = (q^2R_g^2)^{-D_f/2}, \quad \text{power-law regime} \quad (4)$$

where the boundary between the small q (Guinier) regime and the power-law regime is $(qR_g)^2 = 3D_f/2$, chosen to match the value and derivative of $f(qR_g)$ where the regimes meet, following Dobbins and Megaridis (1991). The total scattering cross section then becomes:

$$C_s^a = N^2 C_s^p g(\lambda, R_g, D_f) \quad (5)$$

where $g(\lambda, R_g, D_f)$ takes on different forms according to whether the power-law regime is reached for $\theta \leq 180$ deg; see Köylü and Faeth (1994) for these expressions.

The mean optical cross sections of populations of randomly oriented polydisperse aggregates (polydisperse aggregates) are found by integrating over all aggregate sizes, as follows:

$$\bar{C}_j^a = \int_{N=1}^{\infty} C_j^a(n)p(N)dN; \quad j = pp, s, a \quad (6)$$

where $p(N)$ is the measured size distribution of the aggregate population. In general, Eq. (6) must be integrated numerically when scattering extends over both the Guinier and power-law regimes. However, simple closed-form expressions are possible when all the aggregates are either in the Guinier ($p(N) \ll 1$ for $N \geq N_c$) or power-law ($p(N) \ll 1$ for $N \leq N_c$) regimes, where

$$N_c = k_f(3D_f/(2q^2d_p^2))^{D_f/2} \quad (7)$$

This yields (Köylü and Faeth, 1993b):

$$\bar{C}_w^a(\theta) = \bar{N}^2 C_w^p \exp(-q^2\bar{R}_{gG}^2/3), \quad \text{Guinier regime} \quad (8)$$

$$\bar{C}_w^a(\theta) = \bar{N}^2 C_w^p (q^2\bar{R}_{gL}^2)^{-D_f/2}, \quad \text{power-law regime} \quad (9)$$

The mean-squared radius of gyration in the limiting expressions of Eqs. (8) and (9) is found as a N^2-weighted average in the Guinier regime, and as fractal dimension-weighted average in the power-law regime, as follows:

$$\bar{R}_{gG}^2 = \int_{N=1}^{\infty} R_g(N)^2 N^2 p(N)dN \Big/ \int_{N=1}^{\infty} N^2 p(N)dN, \quad \text{Guinier regime} \quad (10)$$

$$\bar{R}_{gL}^2 = \left[\int_{N=1}^{\infty} R_g(N)^{2D_f} p(N)dN \Big/ \int_{N=1}^{\infty} R_g(N)^{D_f} p(N)dN\right]^{2/D_f}, \quad \text{power-law regime} \quad (11)$$

The general expression for the total scattering cross section of the polydisperse aggregate population is

$$\bar{C}_s^a = C_s^p \int_{N=1}^{\infty} N^2 g(\lambda, R_g, D_f)p(N)dN \quad (12)$$

which must be numerically integrated in both scattering regimes. The absorption cross section of the polydisperse aggregate population is evaluated quite simply for RDG-PFA scattering, as follows:

$$\bar{C}_a^a = \bar{N}C_a^p \quad (13)$$

Notably, Köylü and Faeth (1994) determined absorption cross sections for overfire soot aggregates by direct measurements of scattering and extinction cross sections, finding good agreement with Eq. (13). Finally, the albedo is defined in the usual manner, $\bar{A}^a = \bar{C}_s^a/(\bar{C}_s^a + \bar{C}_a^a)$.

Other Scattering Theories. Other approximate scattering theories that were evaluated using the present measurements included Rayleigh scattering, Mie scattering for an equivalent sphere, and the RDG-PFA approach of Dobbins and Megaridis (1991). The Rayleigh and Mie scattering theories are well known; see Bohren and Huffman (1983) for the complete formulations. The equivalent diameter for the Mie scattering computations was taken to be the volume mean diameter of the aggregate population, in the usual manner (Köylü and Faeth, 1993):

$$D_{30} = \bar{N}^{1/3}d_p \quad (14)$$

The RDG-PFA approach of Dobbins and Megaridis (1991) is identical to the present formulation when all the aggregates are in the Guinier regime. Scattering in the power-law regime is found, however, by using the limiting expression of Eq. (9) with $\bar{R}_{gL}^2$ replaced by $\bar{R}_{gG}^2$. The two regimes are connected by requiring continuity of $\bar{C}_w^a(\theta)$ through the first derivative with respect to $q^2\bar{R}_{gG}^2$, analogous to Eqs. (3) and (4) for an individual aggregate. Thus, the weighting of the scattering properties by the aggregate size distribution function is somewhat distorted in the transition and power-law regimes. This tends to underestimate both the extent of the transition regime in terms of $q^2\bar{R}_{gG}^2$, as well as scattering cross sections in the transition and power-law regimes; see Freltoft et al. (1986), Köylü and Faeth (1994), and Sorensen et al. (1992).

Results and Discussion

Soot Structure Measurements. The general appearance of the soot aggregates in the ethylene and acetylene/air flames is illustrated in the TEM photographs appearing in Figs. 2 and 3. The soot aggregates had smaller primary particle diameters, and larger numbers of primary particles per aggregate, in the ethylene/air flame than the acetylene/air flame. However, the variation of aggregate properties within each flame was modest over the range of streamwise conditions that were considered. The present results are qualitatively similar to other TEM observations of soot at fuel-rich conditions in laminar diffusion flames (Dobbins and Megaridis, 1987). In particular, the soot consists of open (rather than compact) structures of aggregated primary particles that have nearly constant diameters. The aggregates exhibit a broad range of sizes, with the largest aggregates having maximum dimensions on the order of 1 μm. This yields aggregate optical size parameters, based on the maximum aggregate dimension, greater than 5, which implies significant potential for departure from Rayleigh scattering behavior. Such behavior was

Fig. 2 Typical TEM photograph of soot in the ethylene/air flame: x/d = 3.50

Fig. 3 Typical TEM photograph of soot in the acetylene/air flame: x/d = 3.15

confirmed by aggregate scattering measurements to be discussed later.

The TEM measurements of soot structure properties are summarized in Table 2 for the four test conditions that were considered. Primary particle diameters were obtained by measuring roughly 200–300 primary particles within a sample of 20 aggregates, to yield uncertainties (95 percent confidence) of $\bar{d}_p$ less than 2 percent. The standard deviations of the diameters about $\bar{d}_p$ are relatively small, less than 18 percent, which supports the constant primary particle diameter assumption of the RDG-PFA scattering theory.

Aggregate properties in Table 2 were found using a sample of 200 aggregates at each condition. This yielded uncertainties of $\bar{N}$ (95 percent confidence) less than 20 percent. The standard deviations of $\bar{N}$ are comparable to $\bar{N}$ itself, which is characteristic of the broad size distributions of typical soot aggregate populations (Dobbins and Megaridis, 1987; Köylü and Faeth, 1992). The log-normal size distribution function provided a reasonable fit of the present measurements, similar to overfire soot aggregates (Köylü and Faeth, 1992), although the measurements were used directly to predict scattering properties, as noted earlier. The moment, $\bar{N}^2$, plays a crucial role in the scattering properties of soot aggregates (this is particularly evident from Eqs. (8) and (9) for limiting conditions). Unfortunately, it is not practical to obtain a very accurate determination of this moment by sampling due to the broad size distribution of soot aggregates. Thus, uncertainties of $\bar{N}^2$ (95 percent confidence) were only less than 40 percent. Aggregate fractal dimensions were found as described by Köylü and Faeth (1992) to yield uncertainties (95 percent confidence) less than 0.06. The present values of D_f were in the range 1.73–1.77, which is comparable to earlier sampling measurements at both under- and overfire conditions for a wide variety of fuels; see Megaridis and Dobbins (1990), Köylü and Faeth (1992), and references cited therein. This suggests that D_f might have a universal value for soot aggregates in diffusion flames, which would vastly simplify measurements needed to define aggregate scattering properties. Values of D_{30} were computed from Eq. (14), yielding values of roughly 90 and 180 nm for ethylene and acetylene soot, respectively. Thus, the aggregate optical size parameters based on this dimension are in the range 0.5–1.2, so that Rayleigh scattering from aggregates is questionable, as noted earlier.

Evaluation of Scattering Theories. Soot optical properties were computed using the refractive indices of Dalzell and Sarofim (1969), i.e., $m = 1.57 + 0.56i$ at a wavelength of 514.5 nm, in order to be consistent with earlier work (Köylü and Faeth, 1992, 1993, 1994). However, this choice also is justified by the soot scattering observations of Köylü and Faeth (1994), where it was found that the refractive indices of Dalzell and Sarofim (1969) yielded values of $F(m)/E(m)$ that were in better agreement with measurements than other values in the literature.

In order to evaluate the scattering theories, measured volumetric optical cross sections must be related to predicted optical cross sections from a knowledge of the number of aggregates per unit volume, as follows:

$$\bar{Q}_j^a = n_a \bar{C}_j^a; \quad j = pp, s, a \tag{15}$$

Table 2 Summary of soot structure properties from TEM measurements[a]

x/d (-)	$\bar{d}_p(\sigma_p)$ (nm)	$\bar{N}(\sigma_N)$ (-)	$\bar{N}^2/\bar{N}$ (-)	D_f (-)	D_{30} (nm)
Ethylene/air flames:					
3.50	24(3.9)	50(46)	91	1.73	88
4.90	21(3.7)	83(76)	154	1.73	92
Acetylene/air flames:					
2.10	53(6.4)	31(35)	70	1.77	166
3.15	54(6.4)	43(48)	97	1.74	189

[a]For the fuel-rich region of buoyant laminar diffusion flames at normal temperature and pressure.

Table 3 Summary of soot scattering properties[a]

Flame	Ethylene/Air		Acetylene/Air	
x/d	3.50	4.90	2.10	3.15
Primary particles:				
x_p (-)	0.147	0.128	0.324	0.330
$\bar{C}^p_{vv}$ (nm²/sr)	0.0144	0.0065	1.67	1.87
$\bar{C}^p_s$ (nm²)	0.121	0.054	14.0	15.7
A^p (-)	0.0012	0.0018	0.0196	0.0185
n_p (cm⁻³) × 10⁻¹⁰	32	40	9.7	9.3
Aggregates:				
$\bar{C}^a_{vv}(90°)$ (nm²/sr)	24.1	25.2	478	719
$\bar{C}^a_s$ (nm²) × 10⁻³	0.23	0.26	5.7	9.6
$\bar{A}^a$ (-)	0.062	0.063	0.20	0.22
$\bar{p}^a_v(90°)$	0.012	0.011	0.026	0.025
n_a (cm⁻³) × 10⁻⁹	6.30	4.80	3.13	2.17

[a]For the fuel-rich region of buoyant laminar diffusion flames at normal temperature and pressure at 514.5 nm. Soot refractive indices from Dalzell and Sarofim (1969).

while $n_p = \bar{N} n_a$. During the earlier study of overfire soot aggregates (Köylü and Faeth, 1994), the value of n_a was found from direct laser absorption measurements of $\bar{Q}^a_a$, with $\bar{C}^a_a$ computed from Eq. (13) given $\bar{N}$ from the structure measurements. An alternative procedure was used during the present investigation, however, in order to avoid the relatively large uncertainties of volumetric absorption coefficient measurements in the present flame environments. In particular, variable soot concentrations imply that laser extinction measurements for chord-like paths through the flames must be deconvoluted, which yields large experimental uncertainties near the axis where present measurements were made (Santoro et al., 1983). Thus, scattering measurements were used instead, based on predicted values of $\bar{C}^a_{vv}(\theta)$ from Eq. (9) in the power-law regime. This was reasonable because scattering at present test conditions exhibited power-law regimes that could be correlated according to Eq. (9). Additionally, the present RDG-PFA scattering theory yielded good predictions in the power-law regime for the large soot aggregates found in the overfire region of buoyant turbulent diffusion flames (Köylü and Faeth, 1994). Finally, use of the RDG scattering approximation is better justified in the power-law regime than the Guinier regime, based on both theoretical and computational considerations (Nelson, 1989).

Reference soot optical properties for the four test conditions, along with n_a and n_p, are summarized in Table 3. Values of x_p are in the range 0.128–0.330, which marginally places the individual primary particles in the Rayleigh scattering regime (Kerker, 1969). The values of $\bar{A}^a$ are 10–100 times larger than A^p, highlighting the much larger scattering from aggregates than from individual primary particles. The albedo is a measure of the error incurred when soot volume fractions are computed from laser extinction measurements using the Rayleigh scattering approximation. Thus, such errors would be in the range 7–28 percent for present conditions, with the higher values being comparable to the properties of soot aggregates in the overfire region (Köylü and Faeth, 1994). However, corrections of this magnitude still are rather small in comparison to effects of current uncertainties concerning soot refractive indices. Present values of n_p in the range 10^{11}–10^{12} primary particles per cubic centimeter are comparable to earlier measurements of Dobbins et al. (1990) and Megaridis and Dobbins (1990) for similar flame conditions, helping to justify the present determinations of n_p and n_a from scattering measurements.

Measured values of $\bar{Q}^a_{vv}(\theta)$ are plotted as a function of qd_p in Fig. 4 for all four test conditions, along with predictions based on the present RDG-PFA scattering theory. The substantial departure from Rayleigh scattering behavior, where $\bar{Q}^a_{vv}(\theta)$ would be independent of qd_p, is quite evident, with forward scattering being roughly an order of magnitude larger than back scattering. A power-law regime, which should yield a straight line correlation with a slope of $-D_f$ in Fig. 4 (see Eq. (9)) is observed at all test conditions. However, only the ethylene soot aggregates, which are smaller than the acetylene soot aggregates, exhibit a reasonable approach to the Guinier regime where both $\bar{Q}^a_{vv}(\theta)$ and $\bar{C}^a_{vv}(\theta)$ are relatively independent of qd_p from Eq. (8), and $\bar{Q}^a_{vv}(\theta)/Q^p_{vv}$ approaches $\bar{N}^2/\bar{N}$ from Eqs. (8) and (15). Thus, many of the data in Fig. 4 are in the extended transition regime that involves complex polydisperse aggregate effects.

Two predictions based on the present RDG-PFA scattering theory are illustrated in Fig. 4, one based entirely on the present TEM soot structure measurements, and the other based on refitted soot aggregate structure properties to match the scattering measurements. The discrepancies between predictions based on the structure measurements and the scattering measurements are smaller than those observed for large soot aggregates (Köylü and Faeth, 1994), and generally are within experimental uncertainties. In particular, the discrepancies for ethylene soot aggregates are negligible while those for the larger acetylene soot aggregates are less than 37 percent. Nevertheless, it should be recalled that the present predictions are matched in the power-law regime through the method used to find n_a; therefore, an alternative approach to find n_a would increase the discrepancies between predictions and measurements.

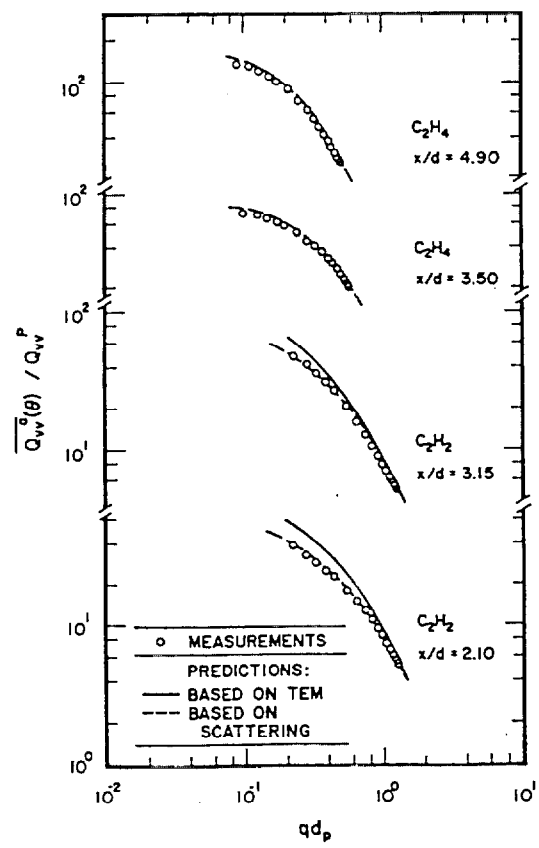

Fig. 4 Measured and predicted volumetric vv soot scattering cross sections in the ethylene and acetylene/air flames as a function of the modulus of the scattering vector

Table 4 Soot structure and optical properties from thermophoretic sampling (TS) and light scattering (LS) measurements[a]

x/d	$(\bar{R}^2_{gL})^{1/2}$ (nm)		$\bar{R}(^2_{gO})^{1/2}$ (nm)		D_f		$\bar{A}^a$	
	TS	LS	TS	LS	TS	LS	TS	LS
Ethylene/air flames:								
3.50	97	90	121	117	1.73	1.72	0.061	0.062
4.90	115	111	144	140	1.73	1.74	0.060	0.063
Acetylene/air flames:								
2.10	179	137	241	185	1.77	1.77	0.21	0.20
3.15	224	163	297	200	1.74	1.76	0.23	0.22

[a]For the fuel-rich region of buoyant laminar diffusion flames at normal temperature and pressure for a wavelength of 514.5 nm. Soot refractive indices from Dalzell and Sarofim (1969).

Based on past experience, it was felt that the sampling limitations of the soot structure measurements, particularly the higher moments of the aggregate size distribution, were primarily responsible for the discrepancies between the scattering predictions and measurements seen in Fig. 4 (Köylü and Faeth, 1994). Thus, the higher moments and the aggregate fractal dimensions were refitted to yield the predictions based on scattering measurements illustrated in Fig. 4. This involved keeping d_p and the lower moment $\bar{N}$ the same as before, while adjusting the higher moments. These adjustments will be represented by $\bar{R}^2_{gO}$ and $\bar{R}^2_{gL}$ in the following. The results illustrated in Fig. 4 indicate that the present RDG-PFA scattering theory provides a reasonable basis to fit the higher moments of soot structure properties based on measured scattering properties in this manner. The resulting values of the adjusted parameters from the light scattering measurements, along with the values found directly from the TEM sampling measurements, are summarized in Table 4. Differences between the TEM sampling and light scattering determinations of the moments for ethylene soot, and the fractal dimensions of both ethylene and acetylene soot, are small in comparison to experimental uncertainties. The differences between the two determinations of higher moments are larger for acetylene soot but still are comparable to anticipated experimental uncertainties. Values of the soot albedo predicted assuming RDG behavior for absorption through Eq. (13) and using the two sets of structure properties, also are listed in Table 4. The results are nearly the same, which is helpful because estimates of the soot albedo are required to evaluate potential errors of laser extinction measurements of soot concentrations. Nevertheless, a more definitive assessment of albedo predictions would be desirable, based on direct measurement of absorption.

Measured and predicted angular scattering patterns of ethylene and acetylene soot are illustrated in Figs. 5 and 6, respectively. These results are for the lowest position in the ethylene flame and the highest position in the acetylene flame, which spans the range of soot aggregate sizes (in terms of D_{30}). The predictions are based on the refitted soot structure properties from the light scattering measurements, which are in excellent agreement with measured values of $\bar{C}^a_{vv}(\theta)$, as discussed in connection with Fig. 4. Similar to Köylü and Faeth (1994), the formulation for $\bar{C}^a_{hh}(\theta)$ was modified from the approach based on Eq. (2) in order to account for observed depolarization phenomena. This was done analogous to Rayleigh scattering theory as follows (Rudder and Bach, 1968):

$$\bar{C}^a_{hh}(\theta) = \bar{C}^a_{vv}(\theta)[(1 - \bar{\rho}^a_v)\cos^2\theta + \bar{\rho}^a_v] \qquad (16)$$

The corresponding estimates of hv and vh scattering cross sections are:

$$\bar{C}^a_{hv} = \bar{C}^a_{vh} = \bar{C}^a_{vv}(90°)\bar{\rho}^a_v \qquad (17)$$

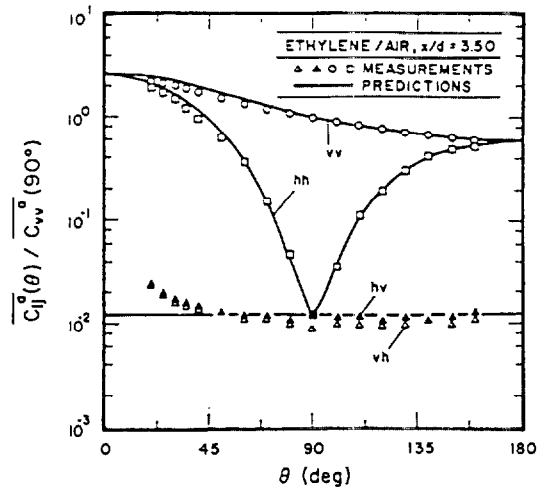

Fig. 5 Measured and predicted angular soot scattering patterns in the ethylene/air flame: x/d = 3.50

The measured values of $\bar{\rho}^a_v(\theta)$ at $\theta = 90°$ are summarized in Table 3; as noted earlier, their magnitudes are similar to the values observed by Köylü and Faeth (1994) for overfire soot. The present results for $\bar{C}^a_{hh}(\theta)$, $\bar{C}^a_{hv}(\theta)$ and $\bar{C}^a_{vh}(\theta)$ also are in qualitative agreement with earlier findings for the much larger overfire soot aggregates (Köylü and Faeth, 1994): Eq. (16) is in excellent agreement with measured values of $\bar{C}^a_{hh}(\theta)$ while Eq. (17) is effective except for the forward-scattering direction where the measured values show a steady increase as the forward scattering direction is approached. It is not known at this point whether the increase of hv and vh scattering as forward scattering is approached follows from the strong forward scattering of soot aggregates or whether it is caused by experimental difficulties. In particular, experimental uncertainties for the vh and hv scattering components increase in the forward scattering direction due to effects of polarization vector misalignment when scattering is strong (Köylü and Faeth, 1994). Clearly, additional consideration of the depolarization ratios of soot aggregates would be useful; however, vh and hv scattering levels are small and have little

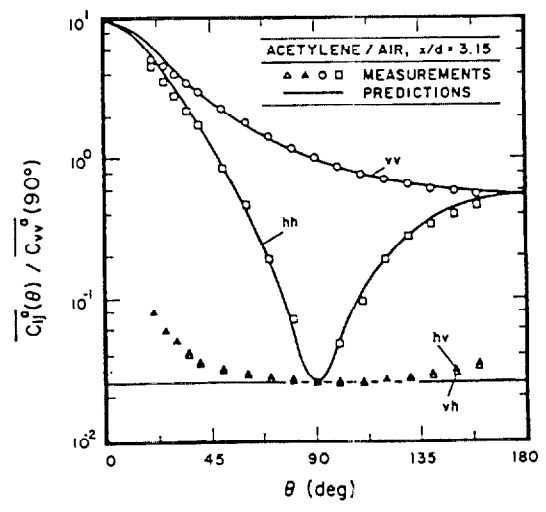

Fig. 6 Measured and predicted angular soot scattering patterns in the acetylene/air flame: x/d = 3.15

effect on total scattering estimates for most conditions of interest. Thus, uncertainties about the evaluation of Eq. (17) in the forward-scattering direction are not very important.

Finally, measured values of $\bar{Q}^a_w(\theta)$ along with the predictions from the various approximate theories are plotted as a function of qd_p in Fig. 7. Results for the ethylene/air flame at $x/d = 4.90$ are illustrated. These conditions correspond to the largest $\bar{N}$ over the present test range, although findings at other conditions were similar. Predictions shown on the plot include Mie scattering for an equivalent sphere, RDG-PFA scattering using the formulation of Dobbins and Megaridis (1991) and RDG-PFA scattering using the formulation of Köylü and Faeth (1994). The Mie scattering predictions are based on D_{30} from Table 2. The RDG-PFA predictions are based on the structure properties from the TEM measurements.

Rayleigh scattering predictions are not illustrated in Fig. 7 because they are totally unsuitable, yielding $\bar{Q}^a_w(\theta)/\bar{Q}^p_w = 1$, which is off the scale of the figure. Typical of past evaluations of the Mie scattering approximation for an equivalent sphere (Köylü and Faeth, 1993), this approximation is not very satisfactory for large soot aggregates. In particular, although Mie scattering theory yields the correct order of magnitude of the scattering level for the present conditions, the angular variation of $\bar{Q}^a_w(\theta)$ is substantially underestimated. Naturally, both RDG-PFA theories yield the same results at small qd_p in the Guinier regime where their formulations are identical. However, the approach of Dobbins and Megaridis (1991) underestimates both the extent of the transition regime and the magnitude of $\bar{Q}^a_w(\theta)$ in the transition and power-law regimes. This occurs because the averaging procedure used by Dobbins and Megaridis (1991) does not account for different weightings of optical properties in the Guinier and power-law regimes. This difficulty in the power-law regime is significant because this regime tends to dominate total scattering computations, and comprises the most accessible angle range for scattering measurements used to find soot structure, for typical soot aggregates.

Conclusions

The optical properties of underfire soot were studied in order to extend an earlier evaluation of approximate soot scattering theories in the power-law (large-angle) regime to the Guinier (small-angle) regime. Test conditions included laminar ethylene/air and acetylene/air diffusion flames, which provided a range of soot aggregate optical properties spanning both the Guinier and power-law scattering regimes. The main conclusions of the study are as follows:

1 The approximate RDG-PFA scattering theory of Köylü and Faeth (1994) yielded predictions that agreed with present measurements within experimental uncertainties. Combined with earlier findings for large overfire soot aggregates, reasonably good performance of this approach has been established for soot from a variety of fuels over the following ranges: x_p of 0.128–0.330, $\bar{N}$ of 31–467, $\bar{N}^2/\bar{N}$ of 70–1330, $\bar{C}^a_w(0°)/\bar{C}^a_w(180°)$ of 10–1000 and $\bar{A}^a$ of 0.06–0.29 (with soot structure properties based on TEM measurements).

2 The main limitation of the approach involves accurate determination of higher order moments, such as $\bar{N}^2$, of the aggregate size distribution function from sampling measurements; thus, it is recommended that these parameters be determined from scattering measurements whenever possible. The performance of other approximate soot aggregate scattering theories generally was not satisfactory over the same range of conditions: Rayleigh scattering substantially underestimated scattering levels, Mie scattering for an equivalent sphere yielded poor estimates of the angular variation of differential scattering cross sections, and RDG-PFA scattering using the approach of Dobbins and Megaridis (1991) underestimated both the extent of the transition regime and scattering levels in the power-law regime.

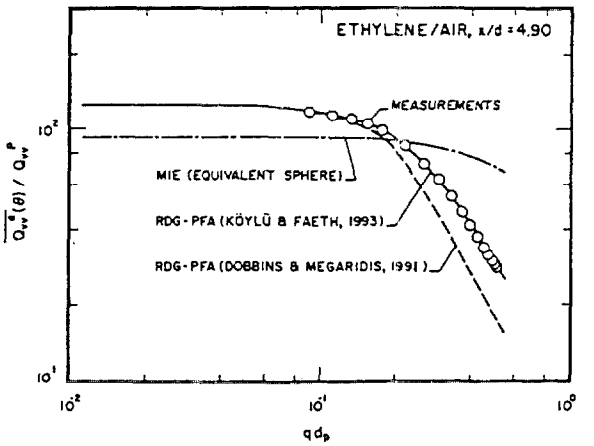

Fig. 7 Various predictions and measurements of volumetric vv soot scattering cross sections in the ethylene/air flame: $x/d = 4.90$

3 The fractal dimensions of soot aggregates appear to be nearly universal over the same range of conditions; for example, combined results for both TEM and light scattering measurements yielded $D_f = 1.77$ with a standard deviation of 0.04. The TEM and light scattering measurements of D_f also were in good agreement, within 1 percent.

4 Past proposals for the use of light scattering measurements to infer soot structure properties, e.g., Dobbins et al. (1990) and Puri et al. (1993), should be re-examined in view of present findings. In particular, scattering from typical soot aggregates in the underfire region is dominated by the transition regime. Unfortunately, optical properties within the transition regime are unusually complex so that approximations of solely Guinier or power-law scattering, which simplify the determination of structure properties, generally are not appropriate for interpreting scattering measurements.

Acknowledgments

This research was supported by the Building and Fire Research Laboratory of the National Institute of Standards and Technology, Grant No. 60NANB1D1175, with H. R. Baum serving as Scientific Officer; and by NASA, Grant No. NAG3-1245, under the technical management of D. L. Urban of the Lewis Research Center. The authors also wish to acknowledge the help of the staff of the Electron Microbeam Analysis Laboratory at the University of Michigan.

References

Bohren, C. F., and Huffman, D. R., 1983, *Absorption and Scattering of Light by Small Particles*, Wiley, New York, pp. 477–482.

Dalzell, W. H., and Sarofim, A. F., 1969, "Optical Constants of Soot and Their Application to Heat Flux Calculations," ASME JOURNAL OF HEAT TRANSFER, Vol. 91, pp. 100–104.

Dalzell, W. H., Williams, G. C., and Hottel, H. C., 1970, "A Light Scattering Method for Soot Concentration Measurements," *Combust. Flame*, Vol. 14, pp. 161–170.

Dobbins, R. A., and Megaridis, C. M., 1987, "Morphology of Flame-Generated Soot as Determined by Thermophoretic Sampling," *Langmuir*, Vol. 3, pp. 254–259.

Dobbins, R. A., Santoro, R. J., and Semerjian, H. G., 1990, "Analysis of Light Scattering From Soot Using Optical Cross Sections for Aggregates," *Twenty-Third Symposium (International) on Combustion*, The Combustion Institute, Pittsburgh, PA, pp. 1525–1532.

Dobbins, R. A., and Megaridis, C. M., 1991, "Absorption and Scattering of Light by Polydisperse Aggregates," *Appl. Optics*, Vol. 30, pp. 4747–4754.

Erickson, W. D., Williams, G. C., and Hottel, H. C., 1964, "Light Scattering Measurements on Soot in a Benzene–Air Flame," *Combust. Flame*, Vol. 8, pp. 127–132.

Freltoft, T., Kjems, J. K., and Sinha, S. K., 1986, "Power-Law Correlations and Finite Size Effects in Silica Particle Aggregates Studied by Small-Angle Neutron Scattering," *Physical Review B*, Vol. 33, pp. 269–275.

Jullien, R., and Botet, R., 1987, *Aggregation and Fractal Aggregates*, World Scientific Publishing Co., Singapore, pp. 45–60.

Kerker, M., 1969, *The Scattering of Light*, Academic Press, New York, pp. 414–486.

Köylü, Ü. Ö., and Faeth, G. M., 1992, "Structure of Overfire Soot in Buoyant Turbulent Diffusion Flames at Long Residence Times," *Combust. Flame*, Vol. 89, pp. 140–156.

Köylü, Ü. Ö., and Faeth, G. M., 1993, "Radiation Properties of Flame-Generated Soot," ASME JOURNAL OF HEAT TRANSFER, Vol. 115, pp. 409–417.

Köylü, Ü. Ö., and Faeth, G. M., 1994, "Optical Properties of Overfire Soot in Buoyant Turbulent Diffusion Flames at Long Residence Times," ASME JOURNAL OF HEAT TRANSFER, Vol. 116, pp. 152–159.

Lin, M. Y., Lindsay, H. M., Weitz, D. A., Ball, R. C., Klein, R., and Meakin, P., 1989, "Universality of Fractal Aggregates as Probed by Light Scattering," *Proc. Roy. Soc. London A*, Vol. 423, pp. 71–87.

Magnussen, B. F., 1974, "An Investigation Into the Behavior of Soot in a Turbulent Free Jet C_2H_2-Flame," *Fifteenth Symposium (International) on Combustion*, The Combustion Institute, Pittsburgh, PA, pp. 1415–1425.

Martin, J. E., and Hurd, A. J., 1987, "Scattering from Fractals," *J. Appl. Cryst.*, Vol. 20, pp. 61–78.

Megaridis, C. M., and Dobbins, R. A., 1990, "Morphological Description of Flame-Generated Materials," *Combust. Sci. Tech.*, Vol. 77, pp. 95–109.

Nelson, J., 1989, "Test of a Mean Field Theory for the Optics of Fractal Clusters," *J. Modern Optics*, Vol. 36, pp. 1031–1057.

Puri, R., Richardson, T. F., Santoro, R. J., and Dobbins, R. A., 1993, "Aerosol Dynamic Processes of Soot Aggregates in a Laminar Ethene Diffusion Flame," *Combust. Flame*, Vol. 92, pp. 320–333.

Rosner, D. E., Mackowski, D. W., and Garcia-Ybarra, P., 1991, "Size- and Structure-Insensitivity of the Thermophoretic Transport of Aggregated Soot Particles," *Combust. Sci. Tech.*, Vol. 80, pp. 87–101.

Rudder, R. R., and Bach, D. R., 1968, "Rayleigh Scattering of Ruby-Laser Light by Neutral Gases," *J. Opt. Soc. Amer.*, Vol. 58, pp. 1260–1266.

Santoro, R. J., Semerjian, H. B., and Dobbins, R. A., 1983, "Soot Particle Measurements in Diffusion Flames," *Combust. Flame*, Vol. 51, pp. 203–218.

Sorensen, C. M., Cai, J., and Lee, N., 1992, "Test of Static Structure Factors for Describing Light Scattering From Fractal Soot Aggregates," *Langmuir*, Vol. 8, pp. 2064–2069.

van de Hulst, H. C., 1957, *Light Scattering by Small Particles*, Dover Publications, New York.

Wersborg, B. L., Howard, J. B., and Williams, G. C., 1972, "Physical Mechanisms in Carbon Formation in Flames," *Fourteenth Symposium (International) on Combustion*, The Combustion Institute, Pittsburgh, PA, pp. 929–940.

Appendix B: Farias et al. (1995a)

Computational Evaluation of Approximate Rayleigh–Debye–Gans/Fractal-Aggregate Theory for the Absorption and Scattering Properties of Soot

T. L. Farias
Graduate Student.

M. G. Carvalho
Professor.
Mem. ASME

Mechanical Engineering Department,
Instituto Superior Técnico,
1096 Lisbon, Portugal

Ü. Ö. Köylü
Research Fellow.

G. M. Faeth
Professor.
Fellow ASME

Department of Aerospace Engineering,
The University of Michigan,
Ann Arbor, MI 48109-2118

A computational evaluation of an approximate theory for the optical properties of soot is described, emphasizing the small-angle (Guinier) regime. The approximate theory (denoted RDG-FA theory) is based on the Rayleigh–Debye–Gans scattering approximation while treating soot as mass-fractal aggregates of spherical primary particles that have constant diameters and refractive indices. The approximate theory was evaluated by more exact predictions from the solution of the volume integral equation formulation of the governing equations, using the method of moments, and based on the ICP algorithm of Iskander et al. (1989). Numerical simulations were used to construct statistically significant populations of soot aggregates having appropriate fractal properties and prescribed numbers of primary particles per aggregate. Optical properties considered included absorption, differential scattering, and total scattering cross sections for conditions typical of soot within flame environments at wavelengths in the visible and the infrared. Specific ranges of aggregate properties were as follows: primary particle optical size parameters up to 0.4, numbers of primary particles per aggregate up to 512, mean fractal dimensions of 1.75, mean fractal prefactors of 8.0, and refractive indices typical of soot. Over the range of the evaluation, ICP and RDG-FA predictions generally agreed within numerical uncertainties (ca. 10 percent) within the Guinier regime, complementing similar performance of RDG-FA theory in the power-law regime based on recent experiments. Thus, the use of approximate RDG-FA theory to estimate the optical properties of soot appears to be acceptable—particularly in view of the significant uncertainties about soot optical properties due to current uncertainties about soot refractive indices.

Introduction

Soot is present within most practical nonpremixed hydrocarbon-fueled flames, which affects their structure, radiation, and pollutant emission properties (Köylü and Faeth, 1993). Thus, the absorption and scattering (optical) properties of soot are needed to predict the continuum radiation properties of soot and to interpret nonintrusive optical measurements to find soot concentrations and structure. Soot optical properties are a challenging problem, however, due to the complexity of soot structure. For example, while soot generally consists of small spherical primary particles that individually satisfy the Rayleigh scattering approximation, these primary particles combine into branched aggregates that exhibit neither Rayleigh nor Mie scattering behavior (Dalzell et al., 1970; Jullien and Botet, 1987; Köylü and Faeth, 1993). However, a potentially useful approximate theory for soot optical properties (denoted RDG-FA theory in the following) recently has been developed, based on the Rayleigh–Debye–Gans (RDG) scattering approximation while assuming that soot aggregates are mass-fractal objects (Jullien and Botet, 1987; Martin and Hurd, 1987; Dobbins and Megaridis, 1991; Köylü and Faeth, 1994a). In particular, the approximate RDG-FA theory provides a computationally tractable way of treating complex populations of soot aggregates having widely varying numbers of primary particles per aggregate that must be considered for practical applications (Köylü and Faeth, 1993, 1994a). Nevertheless, past theoretical and experimental evaluations of RDG-FA theory have not been definitive due to computational and experimental limitations (Köylü and Faeth, 1993, 1994a, b). Thus, the objective of the present investigation was to complete an additional theoretical evaluation of RDG-FA theory for soot, based on computations using a more exact theory (that unfortunately is not tractable for estimates of the optical properties of practical soot aggregates) for populations of mass-fractal aggregates having prescribed properties.

Although RDG-FA theories have been applied to estimate soot scattering properties and to interpret scattering measurements in order to find soot structure properties (Dobbins et al., 1990; Puri et al., 1993; Sorensen et al., 1992), there are significant uncertainties about some of the approximations of the theory for soot aggregates. In particular use of the RDG approximation requires that both $|m-1| \ll 1$ and $2x_p|m-1| \ll 1$ (Bohren and Huffman, 1983; Kerker, 1969; van de Hulst, 1957), which is questionable due to the large refractive indices of soot. Additionally, Berry and Percival (1986) argue that RDG theory should be effective for mass-fractal objects having $D_f < 2$, which is true for soot aggregates, when

$$N \ll x_p^{-D_f} \tag{1}$$

or if this criterion is not satisfied, when

$$x_p \ll \left[\frac{|m^2-1|2^{1-D_f}(D_f(D_f+1))^{D_f/2}}{3(D_f-1)(2-D_f)}\right]^{1/(D_f-3)} \tag{2}$$

The first criterion is rarely satisfied for soot aggregates. The second criterion generally requires $x_p \ll 0.15$, which also is not sat-

Contributed by the Heat Transfer Division for publication in the JOURNAL OF HEAT TRANSFER. Manuscript received by the Heat Transfer Division December 1993; revision received April 1994. Keywords: Combustion, Fire/Flames, Radiation. Associate Technical Editor: W. L. Grosshandler.

isfied for a very wide range of soot properties, particularly in the visible portion of the spectrum, which usually is used for optical measurements of soot structure. Finally, recent computational studies suggest significant effects of multiple scattering for large soot aggregates, which is ignored when the RDG approximation is used (Berry and Percival, 1986; Chen et al., 1990; Ku and Shim, 1992a, b; Nelson, 1989). Thus, additional evaluation of RDG-FA theory is required before it can be recommended for predictions of soot optical properties.

In spite of these concerns about RDG-FA theory, however, recent experimental evaluations of the approach have been encouraging. These evaluations involved comparing RDG-FA scattering predictions, based on measured soot structure properties from thermophoretic sampling and analysis by transmission electron microscopy, with in situ scattering measurements for the same soot aggregate population. This work involved both large soot aggregates in the fuel-lean (overfire) region of buoyant turbulent diffusion flames, which emphasized the large-angle (power-law) scattering regime (Köylü and Faeth, 1994a), and small soot aggregates in the fuel-rich (underfire) region of laminar diffusion flames, which emphasized the small-angle (Guinier) scattering regime (Köylü and Faeth, 1994b). The predictions and measurements agreed within experimental uncertainties for both the power-law and Guinier regimes. This finding was reasonably definitive within the power-law regime, where the soot aggregate fractal properties that dominate aggregate scattering properties could be found accurately from structure measurements. The evaluation was less definitive in the Guinier regime, however, due to difficulties of accurately measuring both scattering properties at small angles and the higher moments of the aggregate size distribution function (e.g., $\bar{N}^2$) that dominate scattering properties at small angles (Köylü and Faeth, 1994a, b). This limitation is unfortunate because multiple-scattering effects that could compromise the use of RDG-FA theory are most significant in the Guinier regime (Nelson, 1989).

Existing computer simulations of the optical properties of soot also do not provide an adequate basis for evaluating RDG-FA scattering theory. In particular, problems of computational tractability for past computer simulations imply that they either involve fundamentally accurate solutions for small nonfractal aggregates where effects of multiple and self-induced scattering are small, or approximate solutions having uncertain accuracy for the large soot aggregates of interest for practical flames (Köylü and Faeth, 1993). Additionally, existing computations have been limited to relatively small samples of both orientations of given aggregates and aggregate configurations, raising questions about the statistical significance of the results (Köylü and Faeth, 1993).

To summarize, while the approximate RDG-FA approach offers a promising treatment of the optical properties of practical soot aggregates, past experimental and theoretical evaluations have not provided a definitive assessment of the approach over the full range of interest. In particular, although acceptable performance of RDG-FA theory has been established in the power-law regime, comparable assessment in the Guinier regime has not been achieved. Thus, the objective of the present investigation was to undertake a theoretical evaluation of RDG-FA theory, emphasizing the Guinier regime. The evaluation was based on computations using the ICP approach of Iskander et al. (1989), which provides a more exact treatment of aggregate scattering in the Guinier regime than RDG-FA theory, by including effects of multiple and self-induced scattering. Problems of defining the higher moments of the size distribution functions of polydisperse aggregates during experiments were avoided by using numerical simulations to generate aggregates having prescribed sizes and mass-fractal properties.

Theoretical Methods

RDG-FA Scattering Theory. The RDG-FA scattering theory is based on methods described by Freltoft et al. (1986), Jullien and Botet (1987), Lin et al. (1989), Martin and Hurd (1987), and Dobbins and Megaridis (1991). Present considerations, however, will be limited to the extended version due to Köylü and Faeth (1994a), which allows for the presence of the power-law regime when finding total scattering cross sections because this regime is important for large aggregates. The major assumptions of this approach with respect to soot aggregate physical properties are as follows: spherical primary particles have constant diameters, primary particles have uniform refractive indices, primary particles just touch one another, and the aggregates are mass-fractal objects. Justifications of these assumptions for soot aggregates are discussed by Köylü and Faeth (1993, 1994a).

The mass fractal approximation for aggregates of constant-diameter spherical primary particles implies the following relationship between the number of primary particles in an aggregate, N, and the radius of gyration of the aggregate, R_g (Jullien and Botet, 1987):

$$N = k_f(R_g/d_p)^{D_f} \tag{3}$$

The fractal dimension and prefactor in Eq. (3), D_f and k_f, appear to be relatively universal properties of soot aggregates, e.g., recent measurements for a variety of soot in flame environments indicate $D_f = 1.77$ and $k_f = 8.1$, with standard deviations of 2 and 10 percent, respectively (Köylü and Faeth, 1993, 1994a, b). Thus, Eq. (3) provides a critical relationship between N, a quantity that is readily measured, and R_g, an important parameter required by RDG scattering theory.

Nomenclature

C = optical cross section
d_e = equivalent sphere diameter
d_i = diameter of object i
d_p = primary particle diameter
D_f = mass fractal dimension, Eq. (3)
$E(m)$ = refractive index function $= \mathrm{Im}((m^2-1)/(m^2+2))$
$f(qR_g)$ = aggregate form factor, Eq. (5)
$F(m)$ = refractive index function $= |(m^2-1)/(m^2+2)|^2$
$g(\lambda, R_g, D_f)$ = aggregate total scattering factor, Eq. (8)
i = $(-1)^{1/2}$
k = wave number $= 2\pi/\lambda$
k_f = fractal prefactor, Eq. (3)
m = refractive index of object $= n + i\kappa$
n = real part of refractive index of object
N = number of primary particles in an aggregate
q = modulus of scattering vector $= (4\pi/\lambda)\sin(\theta/2)$
R_g = radius of gyration of an object
x_i = optical size parameter based on d_i; $x_i = \pi d_i/\lambda$
θ = angle of scattering from forward direction
κ = imaginary part of refractive index of object
λ = wavelength of radiation
ρ_v^a = depolarization ratio

Subscripts

a = absorption
e = optically equivalent object
h = horizontal polarization
i = property of primary particle i
ij = incident (i) and scattered (j) polarization directions
s = total scattering
v = vertical polarization

Superscripts

a = aggregate property
p = primary particle property
$\bar{(\ )}$ = mean value over aggregate size distribution

In addition to the RDG approximation, it is also assumed that the primary particles are small enough to satisfy the Rayleigh scattering approximation as individual particles. This is reasonable because primary particle optical size parameters generally are less than 0.4 for soot in the visible and infrared wavelength ranges, which implies that the total scattering and absorption cross sections of individual primary particles are within 1 and 5 percent, respectively, of estimates based on the Rayleigh scattering approximation for refractive indices typical of soot (Köylü and Faeth, 1993). This yields the following expressions for the absorption and scattering cross sections of individual primary particles (Bohren and Huffman, 1983; Kerker, 1969):

$$C_a^p = 4\pi x_p^3 E(m)/k^2,$$

$$C_s^p = 8\pi x_p^6 F(m)/(3k^2), \quad C_w^p = x_p^6 F(m)/k^2 \quad (4)$$

In Eq. (4), and the following equations, subscripts for differential scattering cross sections denote the direction of polarization vectors with respect to the scattering plane defined by the light source, the aggregate and the observer: v and h designate polarization vectors normal and parallel to this plane while the first and second subscripts designate incident and scattered light.

Under the RDG approximation, differential scattering cross sections for aggregates of a given size (after averaging over all orientations of each aggregate within a statistically significant monodisperse aggregate population) satisfy the following formulas (Kerker, 1969):

$$C_w^a(\theta) = C_{hh}^a(\theta)/\cos^2\theta = N^2 C_w^p f(qR_g) \quad (5)$$

The form factor, $f(qR_g)$, is expressed as follows in the Guinier and power-law regimes (Freltoft et al., 1986; Jullien and Botet, 1987; Lin et al., 1989; Martin and Hurd, 1987):

$$f(qR_g) = \exp(-(qR_g)^2/3), \quad \text{Guinier regime} \quad (6)$$

$$f(qR_g) = (qR_g)^{-D_f}, \quad \text{power-law regime} \quad (7)$$

Adopting the proposal of Dobbins and Megaridis (1991), the boundary between the Guinier and power-law regimes is taken to be $(qR_g)^2 = 3D_f/2$, which is chosen to match the value and the derivative of $f(qR_g)$ where the two regimes meet. The total scattering cross section then becomes:

$$C_s^a = N^2 C_s^p g(\lambda, R_g, D_f) \quad (8)$$

where $g(\lambda, R_g, D_f)$ has different forms if the power-law regime is reached for $\theta \leq 180$ deg, or not; see Köylü and Faeth (1994a) for these expressions. It also is assumed that absorption is not affected by aggregation, while the extinction cross section is the sum of the absorption and scattering cross sections by definition, i.e.,

$$C_a^a = NC_a^p, \quad C_e^a = C_a^a + C_s^a \quad (9)$$

The corresponding formulation for a polydisperse aggregate population, which is not needed here, can be found from Köylü and Faeth (1994a).

ICP Scattering Theory. Ku and Shim (1992a, b) review theories of aggregate optical properties more accurate than the RDG approximation. Various methods are considered but those of Borghese et al. (1984), Jones (1979a, b), Purcell and Pennypacker (1973), and Iskander et al. (1989) are emphasized. Borghese et al. (1984) developed an exact solution for the optical properties of clusters of spheres but this approach is computationally intensive and its practical accuracy is limited by the truncation of series expansions. The popular Jones (1979a, b) formulation, after correction of errors found by Kumar and Tien (1989) and Ku (1991), only includes multiple-scattering terms up to second order (based on the reciprocal of the distance between primary particles) and it was found to be less reliable than the rest. The Iskander et al. (1989) and Purcell and Pennypacker (1973) formulations both include multiple-scattering terms up to third order in the reciprocal distance between primary particles; however, the latter formulation omits a self-interaction term that can be significant for practical aggregates. Based on these considerations, Ku and Shim (1992b) conclude that the ICP formulation of Iskander et al. (1989) was superior to the rest; therefore, this approach was adopted for the present calculations.

The soot aggregate structure approximations of the ICP and RDG-FA calculations were the same. In addition, each primary particle constituted an ICP computational cell, which implies that individual primary particles satisfy the Rayleigh scattering approximation, i.e., the internal electrical fields of primary particles are assumed to be uniform. This approximation is reasonable because errors are less than 10 percent for cross sections and near-forward scattering when $x_p < 0.8|(m^2 + 5)/(2m^2 + 1)|$, taking individual primary particles to be ICP computational cells (Ku and Shim, 1992b). The refractive index factor in this expression is roughly unity for soot, so that present calculations satisfied the criterion with a significant margin for $x_p \leq 0.4$.

The ICP approach involves first determining the internal field of each primary particle, and then finding the optical cross sections resulting from these fields. The formulation for these calculations is lengthy and Iskander et al. (1989) and Ku and Shim (1992b) should be consulted for details. Present results were obtained as averages obtained over various orientations of individual aggregates with respect to the direction of the incident field (in equally spaced spherical coordinate angles) and over populations of fractal aggregates of specified size, N, unless otherwise noted.

Simulation of Aggregates. Mountain and Mulholland (1988) generated aggregates using a simulation of cluster/cluster aggregation based on solution of the Langevin equations. This approach yields fractal aggregates that satisfy the power-law relationship of Eq. (3) with $1.7 < D_f < 1.9$ and k_f circa 5.5, for $N > 10$. These sample aggregates subsequently were used by Chen et al. (1990) for ICP calculations of aggregate scattering properties. However, a larger sample of aggregates was required for the present work, and it was desired to have $1.7 < D_f < 1.8$ and k_f circa 8.0 in order to correspond to recent observations of the fractal properties of soot aggregates (Köylü and Faeth, 1992, 1994a, b). As a result, an alternative aggregate simulation was used during the present investigation. The present numerical simulations of aggregates sought to create populations of aggregates by cluster/cluster aggregation, following Jullien and Botet (1987). The process started with individual and pairs of primary particles, which then were attached to each other randomly, assuming uniform distributions of the point and orientation of attachment but rejecting configurations where primary particles intersected. This procedure was continued in order to form progressively larger aggregates, but with the additional restriction that the aggregates should have $1.7 < D_f < 1.8$ and k_f circa 8 for $N > 8$. It was observed that D_f fell naturally in the range 1.6–1.9 for $N > 48$ during these simulations; therefore, few cluster/cluster combinations were rejected for inappropriate fractal properties when larger aggregates were constructed. Similarly, for D_f in the range 1.7–1.8, the value of k_f fell naturally near $k_f = 8.0$ for statistically significant populations of aggregates.

Projected images of typical aggregates constructed using the present simulation are illustrated in Fig. 1 for $N = 16$, 64, and 256, which cover the range of mean aggregate sizes observed in nonpremixed flames (Köylü and Faeth, 1992, 1993, 1994a, b). The appearance of the aggregates varies considerably with the direction of projection, and from aggregate to aggregate within a population of given size. Nevertheless, the simulated aggregates are qualitatively similar to both past experimental observations of soot aggregates (Dalzell et al., 1970; Jullien and Botet, 1987; Köylü and Faeth, 1992, 1994a, b) and other numerical simulations of soot aggregates (Chen et al., 1990; Jullien and Botet, 1987; Mountain and Mulholland, 1988; Nelson, 1989). Combined with their prescribed fractal properties, this suggests

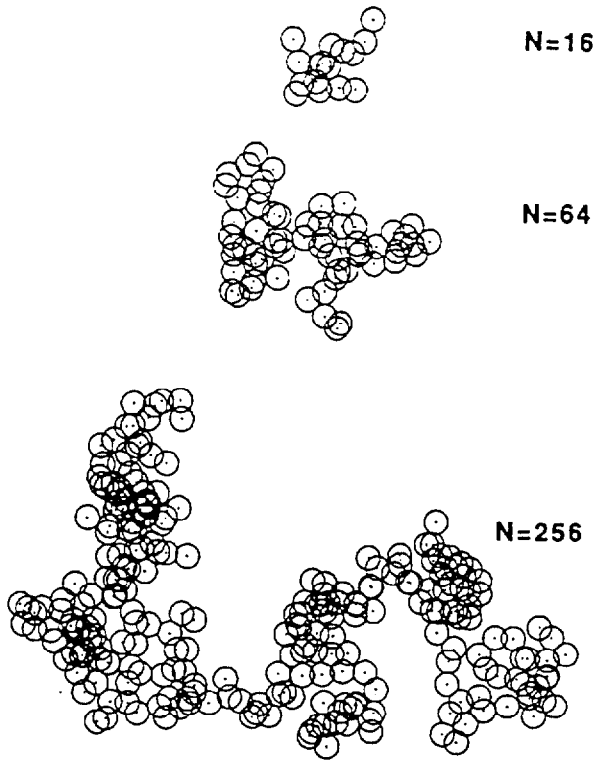

Fig. 1 Projected images of typical aggregates used in the computations for N = 16, 64, and 256

that the present simulated aggregate populations are reasonably representative of the structure of the soot aggregates found in flame environments.

Results and Discussion

Evaluation of ICP Predictions

Spherelike Aggregate. The ICP algorithm was checked by computing the scattering properties of spherelike aggregates, and comparing these results with Mie scattering predictions for an optically equivalent sphere. The configuration of the spherelike aggregate was similar to the arrangement considered by Purcell and Pennypacker (1973) and Ku and Shim (1992b), involving 136 spherical primary particles in a cubical lattice with the aggregate having a spherical outer boundary. For this arrangement, each primary sphere is bounded by a cube having an edge length of d_p, so that the diameter of the equivalent sphere is given by $d_e = (6N/\pi)^{1/3} d_p$, or $d_e = 6.38 d_p$ for $N = 136$. In order to apply Mie scattering predictions to this aggregate, the following Maxwell–Garnett relationship was used to find the effective refractive indices for the equivalent sphere, m_e, noting that the volume fraction of the primary particle within its surrounding cubical volume is $\pi/6$ (Ku and Shim, 1992b):

$$(m_e^2 - 1)/(m_e^2 + 2) = (\pi/6)(m^2 - 1)/(m^2 + 2) \quad (10)$$

The present calculations were carried out for various values of x_p with $m = 1.60 + 0.60i$, which is a typical value of the complex refractive index of soot (Charalampopoulos, 1992). This implies $m_e = 1.33 + 0.25i$ from Eq. (10).

Predictions of normalized differential scattering patterns, $k^2 C_{vv}^s(\theta)$, as a function of θ and x_p, are illustrated in Fig. 2 for the spherelike aggregate. The results include Mie scattering predictions for an equivalent sphere, as well as ICP predictions for both a single orientation and averaged over 128 orientations of the aggregate. At small angles, within the Guinier regime, effects of orientation averaging are small and the agreement between the Mie and ICP predictions is excellent for the full range of x_p considered ($x_p \leq 0.5$). This behavior agrees with the small-angle criterion for ICP cell sizes of Ku and Shim (1992b), discussed earlier, and helps to justify the use of ICP predictions to evaluate RDG-FA theory in the Guinier regime. ICP also yields similar performance for the complete range of scattering angles for $x_p \leq 0.25$. At large angles for $x_p = 0.5$, however, effects of orientation averaging become more important, as discussed subsequently, and there are considerable discrepancies between ICP and Mie scattering predictions, which are caused by truncation errors due to excessively large ICP cell sizes. Thus, the use of ICP to estimate the differential scattering properties of aggregates having large x_p is questionable at large angles.

Fractal Aggregates. The next issues to be established are the number of orientations (in spherical coordinate angles, as noted earlier) of individual aggregates, and the number of individual aggregates, that should be averaged in order to obtain statistically significant ICP predictions. The required numbers of realizations increased with increasing N, m, and x_p; therefore, effects of averaging are illustrated in Fig. 3 for $N = 256$, $m = 1.57 + 0.57i$, and $x_p = 0.4$, which represents a conservative condition for present calculations and a typical refractive index of soot (Charalampopoulos, 1992). The results shown include vv scattering patterns for a single realization (a particular aggregate and orientation) as well as average values and standard deviations for 128 orientations of one aggregate and single orientations (each) of a population of 128 aggregates. The results for a single realization exhibit a complex scattering pattern, particularly at larger scat-

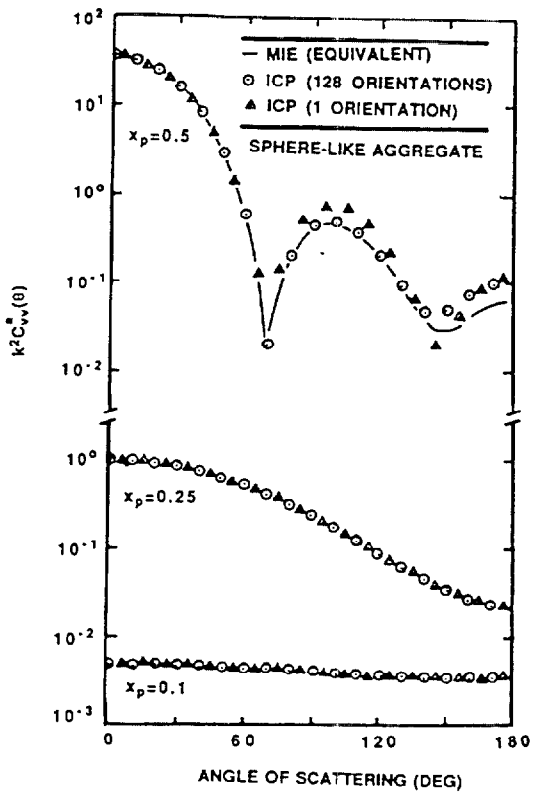

Fig. 2 Normalized vv scattering patterns for a spherelike aggregate, computed using ICP and Mie scattering for an equivalent sphere (N = 136, $m = 1.60 + 0.60i$, $m_e = 1.33 + 0.25i$, $x_e = 6.38x_p$)

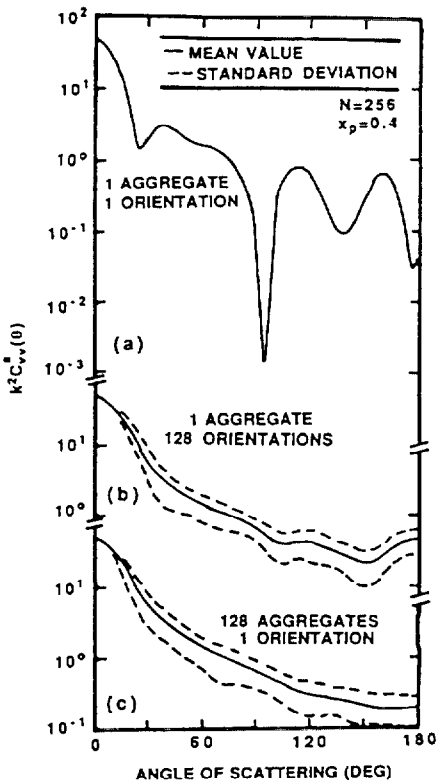

Fig. 3 Normalized *vv* scattering patterns for fractal aggregates computed using ICP (N = 256, D_f = 1.72, k_f = 8.0, λ = 514.5 nm, m = 1.57 + 0.57i and x_p = 0.4): (a) results for a single aggregate and orientation, (b) results for a single aggregate averaged over 128 orientations, (c) results for a single orientation averaged over 128 aggregates

tering angles, due to interference effects for this particular aggregate array and incident wave propagation direction. Naturally, such patterns are not observed for scattering from practical soot aggregates because aggregate orientations are random and scattering patterns involve averages over very large aggregate populations.

The smoothing of scattering patterns due to averaging is evident from the results considering orientation and aggregate averaging in Fig. 3. Thus, the scattering patterns based on averages decay smoothly, and optical properties are relatively independent of the method of averaging, at small and moderate angles ($\theta <$ 30 deg), which is critical for present evaluation of RDG-FA theory. Oscillations begin to appear with increasing angle, particularly when only one aggregate is considered; nevertheless, the performance of ICP for $x_p = 0.4$ is suspect at these conditions in any event, based on the results discussed in connection with Fig. 2. Similarly, the standard deviations of the cross sections over the sample populations progressively increase with increasing scattering angle. This latter behavior is similar to results found by Mountain and Mulholland (1988) for RDG scattering calculations using numerically simulated populations of aggregates, and reflects the increasing importance of the aggregate arrangement as the scattering angle increases. For example, under the RDG scattering approximation, the form factor is nearly unity in the small-angle (Guinier) scattering regime and scattering mainly depends upon the number of primary particles in the aggregates, see Eq. (6). In contrast, the form factor depends strongly on the aggregate arrangement through the values of R_g and D_f in the large-angle (power-law) scattering regime; see Eq. (7). Thus, the largest angle controls the requirements for sampling to achieve statistically significant ICP predictions of differential scattering patterns.

Based on the previous considerations, 64 aggregates, each sampled at 16 orientations, were used to obtain a numerical uncertainty (95 percent confidence) less than 10 percent for ICP predictions of differential scattering cross sections at 180 deg. Fewer realizations were required to obtain statistically significant absorption and total scattering cross sections. Thus, using as few as four orientations of eight aggregates still yielded numerical uncertainties (95 percent confidence) less than 5 percent for ICP predictions of these two cross sections. Naturally, these estimates do not include effects of deficiencies of ICP predictions at large angles and x_p, noted earlier.

Evaluation of RDG-FA Predictions

Differential Scattering Cross Sections. Figure 4 is an illustration of RDG-FA and ICP predictions of $C^a_w(\theta)/(NC^p_w)$ as a function of the radiation momentum, qd_p, for aggregates having $D_f = 1.75$, $k_f = 8.0$, $m = 1.57 + 0.57i$, and x_p up to 0.4 for λ = 514.5 nm. The results for large x_p represent severe conditions: rather large primary particles, refractive indices typical of soot, and a wavelength provided by argon-ion lasers that frequently is used for nonintrusive measurements of soot properties. Results are plotted for aggregates of various size, considering N = 16, 64, and 256—the last representing a reasonable limit for ICP calculations in view of current computer capabilities and the sampling requirements needed to achieve the computational uncertainties stated earlier, and representative of maximum mean aggregate sizes observed in nonpremixed flames (Köylü and Faeth, 1992, 1993, 1994a, b). The predictions are terminated at values of qd_p that correspond to θ = 180 deg.

The RDG-FA results illustrated in Fig. 4 exhibit extended Guinier regimes for the range of aggregate properties considered, reaching $C^a_w(\theta)/(NC^p_w) = N$ at small values of qd_p, as anticipated from Eqs. (5) and (6). It is seen that there are progressively larger regions of power-law behavior, where the slopes of the RDG-FA plots approach $-D_f$ according to Eqs. (5) and (7), as both x_p and N increase. This can be explained by noting that the maximum value of $qd_p = 4x_p$ at θ = 180 deg, which implies a greater range of qd_p as x_p increases, while the boundary between the Guinier and power-law regimes can be represented as $qd_p = (3D_f/2)^{1/2}(k_f/N)^{1/D_f}$, which implies smaller values of qd_p at the onset of the power-law regime as N increases for given aggregate fractal properties. Another feature of the normalization used in Fig. 4 is that the RDG-FA results become universal in the power-law regime for given aggregate fractal properties. This can be seen by eliminating R_g from Eqs. (5) and (7), using Eq. (3), to yield the following relationship for the power-law regime:

$$C^a_w(\theta)/(NC^p_w) = k_f(qd_p)^{-D_f} \qquad (11)$$

Thus, RDG-FA predictions only depend on the values of the fractal properties and qd_p within the power-law regime, and reach an intercept of $k_f = 8.0$ at $qd_p = 1$ if this value of qd_p is within the power-law regime.

For the conditions considered in Fig. 4, the comparison between ICP and RDG-FA predictions is excellent throughout the Guinier regime. For example, the maximum discrepancy between the two predictions within the Guinier regime is roughly 15 percent for forward scattering at $x_p = 0.4$ and $N = 256$ (see Fig. 4*c*). Additionally, discrepancies at other conditions within the Guinier regime generally are less than 10 percent, with comparable agreement over the entire available range of scattering angles for $x_p \leq 0.2$ (see Figs. 4*a*, *b*). Thus, for the range of conditions where ICP predictions are reliable, in view of the results discussed in connection with Fig. 2, RDG-FA predictions seem generally satisfactory based on agreement with ICP predictions.

The comparison between RDG-FA and ICP predictions is less satisfactory in the power-law regime for $x_p = 0.4$ (see Fig. 4*c*); however, this behavior does not imply a deficiency of RDG-FA

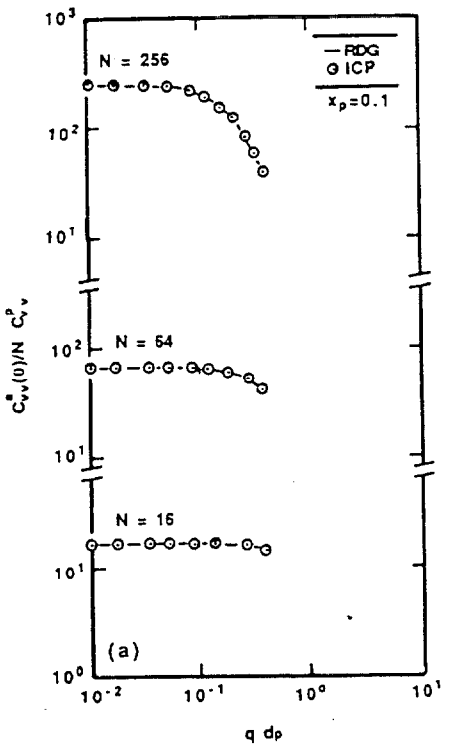

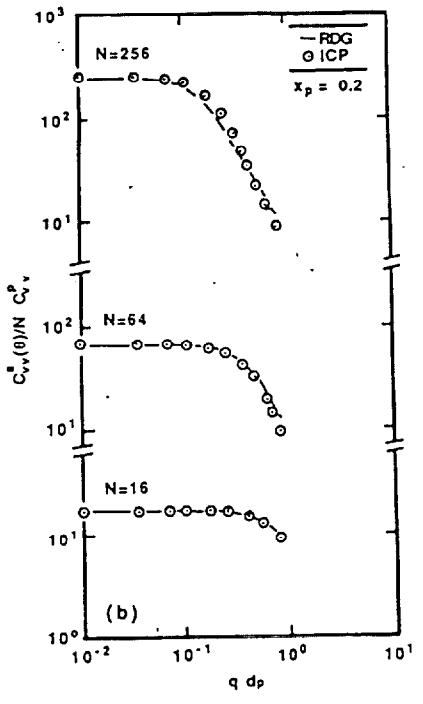

Fig. 4 Normalized *vv* scattering cross sections as a function of the radiation momentum for fractal aggregates of various size, computed using the ICP and RDG-FA methods (D_f = 1.75, k_f = 8.0, λ = 514.5 nm, m = 1.57 + 0.57i): (*a*) x_p = 0.1, (*b*) x_p = 0.2, (*c*) x_p = 0.4

theory. In particular, past experimental evaluations in the power-law regime are reasonably definitive and indicate satisfactory performance for RDG-FA theory (Köylü and Faeth, 1994a, b), as noted earlier. In contrast, ICP predictions are not very satisfactory at large angles and x_p due to truncation errors, as discussed in connection with Fig. 2. The main problem is that ICP overestimates the rate of decrease of $C^a_{vv}(\theta)$ with increasing qd_p for soot aggregates in the power-law regime. This behavior yields slopes of the ICP plots in Fig. 4(*c*) that are greater than $-D_f$ from Eq. (11), which contradicts a well-established property of soot aggregates having an extended power-law regime (Köylü and Faeth, 1993, 1994a, b).

Normalized differential scattering patterns found from both the ICP and RDG-FA theories are illustrated in Fig. 5. The results are plotted as $k^2C^a_{vv}(\theta)$ in order to highlight effects of aggregate size on differential scattering patterns. The aggregate properties for these calculations are the same as Fig. 4, except that only the worst-case condition, x_p = 0.4, has been illustrated. For the properties used to construct Fig. 5, scattering is in the power-law regime at 90 deg for the RDG-FA predictions. Then evaluating $C^a_{vv}(\theta)$ at 0 and 90 deg from Eqs. (5)–(7) yields:

$$C^a_{vv}(0\text{ deg})/C^a_{vv}(90\text{ deg}) = C^a_{hh}(0\text{ deg})/C^a_{vv}(90\text{ deg}) = N(2\sqrt{2}x_p)^{D_f}/k_f \quad (12)$$

Thus, Eq. (12) explains the increase of the normalized *vv* and *hh* scattering cross sections in the forward-scattering direction seen in Fig. 5 as N is increased, as well as a corresponding increase when x_p is increased, which is not illustrated in the figure. Similarly, within the power-law regime, Eqs. (5) and (7) yield:

$$C^a_{vv}(\theta)/C^a_{vv}(90\text{ deg}) = C^a_{hh}(\theta)/(\cos^2\theta C^a_{vv}(90\text{ deg})) = (\sqrt{2}\sin(\theta/2))^{-D_f} \quad (13)$$

Thus, Eq. (13) implies that variations of *vv* and *hh* differential scattering cross sections with scattering angle are controlled by D_f in the power law regime.

The RDG-FA predictions of $C^a_{hh}(\theta)$ in Fig. 5 were corrected for effects of depolarization ratios by analogy to Rayleigh scattering theory (Rudder and Bach, 1968) using the approach of

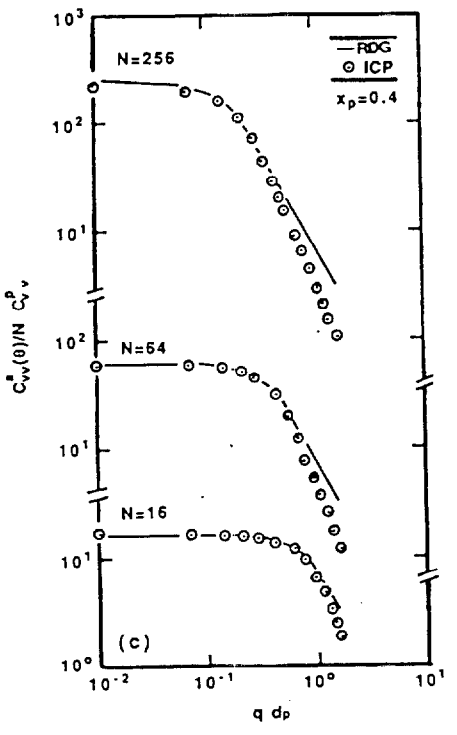

Fig. 4. (Continued)

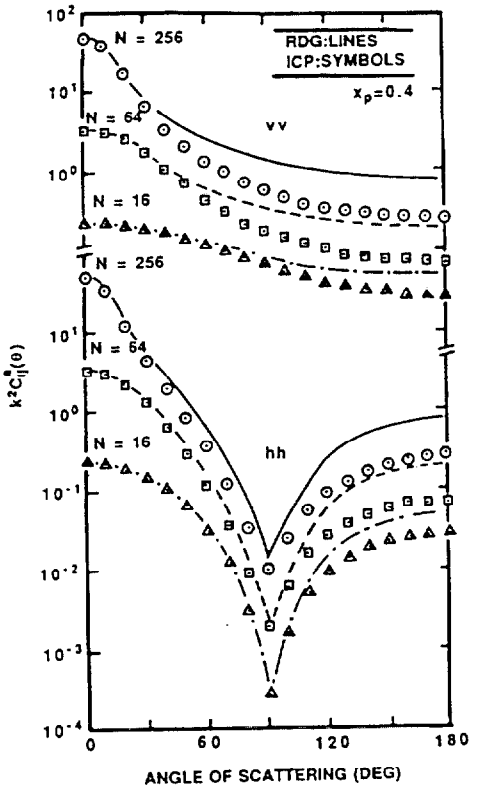

Fig. 5 Normalized scattering patterns for fractal aggregates of various size, computed using the ICP and RDG-FA methods (D_f = 1.75, k_f = 8.0, λ = 514.5 nm, m = 1.57 + 0.57i, and x_p = 0.4)

Köylü and Faeth (1994a). These corrections were based on depolarization ratios, ρ_v^a = 0.0035, 0.0071, 0.0113, for N = 16, 64, and 256, respectively, from the ICP predictions. After correcting $C_{hh}^a(\theta)$ for RDG-FA predictions in this manner, the agreement between RDG-FA and ICP predictions in Fig. 5 is within numerical uncertainties throughout the Guinier regime (roughly θ < 20, 40, and 90 deg for N = 256, 64, and 16, respectively). As discussed earlier, ICP predictions underestimate scattering levels at larger angles due to truncation errors at large x_p, accounting for the discrepancies between the two predictions in this region. However, results similar to Fig. 5 indicated good agreement between the two theories at all angles for $x_p \leq 0.2$, similar to the findings illustrated in Fig. 4.

Effects of refractive indices on the comparison between ICP and RDG-FA predictions also were considered. The variations of m were carried out by taking $n = 1 + \kappa$ and $|m - 1|$ = 0.2, 0.4, and 0.8. This procedure yields progressively increasing refractive indices with the largest values corresponding to typical values for soot in the visible wavelength range (Charalampopoulos, 1992). Other properties of these calculations were similar to the results illustrated in Figs. 4 and 5. The comparison between ICP and RDG-FA predictions of the differential scattering cross sections as refractive indices varied was similar to results discussed in connection with Figs. 4 and 5. In particular, the agreement between the two predictions was within numerical accuracies at small and moderate angles (roughly θ < 30 deg), while ICP predictions tended to underestimate scattering levels at large angles where they are less reliable.

Absorption and Total Scattering. The last phase of the present evaluation of RDG-FA theory was to consider absorption and total scattering cross sections. Figure 6 is an illustration of normalized absorption and total scattering cross sections from the ICP and RDG-FA predictions plotted as a function of N for various values of x_p. The other parameters of these calculations were similar to Figs. 4 and 5; that is, D_f = 1.75, k_f = 8.0, λ = 514.5 nm and m = 1.57 + 0.57i. As noted earlier, reduced sampling requirements to obtain statistically significant values of these cross sections allowed maximum values of N up to 512 to be considered for the ICP predictions.

The ICP predictions of normalized absorption cross sections, $C_a^a/(NC_a^p)$, remain within 10 percent of unity for the conditions illustrated in Fig. 6, even including questionable values for x_p = 0.4 at large N. This is in good agreement with RDG-FA predictions where this ratio is unity from Eq. (9), i.e., the absorption of primary particles in aggregates is identical to the absorption of individual primary particles. In contrast, both predictions of $C_s^a/(NC_s^p)$ increase with increasing N, with the rate of increase gradually decreasing as N increases. This latter effect is observed because fractal aggregate scattering becomes saturated at large N for D_f < 2; in contrast, for D_f > 2, $C_s^a/(NC_s^p)$ continues to increase without bound as N increases (Berry and Percival, 1986; Dobbins and Megaridis, 1991). In particular, RDG-FA theory yields the following expression for $C_s^a/(NC_s^p)$ at large N (Köylü and Faeth, 1994a):

$$C_s^a/(NC_s^p) = k_f(4x_p)^{-D_f}(3/(2 - D_f) - 12/((6 - D_f)(4 - D_f))) \quad (14)$$

Thus, for given fractal properties, $C_s^a/(NC_s^p)$ is independent of N for large N, with this plateau value tending to decrease as x_p increases. Present predictions in Fig. 6 do not extend to large enough values of N to reach the plateau condition; however, both predictions are in good agreement over the range of conditions that are illustrated for $x_p \leq 0.2$. In contrast, problems with ICP predictions at large angles for x_p = 0.4 (see Fig. 5) cause greater discrepancies between the two theories for large N. Similar calculations over the range of refractive indices considered yielded the same general behavior.

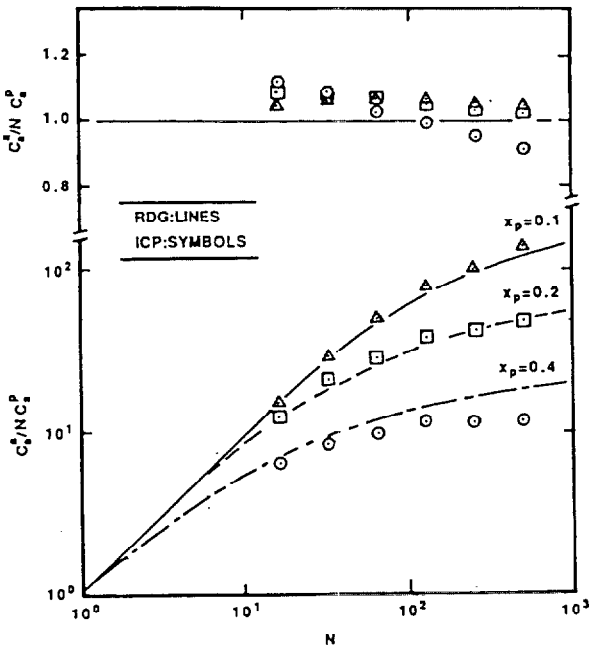

Fig. 6 Normalized absorption and total scattering cross sections as a function of aggregate size for fractal aggregates having various x_p, computed using the ICP and RDG-FA methods (D_f = 1.75, k_f = 8.0, λ = 514.5 nm, m = 1.57 + 0.57i)

Conclusions

An evaluation of an approximate RDG-FA theory for the optical properties of soot aggregates, emphasizing the Guinier regime, was completed based on predictions using the more precise ICP theoretical approach due to Iskander et al. (1989). Conditions considered during the evaluation were selected to approximate the properties of soot aggregates in the visible and near-infrared portions of the spectrum, as follows: x_p up to 0.4, N up to 512, $D_f = 1.75$, $k_f = 8.0$ and refractive indices typical of soot. The main conclusions of the study are as follows:

1 RDG-FA and ICP predictions of absorption cross sections, and of differential scattering cross sections within the Guinier regime, generally agreed within numerical uncertainties (ca. 10 percent) over the range of the evaluation. Combined with reasonable performance of RDG-FA predictions during recent experimental evaluations (Köylü and Faeth, 1994a, b), these results suggest that RDG-FA theory should replace other approximate theories of soot optical properties, such as Rayleigh scattering and Mie scattering for an equivalent sphere, which have not been very effective during recent experimental and computational evaluations (Köylü and Faeth, 1993, 1994a, b).

2 Present calculations using the ICP approach were not satisfactory at large scattering angles for aggregates having $x_p > 0.25$, based on evaluations using Mie scattering predictions for a spherelike aggregate and well-established RDG-FA predictions in the power-law regime for soot aggregates. This difficulty is due to the truncation errors caused by excessively large ICP cell sizes and might be avoided by dividing each primary particle in an aggregate into several ICP cells. This approach, and other methods of treating large aggregates having large x_p, merit further study.

3 Effects of aggregate size mainly dominate scattering properties in the Guinier regime, while the power-law regime exhibits nearly universal behavior independent of aggregate size. Thus, forward-scattering properties, rather than dissymmetry ratios, provide the most reliable indication of aggregate size for large aggregates where scattering properties are dominated by the power-law regime.

4 Variations of refractive indices over the range typical of current uncertainties about these properties yielded far greater variations of optical cross sections than uncertainties concerning RDG-FA predictions for the aggregate properties considered during the present investigation. Thus, current uncertainties about soot refractive indices are the main limitation for accurate estimates of the continuum radiation properties of soot, and the application of nonintrusive optical diagnostics to measure soot concentrations and structure.

Acknowledgments

One of the authors (T.L.F.) would like to acknowledge scholarship support under the JNICT-CIENCIA BOLSAS Program (BD/860/90-IB). Two of the authors (Ü.Ö.K. and G.M.F.) would like to acknowledge support from the Building and Fire Research Laboratory of the National Institute of Standards and Technology (Grant No. 60NANB1D1175) and the Microgravity Combustion Science Program of NASA (Contract No. NAG3-1245). The collaboration between Instituto Superior Técnico and the University of Michigan is sponsored by AGARD Support Project P-101.

References

Berry, M. V., and Percival, I. C., 1986, "Optics of Fractal Clusters Such as Smoke," *Optica Acta*, Vol. 33, pp. 577–591.

Bohren, C. F., and Huffman, D. R., 1983, *Absorption and Scattering of Light by Small Particles*, Wiley, New York, pp. 477–482.

Borghese, F., Denti, P., Saija, R., Toscano, G., and Sindoni, O. I., 1984, "Multiple Electromagnetic Scattering From a Cluster of Spheres. I. Theory," *Aerosol Sci. Tech.*, Vol. 3, pp. 227–235.

Charalampopoulos, T. T., 1992, "Morphology and Dynamics of Agglomerated Particulates in Combustion Systems Using Light Scattering Techniques," *Prog. Energy Combust. Sci.*, Vol. 18, pp. 13–45.

Chen, H. Y., Iskander, M. F., and Penner, J. E., 1990, "Light Scattering and Absorption by Fractal Agglomerates and Coagulations of Smoke Aerosols," *J. Modern Optics*, Vol. 37, pp. 171–181.

Dalzell, W. H., Williams, G. C., and Hottel, H. C., 1970, "A Light Scattering Method for Soot Concentration Measurements," *Combust. Flame*, Vol. 14, pp. 161–170.

Dobbins, R. A., Santoro, R. J., and Semerjian, H. G., 1990, "Analysis of Light Scattering From Soot Using Optical Cross Sections for Aggregates," *Twenty-Third Symposium (International) on Combustion*, The Combustion Institute, Pittsburgh, PA, pp. 1525–1532.

Dobbins, R. A., and Megaridis, C. M., 1991, "Absorption and Scattering of Light by Polydisperse Aggregates," *Appl. Optics*, Vol. 30, pp. 4747–4754.

Freltoft, T., Kjems, J. K., and Sinha, S. K., 1986, "Power-Law Correlations and Finite Size Effects in Silica Particle Aggregates Studied by Small-Angle Neutron Scattering," *Physical Review B*, Vol. 33, pp. 269–275.

Iskander, M. F., Chen, H. Y., and Penner, J. E., 1989, "Optical Scattering and Absorption by Branched Chains of Aerosols," *Appl. Optics*, Vol. 28, pp. 3083–3091.

Jones, A. R., 1979a, "Electromagnetic Wave Scattering by Assemblies of Particles in the Rayleigh Approximation," *Proc. Roy. Soc. London*, Vol. A366, pp. 111–127.

Jones, A. R., 1979b, "Scattering Efficiency Factors for Agglomerates of Small Spheres," *J. Phys. D: Appl. Phys.*, Vol. 12, pp. 1661–1672.

Jullien, R., and Botet, R., 1987, *Aggregation and Fractal Aggregates*, World Scientific Publishing Co., Singapore, pp. 46–60.

Kerker, M., 1969, *The Scattering of Light*, Academic Press, New York, pp. 414–486.

Köylü, Ü. Ö., and Faeth, G. M., 1992, "Structure of Overfire Soot in Buoyant Turbulent Diffusion Flames at Long Residence Times," *Combust. Flame*, Vol. 89, pp. 140–156.

Köylü, Ü. Ö., and Faeth, G. M., 1993, "Radiation Properties of Flame-Generated Soot," ASME Journal of Heat Transfer, Vol. 115, pp. 409–417.

Köylü, Ü. Ö., and Faeth, G. M., 1994a, "Optical Properties of Overfire Soot in Buoyant Turbulent Diffusion Flames at Long Residence Times," ASME Journal of Heat Transfer, Vol. 116, pp. 152–159.

Köylü, Ü. Ö., and Faeth, G. M., 1994b, "Optical Properties of Soot in Buoyant Laminar Diffusion Flames," ASME Journal of Heat Transfer, Vol. 116, pp. 971–979.

Ku, J. C., 1991, "Correction for the Extinction Efficiency Factors Given in the Jones Solution for Electromagnetic Scattering by Agglomerates of Small Spheres," *J. Phys. D: Appl. Phys.*, Vol. 24, pp. 71–75.

Ku, J. C., and Shim, K.-H., 1992a, "Optical Diagnostics and Radiative Properties of Simulated Soot Agglomerates," ASME Journal of Heat Transfer, Vol. 113, pp. 953–958.

Ku, J. C., and Shim, K.-H., 1992b, "A Comparison of Solutions for Light Scattering and Absorption by Agglomerated or Arbitrarily-Shaped Particles," *J. Quant. Spect. and Rad. Trans.*, Vol. 47, pp. 201–220.

Kumar, S., and Tien, C. L., 1989, "Effective Diameter of Agglomerates for Radiative Extinction and Scattering," *Combust. Sci. Tech.*, Vol. 66, pp. 199–216.

Lin, M. Y., Lindsay, H. M., Weitz, D. A., Ball, R. C., Klein, R., and Meakin, P., 1989, "Universality of Fractal Aggregates as Probed by Light Scattering," *Proc. Roy. Soc. London*, Vol. A423, pp. 71–87.

Martin, J. E., and Hurd, A. J., 1987, "Scattering From Fractals," *J. Appl. Cryst.*, Vol. 20, pp. 61–78.

Mountain, R. D., and Mulholland, G. W., 1988, "Light Scattering From Simulated Smoke Agglomerates," *Langmuir*, Vol. 4, pp. 1321–1326.

Nelson, J., 1989, "Test of a Mean Field Theory for the Optics of Fractal Clusters," *J. Modern Optics*, Vol. 36, pp. 1031–1057.

Purcell, E. M., and Pennypacker, C. R., 1973, "Scattering and Absorption of Light by Nonspherical Dielectric Grains," *Astrophys. J.*, Vol. 186, pp. 705–714.

Puri, R., Richardson, T. F., Santoro, R. J., and Dobbins, R. A., 1993, "Aerosol Dynamic Processes of Soot Aggregates in a Laminar Ethene Diffusion Flame," *Combust. Flame*, Vol. 92, pp. 320–333.

Rudder, R. R., and Bach, D. R., 1968, "Rayleigh Scattering of Ruby-Laser Light by Neutral Gases," *J. Opt. Soc. Amer.*, Vol. 58, pp. 1260–1266.

Sorensen, C. M., Cai, J., and Lee, N., 1992, "Test of Static Structure Factors for Describing Light Scattering From Fractal Soot Aggregates," *Langmuir*, Vol. 8, pp. 2064–2069.

van de Hulst, H. C., 1957, *Light Scattering by Small Particles*, Dover Publications, New York.

Appendix C: Faeth and Köylü (1995)

Combust. Sci. and Tech., 1995, Vol. 108, pp. 207–229
Reprints available directly from the publisher
Photocopying permitted by license only

© 1995 OPA (Overseas Publishers Association)
Amsterdam B.V. Published in The Netherlands
under license by Gordon and Breach Science
Publishers SA
Printed in Malaysia

Soot Morphology and Optical Properties in Nonpremixed Turbulent Flame Environments

G. M. FAETH and Ü. Ö. KÖYLÜ *Department of Aerospace Engineering*
The University of Michigan, Ann Arbor, MI 48109-2118, U.S.A.

(Received June 21, 1995)

ABSTRACT—Motivated by the importance of soot to the emission of particulates and other pollutants from combustion processes, current understanding of soot morphology and optical properties is reviewed, emphasizing nonpremixed flame environments. The understanding of soot morphology in flames has grown rapidly in recent years due to the development of methods of thermophoretic sampling and analysis by transmission electron microscopy (TEM). The results show that soot consists of nearly spherical primary particles, having diameters generally less than 60 nm, which collect into open structured aggregates that are mass fractal objects. Aggregates grow by cluster/cluster aggregation to yield broad aggregate size distributions with the largest aggregates containing thousands of primary particles and reaching dimensions of several μm. The optical properties of soot aggregates generally are not suited for the Rayleigh and Mie scattering approximations which has led to the development of approximate Rayleigh-Debye-Gans (RDG) scattering models for polydisperse fractal aggregate populations of soot. Evaluation of RDG models for conditions where both soot structure and scattering properties are known indicates encouraging agreement between predictions and measurements at both visible and infrared wavelengths, as well as reasonable accuracy for Rayleigh scattering theories in the infrared. Thus, there is potential for nonintrusive measurements of both soot concentrations and structure in flame environments, which should be helpful for diagnosing problems of particulate and pollution emissions from combustion processes. However, additional work is needed to realize this potential, including: reliable solutions of the inverse problem, to yield soot properties from scattering and extinction measurements, must be developed; existing uncertainties about soot refractive indices, including effects of fuel type and flame conditions, must be resolved; and more definitive assessment of the limitations of existing approximate theories for soot optical properties must be obtained.

Key Words: Soot structure, soot scattering, optical diagnostics, soot refractive indices

NOMENCLATURE

C	Optical cross section
d_p	Primary particle diameter
D_f	Mass fractal dimension
$E(\mathrm{m})$	Refractive index function, Im $((\mathrm{m}^2-1)/(\mathrm{m}^2+2))$
$f(qR_g)$	Aggregate form factor, Equation (3)
f_s	Soot volume fraction
f_{VA}, f_{VR}	Soot volume fractions from aggregate and Rayleigh theories
$F(m)$	Refractive index function $\lvert(m^2-1)/(m^2+2)\rvert^2$
$g(kR_g, D_f)$	Aggregate total scattering factor
i	$(-1)^{1/2}$
k	Wave number, $2\pi/\lambda$
k_f	Fractal prefactor

m	Refractive index of soot, $n + i\kappa$
n	Real part of refractive index of soot
N	Number of primary particles per aggregate
N_c	Aggregate size at onset of power-law regime, Equation (8)
$p(N)$	Probability density function of aggregate size
q	Modulus of scattering vector, $2k\sin(\theta/2)$
Q	Volumetric optical cross section
R_g	Radius of gyration of an aggregate
$\bar{R}_{gG}^2$	Mean square radius of gyration for the Guinier regime
$\bar{R}_{gL}^2$	Mean square radius of gyration for the power-law regime
x_p	Primary particle size parameter, $\pi d_p/\lambda$
θ	Angle of scattering from forward direction
κ	Imaginary part of refractive index of soot
λ	Wavelength of radiation
ρ	Density
ρ_{sa}	Ratio of scattering to absorption cross section

Subscripts

a	absorption
d	differential
e	extinction
h	horizontal polarization
ij	incident (i) and scattered (j) polarization direction
s	total scattering
v	vertical polarization

Superscripts

a	aggregate property
p	primary particle property
$(\bar{\ })$	mean value over a polydisperse aggregate population

INTRODUCTION

Practical hydrocarbon-fuled flames generally contain and emit soot, which affects their structure, and their radiation, pollutant and particulate emission properties. Thus, numerous studies of soot processes in flame environments have been reported. In spite of this interest, however, processes of soot nucleation, growth and oxidation in flames are unusually complex and their current understanding is very incomplete. This is unfortunate because anticipated regulations will impose new and more stringent limitations on the emissions of particulates (largely soot) and pollutants from combustion processes, which will be difficult to satisfy without an improved technology base concerning combustion-generated soot. Enhanced experimental capabilities are required to study soot processes in flames, with optical diagnostics being favored because they are convenient and nonintrusive. Thus, the objective of the present paper is to

review current understanding of soot optical properties needed to develop reliable optical diagnostics for soot concentrations and structure.

Most practical hydrocarbon-fueled flames contain soot, which motivates study of soot phenomena as a necessary step toward the development of detailed numerical simulations of combustion processes, i.e., computational combustion. In particular, the significance of soot chemistry for practical flames is highlighted by the impact of soot on the emission of other pollutants. For example, while soot particles themselves constitute an obvious, and generally visible, emission of unburned hydrocarbons, they also can serve as a carrier for other undesirable pollutants like PAH (Lahaye and Prado, 1981). Another interaction is the well-known trade-off between NO_x emissions and the emission of soot particulates and carbon monoxide which limits capabilities to meet requirements for all regulated emissions using existing combustion modification technologies (Bowman, 1992). The correlation between soot and carbon monoxide emissions is well known (Tewarson, 1988), and it is not surprising because both emissions result from incomplete combustion of fuel carbon, e.g., carbon monoxide is the main product of the oxidation of soot and is likely to be present as long as soot is present. This relationship is quantified in Figure 1 for turbulent diffusion flames burning in air at long residence times where both soot and carbon monoxide generation factors (kg of soot and carbon monoxide emitted per kg of fuel carbon burned) are independent of the residence time. It is evident that there is a strong correlation

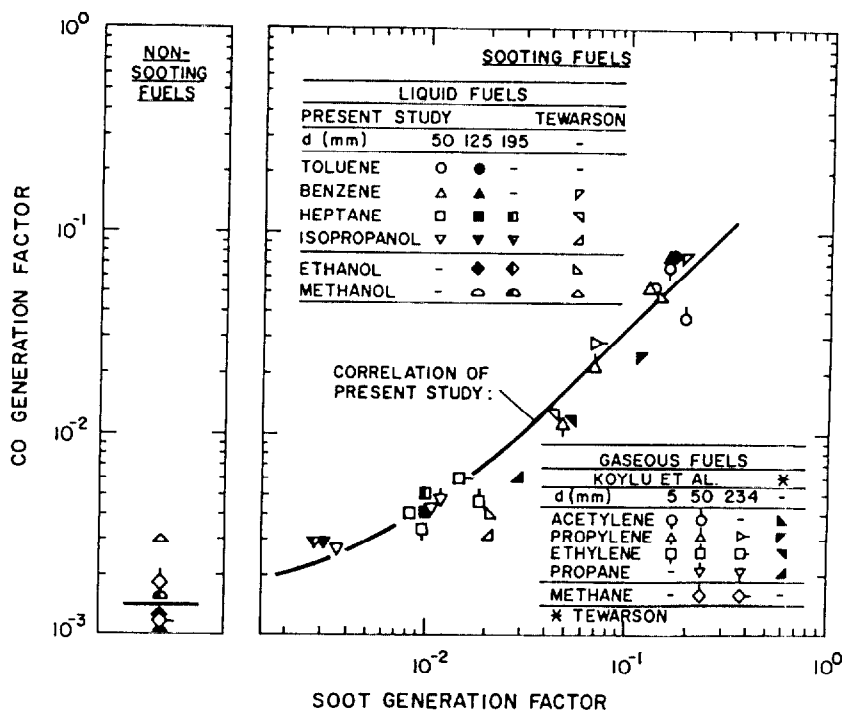

FIGURE 1 Carbon monoxide generation factors as a function of soot generation factors for turbulent diffusion flames in air. Measurements from Köylü and Faeth (1991), Köylü *et al.* (1991) and Tewarson (1988).

between soot and carbon monoxide emissions, relatively independent of fuel type, with heavily sooting fuels emitting roughtly 0.37 kg of carbon monoxide per kg of fuel carbon burned (Köylü and Faeth, 1991). Thus, progress toward understanding pollutant emissions from practical combustion devices clearly will require an improved understanding of soot processes in flames.

Studies of soot nucleation, growth and oxidation in flame environments depend on measurements to a significant degree, due to the complexity of these phenomena. The use of intrusive probes for measurements of soot properties has not been popular, however, due to concern about the disturbances caused by intrusive probes on flame structure. In particular, problems of probes are severe in soot-containing flame environments due to thermophoretic deposition of soot particles on surfaces. This causes probes to clog and to grow soot deposits to sizes that clearly disturb test flames. Thus, nonintrusive optical methods have been emphasized, generally using laser extinction and scattering in the visible to infer soot concentrations and surface areas relevant to heterogeneous soot chemistry. These measurements generally are interpreted based on either the Rayleigh scattering approximation at the small particle limit or the Mie scattering approximation for an equivalent spherical particle. Nevertheless, even early studies raised questions about the general validity of these methods. For example, transmission electron microscopy (TEM) measurements for premixed acetylene, benzene and propane flames showed that soot consisted of small spherical primary particles collected into open structured aggregates having a broad distribution of sizes; additionally, many aggregates were too large for reasonable application of the Rayleigh scattering approximation, and too open structured for proper representation as equivalent compact spheres using the Mie scattering approximation (Erickson *et al.*, 1964; Dalzell *et al.*, 1970; Wersborg *et al.*, 1972). Furthermore, direct measurements at these conditions confirmed these concerns about soot scattering properties: strong forward scattering was observed which is not representative of Rayleigh scattering behavior, while use of the Mie scattering approximation for an equivalent sphere still did not provide an adequate fit of the data (Erickson *et al.*, 1964; Dalzell *et al.*, 1970; Wersborg *et al.*, 1972; Magnussen, 1974). Subsequently, the absence of reliable nonintrusive and intrusive diagnostics for soot has remained as a major impediment to definitive measurements needed to study soot phenomena in flame environments.

Recently, more effective theories of soot optical properties have been developed which appear to have the potential to remove past limitations and provide reliable nonintrusive optical diagnostic for soot properties in flames. These methods are based on the Rayleigh-Debye-Gans scattering approximation while treating soot aggregates as polydisperse collections of mass fractal aggregates (denoted the RDG-PFA scattering approximation in the following), see Jullien and Botet (1987), Martin and Hurd (1987), Dobbins and Megaridis (1991) and Köylü and Faeth, (1992b, c). The objective of this review is to describe the RDG-PFA approach and its evaluation, and to highlight areas where research is needed so that RDG-PFA theory can be exploited to establish reliable nonintrusive optical diagnostics for soot properties. The paper begins with consideration of the structure of soot aggregates and existing evidence for their characterization as mass fractal objects. Soot optical properties are then considered, treating RDG-PFA scattering theory, its evaluation based on scattering measurements, the implications of the theory for measuring soot properties, and issues that still must be resolved to achieve reliable measurements of soot properties.

SOOT PHYSICAL PROPERTIES

General Properties

The physical properties of soot aggregates must be addressed in order to properly model their optical properties; therefore, they will be considered first. Numerous TEM photographs of soot aggregates at various flame conditions have appeared in the literature, all indicating a reasonably generic morphology or structure, see Dalzell *et al.* (1970), Dobbins and Megaridis (1987), Erickson *et al.* (1964), Köylü and Faeth (1992, 1993c), Medalia and Heckman (1969), Nelson (1989), Samson *et al.* (1987) and Wersborg *et al.* (1973) for examples. A typical TEM photograph of soot aggregates appears in Figure 2. These conditions involve soot emitted from long residence time turbulent acetylene/air diffusion flames where emitted soot properties are independent of residence time (Köylü and Faeth, 1992). The aggregates in the photograph are somewhat large, due to the long residence time available for aggregation, but otherwise they are representative of soot found in flame environments.

Quantitative examination of soot aggregates generally indicates that the aggregates consist of nearly spherical primary particles having relatively uniform diameters at

FIGURE 2 TEM photograph of typical soot aggregates emitted from turbulent acetylene/air diffusion flames. From Köylü and Faeth (1992).

a given flame condition. The primary particles tend to be somewhat merged, rather than just touching at points, due to soot growth subsequent to the joining of adjacent primary particles. Nevertheless, models of soot aggregates as monodisperse spherical primary particles that just touch one another are a reasonable approximation of TEM observations, and this approximation generally has been adopted for studies of soot optical properties.

As seen in Figure 2, soot aggregates have branched and open structures with a large variation of the number of primary particles per aggregate even at a given flame condition. Thus, the open structure of soot aggregates does not suggest that their optical properties can be modeled effectively by treating them as equivalent spherical objects having the same volume. Additionally, the largest aggregates have dimensions of several μm, exceeding the wavelength of light in the visible portion of the spectrum, which raises questions about the use of the small particle (Rayleigh) scattering limit to treat their optical properties. As discussed earlier, these concerns are amply justified by observations of soot scattering properties that were not consistent with either of these scattering approximations.

Other measurements of the physical properties of soot aggregates relate to their density, porosity and composition. Not surprisingly, these properties generally are found to be similar to carbon blacks with two major exceptions: soot during the last stages of oxidation has significant porosity, even extending to the presence of hollow cenospheres; and soot from some internal engine combustion processes (like diesel engines at heavily sooting conditions) contain high levels of volatile matter (Lahaye and Prado, 1981). Otherwise, soot densities are typical of carbon blacks, e.g., values in the range 1820–2050 kg/m^3, see Dobbins *et al.* (1993) and references cited therein. Soot aggregates also appear to be relatively nonporous with measurements of surface area compatible with shapes observed on TEM photographs except as noted earlier. Finally, soot mainly consists of carbon. For example, soot emitted from long residence time turbulent diffusion flames (involving the combustion of toluene, benzene, acetylene, propylene and propane burning in air) had the following elemental mole ratio ranges: C:H of 8.3–18.3, C:O of 58–109, C:N of 292–976. However, the presence of volatiles, as well as annealing processes at high temperatures, can affect concentrations of noncarbon substances, and possibly optical properties like soot refractive indices as well. Finally, TEM microstructure studies showing somewhat different structure near the core and at the surface of primary particles, as well as the formation of pores and cenospheres at high levels of soot oxidation, raise questions about the uniformity of primary particle properties (Lahaye and Prado, 1981). Thus, while models of soot optical properties generally adopt approximations of uniform primary particle properties, and ignore potential variations of refractive indices with fuel type and flame conditions, these approximations clearly merit additional scrutiny.

Primary Particle Size

Recent measurements of soot aggregate properties in flame environments have employed thermophoretic sampling and analysis by TEM. This is reasonably reliable because effects of aggregate size bias are fortuitously rather small for thermophoretic sampling, assuring representative statistics (Rosner *et al.*, 1991), while TEM analysis is

not dependent upon questionable approximations about the optical properties of soot. This work has included both the fuel-rich and fuel-lean regions of laminar diffusion flames (Dobbins and Megaridis, 1987; Megaridis and Dobbins, 1990; Köylü and Faeth, 1993c; Samson *et al.*, 1987) as well as soot emitted from long residence time turbulent diffusion flames (Köylü and Faeth, 1992). Some typical structure properties of soot aggregates, including primary particle diameters, are summarized in Table I for soot emitted from long residence time turbulent flames of various fuels burning in air. This soot is representative of soot emitted from combustion processes, and also is of interest for evaluation of predictions of soot optical properties to be discussed later.

Primary particle diameters at a given flame condition are nearly monodisperse. For example, the standard deviations of the primary particles listed in Table I were in the range 17–25% of the mean primary particle diameter. Primary particle size distributions can be fitted accurately to log normal distribution functions but due to their small standard deviations are approximated reasonably well by Gaussian functions (Köylü and Faeth, 1992). Mean primary particle diameters vary with flame condition and fuel type but diameters less than 60 nm generally are observed in flame environments, with the largest diameters associated with heavily sooting fuels, see Table I. This implies primary particle size parametes, $x_p < 0.4$ for $\lambda > 500$ nm, so that it is reasonable to assume that individual primary particles behave like Rayleigh scattering particles, i.e., total scattering and absorption cross sections are within 1 and 5%, respectively, of estimates based on the Rayleigh scattering approximation for individual primary particles (Köylü and Faeth, 1993a).

Aggregate Properties

Soot aggregates are small near the soot inception point but they aggregate rapidly with $\bar{N}$ in the range 200–600 for soot emitted from turbulent diffusion flames, see Table I. Unlike primary particle diameters, however, aggregate size distributions are quite broad, with standard deviations comparable to $\bar{N}$ and large values of the second moment of the distribution, $\bar{N}^2/(\bar{N})^2$, e.g., values up to 3.3 have been observed for soot emissions. Nevertheless, aggregate size distributions are reasonably represented by

TABLE I

Structure of soot emitted from long residence time turbulent diffusion flames[a]

Fuel	$\bar{d}_p$ (nm)	$\bar{N}$	$\bar{N}^2/(\bar{N})^2$	D_f	$(\bar{R}_g^2)^{1/2}$ (nm)
Toluene	51	526	3.23	1.73	672
Acetylene	47	417	3.20	1.79	481
Benzene	50	552	2.71	1.71	686
Propylene	41	460	2.61	1.75	431
Ethylene	32	467	2.42	1.73	376
n-Heptane	35	260	2.05	1.73	299
Propane	30	364	2.56	1.74	305
Isopropanol	31	255	2.61	1.70	275

[a] From Köylü and Faeth (1992), r.m.s. value of R_g found assuming $D_f = 1.81$ and $k_f = 8.1$ from Köylü and Faeth (1993b).

a log normal distribution function (Dobbins and Megaridis, 1987; Köylü and Faeth, 1992; Lahaye and Prado, 1981). Based on the properties of this distribution function, 95% of the soot aggregates summarized in Table I would contain 30–1800 primary particles. This means that the optical properties of aggregates are complex in the visible—ranging from Rayleigh scattering for small aggregates, where each primary particle essentially scatters light independently, to significant interactions between scattering from the individual primary particles of large aggregates.

Numerous recent evaluations have shown that flame-generated soot aggregates exhibit mass fractal-like behavior with a Hausdorf or fractal dimension, $D_f < 2$, even when the number of primary particles in an aggregate is small (Jullien and Botet, 1987; Köylü and Faeth, 1992, 1993c; Megaridis and Dobbins, 1990; Samson *et al.*, 1987). Mountain and Mulholland (1988) have carried out stochastic simulations of the aggregation process finding that cluster/cluster aggregation yields properties similar to soot aggregates, with the progressive buildup of aggregate size leading naturally to scaling relationships representative of fractal behavior. The fractal dimension has important implications for soot optical properties because the scattering per primary particle continues to grow as the size of the aggregate increases for $D_f > 2$ but reaches a constant saturated value for $D_f < 2$ (Berry and Percival, 1986; Dobbins and Megaridis, 1991; Nelson, 1989).

The mass fractal approximation implies the following relationship between the primary particle diameter, the number of primary particles, and the radius of gyration of the aggregate (Jullien and Botet, 1987):

$$N = k_f(R_g/d_p)^{D_f} \tag{1}$$

where k_f is the fractal prefactor and the aggregates are assumed to consist of monodisperse nonoverlapping primary particles. Results summarized in Table I indicate that the fractal dimensions of soot emitted from flames are relatively independent of fuel type. Recent studies of soot within laminar diffusion flames, where aggregates are still relatively small, yield fractal dimensions in the range 1.7–1.8 as well (Köylü and Faeth, 1993c; Megaridis and Dobbins, 1990). Fractal prefactors have received less attention, however, recent determinations based on both TEM and scattering measurements for various flame conditions suggest values in the range 7.0–9.2 (Köylü and Faeth, 1992, 1993b; Puri *et al.*, 1993). Thus, unlike other aggregate structure properties, D_f and k_f appear to be relatively durable properties of soot in flame environments.

SOOT OPTICAL PROPERTIES

General Description

In view of the difficulties encountered when using the Rayleigh and Mie scattering approximations for soot optical properties, recent work has focused on the Rayleigh-Debye-Gans (RDG) scattering approximation. The RDG approximation implies that effects of multiple- and self-scattering are ignored so that the electromagnetic fields within each primary particle are the same as the incident field, and differences between the phase shift of light scattered from various points within a particular primary

particle are ignored. This requires that both $|m-1| \ll 1$ and $2x_p|m-1| \ll 1$ (Kerker, 1969; van de Hulst, 1957; Bohren and Huffman, 1983), which is questionable for soot aggregates due to the relatively large refractive indices of soot. In addition, recent computational studies suggest significant effects of multiple scattering for large soot aggregates, similar to those summarized in Table I, see Berry and Percival (1986), Chen *et al.* (1990), Ku and Shim (1992) and Nelson (1989). Thus, the RDG scattering approximation requires evaluation with experiments as discussed in the following.

Major assumptions concerning soot physical properties, used in RDG scattering theories, can be summarized as follows: spherical primary particles having constant diameter, primary particles just touch one another, uniform refractive indices, log normal aggregate size distributions and the aggregates are mass fractal-like objects that satisfy Equation (1) with constant values of D_f and k_f.

RDG-PFA Theory

The RDG-PFA scattering theory is based on methods described by Freltoft *et al.* (1986), Jullien and Botet (1987), Lin *et al.* (1989), Martin and Hurd (1987) and Dobbins and Megaridis (1991) for a single aggregate, as extended by Köylü and Faeth (1993b) for polydisperse aggregate populations. Only the main results of RDG-PFA scattering theory will be summarized in the following, original sources should be consulted for details.

Under the present assumptions, primary particles satisfy the Rayleigh scattering approximation, yielding the following expressions for their optical properties (Bohren and Huffman, 1983; Kerker, 1969):

$$C_a^p = 4\pi x_p^3 E(m)/k^2, \quad C_s^p = 8\pi x_p^6 F(m)/(3k^2), \quad C_{vv}^p = x_p^6 F(m)/k^2 \tag{2}$$

In Equation (2) and the following equations, subscripts for differential scattering cross sections denote the direction of polarization vectors with respect to the scattering plane defined by the light source, the soot aggregate and the observer; v and h denote polarization vectors normal and parallel to this plane, respectively; and the first and second subscripts refer to incident and scattered light, respectively.

The treatment of aggregate optical properties begins with the scattering cross sections for a single fractal aggregate under the RDG approximation (Kerker, 1969):

$$C_{vv}^a(\theta) = C_{hh}^2(\theta)/\cos^2\theta = N^2 C_{vv}^p f(qR_g) \tag{3}$$

The form factor, $f(qR_g)$, is expressed as follows in the small angle (Guinier) and large angle (power-law) regimes (Freltoft *et al.*, 1986; Jullien and Botet, 1987; Lin *et al.*, 1989; Martin and Hurd, 1987):

$$f(qR_g) = \exp(-(qR_g)^2/3), \quad \text{Guinier regime} \tag{4}$$

$$f(qR_g) = (qR_g)^{-D_f}, \quad \text{power-law regime} \tag{5}$$

Following Dobbins and Megaridis (1991), the boundary between the Guinier and power-law regimes is taken to be $(qR_g)^2 = 3D_f/2$, chosen to match the value and

derivative of $f(qR_g)$ where the two regimes meet. The total scattering cross section then becomes:

$$C_s^a = N^2 C_s^p g(\lambda, R_g, D_f) \tag{6}$$

where $g(\lambda, R_g, D_f)$ has different forms if the power-law regime is reached for $\theta \leq 180°$ or not, see Köylü and Faeth (1993b) for these expressions.

The mean optical cross sections of populations of randomly oriented polydisperse aggregates are found by integrating over all aggregate sizes, as follows:

$$\bar{C}_j^a = \int_{N=1}^{\infty} C_j^a(N) p(N) dN; \quad j = pp, s, a \tag{7}$$

where $p(N)$ is the aggregate size distribution function. Equation (7) must be integrated numerically when scattering extends over both the Guinier and power-law regimes. However, simple closed form expressions are possible when all aggregates are either in the Guinier ($p(N) \ll 1$ for $N \geq N_c$) or power-law ($p(N) \ll 1$ for $N \leq N_c$), where

$$N_c = k_f (3D_f/(2q^2 d_p^2))^{D_f/2} \tag{8}$$

This yields:

$$\bar{C}_{vv}^a(\theta)/C_{vv}^p = \bar{N}^2 \exp(-q^2 \bar{R}_{gG}^2/3), \quad \text{Guinier regime} \tag{9}$$

$$\bar{C}_{vv}^a(\theta)/C_{vv}^p = \bar{N} k_f (q d_p)^{-D_f} = \bar{N}^2 (q^2 \bar{R}_{gL}^2)^{-D_f/2}, \quad \text{power-law regime} \tag{10}$$

where expressions for $\bar{R}_{gG}^2$ and $\bar{R}_{gL}^2$ can be found in Köylü and Faeth (1993c). The general expression for the total scattering cross section of a polydisperse aggregate population is

$$\bar{C}_s^a = C_s^p \int_{N=1}^{\infty} N^2 g(\lambda, R_g, D_f) p(N) dN \tag{11}$$

which must be numerically integrated in both scattering regimes. The absorption cross section is evaluated quite simply, as follows:

$$\bar{C}_a^a = \bar{N} C_a^p \tag{12}$$

Evaluation of RDG-PFA Predictions

Existing computer simulations of the optical properties of soot do not provide an adequate basis for evaluating approximate scattering theories because they involve either fundamentally accurate solutions for small aggregates where effects of multiple- and self-induced scattering are small, or approximate solutions having uncertain accuracy for the large soot aggregates of interest for practical flames (Köylü and Faeth, 1993a).

The predictions of RDG-PFA theory have been evaluated for conditions where both soot structure and scattering properties were measured. These evaluations included the large soot aggregates emitted from long residence time turbulent diffusion flames (see Table I for the properties of this soot), as well as relatively small soot aggregates found at fuel-rich conditions within laminar ethylene and acetylene/air diffusion flames

(Köylü and Faeth, 1993b, c). This range of conditions was studied in order to adequately cover the Guinier (for small aggregates) and power-law (for large aggregates) regimes. Measured volumetric optical cross sections were converted to optical cross sections, and vice versa, assuming that absorption is not affected by aggregation, which follows from Equation (12) based on RDG theory, but also is accurate within experimental uncertainties for scattering properties (ca. 20%) based on more complete scattering theories allowing for effects of multiple- and self-induced scattering (Chen *et al.*, 1990; Farias and Carvalho, 1993; Iskander *et al.*, 1989; Köylü and Faeth, 1993a). This approximation yields:

$$\bar{C}_j^a(\theta) = \pi \bar{N} d_p^3 \bar{Q}_j^a(\theta)/(6 f_s), \quad j = pp, s, a \tag{13}$$

where $\bar{N}$ and d_p were found from TEM measurements and f_s from extinction and scattering measurements. Finally, all computations employed the refractive indices of Dalzell and Sarofim (1969) in order to be consistent with earlier work (Köylü and Faeth, 1992, 1993a), and because they were preferred based on scattering measurements to be discussed later.

Measured and predicted values of $\bar{Q}_{vv}^a(\theta)$ are plotted as a function of qd_p in Figure 3 for soot emitted from long residence time flames fueled with acetylene, propylene, ethylene and propane. The substantial departure from Rayleigh scattering behavior (where $\bar{Q}_{vv}^a(\theta)$ would be independent of qd_p) is evident, with forward scattering roughly 100 times larger than back scattering for all the fuels. In fact, the large size of the aggregates prevented fully reaching the Guinier regime even though scattering angles as small as 5° were considered, however, the measurements provide an extended range within the power-law regime. Within this regime Equations (10) and (13) yield D_f and k_f from the slope and magnitude of plots of $\bar{Q}_{vv}^a(\theta)/\bar{Q}_{vv}^p$ as a function of qd_p from Figure 3. These values are summarized in Table II for the four fuels, along with values found from TEM measurements of soot structure from Köylü and Faeth (1992) and Puri *etal.* (1993). The scattering measurements are seen to be in good agreement with the TEM measurements.

Two sets of predictions based on RDG-PFA theory are illustrated in Figure 3, one set entirely based on TEM measurements of soot structure, and the other set based on refitting the higher moments, $\bar{N}^2/(\bar{N})^2$, of the aggregate size distribution functions in order to best fit the scattering predictions and measurements, keeping all other structure properties the same. This was done because the higher moment was not found very accurately during the TEM structure measurements (experimental uncertainties were only less than 40–90%) due to the broad size distribution of aggregates (Köylü and Faeth, 1992). Predictions based on refitted structure properties are seen to be in good agreement with the measurements, while the required changes of the higher moments of the size distribution functions were within experimental uncertainties. Evaluation of predictions of extinction at 632.8 and 1152 nm also was reasonably satisfactory with differences between predictions and measurements less than 18%.

An obvious weakness of the evaluation of predictions using large soot aggregates is that the aggregates were to large to reach the Guinier regime. This was rectified during subsequent work considering relatively small soot aggregates observed at fuel-rich conditions in laminar flames (Köylü and Faeth, 1993c). In this case, the predictions based on TEM structure measurements agreed with the scattering measurements

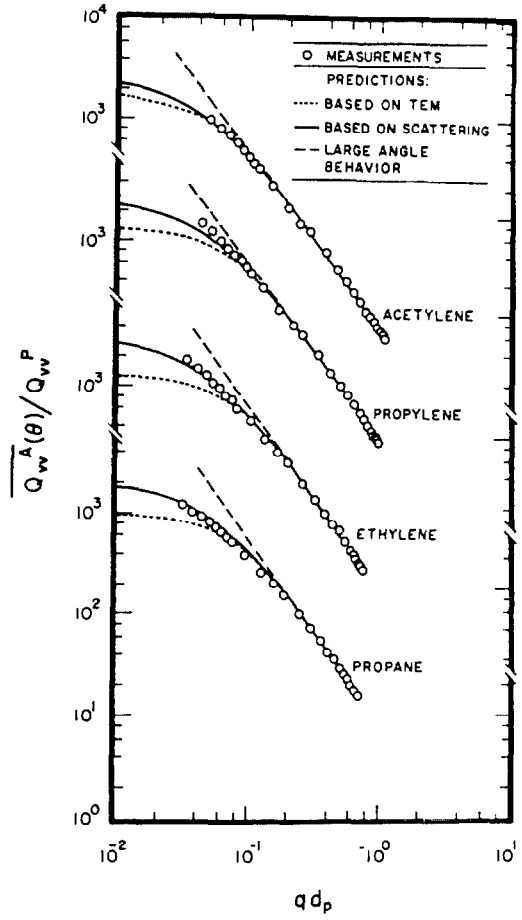

FIGURE 3 Measured and predicted volumetric vv cross sections as a function of the modulus of the scattering vector for soot emitted from turbulent diffusion flames in air. From Köylü and Faeth (1992).

within 37%, while refitting the higher moments of the aggregate size distribution function, within their experimental uncertainties, yielded results similar to the fitted predictions illustrated in Figure 3.

A final test of the RDG-PFA predictions involved the consideration of scattering patterns. Typical results are illustrated in Figures 4 and 5 for the smallest and largest soot aggregates studied, in order to indicate the range of behavior observed. Predictions on these figures are seen to be in reasonably good agreement with the measurements. Comparing the $\bar{C}^a_{vv}(\theta)$ plotted in Figures 4 and 5 illustrates the effect of aggregate size on scattering patterns, with the very strong forward scattering observed for large aggregates evolving toward a uniform distribution of scattering, typical of Rayleigh scattering (see Equation (2)), as the aggregates become smaller. The variation of the slope of $\bar{C}^a_{vv}(\theta)$ at angles in the range 45–135° often is used for nonintrusive measurements of aggregate size (Dobbins *et al.*, 1990), e.g., dissymmetry ratios, $\bar{C}^a_{vv}(45°)/\bar{C}^a_{vv}(135°)$,

TABLE II

Soot aggregate fractal properties from thermophoretic sampling and light scattering measurements[a]

Fuel	Acetylene	Propylene	Ethylene	Propane
Fractal Dimension, D_f:				
Thermophoretic sampling	1.79	1.75	1.73	1.74
Light scattering	1.85	1.84	1.83	1.77
Fractal Prefactor, k_f:				
Thermophoretic sampling[b]	9.2	–	8.6	–
Light scattering[c]	7.0	8.6	8.8	8.0

[a] For soot emitted from long residence time turbulent diffusion flames, from Köylü and Faeth (1993b).
[b] From Puri *et al.* (1993).
[c] Based on the soot refractive indices of Dalzell and Sarofim (1969).

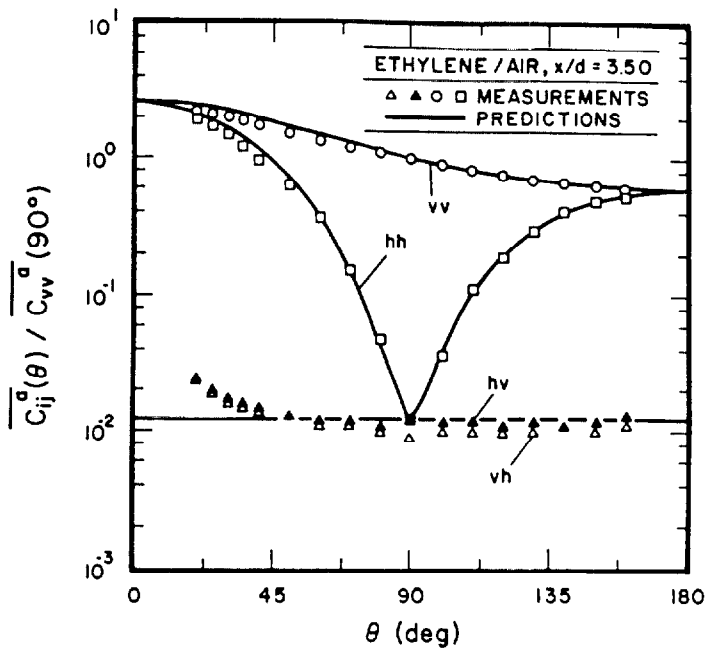

FIGURE 4 Measured and predicted angular soot scattering patterns for small soot aggregates in ethylene/air diffusion flames. From Köylü and Faeth (1993c).

are seen to be larger for the large soot aggregates of Figure 4 than the small soot aggregates of Figure 5. However, this approach must be used with caution: dissymmetry ratios for angles in the range 45–135° are not very sensitive to aggregate size for $\bar{N} > 100$ (Köylü and Faeth, 1993a), and become insensitive to aggregate size once again for small aggregates approaching the small particle (Rayleigh) scattering limit. In contrast, effects of aggregate size are most evident at small scattering angles ($\theta < 45°$), which provides a more reliable regime for nonintrusive measurements of aggregate size.

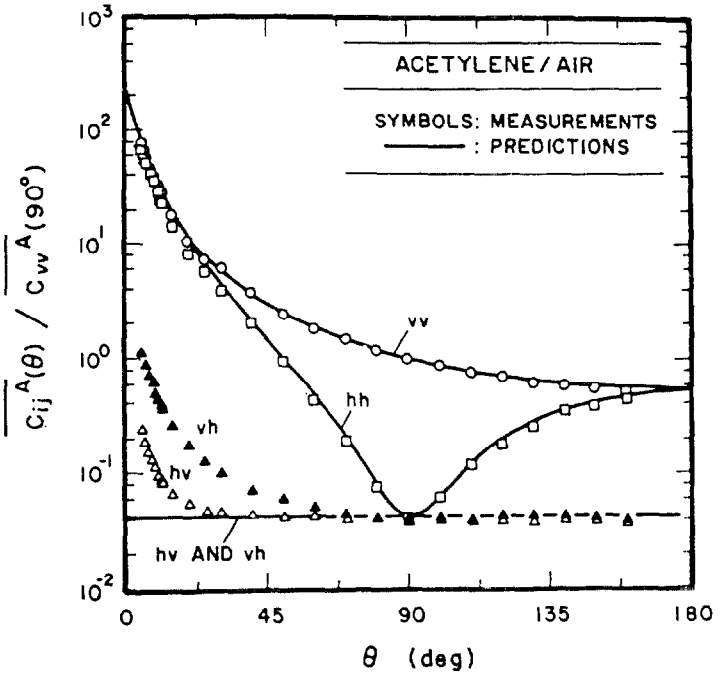

FIGURE 5 Measured and predicted angular scattering patterns for large soot aggregates in acetylene/air diffusion flames. From Köylü and Faeth (1993b).

Results at other test conditions were similar to the findings illustrated in Figures 3–5. Thus, RDG-PFA theory yielded predictions that agreed with measurements, within experimental uncertainties, over the following ranges: x_p of 0.128–0.330, $\bar{N}$ of 31–467, $\bar{N}^2/(\bar{N})^2$ of 1.82–3.23, $\bar{C}^a_{vv}(0°)/\bar{C}^a_{vv}(180°)$ of 10–1000 and values of the albedo of 0.06–0.29.

Implications of Soot Scattering Properties

Further evaluation of the RDG-PFA theory for soot optical properties would be desirable. In particular, the studies of Köylü and Faeth (1993a, b) involved a limited range of soot aggregate properties and problems of adequately measuring the higher moments of the aggregate size distribution using TEM compromised the evaluation to some extent. Uncertainties also remain about effects of primary particles, nonuniformity of primary particle physical properties, and variations of fractal properties and refractive indices as a function of fuel type and flame condition. Some of these issues can be addressed by computer simulations using more advanced theories than the RDG approximation, e.g., the methods developed by Borghese *et al.* (1984) and Iskander *et al.* (1989). Nevertheless, the evaluation of RDG-PFA scattering theory has been reasonably promising thus far; therefore, it is worthwhile to exploit the theory to gain insight about potential nonintrusive optical diagnostics for soot properties.

Laser extinction often is used to measure soot concentrations in flame environments, with the measurements interpreted based on the small-particle (Rayleigh) scattering

approximation, see Faeth *et al.* (1989), Köylü and Faeth (1993a), Santoro *et al.* (1983), Tien and Lee (1982), and references cited therein. Under the Rayleigh scattering approximation, scattering is negligible so that extinction and absorption are essentially identical and extinction measurements are proportional to the volume fraction of soot in the optical path through Equation (1). Nevertheless, the differential scattering cross sections illustrated in Figures 3–5 indicate significant scattering levels for large soot aggregates so that attributing all the extinction to absorption can overestimate soot volume fractions significantly.

The effect of the departure of soot aggregate scattering from the Rayleigh scattering limit on laser extinction measurements of soot volume fractions is illustrated in Figure 6. This is a plot of the ratio of the total scattering to absorption cross sections, $\bar{\rho}_{sa}$, based on RDG-PFA theory, as a function of mean aggregate size (Köylü and Faeth, 1992). Results are illustrated for two different wavelengths (note the different scales of the ordinates of the two plots): 632.8 nm, which is representative of wavelengths used to find soot volume fractions from laser extinction measurements, and 2000 nm which is representative of wavelengths where radiant emission from flames is relatively large. The results are presented as $\bar{\rho}_{sa}E(m)/F(m)$ to avoid complications of the uncertainties of soot refractive indices, this parameter also is proportional to the fractional error incurred by using the Rayleigh scattering approximation to find soot volume fractions from laser extinction measurements. These plots have been constructed using the soot properties of Table I, except for varying $\bar{N}$, with the data symbols on each plot indicating behavior for the actual $\bar{N}$ of each fuel.

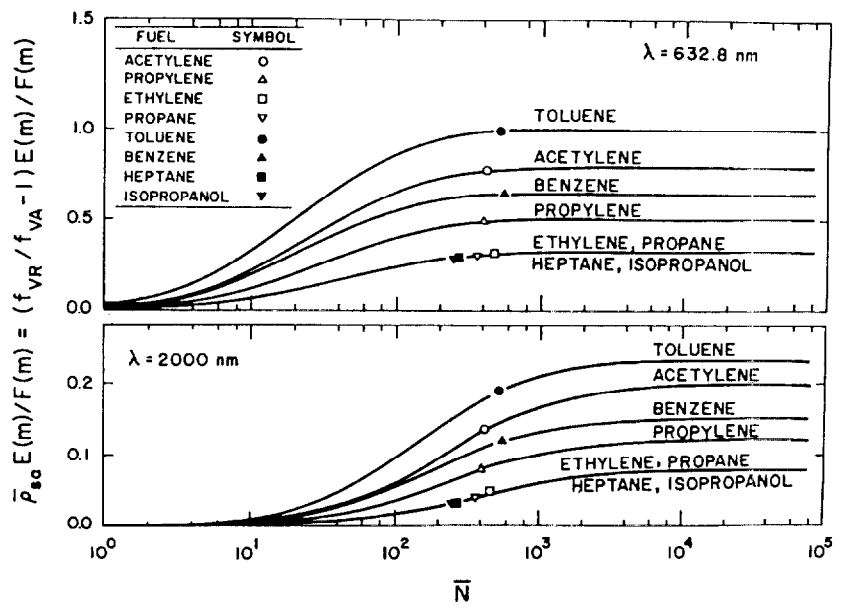

FIGURE 6 Ratios of scattering to absorption cross sections as a function of aggregate size for soot aggregates. From Köylü and Faeth (1992).

Results illustrated in Figure 6 show the transition between nearly Rayleigh scattering behavior for small aggregates, $\bar{\rho}_{sa} \approx 0$, to conditions where $\bar{\rho}_{sa}$ becomes independent of aggregate size (or saturated scattering) for large aggregates. Saturated scattering is characteristic of scattering from fractal objects having $D_f < 2$; for $D_f > 2$, $\bar{\rho}_{sa}$ would continue to increase as $\bar{N}$ increases (Berry and Percival, 1986; Dobbins and Megaridis, 1991). The variation of $\bar{\rho}_{sa}$ with fuel type and wavelength seen in Figure 6 is caused by variations of primary particle size parameters, e.g., $\bar{\rho}_{sa} \sim x_p^{3-D_f}$ within the saturated scattering regime (Dobbins and Megaridis, 1991). The large soot aggregates summarized in Table I approach saturated scattering at 632.8 nm, and are intermediate between Rayleigh and saturated aggregate scattering at 2000 nm. The additional scattering from aggregates causes soot volume fractions for these large aggregates to be significantly overestimated when laser extinction measurements are analyzed using the Rayleigh scattering approximation. For example, noting that $F(m)/E(m)$ is of order unity, as discussed later, such measurements at 632.8 nm overestimate soot volume fractions by nearly a factor of two for a heavily sooting material like toluene and by roughly 30% for lightly sooting materials like ethylene, propane, n-heptane and isopropanol. Thus, it appears that some consideration of scattering is required for laser extinction measurements of soot volume fractions in the visible, unless evidence is available that both primary particle diameters and aggregate sizes are small.

Effects of scattering on laser extinction measurements of soot volume fractions become smaller at longer wavelengths, as seen from the results at a wavelength of 2000 nm in Figure 6. This is illustrated more directly in Figure 7, where $\bar{\rho}_{sa}$ is plotted as a function of wavelength for the large soot aggregates summarized in Table I. It is seen

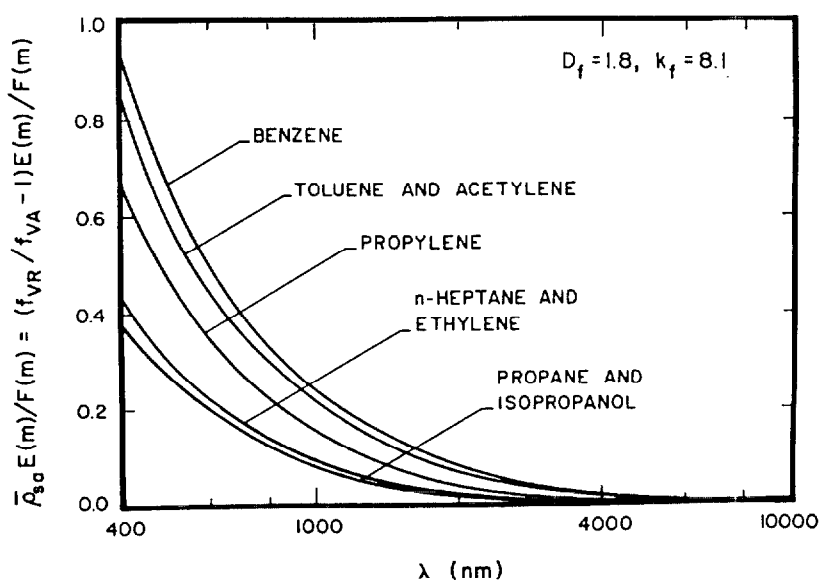

FIGURE 7 Mean ratios of scattering to absorption cross sections as a function of wavelength for soot aggregates from turbulent diffusion flames in air. From Köylü and Faeth (1993b).

that $\bar{\rho}_{sa}$ progressively decreases with increasing wavelength, reaching values less than 20% for wavelengths greater than 2000 nm, even for very large toluene soot aggregates. Thus, extinction measurements in the infrared offer a simple means of measuring soot volume fractions without the complications of simultaneous measurements of scattering or soot structure, as long as wavelengths are chosen to avoid effects of absorption from infrared gas bands. Additionally, results of Figures 6 and 7 suggest relatively small effects of scattering on the radiation properties of soot aggregates in flame environments, where the significant wavelengh range is in the infrared.

Nonintrusive optical measurements of soot structure and concentration properties impose somewhat different requirements. For example, it has just been noted that soot concentrations are most easily measured at the Rayleigh scattering conditions, howvers, these same conditions provide relatively little information about soot structure. In particular, primary particles scatter essentially independently in the Rayleigh scattering regime; therefore, no inforamtion about aggregate properties can be found at these conditions. Additionally, C_{vv}^{p} is independnet of scattering angle from Equation (2) so that dissymmetry ratios are unity and independent of primary particle diameter. Only the primary particle diameter is available, based on absolute scattering measurements to find $\bar{\rho}_{sa}$ and then using Equation (2), e.g. $x_p = (3\bar{\rho}_{sa}E(m)/(2F(m)))^{1/3}$.

Similar to the Rayleigh scattering regime, the saturated scattering regime, which is dominated by power-law scattering behavior, has limited capabilities for inferring soot structure properties. At these conditions, the slope of plots of $\bar{Q}_{vv}^{a}(\theta)$ as a function of qd_p yields the fractal dimension but this property is relatively universal for soot aggregates in any event. A corollary of this behavior is that dissymmetry ratios are relatively independent of aggregate size, as discussed in connection with Figures 4 and 5. Thus, direct measurements of $\bar{C}_{vv}^{a}(\theta)$ and $\bar{C}_{a}^{a}$ can yield d_p through Equations (10) and (12) if the fractal properties D_f and k_f can be reliably prescribed, implying structure information and absolute scattering measurement requirements somewhat analogous to the Rayleigh scattering regime.

Scattering in the small-angle (Guinier) regime provides conditions where soot aggregate structure can be found using nonintrusive optical methods. Dobbins *et al.* (1990) have considered this inverse problem using RDG-PFA theory, however, their polydisperse aggregate considerations were limited to conditions where all aggregates were in the Guinier regime, see Köylü and Faeth (1993b, c) for a discussion of this issue. These conditions probably were not met for the ethylene soot aggregates that were measured by Dobbins *et al.* (1990). In particular, they found values of $\bar{\rho}_{sa}$ up to 30% at a wavelength of 632.8 nm, which would imply nearly saturated behavior, with scattering dominated by the power-law regime, based on the results for ethylene soot illustrated in Figure 6. Thus, while Dobbins *et al.*(1990) provide an interesting example of inferring soot structure properties from scattering measurements based on RDG-PFA theory, their conclusions should be considered with caution until the impact of power-law scattering on their results has been assessed.

Köylü and Faeth (1993b, c) also report results where soot structure properties were inferred from soot scattering properties, as discussed earlier. However, this was a mixed approach where scattering and TEM measurements were combined in order to optimize the higher-order moments of the aggregate size distribution function. Thus, algorithms to infer the properties of the soot aggregate size distribution function from

extinction and scattering measurements in the Guinier regime must still be developed and evaluated. As discussed earlier, primary particle diameters can be found from scattering measurements in the Rayleigh and power-law regimes; an approch to yield primary particle diameters in the Guinier regime clearly is of interest as well.

Refractive Indices

Computations of soot optical properties require accurate refractive indices for their wavelength range of interest, typically 0.1–10 μm, in order to treat optical diagnostics and continuum radiation for soot. In particular, $E(m)$ is needed for estimates of absorption, $F(m)$ is needed for estimates of scattering and the ratio $F(m)/E(m)$ is needed for estimates of the importance of scattering as well as for nonintrusive determinations of primary particle diameters using RDG-PFA and Rayleigh scattering theories. Thus, current understanding of soot refractive indices is briefly reviewed in the following, see Chang and Charalampopoulos (1990), Charalampopoulos (1992), Tien and Lee (1982), and Viskanta and Mengüc (1987), and references cited therein, for a more complete discussion.

Early determinations of soot volume fractions involved *ex situ* reflection coefficient measurements from compressed soot samples removed from flames, see Dalzell and Sarofim (1969), Felske *et al.* (1984) and references cited therein. These approaches were questioned, however, based on potential modification of soot properties by sampling and compression, as well as effects of surface roughness and voids on reflectance properties that are difficult to evaluate (Felske *et al.*, 1984; Lee and Tien, 1980; Charalampopoulos, 1992). Thus, most recent work has involved *in situ* measurements of extinction and scattering within both premixed and nonpremixed (diffusion) flames, see Chang and Charalampopoulos (1990), Charalampopoulos (1992), Lee and Tien (1980), Roessler and Faxvog (1980) and Vaglieco *et al.* (1990) for examples. Unfortunately, these determinations did not involve characterization of soot structure and employed Rayleigh and Mie scattering approximations whose accuracy is questionable based on results discussed here. Additionally, the extinction and scattering measurements must be supplemented by other information in order to find refractive indices. Three methods for providing auxiliary information have been used: Drude-Lorentz dispersion models for the wavelength dependence of soot refractive indices (Dalzell and Sarofim, 1969; Lee and Tien, 1980), Kramers-Krönig relationships based on the causality requirements of inputs and outputs of passive physical systems (Chang and Charalampopoulos, 1990; Charalampopoulos, 1992), and results based on other measurements that ultimately rest on either dispersion models or Kramers-Krönig relationships (Vagiieco *et al.*, 1990). Unfortunately, there are considerable differences of empirical dispersion model constants among the various investigations while use of Kramers-Krönig relationships invariably requires uncertain extrapolations of soot refractive indices to ranges that can not be measured because the wavelength range, $0-\infty$, is involved in these computations. Thus, there are significant uncertainties about all existing measurements of soot refractive indices, which constitutes a major impediment to proper characterization of soot optical properties.

Results concerning the effects of fuel type and flame condition on soot refractive indices are somewhat contradictory. Early work suggested that soot refractive indices

were relatively independent of fuel type and did not find significant effects of flame condition, including effects of H/C ratio and temperature (Tien and Lee, 1992). However, later work reported significantly lower refractive indices when the soot contained high levels of volatile matter, as well as effects of annealing of soot in the high-temperature post-flame region of premixed flames where it was hypothesized that refractive indices increased due to removal of hydrogen near the surface of the soot particles by reactive effects (Charalampopoulos, 1992). These effects are difficult to resolve, however, due to the fundamental limitations of the methods used to measure soot volume fractions, discussed earlier. For example, continued aggregation of soot in post flame gases can easily be interpreted as an increase in soot refractive indices when using questionable Rayleigh and Mie scattering approximations to estimate soot optical properties.

Typical measurements of the real and imaginary parts of the refractive indices of soot, extending over the wavelength range 0.1–20 μm, are illustrated in Figure 8. The following measurements are shown on the figure: acetylene soot based on the reflectance of acetylene soot pellets and a dispersion model (Dalzell and Sarofim, 1969); polystyrene and plexiglass soot based on *in situ* extinction measurements in diffusion flames and a dispersion model (Lee and Tien, 1980); and propane soot based on *in situ* extinction measurements in premixed flames and the use of Kramers-Krönig relationships (Chang and Charalampopoulos, 1990). It is evident that there are significant differences among these evaluations of soot refractive indices, including other measurements in the literature would yield even wider variations (Charalampopoulos, 1992). These differences can be attributed to approximations used to interpret the optical measurements, effects of fuel type, and effects of flame conditions—particularly the temperature for the near ultraviolet region (Lee and Tien, 1980). However, concerns about the approximate theories used to interpret the data are an overriding consider-

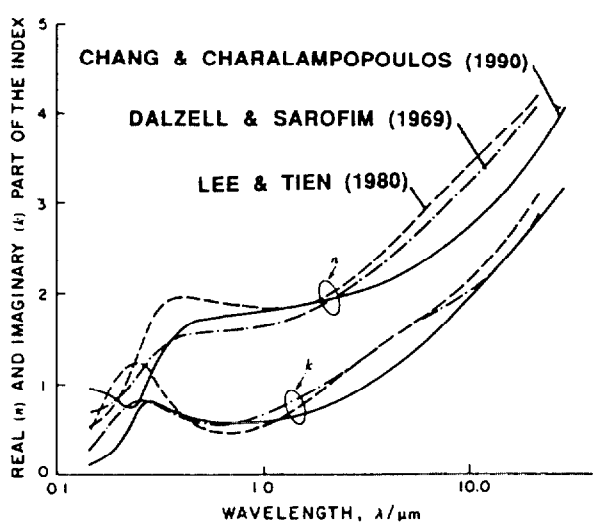

FIGURE 8 Measurements of soot refractive indices as a function of wavelength. From Chang and Charalampopoulos (1990).

ation and it is difficult to see how the other issues can be resolved until a sound method for measuring soot refractive indices has been established. Careful characterization of soot structure properties coupled with the use of RDG-PFA scattering theory certainly merits consideration as a means of measuring soot refractive indices more reliably.

Variations of soot refractive indices within the range illustrated in Figure 8 have a substantial effect on estimations of soot optical properties. This can be seen from results in Table III, where the refractive indices, $E(m)$, $F(m)$ and the ratio $F(m)/E(m)$ are summarized for wavelengths of 514.5 and 1000 nm. Results in the table are based on the measurements of Dalzell and Sarofim (1969), Lee and Tien (1980) and Chang and Charalampopoulos (1990). The variations of refractive index properties over these three studies are substantial: roughly 40% for $E(m)$, 80% for $F(m)$ and 90% for $F(m)/E(m)$. From Equations (2), (3) and (6), it is evident that uncertainties in $E(m)$, $F(m)$ and $F(m)/E(m)$ yield corresponding uncertainties in absorption, scattering, and soot volume fractions. Thus, effects of uncertainties of refractive index properties are comparable to effects of aggregate scattering in the visible, illustrated in Figure 6, and persist into the infrared as well.

Köylü and Faeth (1993b) have reported a very limited independent assessment of soot refractive indices at 514.5 nm, based on RDG-PFA scattering predictions and measurements in the power-law regime for large soot aggregates emitted from long residence time turbulent diffusion flames. For these conditions, Equations (2) and (10) can be rearranged to yield:

$$F(m)/E(m) = 4\pi(q d_p)^{D_f} \bar{Q}^a_{vv}/(k_f x_p^3 \bar{Q}^a_a) \tag{14}$$

Then using measured values of d_p, k_f, D_f, $\bar{Q}^a_{vv}$ and $\bar{Q}^a_a$, it was found that $F(m)/E(m) = 0.74$ with a standard deviation of 0.09 over all the conditions illustrated in Figure 3. Referring to Table III, this result is in best agreement with the measurements of Dalzell

TABLE III

Refractive index properties of soot

Source	n	k	$E(m)$	$F(m)$	$F(m)/E(m)$
$\lambda = 514.6$ nm:					
Dalzell and Sarofim (1969)[a]	1.57	0.56	0.26	0.22	0.84
Lee and Tien (180)[b]	1.90	0.55	0.19	0.30	1.58
Chang and Charalampopoulos (1990)[c]	1.63	0.48	0.21	0.20	0.95
$\lambda = 1000$ cm:					
Dalzell and Sarofim (1969)[a]	1.65	0.72	0.31	0.30	0.97
Lee and Tien (1980)[b]	1.90	0.80	0.27	0.39	1.44
Chang and Charalampopoulos (1990)[c]	1.65	0.50	0.22	0.22	1.00

[a] For acetylene soot pellets at room temperature.
[b] For polystyrene and plexiglass diffusion flames.
[c] For the post flame region of fuel-rich premixed propane/oxygen flames.

and Sarofim (1969), suggesting that the soot aggregate scattering approximations used by Tien and Lee (1980) and Chang and Charalampopoulos (1990) may have compromised their results. Nevertheless, more study clearly is needed to resolve the current unacceptably large uncertainties of soot refractive indices.

CONCLUSIONS

Existing information concerning the structure and optical properties of soot within diffusion flame environments was reviewed. The main conclusions from the review are as follows:

1. Soot consists of nearly spherical and monodisperse primary particles collected into mass fractal aggregates exhibiting a log normal distribution function for the number of primary particles per aggregate. While primary particle diameters and aggregate sizes vary with fuel type and flame condition, the fractal dimension and prefactor appear to be relatively robust properties with $D_f = 1.77$ and $k_f = 8.1$ (with standard deviations of 2 and 10%, respectively) based on recent sampling and light scattering measurements.
2. Use of the Rayleigh-Debye-Gans scattering approximation, in conjuction with the fractal properties of polydisperse soot aggregates, yields predictions of soot scattering properties that agreed with measurements within experimental uncertainties. The evaluation considered soot from a variety of fuels over the following test ranges: x_p of 0.128–0.330, $\bar{N}$ of 31–467 and $\bar{N}^2/(\bar{N})^2$ of 1.82–3.23. However, additional evaluation of this methodology would be desirable, emphasizing small-angle (Guinier) behavior, larger values of primary particle diameters and aggregate sizes, and effects of departures of actual soot geometry and physical properties from spherical primary particles in point contact and having uniform refractive indices.
3. The performance of other widely used soot aggregate scattering theories generally was not satisfactory over the same range of conditions: Rayleigh scattering underestimated scattering levels and yielded extinction cross sections up to roughly less than half the correct values for large soot aggregates in the visible portion of the spectrum, while Mie scattering for an equivalent sphere gave inconsistent results because the optical properties of open-structured wispy aggregates having fractal dimensions less than 2 are not well represented by compact objects. Nevertheless, errors from use of the Rayleigh scattering approximation are small in comparison to other uncertainties in the infrared, where this approximation can be used for predictions of the radiative properties of soot and interpretation of extinction measurements to find soot volume fractions.
4. Use of Rayleigh-Debye-Gans polydisperse fractal aggregate theory provides a potential for nonintrusive measurements of both soot concentrations and structure in flame environments but several areas of uncertainty must be addressed to realize this potential, as follows: reliable solution algorithms for the inverse problem, to infer soot structure from scattering and extinction measurements, must be developed; and effects of fuel type and of flame conditions on soot refractive indices must be better understood. In particular, long-standing uncer-

tainties and controversies concerning the refractive indices of soot are the greatest impediment for reliable nonintrusive optical diagnostics to find soot properties in flame environments and resolving these difficulties merits high priority for future research.

ACKNOWLEDGEMENTS

The authors' research on soot structure and optical properties is supported by the Building and Fire Research Laboratory of the National Institute of Standards and Technology, Grant No. 60NANB1D1175, with H. R. Baum serving as Scientific Officer; the Microgravity Science and Applications Division of NASA, Grant No. NAG3-1245, under the technical management of D.L. Urban of the Lewis Rresearch Center; and the Office of Naval Research, Grant No. N00014-93-1-0321 with G. D. Roy serving as program manager.

REFERENCES

Berry, M. V. and Percival, I. C. (1986). Optics of Fractal Clusters such as Smoke. *Optica Acta*, **33**, 577.

Bohren, C. F. and Huffman, D. R. (1983). *Absorption and Scattering of Light by Small Particles*, John Wiley and Sons, New York, pp. 477–482.

Borghese, F., Denti, P., Saija, R., Toscano, G. and Sindoni, O. I. (1984). Multiple Electromagnetic Scattering from a Cluster of Spheres. I. Theory. *Aerosol Sci. Tech.*, **3**, 227.

Bowman, C. T. (1992). Control of Combustion-Generated Nitrogen Oxide Emissions Driven by Regulation. *Twenty-Fourth Symposium (International) on Combustion*, The Combustion Institute, Pittsburgh, pp. 859–878.

Chang, H. and Charalampopoulos, T. T. (1990). Determination of the Wavelength Dependence of Refractive Indices of Flame Soot. *Proc. R. Soc. London* **A430**, 577.

Charalampopoulos, T. T. (1992). Morphology and Dynamics of Agglomerated Particulates in Combustion Systems Using Light Scattering Techniques. *Prog. Energy Combust. Sci.*, **18**, 13.

Chen, H. Y., Iskander, M. F. and Penner, J. E. (1990). Light Scattering and Absorption by Fractal Agglomerates and Coagulations of Smoke Aerosols. *J. Modern Optics*, **2**, 171.

Dalzell, W. H. and Sarofim, A. F. (1969). Optical Constants of Soot and Their Application to Heat Flux Calculations. *J. Heat Trans.*, **91**, 100.

Dalzell, W. H., Williams, G. C. and Hottel, H. C. (1970). A Light Scattering Method for Soot Concentration Measurements. *Combust. Flame*, **14**, 161.

Dobbins, R. A. and Megaridis, C. M. (1987). Morphology of Flame-Generated Soot as Determined by Thermophoretic Sampling. *Langmuir*, **3**, 254.

Dobbins, R. A. and Megaridis, C. M. (1991). Absorption and Scattering of Light by Polydisperse Aggregates. *Appl. Optics*, **30**, 4747.

Dobbins, R. A., Santoro, R. J. and Semerjian, H. G. (1990). Analysis of Light Scattering From Soot Using Optical Cross Sections for Aggregates. *Twenty-Third Symposium (International) on Combustion*. The Combustion Institute, Pittsburgh, pp. 1525–1532.

Dobbins, R. A., Mulholland, G. W. and Bryner, N. P. (1993). Comparison of a Fractal Smoke Optics Model with Light Extinction Measurements. *Atmospheric Environment*, in press.

Erickson, W. D., Williams, G. C. and Hottel, H. C. (1964). Light Scattering Measurements on Soot in a Benzene-Air Flame. *Combust. Flame*, **8**, 127.

Faeth, G. M., Gore, J. P., Chuech, S. G. and Jeng, S.-M. (1989). Radiation from Turbulent Diffusion Flames. *Annual Review of Numerical Fluid Mechanics and Heat Transfer*, **2**, 1.

Farias, T. and Carvalho, M. G. (1993). Personal Communication.

Felske, J. D., Charalampopoulos, T. T. and Hura, H. (1984). Determination of the Refractive Indices of Soot Particles From the Reflectivities of Compressed Soot Pellets. *Combust. Sci. Tech.*, **37**, 263.

Freltoft, T., Kjems, J. K. and Sinha, S. K. (1986). Power-Law Correlations and Finite Size Effects in Silica Particle Aggregates Studied by Small-Angle Neutron Scattering. *Physical Review*, **B33**, 269.

Iskander, M. F., Chen, H. Y. and Penner, J. E. (1989). Optical Scattering and Absorption by Branched Chains of Aerosols. *Appl. Optics*, **28**, 3083.

Jullien, R. and Botet, R. (1987).*Aggregation and Fractal Aggregates*, World Scientific Publishing Co., Singapore, pp. 46–50.

Kerker, M. (1969). *The Scattering of Light*, Academic Press, New York, pp. 414–486.

Köylü, Ü. Ö. and Faeth, G. M. (1991). Carbon Monoxide and Soot Emissions from Liquid-Fueled Buoyant Turbulent Diffusion Flames. *Combust. Flame*, **87**, 61.

Köylü, Ü. Ö. and Faeth, G. M. (1992). Structure of Overfire Soot in Buoyant Turbulent Diffusion Flames at Long Residence Times. *Combust. Flame*, **89**, 140.

Köylü, Ü. Ö. and Faeth, G. M. (1993a). Radiative Properties of Flame-Generated Soot. *J. Heat Trans.* **115**, 409.

Köylü, Ü. Ö. and Faeth, G. M. (1993b). Optical Properties of Overfire Soot in Buoyant Turbulent Diffusion Flames at Long Residence Times. *J. Heat. Trans.*, in press.

Köylü, Ü. Ö. and Faeth, G. M. (1993c). Optical Properties of Soot in Buoyant Laminar Diffusion Flames. *J. Heat. Trans.* in press.

Köylü, Ü. Ö., Sivathanu, Y. R. and Faeth, G. M. (1991). *Third International Symposium on Fire Safety Science*, Elsevier, London, pp. 625–634.

Laheay, J. and Prado, G. (1981). Morphology and Internal Structure of Soot and Carbon Blacks. in Siegla, D. C. and Smith, G. W. (eds.), *Particulate Carbon*, Plenum Press, New York, pp. 33–55.

Lee, S. C. and Tien, C. L. (1980). Optical Constants of Soot in Hydrocarbon Flames. *Eighteenth Symposium (International) on Combustion*, The Combustion Institute, Pittsburgh, pp. 1159–1166.

Lin, M. Y., Lindsay, H. M., Weitz, D. A., Ball, R. C., Klein, R. and Meakin, P. (1989). Universality of Fractal Aggregates as Probed by Light Scattering. *Proc. Roy. Soc. London*, **A423**, 71.

Magnussen, B. F. (1974). An Investigation into the Behavior of Soot in a Turbulent Free Jet C_2H_2-Flame, *Fifteenth Symposium (International) on Combustion*, The Combustion Institute, Pittsburgh, pp. 1415–1425.

Martin, J. E. and Hurd, A. J. (1987). Scattering from Fractals. *J. Appl. Cryst.*, **20**, 61.

Medalia, A. I. and Heckman, F. A. (1969). Morphology of Aggregates—II. Size and Shape Factors of Carbon Black Aggregates from Electron Microscopy. *Carbon*, **7**, 567.

Megaridis, C. M. and Dobbins, R. A. (1990). Morphological Description of Flame-Generated Materials. *Combust. Sci. Tech*, **77**, 95.

Mountain, R D. and Mulholland, G. W. (1988). Light Scattering from Simulated Smoke Agglomerates. *Langmuir*, **4**, 1321.

Nelson, J. (1989). Test of a Mean Field Theory for the Optics of Fractal Clusters. *J. Modern Optics*, **36**, 1031.

Newman, J. S. and Steciak, J. (1987). Characterization of Particulates from Diffusion Flames. *Combust. Flame*, **67**, 55.

Puri, R., Richardson, T. F., Santoro, R. J. and Dobbins, R. A. (1993). Aerosol Dynamic Processes of Soot Aggregates in a Laminar Ethene Diffusion Flame. *Combust. Flame*, **92**, 320.

Rossler, D. M. and Faxvog, F. R. (1980). Optical Properties of Agglomerated Acetylene Smoke Particles at 0.5145 μm and 10.6 μm wavelengths. *J. Opt. Soc. Am.*, **70**, 230.

Rosner, D. E., Mackowski, D. W. and Garcia-Ybarra, P. (1991). Size- and Structure-Insensitivity of the Thermophoretic Transport of Aggregated 'Soot' Particles in Gases. *Combust. Sci. Tech.* **80**, 87.

Samson, R. J., Mulholland, G. W. and Gentry, J. W. (1987). Structural Analysis of Soot Agglomerates. *Langmuir*, **3**, 272.

Santoro, R. J., Semerjian, H. B. and Dobbins, R. A. (1983). Soot Particle Measurements in Diffusion Flames. *Combust. Flame*, **51**, 203.

Tewarson, A. (1988). Generation of Heat and Chemical Compounds in Fires, in *SPFE Handbook on Fire Protection Engineering*, National Fire Protection Association, Quincy, MA, pp. 1–179.

Tien, C. L. and Lee, S. C. (1982). Flame Radiation. *Prog. Energy Combust. Sci.*, **8**, 41.

Vaglieco, B. M., Beretta, F. and D'Alessio, A. (1990). In Situ Evaluation of the Soot Refractive Index in the UV-Visible from the Measurements of Scattering and Extinction Coefficients in Rich Flames. *Combust. Flame*, **79**, 259.

van de Hulst, H. C. (1957). *Light Scattering by Small Particles*, Dover Publication, New York.

Viskanta, R. amd Mengüc, M. P. (1987). Radiation Heat Transfer in Combustion Systems. *Prog. Energy Combust. Sci.*, **13**, 97.

Wersborg, B. L., Howard, J. B. and Williams, G. C. (1972). Physical Mechanisms in Carbon Formation in Flames. *Fourteenth Symposium (International) on Combustion*, The Combustion Institute, Pittsburg, pp. 929–940.

Appendix D: Köylü et al. (1995)

Fractal and Projected Structure Properties of Soot Aggregates

Ü. Ö. KÖYLÜ and G. M. FAETH*
Department of Aerospace Engineering, The University of Michigan, Ann Arbor, Michigan 48109-2118, U.S.A.

T. L. FARIAS and M. G. CARVALHO
Mechanical Engineering Department, Instituto Superior Técnico, 1096 Lisbon, Portugal

The structure of soot aggregates was investigated, emphasizing the fractal properties as well as the relationships between the properties of actual and projected soot images. This information was developed by considering numerically simulated soot aggregates based on cluster–cluster aggregation as well as measured soot aggregates based on thermophoretic sampling and analysis by transmission electron microscopy (TEM) of soot for a variety of fuels (acetylene, propylene, ethylene, and propane) and both laminar and turbulent diffusion flame conditions. It was found that soot aggregate fractal properties are relatively independent of fuel type and flame condition, yielding a fractal dimension of 1.82 and a fractal prefactor of 8.5, with experimental uncertainties (95% confidence) of 0.08 and 0.5, respectively. Relationships between the actual and projected structure properties of soot, e.g., between the number of primary particles and the projected area and between the radius of gyration of an aggregate and its projected image, also are relatively independent of fuel type and flame condition.

NOMENCLATURE

A_a	projected area of an aggregate
A_p	cross-sectional area of a primary particle, $\pi d_p^2/4$
d	burner diameter
d_p	diameter of primary particle
D_f	aggregate fractal dimension
k_a	projected area prefactor, Eq. 2
k_f	fractal prefactor based on R_g, Eq. 1
k_{fL}	fractal prefactor based on $(LW)^{1/2}$, Eq. 5
L	projected maximum length of aggregate
N	number of primary particles in an aggregate
R_g, $R_g(3D)$	radius of gyration of an aggregate
$R_g(2D)$	radius of gyration of projected aggregate image
W	maximum projected aggregate width normal to L
x	height above burner, coordinate direction
x_p	primary particle size parameter, $\pi d_p/\lambda$
y	coordinate direction
z	coordinate direction

Greek Symbols

α	projected area exponent
λ	wavelength of light

INTRODUCTION

Practical hydrocarbon fueled flames generally contain and emit soot, which affects their radiation, structure, and pollutant emission properties. These effects have motivated considerable interest in the structure and optical properties of soot, in order to develop nonintrusive methods for measuring soot properties and to estimate the continuum radiation and heterogeneous reaction properties of soot in flame environments. The present investigation seeks to contribute to a better understanding of soot structure, by undertaking a computational and experimental study of the structure of soot aggregates, emphasizing characteristics needed to define soot optical and fractal prop-

* Corresponding author.

COMBUSTION AND FLAME 100: 621–633 (1995)
Copyright © 1995 by The Combustion Institute
Published by Elsevier Science Inc.

0010-2180/95/$9.50
SSDI 0010-2180(94)00147-K

erties, and to understand the relationships between actual and projected soot images.

Earlier work concerning the structure and optical properties of soot has been reviewed by Tien and Lee [1], Viskanta and Mengüc [2], Jullien and Botet [3], and Köylü and Faeth [4]; therefore, consideration of past studies will be brief. Initial studies of the structure of soot by Williams and coworkers [5–7] involved thermophoretic and molecular beam sampling of premixed acetylene, benzene and propane flames, followed by analysis using transmission electron microscopy (TEM). The results showed that soot consisted of small spherical primary particles, having nearly constant diameters, collected into open structured aggregates that had broad distributions of the number of primary particles per aggregate. Subsequent work using thermophoretic sampling and TEM established similar behavior for a variety of fuels and flame conditions, e.g., laminar and turbulent flames as well as premixed and diffusion flames [8–21]. In general, the distributions of primary particle diameters had standard deviations of 15%–25% of the mean primary particle diameter, supporting the observations of nearly uniform primary particle sizes [4]. Additionally, primary particle diameters generally were less than 60 nm, with the largest diameters associated with heavily sooting fuels [4]. This behavior yields primary particle size diameters, $x_p < 0.4$, for wavelengths of interest for optical measurements of soot properties and estimates of continuum radiation from soot ($\lambda > 500$ nm). As a result, it is reasonable to assume that individual primary particles approximate Rayleigh scattering particles, e.g., their total scattering and absorption cross-sections typically are within 1% and 5%, respectively, of estimates based on Mie scattering theory for $\lambda > 500$ nm [4].

Soot aggregates are small near the soot inception point in flames but they aggregate rapidly with the mean number of primary particles per aggregate reaching values in the range 200–600 for soot emitted from large buoyant turbulent diffusion flames [4]. As noted earlier, unlike primary particle diameters, aggregate size distributions are broad; in fact, the standard deviations of aggregate size are comparable to the mean value of the number of primary particles in an aggregate. Thus, aggregate size distributions generally are represented by the log normal size distribution function while 95% of the soot aggregates emitted from large turbulent diffusion flames contain 30–1800 primary particles [4, 19]. This complexity of aggregate size distributions, however, is mitigated by the observation that soot aggregates exhibit mass fractal-like behavior with a Hausdorf or mass fractal dimension, $D_f < 2$, even when the number of primary particles in an aggregate is small [3, 4, 10–21]. The mass fractal approximation implies the following relationship between the primary particle diameter, the number of primary particles in an aggregate and the radius of gyration of an aggregate [3]:

$$N = k_f (R_g/d_p)^{D_f}, \tag{1}$$

where k_f is a constant fractal prefactor and the aggregates are assumed to consist of monodisperse nonoverlapping spherical primary particles, i.e., the mean value of d_p is used in Eq. 1. This fractal-like behavior has important implications for the optical properties of soot which will be discussed next.

Measurements show that flame-generated soot ranges from small aggregates (dimensions on the order of 10 nm) near the start of soot formation, to large aggregates (dimensions on the order of 1 μm) emitted from large buoyant turbulent diffusion flames [3–21]. The larger-sized aggregates are too large for reasonable application of the Rayleigh scattering approximation and are too open structured for proper representation as equivalent compact spheres using the Mie scattering approximation [4]. These difficulties were established by direct measurements of soot scattering properties during early work [5–7]. For example, strong forward scattering was observed which is not representative of Rayleigh scattering behavior, while use of the Mie scattering approximation for an equivalent sphere still did not provide an adequate fit of scattering measurements [5–7]. The former behavior follows because the large soot aggregates in the size distribution dominate scattering properties and are too large to be approximated as Rayleigh scatter-

ing objects. Additionally, the fact that soot aggregates have fractal dimensions less than 2 implies that their structure is too open to be represented by a compact object such as an equivalent Mie scattering sphere [22]. The limitations of the Rayleigh and Mie scattering theories prompted subsequent development of optical theories of soot aggregates based on the Rayleigh–Debye–Gans (RDG) scattering approximation for mass fractal objects involving monodisperse spherical primary particles that just touch one another [3, 4, 11, 17]. The large refractive indices of soot raised questions about the validity of the RDG scattering approximation [4], however, recent work where both soot structure and scattering properties were known, has demonstrated performance of the RDG scattering theory for polydisperse fractal soot aggregates within experimental and computational uncertainties [20, 21, 23].

The reasonably successful evaluation of the RDG scattering theory for soot aggregates provides potential for resolving long-standing problems of the accurate determination of the refractive indices of soot [4, 24, 25], as well as for developing methods of solving the inverse problem so that soot structure properties can be found nonintrusively from scattering measurements [4, 20, 21, 24, 25]. Both these objectives, however, are inhibited by current limitations about the fractal and polydisperse properties of practical soot aggregates in flames. In particular, RDG theory requires values of R_g as a function of N but this determination is inhibited by current uncertainties concerning D_f and more particularly k_f [20, 21, 26]. Additionally, information about k_f requires analysis of actual three-dimensional soot aggregates, which can be facilitated by the availability of relationships between the projected and the actual properties of soot aggregates. Unfortunately, currently available information along these lines is rather limited. In particular, evaluation of relationships between projected and true three-dimensional properties of soot aggregates have only involved small aggregate samples and a few flame conditions [11, 12, 19]. Recent work by Sorensen and coworkers [24, 25] has sought to extend understanding of the projected and fractal properties of soot aggregates, but more development of their experimental methods will be needed for definitive results. Finally, Wu and Friedlander [26] address the fractal properties of aggregates based on existing results for numerically simulated populations of aggregates of spherical primary particles; however, the relevance of these findings to practical soot aggregates must still be established.

In view of current limitations about the structure and optical properties of soot aggregates, the objective of the present investigation was to study soot structure in order to define soot optical and fractal properties, as well as the relationships between actual and projected soot images. This work involved direct evaluation of the relationships between the number of primary particles and the projected image of an aggregate, the relationships between the radius of gyration of an aggregate and properties of its projected image, and the values of the Hausdorf or mass fractal dimensions and prefactors of soot in flame environments. The new information was developed by considering both numerically simulated and experimentally measured soot aggregates. The numerical simulations to create soot aggregates were based on cluster–cluster aggregation along the lines of Jullien and Botet [3], Mountain and Mulholland [13], and Farias et al. [23]. The experimental soot aggregates were obtained from two sources, as follows: the large soot aggregates found in the fuel-lean region of buoyant turbulent diffusion flames in the long residence time regime, where soot generation factors and soot structure are independent of flame position and residence time [19, 20, 27, 28]; and soot aggregates collected in both the fuel-rich and fuel-lean regions of laminar jet diffusion flames [29]. Taken together, the experimental soot properties involve a variety of fuels—acetylene, propylene, ethylene, and propane—burning in air within diffusion flames.

The paper begins with consideration of numerically simulated soot aggregates in order to establish relationships between actual and projected soot aggregate properties. Measured soot aggregate properties are then considered, emphasizing soot fractal properties.

NUMERICALLY SIMULATED AGGREGATES

Aggregate Simulation

Mountain and Mulholland [13] generated soot aggregates using a simulation involving cluster–cluster aggregation based on a solution of the Langevin equations. This approach yields fractal-like aggregates that satisfy the power-law relationship of Eq. 1 with $1.7 < D_f < 1.9$ and k_f ca. 5.5 for $N > 10$. However, a larger sample of aggregates was required for present work, and it was desired to have $1.7 < D_f < 1.8$ and k_f ca. 8.0 in order to correspond to recent experimental observations of the fractal properties of soot aggregates [19–21]. As a result, an alternative aggregate simulation, based on the approach used by Farias et al. [23], was used during the present investigation.

The present aggregate simulation involved creating a population of aggregates by cluster–cluster aggregation, following Jullien and Botet [3]. The simulation began with individual and pairs of primary particles which were attached to each other randomly, assuming uniform distributions of the point and orientation of attachment, while rejecting configurations where primary particles intersected. This procedure was continued in order to form progressively larger aggregates, but with the additional restriction that the aggregates should have $1.7 < D_f < 1.8$ with k_f of 8 for $N > 8$, based on Eq. 1 applied to the computed value of R_g for the aggregate. It was observed that D_f fell naturally in the range 1.6–1.9 for $N > 48$ during these simulations; therefore, few cluster-cluster combinations were rejected for inappropriate fractal properties when larger aggregates were constructed. Similarly, for D_f in the range 1.7–1.8, the value of k_f fell naturally near $k_f = 8.0$ for statistically significant populations of aggregates. Naturally, the numerically simulated aggregates were not useful for investigating aggregate fractal properties because their fractal properties had been prescribed. Nevertheless, these objects were useful for investigating relationships between projected and actual aggregate properties because the simulated aggregates were very similar to actual aggregates while their known geometry vastly simplified determinations of actual and projected aggregate properties.

The population of simulated aggregates involved N in the range 20–1000, considering 20 aggregate sizes. Results for each aggregate size were averaged over 20 different aggregates to yield a total sample of 400 aggregates. In order to fix ideas, a primary particle diameter of 50 nm was used for the simulations, which is typical of soot aggregates for heavily sooting materials [19]. Present results are normalized by d_p or A_p, however, and such normalized results are independent of d_p, at least for d_p less than 60 nm [20, 21].

Projected images of typical aggregates constructed using the present simulation are illustrated elsewhere for $N = 16$, 64, and 256 [23]. An example involving projected images of a given aggregate in three orthogonal directions for $N = 100$, is illustrated in Fig. 1. This partic-

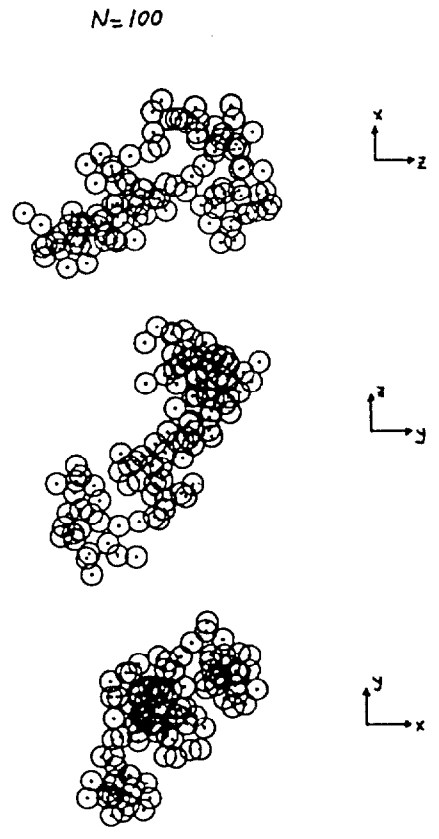

Fig. 1. Projected images of a numerically simulated soot aggregate. $N = 100$. Note that the primary particle diameter used in this simulation was 50 nm.

ular aggregate had $D_f = 1.76$ while $d_p = 50$ nm as noted earlier. Even though the value of N used in Fig. 1 is relatively modest, the dimensions of the aggregate are substantial, reaching maximum projected lengths greater than 1 μm. It is evident that the appearance of an aggregate varies considerably with the direction of the projection; it also varies substantially from aggregate to aggregate within a population of given size [23]. Nevertheless, the present simulated aggregates are qualitatively similar to both past experimental observations of soot aggregates [3, 6, 19–21] and other numerical simulations of soot aggregates [3, 13, 23]. Combined with their prescribed fractal properties, this behavior suggests that the present simulated aggregate populations are reasonably representative of the structure of soot aggregates found in flame environments.

Results and Discussion

The first property studied using the numerically simulated aggregates was the relationship between the number of primary particles in an aggregate and the projected area of the aggregate. Several workers have suggested the following relationship between the projected area of a soot aggregate, A_a, and N [12, 15–17, 19]:

$$N = k_a(A_a/A_p)^{\alpha}, \tag{2}$$

where α is an empirical projected area exponent and k_a is a constant normally taken to be unity. Results for the present simulated aggregates, based on random projections of the aggregates, are plotted according to Eq. 2 in Fig. 2. The power-law correlation of Eq. 2 is seen to provide an excellent fit of the data. The least-squares fit values of the correlation of Eq. 2 are $\alpha = 1.10$ and $k_a = 1.16$ with standard deviations of 0.002 and 0.01, respectively. The value of α is in reasonable agreement with earlier assessments although the present value of k_a exceeds the value of unity used in earlier work [12, 15–17, 19]. Further consideration of these differences will be undertaken when the experimental results are discussed.

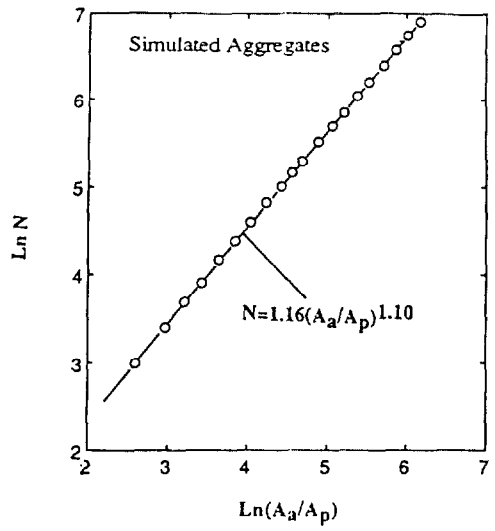

Fig. 2. Number of primary particles as a function of projected area ratio for simulated soot aggregates.

As noted earlier, the radius of gyration is an important aggregate property because it directly affects scattering properties computed using RDG theory. Thus, the simulated aggregates were used to compare actual values of the radius of gyration with values found from projected images of the aggregates. These results are illustrated in Fig. 3 where $R_g(3D)/R_g(2D)$ is plotted as a function of N for N in the range 20–1000. Remarkably, the ratio of the actual to projected radius of gyra-

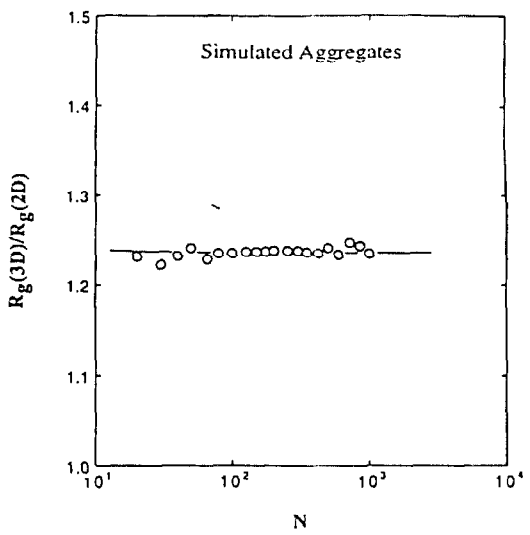

Fig. 3. Ratio of actual to projected radius of gyration as a function of aggregate size for simulated soot aggregates.

tion is essentially independent of N and has a value of 1.24 with a standard deviation less than 0.01, i.e.,

$$R_g(3D) = 1.24R_g(2D). \tag{3}$$

Thus, Eqs. 2 and 3 provide convenient relationships between the properties of projected images of aggregates, and the values of N and R_g needed to assess the fractal properties of aggregates that are defined in Eq. 1.

Direct evaluation of fractal properties from Eq. 1 requires either extensive data reduction of stereopair images or the alternative evaluation from the properties of projected images through Eqs. 2 and 3 that was just discussed. Information of this type is not often available so that several simplified methods based on projected aggregate dimensions have been developed, as discussed by Jullien and coworkers [3, 10]. One approach involves the use of the maximum projected length of the aggregate, L, as follows [3, 10]:

$$N = k_{fL}(L/d_p)^{D_f}. \tag{4}$$

An alternative approach, used during earlier work in this laboratory [19], involves use of the geometric mean of L, and the maximum projected width normal to L, W, as follows [3, 10]:

$$N = k_{fLW}\left((LW)^{1/2}/d_p\right)^{D_f}, \tag{5}$$

where the mean value of d_p is used in the correlations of Eqs. 4 and 5, similar to Eq. 1.

Comparing Eqs. 1, 4 and 5 indicates that L and $(LW)^{1/2}$ in Eqs. 4 and 5, act as surrogates for R_g in the fundamental fractal relationship of Eq. 1. Thus, the relationship between these various lengths is of interest and is illustrated in Fig. 4. These results involve plots of $L/(2R_g)$ and $(LW)^{1/2}/(2R_g)$ as a function of N. Unlike $R_g(3D)/R_g(2D)$, the ratios of either L or $(LW)^{1/2}$ and R_g are seen to decrease as N increases and only approach relatively constant values for $N > 100$, where

$$L/(2R_g) = 1.49, \tag{6}$$

$$(LW)^{1/2}/(2R_g) = 1.17, \tag{7}$$

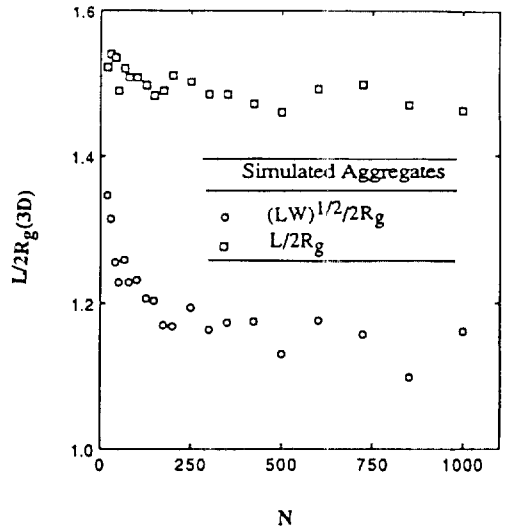

Fig. 4. Number of primary particles as a function of aggregate characteristic dimensions for simulated soot aggregates.

with standard deviations of 0.02 and 0.03, respectively. The smaller value of this ratio for $(LW)^{1/2}$ than for L is quite reasonable because $(LW)^{1/2}$ involves W, which is less than L by definition, for each aggregate. The effect of the variation of this ratio with N is of course negligible when data for large aggregates are processed to find D_f. However, this rarely is the case and the progressive reduction of the ratios generally acts to increase the apparent value of D_f when either L or $(LW)^{1/2}$ is used as a surrogate for R_g. Fortunately, the effect of this variation on determinations of D_f is not large, ca. 5%, as discussed subsequently in connection with experimental measurements of aggregate properties.

Puri et al. [18] also have considered values of $L/(2R_g)$ based on the measurements of Samson et al. [12]. These results were obtained using a 36-aggregate sample of overfire soot from a laminar acetylene flame and yield $L/(2R_g) = 1.78$ [18], which is roughly 20% larger than the present large N results. This behavior probably is caused by the relatively small aggregate sample used by Puri et al. [18], e.g., these results also exhibit an unusually small value of D_f as discussed later.

FLAME-GENERATED AGGREGATES

Experimental Methods

Soot structure also was observed using flame-generated aggregates collected by thermophoretic sampling. Sampling procedures were based on the methods of Dobbins and Megaridis [14–16] with specific techniques identical to past work in this laboratory [19]. The sampling surfaces were the carbon-supported copper grids used to hold TEM specimens (3-mm-diameter 200-mesh copper grids supported by a 20-nm-thick elemental carbon film, SPI Supplies, Philadelphia, part no. 3520C), aligned parallel to the mean flow direction. The probes were stored outside the flame and were inserted briefly into the flame environment using a double-acting pneumatic cylinder. Sampling times were controlled so that soot aggregates covered no more than 10% of the TEM grid in order to avoid overlapping aggregates on the grid. The time of transit of the grids to and from the sampling location through the flame environment was less than 5% of the sampling time so that soot on the grid was representative of the sampling location. This effect is not of any consequence for the soot sampled in the fuel-lean region of buoyant turbulent diffusion flames, however, because the properties of this soot are independent of position in any event [19].

The principles of thermophoretic sampling are discussed elsewhere [15–17, 30–32]. For present conditions, primary particle diameters were less than 60 nm, which implies that primary particle dimensions are smaller than the mean free path for all sampling conditions, so that the thermophoretic velocities of individual primary particles are identical. In addition, Rosner et al. [32] have shown that the thermophoretic velocities of aggregates and individual primary particles agree within 20%, even when the aggregates are larger than mean free path lengths. Thus, effects of intrinsic bias with respect to aggregate size for the present thermophoretic sampling technique are small.

The samples were observed using a JEOL 2000FX analytical electron microscope system with a 1-nm edge-to-edge resolution and sample tilting angles up to $\pm 45°$. Magnifications used for the present measurements were in the range 20,000–300,000. The procedure involved selecting aggregates randomly at low magnification, and then increasing the magnification in order to analyze them. The images were processed using the IMAGE computer algorithm to find projected aggregate areas and dimensions, as well as the projected positions and sizes of primary particles. Images at various angles of projection, as well as stereopairs, were then analyzed independently to find the corresponding three-dimensional properties of aggregates. Latex spheres having a diameter of 91 nm (with a standard deviation of 5.8 nm) were used to calibrate the TEM images. Specific sampling procedures and the experimental uncertainties of the soot structure parameters derived from these measurements will be considered when the results are discussed.

Typical TEM images of a soot aggregate found in the fuel-lean region of a buoyant turbulent ethylene/air diffusion flame are illustrated in Fig. 5. This particular aggregate has a primary particle diameter of 32 nm and contains 295 primary particles, based on observations at various angles of projection, which yields maximum projected dimensions of roughly 900 nm. The results shown in the photographs are for tilt angles of $-45°$, $0°$ and $45°$, which provides a means of locating each primary particle in space for absolute analysis of aggregate structure properties. Other properties of this aggregate are typical of earlier observations in the literature [8–21], as well as the numerically simulated aggregate of similar size illustrated in Fig. 1. In particular, the object is open-structured and consists of primary particles having a nearly constant diameter [4].

Results and Discussion: Turbulent Flames

The most extensive measurements of soot aggregate properties were made for the soot in the fuel-lean region of buoyant turbulent diffusion flames in the long residence time regime. As noted earlier, soot for a particular fuel at these conditions does not depend on position in the fuel-lean region or residence time [19].

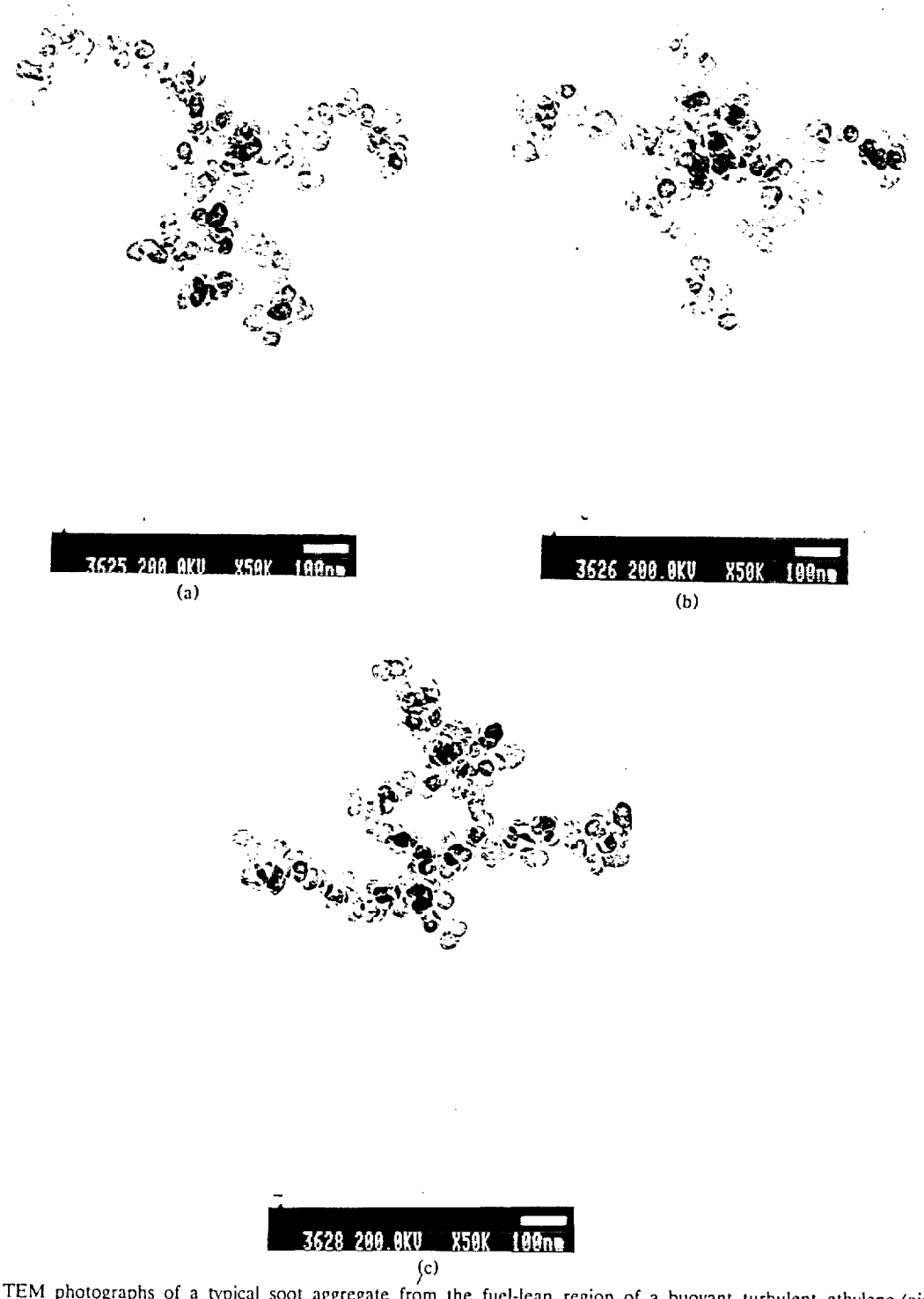

Fig. 5. TEM photographs of a typical soot aggregate from the fuel-lean region of a buoyant turbulent ethylene/air diffusion flame. Angles of projection (a) $-45°$, (b) $0°$, and (c) $45°$. Note, TEM length label is 100 nm long.

Specific measurements involved soot within acetylene, propylene, ethylene, and propane flames, see Ref. [19] for a complete description of experimental conditions. The measurements involved a total of 127 aggregates which contained 10–500 primary particles per aggregate.

The first issue to be considered using the measured aggregate structure properties was the relationship between the number of primary particles in an aggregate and its projected area on a TEM image. These results are illustrated in Fig. 6, for aggregates in the fuel-lean region of buoyant turbulent diffusion flames at long residence times. Composite results for soot from all the fuels are illustrated in Fig. 6. However, even though specific aggregate properties differ for the various flame systems, all the flames yield the same relationship between the number of primary particles in an aggregate and its projected area.

Similar to the simulated results illustrated in Fig. 2, the measured results illustrated in Fig. 6 suggest a correlation between the number of primary particles in an aggregate and its projected area. In fact, the empirical correlation found from the results illustrated in Fig. 6 is

$$N = 1.15(A_a/A_p)^{1.09}, \tag{8}$$

with standard deviations of α and k_a of 0.02 and 0.18, respectively. Within statistical significance, these values are identical to the results found for the numerically simulated aggregates which yielded $\alpha = 1.10$ and $k_a = 1.16$ with smaller standard deviations. Based on these findings it appears that the original correlation of Eq. 2 from Refs. 12, 15–17, and 19 is reasonable, except that k_a should be increased from unity to roughly 1.15. This effect implies that N was somewhat underestimated during earlier evaluations of fractal dimensions, based on expressions similar to Eqs. 4 and 5. This effect modifies values of k_{fL} and k_{fLW} inferred from these measurements but does not influence the determination of the fractal dimension, D_f.

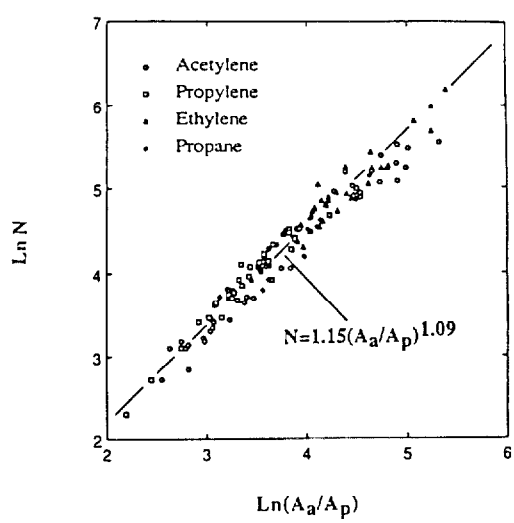

Fig. 6. Number of primary particles as a function of projected area ratio for soot aggregates from the overfire region of buoyant turbulent diffusion flames at long residence times.

The major effort of the present investigation was the determination of fractal prefactor, k_f, in Eq. 1 by measurements of N and R_g for the fuel-lean soot aggregates within buoyant turbulent diffusion flames in the long residence time regime. Similar to the results illustrated in Fig. 6, the fractal properties of aggregates for the various fuels—acetylene, propylene, ethylene and propane—were identical within experimental uncertainties, even though other properties—such as d_p and the mean number of primary particles per aggregate—differed considerably. The measured variation of N with R_g/d_p for the fuel-lean soot aggregates is illustrated in Fig. 7. The scatter of this data is appreciable, reflecting the problems of measuring R_g from projected images of aggregates at various angles. The fractal properties of the aggregates are clearly independent of fuel type, however, even though other properties of the aggregates (e.g., d_p, the mean number of primary particles per aggregate, etc.) differ considerably for soot formed from combustion of the various fuels. The best fit correlation of the measurements in Fig. 7 yields

$$N = 8.5(R_g/d_p)^{1.65}, \tag{9}$$

with standard deviations of D_f and k_f of 0.06 and 2.6, respectively. The standard deviation of k_f is relatively large; nevertheless, due to the relatively large data sample the corresponding uncertainty of the mean value of k_f is modest, i.e., the experimental uncertainty of the mean value of k_f (95% confidence) is 0.45 while the corresponding uncertainty of D_f is 0.12.

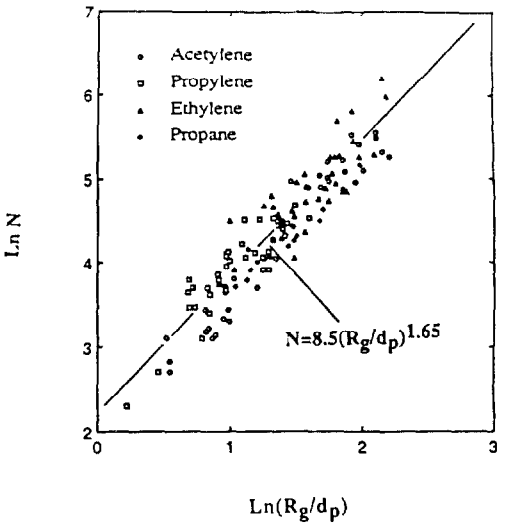

Fig. 7. Number of primary particles as a function of radius of gyration for soot aggregates from the overfire region of buoyant turbulent diffusion flames at long residence times.

The value of the fractal dimension found directly from the results of Fig. 7, $D_f = 1.65$, is somewhat low in comparison to earlier measurements of the same soot based on sampling and scattering determinations [19, 20]. For example, sampling and TEM measurements based on correlations of N as a function of $(LW)^{1/2}$ yielded $D_f = 1.75$ with an experimental uncertainty (95% confidence) of 0.07 over the four fuels [19]. The difference between the earlier and present values of D_f merits some explanation even though its statistical significance is marginal. This behavior follows from the discussion of Fig. 4; namely, that values of D_f based on $(LW)^{1/2}$ are somewhat larger than those based on R_g for a similar range of aggregate sizes, due to the progressive reduction of $(LW)^{1/2}/R_g$ with increasing aggregate size.

A more significant difference between the present value of D_f from Eq. 9, and other results, involves determinations of D_f based on light-scattering measurements [20]. For example, D_f found from the light-scattering measurements yielded a value of 1.82 with an experimental uncertainty (95% confidence) of 0.08 which is significantly greater than the present determination given by Eq. 9. This difference can be explained, however, by noting that the present sampling and TEM analysis yielded a progressive increase of D_f as both the size of largest aggregates and the sample size were increased. This behavior is consistent with larger observed values of D_f for the light-scattering measurements because these results emphasize the largest aggregates in the aggregate size distribution, as well, and clearly involve averages over a large number of aggregates [20]. Based on this observation, the effect of aggregate size on the present determination of D_f was estimated by Richardson extrapolation of the available variation of D_f with maximum aggregate size in the sample from the present data. This procedure involved plotting D_f found for samples containing aggregates smaller than a particular size N, as a function of $1/N$. The resulting plot was nearly linear for $N > 40$ and was extrapolated to $N \to \infty$ in order to obtain an estimate of $D_f = 1.83$ from the present sampling and TEM measurements [20]. Clearly, this value is in good agreement with the light-scattering determinations of $D_f = 1.82$, which also emphasize the largest aggregates in the distribution, as noted earlier.

The variation of k_f with maximum aggregate size in the present samples was less significant than the variation of D_f; therefore, $k_f = 8.5$ from Eq. 9 represents the present best estimate of this parameter. This value agrees within experimental uncertainties with recent estimates of Puri et al. [18] based on measurements of Samson et al. [12] and Megaridis and Dobbins [16]. In particular, analysis of measurements of N and R_g for a 36-aggregate sample of overfire soot from a laminar acetylene flame reported by Samson et al. [12] yielded $k_f = 9.22$ [18]. However, $D_f = 1.40$ for this sample, which is unusually low, so that the value of k_f was questioned based on potential sampling limitations [18]. Other estimates were obtained from measurements of Megaridis and Dobbins [16] for a nonsmoking laminar ethylene/air flame, taking $L/(2R_g) = 1.78$, to yield $k_f = 8.3$ and 8.9 for the two available aggregate samples from Ref. 16. As noted earlier, in connection with the discussion of Fig. 4, this value of $L/(2R_g)$ is somewhat larger than the present findings, although the corresponding values of k_f agree with present results within experimental uncertainties. Other earlier estimates of k_f are based on numerical

simulations of aggregation processes and generally yield values of k_f that are smaller than present estimates; see Wu and Freidlander [26] and references cited therein. An example of this behavior is $k_f = 5.8$, found by Puri et al. [18] based on the cluster-cluster aggregation simulation of Mountain and Mulholland [13]. The reasons for the low values of k_f from these simulations in comparison to subsequent measurements are not understood at the present time.

The fractal properties of the soot in the fuel-lean region of the buoyant turbulent diffusion flames at long residence times also can be considered from the results illustrated in Fig. 8. In this case, N is plotted as a function of the geometric mean projected aggregate size $(LW)^{1/2}$ for the four fuels over the same range of conditions as Fig. 7. The least-squares correlation of the measurements yields $D_f = 1.73$ and $k_{fLW} = 1.54$ with standard deviations of 0.04 and 0.30, respectively. As discussed in connection with Fig. 4, the apparent value of D_f is somewhat larger when found from $(LW)^{1/2}$, 1.73, than the value found from R_g, 1.65, for the same sample. All things considered, however, suggests the following estimates of the fractal properties of the fuel-lean soot: $D_f = 1.82$ with an uncertainty (95% confidence) of 0.08 from the light scattering measurements [20], supported by the extrapolated sampling results of Fig. 7; and $k_f = 8.5$ with an uncertainty (95% confidence) of 0.5, based on the sampling results of Fig. 7.

Results and Discussion: Laminar Flames

The final experimental results involved soot found in a laminar diffusion flame. In this case, samples were obtained at seven different locations along the axis of a weakly-buoyant acetylene/air laminar jet flame at a pressure of 0.25 atm. The test condition involved a burner diameter of 3.3 mm, and a burner exit Reynolds number of 80, which yielded a luminous soot-containing region roughly 50 mm long. Soot was sampled in both the fuel-rich and fuel-lean regions of the flame, over the range x/d of 1.92–13.42, to obtain a total of 618 aggregates with N in the range 5–1500.

The main results considered for soot in the laminar flame involved fractal properties. Measurements to find fractal properties are illustrated in Fig. 9, where N is plotted as a function of $(LW)^{1/2}$. Similar to results obtained from turbulent flames, the fractal properties of the soot illustrated in Fig. 9 were independent of the point where the soot was sampled, even though a range of fuel-lean and fuel-rich con-

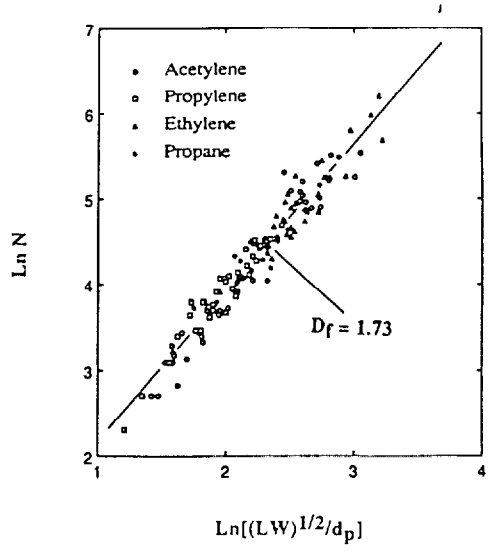

Fig. 8. Number of primary particles as a function of aggregate characteristic dimensions for soot aggregates from the overfire region of buoyant turbulent diffusion flames at long residence times.

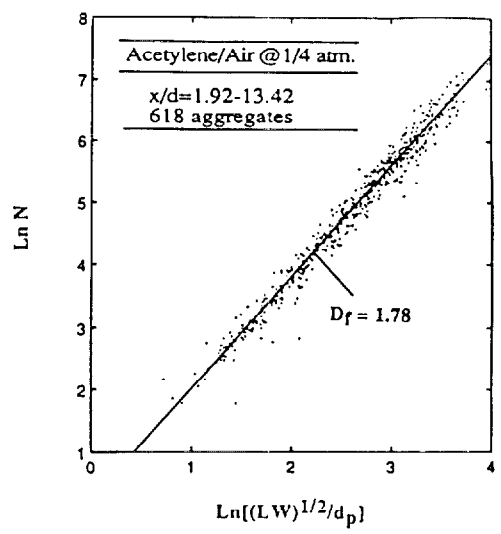

Fig. 9. Number of primary particles as a function of aggregate characteristic dimensions for soot aggregates from the underfire region of a laminar acetylene/air diffusion flame.

ditions were used and properties such as d_p and the mean number of primary particles per aggregate varied considerably with position in the flame. Then, treating all the laminar flame soot as a single sample population with respect to fractal properties yielded a best fit correlation of the measurements according to Eq. 5 with $D_f = 1.78$ and k_{fLW} of 1.33 with standard deviations of 0.012 and 0.23, respectively. The value of D_f for this soot is somewhat larger than the value for overfire soot found in Fig. 8 but this is felt to be due to the progressive increase of D_f with aggregate and sample size discussed in connection with Fig. 7, noting that both the sample size and the maximum value of N is larger for Fig. 9 than Fig. 8. Additionally, the difference between the results of Figs. 8 and 9 are relatively small so that properties of the laminar flame soot are identical to those of the soot within the fuel-lean region of buoyant turbulent diffusion flames at long residence times, within present experimental uncertainties. This finding suggests that the main fractal properties of soot, D_f and k_f, are relatively independent of the fuel and the flame condition.

CONCLUSIONS

Study of the structure of soot aggregates, considering aggregates obtained from numerical simulations using cluster–cluster aggregation, measured properties of soot aggregates from the fuel-lean region of buoyant turbulent diffusion flames at long residence times, and measured properties of soot aggregates from both the fuel-rich and fuel-lean regions of weakly buoyant laminar jet diffusion flames, yielded the following major conclusions:

1. In contrast to primary particle diameters and aggregate size, which vary considerably depending on flame conditions and fuel type, both the fractal properties, and the relationships between actual and projected soot aggregate structure properties, appear to be durable properties of soot that are relatively independent of fuel type and flame condition.
2. The best estimates of the fractal properties of soot aggregates based on present measurements yield $D_f = 1.82$ and $k_f = 8.5$ with experimental uncertainties (95% confidence) of 0.08 and 0.5, respectively. These results agree within experimental uncertainties with earlier determinations from sampling and TEM measurements [12, 16, 18–21].
3. Both computer simulations and experimental measurements indicated that it is possible to characterize soot aggregate structure properties from projected images, yielding $k_a = 1.15$, $\alpha = 1.09$ and $R_g(3D)/R_g(2D) = 1.24$, with standard deviations of these properties of 0.01, 0.002, and 0.01, respectively. The value of α is in good agreement with earlier estimates of this property [1, 15–17, 19]. In contrast, the present value of k_a is significantly larger than earlier estimates of unity for this parameter.
4. Values of the fractal dimension based on the geometric mean aggregate dimension, $(LW)^{1/2}$, were roughly 5% larger than values based on R_g for the aggregate samples considered here. This behavior is caused by a progressive reduction of $(LW)^{1/2}/R_g$ with increasing aggregate size. Additionally, values of D_f from sampling progressively increased as the sample size and the size of the largest aggregate were increased; in contrast, k_f exhibited a relatively small variation with sample and maximum aggregate size over the present range of conditions.

One of the authors (T.L.F.) would like to acknowledge scholarship support under the JNICT-CIENCIA BOLSAS Program (BD / 860 / 90-1B). Two of the authors (Ü.Ö.K and G.M.F.) would like to acknowledge support from the Building and Fire Research Laboratory of the National Institute of Standards and Technology (Grant No. 60NANB1D1175), the Microgravity Combustion Science Program of NASA (Contract No. NAG3-1245), and the Office of Naval Research (Grant No. N00014-93-1-0321). The collaboration between Instituto Superior Técnico and The University of Michigan is sponsored by AGARD, Support Project P-101. The assistance of Tienmin Chu with the TEM measurements is also gratefully acknowledged.

REFERENCES

1. Tien, C. L., and Lee, S. C., *Prog. Energy Combust. Sci.* 8:41–59 (1982).

2. Viskanta, R., and Mengüc, M. P., *Prog. Energy Combust. Sci.* 13:97–160 (1987).
3. Jullien, R., and Botet, R., *Aggregation and Fractal Aggregates*, World Scientific Publishing Co., Singapore, 1987.
4. Köylü, Ü. Ö., and Faeth, G. M., *J. Heat Transf.* 115:409–417 (1993).
5. Erickson, W. D., Williams, G. C., and Hottel, H. C., *Combust. Flame* 8:127–132 (1964).
6. Dalzell, W. H., Williams, G. C., and Hottel, H. C., *Combust. Flame* 14:161–170 (1970).
7. Wersborg, B. L., Howard, J. B., and Williams, G. C., *Fourteenth Symposium (International) on Combustion*, The Combustion Institute, Pittsburgh, 1972, p. 929.
8. Medalia, A. I., and Heckman, F. A., *Carbon* 7:567–582 (1969).
9. Magnussen, B. F., *Fifteenth Symposium (International) on Combustion*, The Combustion Institute, Pittsburgh, 1974, p. 1415.
10. Tence, M., Chevalier, J. P., and Jullien, R., *J. Physi. (Paris)* 47:1989–1998 (1986).
11. Martin, J. E., and Hurd, A. J., *J. Appl. Cryst.* 20:61–78 (1987).
12. Samson, R. J., Mulholland, G. W., and Gentry, J. W., *Langmuir* 3:272–281 (1987).
13. Mountain, R. D., and Mulholland, G. W., *Langmuir* 4:1321–1326 (1988).
14. Dobbins, R. A., and Megaridis, C. M., *Langmuir* 3:254–259 (1987).
15. Megaridis, C. M., and Dobbins, R. A., *Combust. Sci. Technol.* 66:1–16 (1989).
16. Megaridis, C. M., and Dobbins, R. A., *Combust. Sci. Technol.* 71:95–109 (1990).
17. Dobbins, R. A., and Megaridis, C. M., *Appl. Opt.* 30:4747–4754 (1991).
18. Puri, R., Richardson, T. F., Santoro, R. J., and Dobbins, R. A., *Combust. Flame* 92:320–333 (1993).
19. Köylü, Ü. Ö., and Faeth, G. M., *Combust. Flame* 89:140–156 (1992).
20. Köylü, Ü. Ö., and Faeth, G. M., *J. Heat Transf.*, 116:152–159 (1994).
21. Köylü, Ü. Ö., and Faeth, G. M., *J. Heat Transf.*, in press.
22. Berry, M. V., and Percival, I. C., *Optica Acta* 33:577–591 (1986).
23. Farias, T., Carvalho, M. G., Köylü, Ü. Ö., and Faeth, G. M., *J. Heat Transf.*, in press.
24. Sorensen, C. M., Cai, J., and Lu, N., *Appl. Opt.* 31:6547–6557 (1992).
25. Cai, J., Lu, N., and Sorensen, C. M., *Langmuir* 9:2861 (1993).
26. Wu, M. K., and Friedlander, S. K., *J. Colloid Inter. Sci.* 159: 246–248 (1993).
27. Sivathanu, Y. R., and Faeth, G. M., *Combust. Flame* 81:133–149 (1990).
28. Köylü, Ü. Ö., and Faeth, G. M., *Combust. Flame* 87:61–76 (1991).
29. Sunderland, P. B., Köylü, Ü. Ö., and Faeth, G. M., *Combust. Flame*, in press.
30. Hinds, W. C., *Aerosol Technology*, Wiley, New York, 1982, pp. 83, 154.
31. Eisner, A. D., and Rosner, D. E., *Combust. Flame* 6:153–166 (1985).
32. Rosner, D. E., Mackowski, D. W., and Garcia-Ybarra, P., *Combust. Sci. Technol.* 80:87–101 (1991).

Received 28 January 1994; revised 7 June 1994

Appendix E: Köylü and Faeth (1996)

Spectral Extinction Coefficients of Soot Aggregates From Turbulent Diffusion Flames

Ü. Ö. Köylü
Department of Chemical Engineering,
Yale University,
New Haven, CT 06520-8286

G. M. Faeth
Department of Aerospace Engineering,
The University of Michigan,
Ann Arbor, MI 48109-2118

The spectral extinction coefficients of soot aggregates were studied in the fuel-lean (overfire) region of buoyant turbulent diffusion flames. Extinction measurements were carried out in the wavelength region of 0.2–5.2 μm for flames fueled with acetylene, propylene, ethylene, and propane, burning in air. The present measurements were combined with earlier measurements of soot morphology and light scattering at 0.514 μm in order to evaluate the spectral soot refractive indices reported by Dalzell and Sarofim (1969), Lee and Tien (1981), and Chang and Charalampopoulos (1990). The specific extinction coefficients and emissivities were predicted based on Rayleigh–Debye–Gans theory for polydisperse fractal aggregates, which has been recently found to be the best approximation to treat optical cross sections of soot aggregates. The results indicated that available refractive indices of soot do not predict the spectral trends of present measurements in the ultraviolet and infrared regions. Soot complex refractive index was inferred to be $m = 1.54 + 0.48i$ at 0.514 μm, which is surprisingly in best agreement with the values reported by Dalzell and Sarofim (1969). Additionally, specific extinction coefficients of soot aggregates varied with wavelength as $\lambda^{-0.83}$ from the visible to the infrared. Finally, soot refractive indices were found to be relatively independent of fuel type for the visible and infrared spectral regions over the H/C ratio range of 0.08–0.22.

Introduction

Accurate knowledge of the spectral variation of the refractive indices of soot is necessary in order to estimate continuum radiation from luminous flames and to develop in situ optical techniques for measuring soot properties. However, there are fairly large variations among the soot refractive indices reported in the literature, implying uncertainties about which values should be used in a particular application; see, for example, Chang and Charalampopoulos (1990), Charalampopoulos (1992), Tien and Lee (1982), Viskanta and Mengüç (1987), and references cited therein for a complete discussion.

Some earlier determinations of soot refractive indices involved the use of ex-situ reflection methods involving compressed soot pellets sampled from flames; see Dalzell and Sarofim (1969), Felske et al. (1984), and references cited therein. These approaches were criticized, however, based on potential modification of soot properties by sampling and compression, as well as effects of surface roughness and voids on reflectance data that are difficult to evaluate (Felske et al., 1984; Tien and Lee, 1982; Charalampopoulos, 1992). Therefore, most recent work has employed in-situ measurements of scattering and extinction within both premixed and nonpremixed flames; see Habib and Vervisch (1988), Chang and Charalampopoulos (1990), Lee and Tien (1981), and Vaglieco et al. (1990). However, these determinations did not involve characterization of soot morphology and were analyzed using Mie theory whose accuracy to represent the optical cross sections of soot aggregates is questionable; see Dobbins and Megaridis (1991), Köylü and Faeth (1993, 1994a, b), Farias et al. (1995), and references cited therein. Additionally, there was always one more unknown than the measurements, so that a theoretical relationship between the real and imaginary parts of the refractive indices must be introduced, e.g., either the Drude–Lorentz dispersion model or the Kramers–Kronig relationships. Unfortunately, the Drude–Lorentz dispersion model requires constants that are not well known for soot and differ among the various investigations, while the Kramers–Kronig relationships require extinction data in the wavelength range of $0-\infty$, which is not feasible to obtain (Chang and Charalampopoulos, 1990; Felske and Ku, 1992; Lee and Tien, 1981). Moreover, results regarding the effects of fuel type (C/H ratio) on soot refractive indices are also contradictory. The early work of Dalzell and Sarofim (1969), and Lee and Tien (1981) suggested that soot refractive indices were weakly dependent on fuel type, although the specific findings of these studies were substantially different from each other in the visible. On the other hand, later work of Habib and Vervisch (1988), and Charalampopoulos et al. (1989) indicated significant effects of fuel type on soot refractive indices. However, Sivathanu et al. (1993) recently reported that their measurements were most consistent with the values reported by Dalzell and Sarofim (1969), while finding only a weak dependence of fuel type on soot refractive indices. Thus, the objective of the present study was to evaluate the capabilities of the soot refractive indices reported in the literature to treat the spectral extinction properties of soot aggregates, and to investigate the effect of fuel type on refractive indices.

Past work has provided information about soot morphology in the fuel-lean (overfire) region of buoyant turbulent diffusion flames for a variety of gaseous and liquid fuels burning in still air within the long residence time regime (Köylü and Faeth, 1992). In addition, angular scattering and extinction coefficients at 0.514 μm have been measured for the same conditions for flames fueled by the gaseous fuels (Köylü and Faeth, 1994a). Thus, the same conditions were adopted for the present study due to the well-characterized soot environment and the universality of overfire soot in the long residence time regime for a particular fuel. The present measurements included the extinction coefficients of soot in the wavelength region of 0.2–5.2 μm. Four gaseous hydrocarbon fuels—acetylene, propylene, ethylene and propane—were used to study the effect of fuel type (H/C ratio) on spectral refractive indices of soot. The

Contributed by the Heat Transfer Division for publication in the JOURNAL OF HEAT TRANSFER. Manuscript received by the Heat Transfer Division May 1995; revision received December 1995. Keywords: Combustion, Radiation, Thermophysical Properties. Associate Technical Editor: S. H. Chan.

spectral properties, e.g., specific extinction coefficients and emissivities, were predicted based on RDG theory for polydisperse fractal aggregates because this approach has been found to be the best approximation to represent the optical properties of soot aggregates (Köylü and Faeth, 1994a, b; Farias et al., 1995). The spectral soot refractive indices reported by Dalzell and Sarofim (1969), Lee and Tien (1981), and Chang and Charalampopoulos (1990) were chosen for comparison with the present measurements because they are frequently used in heat transfer and combustion studies and they also involve different experimental and data inversion methods.

The paper begins with description of experimental and theoretical methods. This is followed by results, considering earlier scattering measurements at 0.514 μm briefly, comparisons with different soot refractive indices in the literature, and the effect of fuel type on spectral refractive indices, in turn. An experimental correlation for the variation of specific extinction coefficients is also suggested.

Experimental Methods

The present test arrangement was the same as for the earlier light scattering measurements of Köylü and Faeth (1994a). The apparatus consisted of a 50-mm-dia water-cooled burner, which provided buoyant turbulent diffusion flames in the long residence time regime. The burner was located within a larger enclosure with a hood at the top and an adjustable exhaust system to remove the combustion products. The soot emitted from the flames was collected in a sampling duct with a 152-mm-dia exit at the top, which discharged into the main hood of the apparatus. The mixing within the duct was sufficient to yield homogeneous soot properties across the exit of the sampling duct where extinction measurements were carried out.

Three different light sources—a 30 W deuterium lamp (Oriel 6316), a 100 W QTH lamp (Oriel 6333), and a 100 W IR element (Oriel 6363)—were used in the wavelength regions 0.20–0.35, 0.35–2.0, and 2.0–5.2 μm, respectively. CaF_2 lenses were used for spatial filtering and collimating the incident light due to the wide range of wavelengths considered. The light was modulated by an enclosed chopper (Oriel 75155) before passing through the soot samples. Different interference filters were used in front of the detector to make measurements at the wavelength of interest. The reference (without soot) and transmitted (with soot) intensities were measured by a pyroelectric detector (Oriel 70841), which has a flat response in the wavelength range of 0.2–40 μm. The stability of the light sources was insured by measuring reference intensities before and after each test run at each wavelength. The detector output was stored on a computer, sampling at 400 Hz for 30 s for heavily sooting fuels (acetylene and propylene), while the sampling time was doubled to 60 s for lightly soothing fuels (ethylene and propylene) in order to increase signal-to-noise ratios. The results were averaged over three tests at each wavelength to achieve a repeatability within 1 percent.

Experimental uncertainties of the extinction coefficients increased not only with decreasing tendency of the fuel to form soot but also with increasing wavelength, since they were inversely proportional to ln (I/I_o) and sampling times. Specifically, experimental uncertainties (95 percent confidence) were estimated to be generally less than 20 percent for acetylene and propylene, and less than 40 percent for ethylene and propane for present test conditions. It should be noted that the present measurements were also compared to the results of Köylü and Faeth (1994a) at the three laser wavelengths of 0.514, 0.633, and 1.152 μm to check current measurements independently.

Theoretical Methods

Radiative Properties of Polydisperse Soot Aggregates. The complete formulation of Rayleigh–Debye–Gans polydisperse fractal aggregate theory (RDG/PFA) as well as relevant references can be found in Köylü and Faeth (1994a, b). Briefly, assuming that the individual soot particles that combine to form aggregates satisfy Rayleigh approximation ($x_p \leq 0.3$), the various cross sections of an aggregate are expressed in terms of the morphology of the aggregate and the corresponding cross sections of primary particles within the RDG/FA approximation. The mean optical cross sections of populations of randomly oriented polydisperse aggregates are found by integrating over all aggregate sizes using the log-normal aggregate size distribution function. It should be mentioned that this formal integration is necessary, since no single parameter can represent the optical properties of polydisperse aggregates. The optical coefficients (the volumetric cross sections) are the products of the cross sections and the number density of aggregates, as follows:

$$K_j = n\overline{C_j}; \quad j = vv, s, a, e \tag{1}$$

Extinction coefficient is simply the sum of absorption and total scattering, i.e.,

$$K_e = K_a + K_s = K_a(1 + \rho_{sa}) \tag{2}$$

where

$$K_a = K_a^p = \frac{6\pi E(m)}{\lambda} f_v \tag{3}$$

Nomenclature

C = optical cross section
d_p = primary particle diameter
D_f = mass fractal dimension
$E(m)$ = refractive index function = Im $[(m^2 - 1)/(m^2 + 2)]$
f = scattering form factor = $f(qR_g)$
f_v = soot volume fraction
$F(m)$ = refractive index function = $|(m^2 - 1)/(m^2 + 2)|^2$
g = total scattering factor = $g(kR_g)$
$i = (-1)^{1/2}$
I = transmitted light intensity
I_o = reference light intensity
k = wave number = $2\pi/\lambda$
k_f = fractal prefactor
K = optical coefficient
m = refractive index of soot = $\eta + i\kappa$
n = number density of aggregates
N = number of primary particles in an aggregate
q = modulus of scattering vector = $2k \sin(\theta/2)$
R_g = radius of gyration of an aggregate
S = optical path length
x_p = optical size parameter of an individual particle = $\pi d_p/\lambda$
α = correlation constant, Eq. (11)
ϵ = emissivity of soot
η = real part of refractive index of soot
κ = imaginary part of refractive index of soot
λ = wavelength of radiation
θ = scattering angle
ρ_{sa} = ratio of total scattering to absorption cross section
Φ = phase function
Ω_o = single-scattering albedo

Subscripts

a = absorption
e = extinction
s = total scattering
vv = vertically polarized incident and scattered light

Superscripts

p = individual particle property
$(\bar{\ })$ = mean value over a polydisperse aggregate population

and

$$\rho_{sa} = \rho_{sa}^{p} \frac{\overline{N^2 g}}{\overline{N}} \tag{4}$$

Therefore, the absorption coefficients of aggregates and the individual particles composing them are identical. Additionally, ρ_{sa} represents the effect of aggregation on total scattering and is related to albedo by $\rho_{sa} = \Omega_o/(1 - \Omega_o)$. The optical coefficients can be measured directly using light scattering and transmission measurements in a soot-containing environment. Specifically, the transmissivity, I/I_o, for a uniform path length of S is given as follows:

$$\frac{I}{I_0} = \exp(-K_e S) \tag{5}$$

where the quantity, $K_e S$, is called the optical thickness. The underlying requirement for the use of Eq. (5) is to have an optically thin medium, i.e., $K_e S \ll 1$. However, this condition can be relaxed somewhat as long as absorption is the dominant mechanism. In other words, the range of applicability of Eq. (5) is extended further as long as $K_s S \ll 1$ (Bohren and Huffman, 1983).

A useful quantity for radiative heat transfer calculations is the specific extinction coefficient, defined as the extinction coefficient per unit volume fraction of soot. By combining Eqs. (2)–(4), an explicit form for specific extinction coefficient is obtained as follows:

$$\frac{K_e}{f_v} = \frac{6\pi E(m)}{\lambda}\left[1 + \frac{2}{3}\frac{F(m)}{E(m)} x_p^3 \frac{\overline{N^2 g}}{\overline{N}}\right] \tag{6}$$

where $g = g(kR_g)$ is the total scattering factor. This implies that if the soot morphology is known, the right-hand side of Eq. (6) is only a function of the refractive indices. Thus, the specific extinction coefficient is a logical parameter for comparing refractive indices from different sources. The spectral emissivity can be expressed in terms of specific extinction coefficient as follows:

$$\epsilon_\lambda = 1 - \exp\left[-\left(\frac{K_e}{f_v}\right) f_v S\right] \tag{7}$$

Another important radiative property is the phase function (Siegel and Howell, 1981), which is given as follows within RDG/PFA theory:

$$\Phi(\theta) = \Phi^p(\theta)\left(\frac{\overline{N^2 f}}{\overline{N^2 g}}\right) \tag{8}$$

where $f = f(qR_g)$ represents the angular scattering form factor. This formulation implies that the radiative properties of aggregates are substantially different from those of individual particles.

Soot Refractive Indices. Among the mean radiative properties, only the albedo is independent of refractive indices, which are the fundamental quantities required for most practical optical property calculations. In particular, the values of $E(m)$ and the ratios of $F(m)/E(m)$ are needed for both spectral radiative properties and determinations of soot volume fractions; see Eqs. (6) and (7). Thus, the spectral variations of $E(m)$ and the ratio $F(m)/E(m)$ from different sources are illustrated in Fig. 1. Results in the figure are based on the measurements of Dalzell and Sarofim (1969), Lee and Tien (1981), and Chang and Charalampopoulos (1990). It is evident that there are significant differences for $E(m)$ and $F(m)/E(m)$ among these three studies, noting that other determinations in the literature would yield even wider variations (Charalampopoulos, 1992). $E(m)$ values

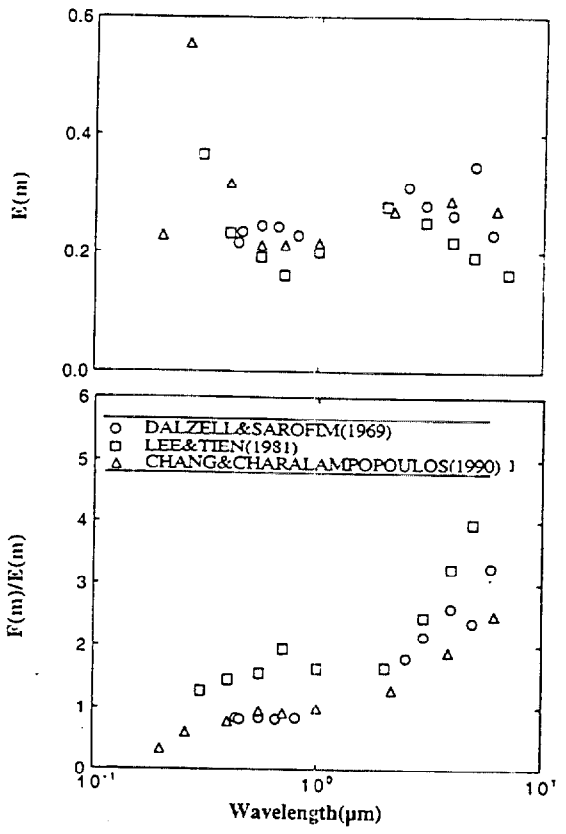

Fig. 1 $E(m)$ values and ratios of $F(m)/E(m)$ as a function of wavelength as determined by Dalzell and Sarofim (1969), Lee and Tien (1981), and Chang and Charalampopoulos (1990)

from the three investigations agree somewhat in the visible; however, there are up to 40 percent differences in the infrared and ultraviolet. Although, the values from Dalzell and Sarofim (1969), and Chang and Charalampopoulos (1990) yield very similar spectral variations of $E(m)$, Lee and Tien (1981) always give lower estimates. On the other hand, there is even less agreement about the ratios of $F(m)/E(m)$ among these three studies with up to 100 percent differences encountered in the infrared. The ratios of $F(m)/E(m)$ from Dalzell and Sarofim (1969), and Chang and Charalampopoulos (1990) agree well in the visible while the estimates from Lee and Tien (1981) are higher than the other two at all wavelengths. These differences among refractive indices result in corresponding uncertainties about radiative properties. Thus, use of refractive indices from a particular source can only be justified by the evidence that they treat measured spectral properties effectively, which was the main motivation for the present investigation.

Results and Discussion

Scattering at 0.514 μm. Measured phase function from the earlier scattering measurements, along with the predictions from the various approximate theories, are plotted as a function of scattering angle in Fig. 2. The measurements are for acetylene soot from the scattering measurements of Köylü and Faeth (1994a) at 0.514 μm, while the predictions are based on TEM characterization of soot morphology from Köylü and Faeth (1992). As can be seen from Fig. 2, soot aggregates scatter strongly in the forward direction; additionally, predictions of the RDG/PFA theory are in good agreement with measurements. However, neither Mie theory for an equivalent diameter nor the

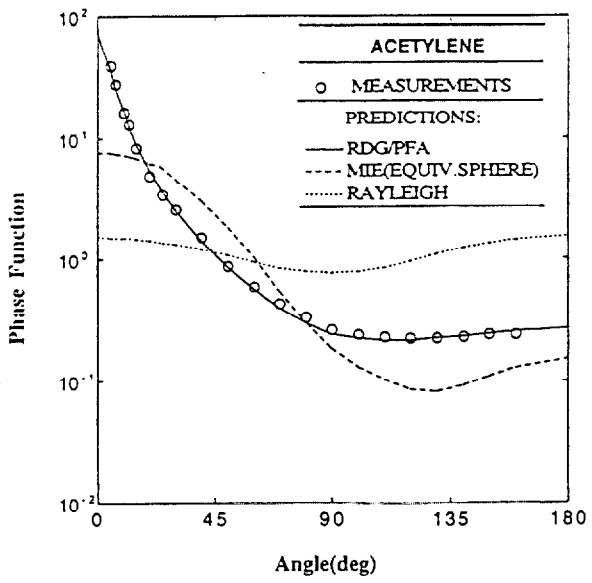

Fig. 2 Various theoretical predictions and measurements of phase function for soot aggregates in the overfire region of turbulent acetylene/air diffusion flame

Rayleigh approximation can predict the angular trends of phase function. These results suggest the importance of aggregate scattering and justifies the use of RDG/PFA theory to estimate spectral properties of soot.

Köylü and Faeth (1994a) reported a limited assessment of soot refractive indices at 0.514 μm based on RDG/PFA theory, which yielded the following relationship for large scattering angles corresponding to the power-law regime:

$$\frac{F(m)}{E(m)} = 4\pi \frac{(qd_p)^{D_f}}{k_f x_p^3} \frac{K_w}{K_a} \tag{9}$$

However, this evaluation was based on an assumed value of fractal prefactor, k_f (appearing in the relationship $N = k_f(R_g/d_p)^{D_f}$ for fractal-like aggregates), and there were still some concerns about the reliability of RDG/FA theory. Later, Köylü et al. (1995) established a value of $k_f = 8.5 \pm 0.5$, independently from three-dimensional reconstructions of TEM images. Additionally, RDG/PFA theory was further evaluated both experimentally (Köylü and Faeth, 1994b) and computationally (Farias et al., 1995), finding satisfactory performance. Thus, it is appropriate to reconsider Eq. (9) in conjunction with the present study.

Using the earlier measurements of soot morphology and light scattering at 0.514 μm, together with values of $k_f = 8.5$ and $D_f = 1.8$, Eq. (9) yields $F(m)/E(m) = 0.78$ with a standard deviation of 0.09 over all the fuels. Since the range of $E(m)$ values from different sources are rather narrow compared to $F(m)$, a value of $E(m) = 0.23$ seems to be reasonable (see Fig. 1). This, together with measured value of $F(m)/E(m)$, yields a complex refractive index of $m = 1.54 + 0.48i$ at 0.514 μm, which is in reasonably good agreement with the measurements of Dalzell and Sarofim (1969) and Chang and Charalampopoulos (1990). However, the refractive indices at this wavelength given by Lee and Tien (1981) yield $F(m)/E(m) = 1.55$, which is almost 100 percent higher than the measured value.

Spectral Extinction Properties of Soot. Measured optical thicknesses, K_eS, in the wavelength range 0.2–5.2 μm, are illustrated in Fig. 3 for all the fuels considered during the present study. The strong gas absorption bands of H_2O at 2.7 μm, and CO_2 at 4.3 μm were avoided during the spectral measurements. The results yielded a maximum extinction coefficient in the ultraviolet region at a wavelength of approximately 0.25 μm for all fuels. Menna and D'Alessio (1982) and Chang and Charalampopoulos (1990) reported similar observations, which seem to be caused by a resonance of soot refractive indices at this wavelength range. In contrast, the behavior of spectral extinction coefficients in the infrared is monotonic, i.e., extinction coefficients decrease with increasing wavelength, as expected.

The present spectral measurements of extinction coefficients will now be used to assess existing refractive indices in the literature. Soot volume fractions are estimated using $m = 1.54 + 0.48i$ at 0.514 μm and applying Eq. (6) at the same wavelength. Knowing the volume fraction and the morphology of soot, then it is possible to evaluate Eq. (6) at each wavelength using refractive indices from different sources and to compare it with measurements. The resulting measured and predicted specific extinction coefficients are plotted as a function of wavelength in Fig. 4. The spectral measurements are for the overfire soot aggregates emitted from propane/air flame, while the predictions are based on RDG/PFA theory using the refractive indices of Dalzell and Sarofim (1969), Lee and Tien (1981), and Chang and Charalampopoulos (1990). The results indicate that the predictions of all three sources are in good agreement with measurements in the visible. However, this may be misleading for the values of Lee and Tien (1981), because it was previously shown that they overestimated scattering by almost 100 percent at 0.514 μm; therefore, the suitable extinction behavior is an artifact of their low values of $E(m)$ compensating for high ratios of $F(m)/E(m)$. Thus, only the refractive indices from Dalzell and Sarofim (1969), and Chang and Charalampopoulos (1990) seem to be acceptable in the visible.

The refractive indices from the three studies overestimate the observed extinction levels by up to a factor of three in the ultraviolet. However, the values from Chang and Charalampopoulos (1990) correctly predict the properties of the resonance of refractive indices near 0.25 μm. Although the measurements of Dalzell and Sarofim (1969), and Lee and Tien (1981) do not extend into this short wavelength region, their dispersion models fail to indicate the presence of the resonance phenomena, as quantified by Menna and D'Alessio (1982). In other

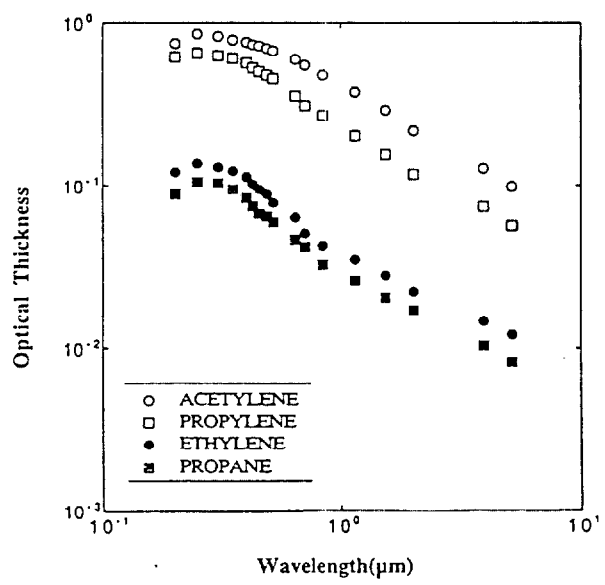

Fig. 3 Measurements of optical thickness as a function of wavelength for soot aggregates in the overfire region of turbulent hydrocarbon diffusion flames

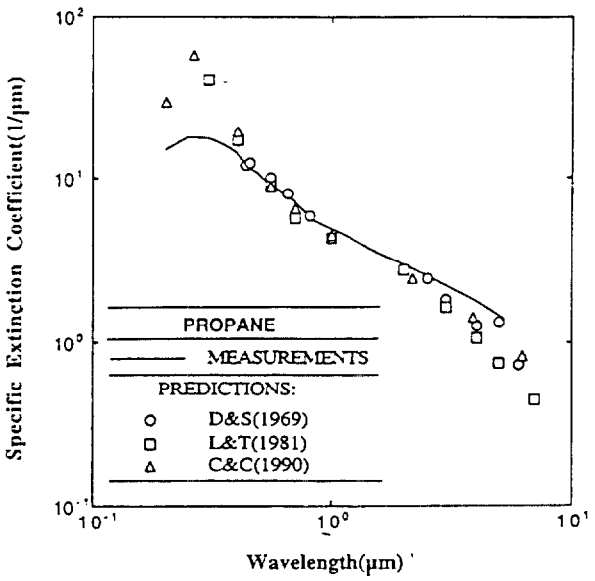

Fig. 4 Predictions of various refractive indices and measurements of spectral specific extinction coefficient of soot aggregates in the overfire region of turbulent propane/air diffusion flame

words, their extinction coefficient estimates would continue to increase with decreasing wavelength, with no peak in the UV. Thus, the magnitude as well as the trend of their refractive indices do not agree with present measurements. At this point, some of the overall poor agreement between predictions and measurements may be caused by the approximations of the RDG/PFA theory because optical size parameters become rather large in the region of the resonance. However, the mean individual particle diameter for propane soot is 30 nm, yielding $x_p = 0.38$ at 0.25 μm. Although this small deviation of individual particles from Rayleigh scattering behavior ($x_p \leq 0.3$) cannot be responsible for the significant differences between measurements and predictions at this wavelength, the performance of RDG/PFA theory in the ultraviolet region of the spectrum certainly merits additional study.

The refractive indices from the three sources yield predictions that begin to deviate from measurements as the wavelength increases from visible into the infrared. Although the values from Dalzell and Sarofim (1969) yield best agreement with measurements in this wavelength range, all three data sets underestimate the measurements of specific extinction coefficients. This is probably due to their low $E(m)$ values in the infrared, as will be demonstrated in the following by evaluating Eq. (6) at $\lambda_1 = 0.514$ μm and $\lambda_2 = 5.2$ μm, and taking the ratio:

$$\frac{E(\lambda_1)}{E(\lambda_2)} = \frac{\lambda_2}{\lambda_1}\frac{K_e(\lambda_2)}{K_e(\lambda_1)}[1 + \rho_{sa}(\lambda_1)] \tag{10}$$

since the scattering is negligible at 5.2 μm, i.e., $\rho_{sa}(\lambda_2) \cong 0$. Noting that all the quantities on the right-hand side of Eq. (10) are known from the measurements, the ratios between $E(m)$ at 5.2 and 0.514 μm can be calculated. This yields $E(5.2\ \mu\text{m})/E(0.514\ \mu\text{m}) = 1.89$ with a standard deviation of 0.18 for all the fuels. This ratio is given by Dalzell and Sarofim (1969), Lee and Tien (1981), and Chang and Charalampopoulos (1990) as 1.38, 1.00, and 1.21, respectively. Thus, the closest agreement is obtained from the refractive indices of Dalzell and Sarofim (1969), underestimating the measured value by 27 percent. Nevertheless, the differences between predictions and measurements are typically 50–100 percent at long wavelengths. These results also suggest a value of $E(m) = 0.42$ at 5.2 μm, when $E(m)$ at 0.514 μm is taken to be 0.23.

The emissivities of the soot aggregates are illustrated as a function of wavelength for propylene in Fig. 5. Spectral emissivities are obtained from Eq. (7) using the measurements of specific extinction coefficients. Again, the predictions are based on the RDG/PFA theory with refractive indices from Dalzell and Sarofim (1969), Lee and Tien (1981), and Chang and Charalampopoulos (1990). Similar to the results for specific extinction coefficients, the predicted emissivities are overestimated in the UV and underestimated in the IR. On the other hand, measurements and predictions are in good agreement for visible wavelengths. Among the three, the refractive indices from Dalzell and Sarofim (1969) appear to be yielding best estimates of emissivities, followed by the results of Chang and Charalampopoulos (1990). It is a puzzling fact that not only this study but also other studies (Sivathanu et al., 1993; Choi et al., 1994; Dobbins et al., 1994) find that the refractive index data from the highly criticized ex-situ reflection measurements of Dalzell and Sarofim (1969) yield predictions that are in good agreement with the scattering/extinction/emission measurements in the visible and near-infrared portions of the spectrum. Why this is so is not clear and certainly merits further investigation. However, the overall differences between the measured and predicted spectral emissivities in the infrared may result in significant differences (20–40 percent) in the total emittance for typical flame temperatures. It should be mentioned that the results for other fuels were similar and will not be discussed here.

Experimental Correlation for Spectral Properties. As discussed in the introduction, it is well established that the Drude–Lorentz model is not only inappropriate for soot-like materials but also involves several unknown parameters. As a result, although it was desirable to obtain spectral refractive indices of soot, application of any dispersion model was avoided. On the other hand, several authors (see, for example, Siegel and Howell (1981), and Siddall and McGrath (1963)) have reported that the specific extinction coefficients of soot varied with wavelength according to:

$$K_e/f_v \propto \lambda^{-\alpha} \tag{11}$$

The use of Eq. (11) is practical in radiative heat transfer calculations for soot, since the expression does not involve the compli-

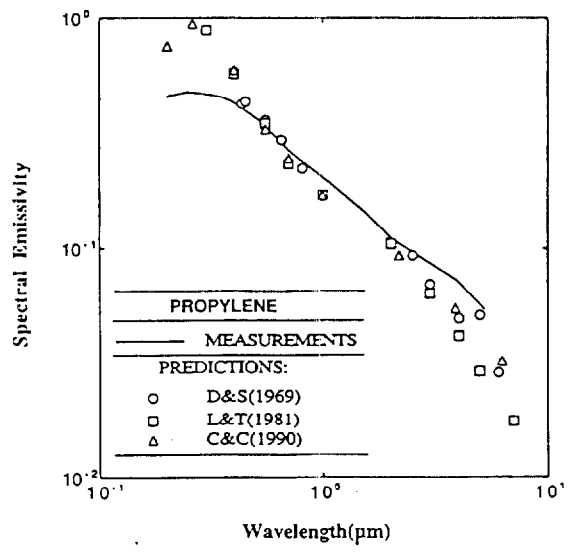

Fig. 5 Predictions of various refractive indices and measurements of emissivity of soot aggregates in the overfire region of turbulent propylene/air diffusion flame

cations of refractive indices. Thus, a similar correlation was sought for the present test conditions. The least-square fits of the measurements in the wavelength range of 0.514–5.2 μm yielded a value of $\alpha = 0.83$ with a standard deviation of 0.04 for the four fuels considered in this study. The values suggested by the refractive indices of Dalzell and Sarofim (1969), Lee and Tien (1981), and Chang and Charalampopoulos (1990) are in the range of 0.94–1.21, which are 13–47 percent higher than the present measurements. Additionally, the experimental correlation given above implies that $E(m)$ should increase slightly with increasing wavelength, i.e., $E(m) \propto \lambda^{0.17}$ in the infrared. This also suggests that the refractive indices of soot are weak functions of wavelength in this part of the spectrum. This behavior, however, differs from the behavior of available refractive indices in the infrared, as can be seen from Fig. 1, which shows a decrease (Dalzell and Sarofim, 1969; Lee and Tien, 1981), or almost no variation (Chang and Charalampopoulos, 1990) of $E(m)$ with increasing wavelength in the infrared.

Other evaluations of α directly from extinction measurements are available in the literature. Siddall and McGrath (1963) extensively studied the spectral behavior of several types of soot in the infrared portion, reporting $\alpha = 0.77-1.25$. However, most of their measurements involved optically thick conditions, where use of Eq. (5) is questionable, as discussed previously. Consistent with this observation, their measurements with avtur kerosine and amyl acetate soot had similar extinction levels to present study and yielded $\alpha = 0.77$ and 0.89, respectively. These values are in excellent agreement with the present measurements, which may imply that the results of the present study can be extended to other types of fuel. Additionally, their claim of variation of α with wavelength should be interpreted with great caution, since the method used to calculate α at each wavelength involved high experimental uncertainties due to taking successive logarithms. Thus, $\alpha = 0.83$ appears to be reasonable with a wavelength range from the visible to infrared.

Effect of Fuel Type on Soot Refractive Indices. Table 1 is a summary of soot refractive index properties found during the present study. The table includes $F(m)/E(m)$ at 0.514 μm, the ratios of the values of $E(m)$ at 5.2 μm and 0.514 μm, and the values of α, representing the spectral variation of refractive indices in the range of 0.514–5.2 μm. As can be seen from Eqs. (9), (10) and (11), these parameters are all obtained without using any assumptions including soot volume fraction. The changes in all three measurements with fuel type were within present experimental uncertainties, suggesting that the refractive indices of soot are relatively independent of fuel type from visible to infrared for the present test conditions. In view of similar observations of Sivathanu et al. (1993) for soot within laminar premixed flames, this weak dependence may apply to other flame environments, simplifying both in-situ soot volume fraction determinations and radiative heat transfer calculations.

Table 1

Fuel	F(0.514 μm)/E(0.514 μm)	E(5.2 μm)/E(0.514 μm)	α
Acetylene	0.66	2.07	0.84
Propylene	0.84	1.77	0.87
Ethylene	0.85	2.01	0.78
Propane	0.77	1.71	0.82
Mean (stand. dev.)	0.78 (0.09)	1.89 (0.18)	0.83 (0.04)

[a] Measurements involve overfire soot for buoyant turbulent diffusion flames burning in air for the designated fuel.

However, additional studies in various flames will be required in order to firmly establish the insensitivity of refractive indices to fuel type.

Conclusions

The spectral extinction coefficients of soot were measured in the wavelength region of 0.2–5.2 μm. Four hydrocarbon fuels were considered in order to vary H/C ratios in the range 0.08 to 0.22. Test conditions were limited to the fuel-lean (overfire) region of buoyant turbulent diffusion flames in the long residence time regime, where soot morphology, and soot scattering properties at 0.514 μm, were known from earlier work (Köylü and Faeth, 1992, 1994a). The results of the present measurements were combined with earlier findings in order to evaluate existing refractive indices in the literature. The major conclusions of the study are as follows:

1 The refractive indices determined by Dalzell and Sarofim (1969), and Chang and Charalampopoulos (1990) were in good agreement with present extinction and scattering measurements in the visible. The values from Lee and Tien (1981), however, gave less satisfactory results in the same wavelength region. Additionally, the present study suggests a complex refractive index of $m = 1.54 + 0.48i$ at 0.514 μm, which is in best agreement with the measurements of Dalzell and Sarofim (1969) at visible wavelengths.

2 The specific extinction coefficients of soot were found to vary with wavelength from visible to infrared according to $K_e/f_v \propto \lambda^{-\alpha}$, where $\alpha = 0.83 \pm 0.08$ for all the fuels considered in this investigation. The spectral refractive indices from Dalzell and Sarofim (1969), Lee and Tien (1981), and Chang and Charalampopoulos (1990) yielded values of α that are 13–47 percent higher than the measured value, which would result in an underestimation of total emittance up to 40 percent for typical flame temperatures.

3 The present spectral extinction measurements, together with previous scattering results, showed that the ratios of $F(m)/E(m)$ at 0.514 μm, the ratios of values of $E(m)$ at 5.2 μm and 0.514 μm, and the values of α, representing the spectral variation of refractive indices in the range of 0.514–5.2 μm did not change with fuel type within experimental uncertainties. All three measurements suggest that soot refractive indices are relatively independent of fuel type for the visible and infrared spectral ranges for the present test conditions.

Acknowledgments

This research was sponsored by the Building and Fire Research Laboratory of the National Institute of Standards and Technology, Grant No. 60NANB1D1175, with K. C. Smyth and H. R. Baum serving as Scientific Officers; and by NASA, Grant No. NAG3-1245, under the technical management of D. L. Urban of the Lewis Research Center. One of the authors (Ü. Ö. K.) would like to acknowledge the partial support by AFOSR, Grant No. 94-0143, with J. M. Tishkoff serving as Technical Monitor.

References

Bohren, C. F., and Huffman, D. R., 1983, *Absorption and Scattering of Light by Small Particles*, Wiley, New York, pp. 69–81.

Chang, H., and Charalampopoulos, T. T., 1990, "Determination of the Wavelength Dependence of Refractive Indices of Flame Soot," *Proc. R. Soc. London A*, Vol. 430, pp. 577–591.

Charalampopoulos, T. T., 1992, "Morphology and Dynamics of Agglomerated Particulates in Combustion Systems Using Light Scattering Techniques," *Prog. Energy Combust. Sci.*, Vol. 18, pp. 13–45.

Charalampopoulos, T. T., Chang, H., and Stagg, B. J., 1989, "The Effects of Temperature and Composition on the Complex Refractive Index of Flame Soot," *Fuel*, Vol. 68, pp. 1173–1179.

Choi, M. Y., Hamins, A., Mulholland, G. W., and Kashiwagi, T., 1994, "Simultaneous Optical Measurement of Soot Volume Fraction and Temperature in Premixed Flames," *Combust. Flame*, Vol. 99, pp. 174–186.

Dalzell, W. H., and Sarofim, A. F., 1969, "Optical Constants of Soot and Their Application to Heat Flux Calculations," ASME JOURNAL OF HEAT TRANSFER, Vol. 91, pp. 100–104.

Dobbins, R. A., and Megaridis, C. M., 1991, "Absorption and Scattering of Light by Polydisperse Aggregates," *Appl. Optics*, Vol. 30, pp. 4747–4754.

Dobbins, R. A., Mulholland, G. W., and Bryner, N. P., 1994, "Comparison of a Fractal Smoke Optics Model With Light Extinction Measurements," *Atmos. Environ.*, Vol. 28, pp. 889–897.

Farias, T. L., Carvalho, M. G., Köylü, Ü. Ö., and Faeth, G. M., 1995, "Computational Evaluation of Approximate Rayleigh-Debye-Gans/Fractal Aggregate Theory for the Absorption and Scattering Properties of Soot," ASME JOURNAL OF HEAT TRANSFER, Vol. 117, pp. 152–159.

Felske, J. D., and Ku, J. C., 1992, "A Technique for Determining the Spectral Refractive Indices, Size and Number Density of Soot Particles From Light Scattering and Spectral Extinction Measurements in Flames," *Combust. Flame*, Vol. 91, pp. 1–20.

Felske, J. D., Charalampopoulos, T. T., and Hura, H., 1984, "Determination of the Refractive Indices of Soot Particles From the Reflectivities of Compressed Soot Pellets," *Combust. Sci. Tech.*, Vol. 37, pp. 263–283.

Habib, Z. G., and Vervisch, P., 1988, "On the Refractive Index of Soot at Flame Temperature," *Combust. Sci. Tech.*, Vol. 59, pp. 261–274.

Köylü, Ü. Ö., and Faeth, G. M., 1992, "Structure of Overfire Soot in Buoyant Turbulent Diffusion Flames at Long Residence Times," *Combust. Flame*, Vol. 89, pp. 140–156.

Köylü, Ü. Ö., and Faeth, G. M., 1993, "Radiative Properties of Flame-Generated Soot," ASME JOURNAL OF HEAT TRANSFER, Vol. 115, pp. 409–417.

Köylü, Ü. Ö., and Faeth, G. M., 1994a, "Optical Properties of Overfire Soot in Buoyant Turbulent Diffusion Flames at Long Residence Times," ASME JOURNAL OF HEAT TRANSFER, Vol. 116, pp. 152–159.

Köylü, Ü. Ö., and Faeth, G. M., 1994b, "Optical Properties of Soot in Buoyant Laminar Diffusion Flames," ASME JOURNAL OF HEAT TRANSFER, Vol. 116, pp. 971–979.

Köylü, Ü. Ö., Faeth, G. M., Farias, T. L., and Carvalho, M. G., 1995, "Fractal and Projected Structure Properties of Soot Aggregates," *Combust. Flame*, Vol. 100, pp. 621–633.

Lee, S. C., and Tien, C. L., 1981, "Optical Constants of Soot in Hydrocarbon Flames," *Eighteenth Symposium (International) on Combustion*, The Combustion Institute, Pittsburgh, pp. 1159–1166.

Menna, P., and D'Alessio, A., 1982, "Light Scattering and Extinction Coefficients for Soot Forming Flames in the Wavelength Range From 200 nm to 600 nm," *Nineteenth Symposium (International) on Combustion*, The Combustion Institute, Pittsburgh, pp. 1421–1428.

Siddall, R. G., and McGrath, I. A., 1963, "The Emissivity of Luminous Flames," *Ninth Symposium (International) on Combustion*, The Combustion Institute, Pittsburgh, pp. 102–110.

Siegel, R., and Howell, J. R., 1981, *Thermal Radiation Heat Transfer*, Hemisphere, New York, pp. 658–669.

Sivathanu, Y. R., Gore, J. P., Janssen, J. M., and Senser, D. W., 1993, "A Study of In Situ Specific Absorption Coefficients of Soot Particles in Laminar Flat Flames," ASME JOURNAL OF HEAT TRANSFER, Vol. 115, pp. 653–658.

Tien, C. L., and Lee, S. C., 1982, "Flame Radiation," *Prog. Energy Combust. Sci.*, Vol. 8, pp. 41–59.

Vaglieco, B. M., Beretta, F., and D'Alessio, A., 1990, "In Situ Evaluation of the Soot Refractive Index in the UV-Visible from the Measurements of the Scattering and Extinction Coefficients in Rich Flames," *Combust. Flame*, Vol. 79, pp. 259–271.

Viskanta, R., and Mengüç, M. P., 1987, "Radiation Heat Transfer in Combustion Systems," *Prog. Energy Combust. Sci.*, Vol. 13, pp. 97–160.

Appendix F: Wu et al. (1997)

Refractive Indices at Visible Wavelengths of Soot Emitted From Buoyant Turbulent Diffusion Flames

J.-S. Wu[1]
Research Fellow

S. S. Krishnan
Graduate Student Research Assistant

G. M. Faeth
Prof., Fellow ASME
gmfaeth@umich.edu

Department of Aerospace Engineering,
The University of Michigan,
Ann Arbor, MI 48109-2118

Measurements of the optical properties of soot, emphasizing refractive indices, are reported for visible wavelengths (350–800 nm). The experiments considered soot in the fuel-lean (overfire) region of buoyant turbulent diffusion flames in the long residence time regime where soot properties are relatively independent of position in the overfire region and residence time. Flames fueled with acetylene, propylene, ethylene, and propane that were burning in still air provided a range of soot physical and structure properties. Measurements included soot composition, density, structure, gravimetric volume fraction, and scattering and absorption properties. These data were analyzed to find soot fractal dimensions, refractive indices, refractive index functions, and dimensionless extinction coefficients assuming Rayleigh-Debye-Gans scattering for polydisperse mass fractal aggregates (RDG-PFA theory). RDG-PFA theory was successfully evaluated using measured scattering properties. Soot fractal dimensions were independent of both fuel type and wavelength, yielding a mean value of 1.77 with a standard deviation of 0.04. Refractive indices were independent of fuel type within experimental uncertainties and were in reasonably good agreement with earlier measurements for soot in the fuel-lean region of diffusion flames due to Dalzell and Sarofim (1969). Dimensionless extinction coefficients were independent of both fuel type and wavelength, yielding a mean value of 5.1 with a standard deviation of 0.5, which is lower than earlier measurements for reasons that still must be explained.

Introduction

Information about the structure and optical properties of soot is needed in order to develop reliable nonintrusive (optical) measurements of soot properties and estimates of continuum radiation due to soot in flame environments. Past work has established some information about soot optical properties as follows: (i) soot consists of nearly monodisperse spherical primary particles that collect into mass fractal aggregates having broad size distributions (Faeth and Köylü, 1995; Jullien and Botet, 1987; Medalia and Heckman, 1969); (ii) soot optical properties in the visible can be approximated by Rayleigh-Debye-Gans scattering from polydisperse mass fractal aggregates, called RDG-PFA theory (Dobbins and Megaridis, 1991; Faeth and Köylü, 1995; Farias et al., 1995; Köylü and Faeth, 1994a, b; Martin and Hurd, 1987); and (iii) current estimates of soot optical properties in flame environments are mainly limited by excessive uncertainties about soot refractive indices (Chang and Charalampopoulos, 1990; Faeth and Köylü, 1995; Tien and Lee, 1982; Vaglieco et al., 1990; Viskanta and Mengüc, 1987). Motivated by these observations, the objective of the present investigation was to experimentally determine soot optical properties at visible wavelengths, emphasizing soot refractive indices.

Earlier studies of soot refractive indices in the visible are briefly reviewed in the following, more details can be found in Chang and Charalampopoulos (1990), Charalampopoulos (1992), Lee and Tien (1980), Tien and Lee (1982), Viskanta and Mengüc (1987), and references cited therein. The earliest determinations of soot refractive indices involved ex situ reflectivity measurements of compressed soot samples (Dalzell and Sarofim, 1969; Felske et al., 1984); these results were questioned, however, due to potential changes of soot properties caused by sample collection and compression as well as potential effects of surface irregularities on measured reflectance properties (Charalampopoulos, 1992; Felske et al., 1984; Tien and Lee, 1982). As a result, subsequent work emphasized in situ measurements of extinction and scattering (Chang and Charalampopoulos, 1990; Charalampopoulos, 1992; Habib and Vervisch, 1988; Lee and Tien, 1980; Vaglieco et al., 1990); unfortunately, these studies also involved a number of the following deficiencies: soot structure generally was not characterized adequately; Rayleigh and Mie scattering approximations were used to interpret the measurements, which have not proven to be very effective for soot aggregates; and questionable approximations involving either Drude-Lorentz dispersion models or Kramers-Krönig causality relationships had to be adopted so that soot refractive indices could be found from the measurements (Dobbins and Megaridis, 1991; Faeth and Köylü, 1995; Köylü and Faeth, 1994a, b, 1996).

In view of these considerations, the present experimental study of soot refractive indices and related optical properties was undertaken; this study considered soot emitted from buoyant turbulent diffusion flames in the long residence time regime where soot properties are relatively independent of position in the fuel-lean (overfire) region and the residence time. A range of soot physical and structure properties were studied by considering flames fueled with acetylene, propylene, and ethylene and propane burning in still air. The approach to find optical properties involved ex situ measurements of soot physical and structure properties, gravimetric measurements of soot volume

[1] Now with the National Space Program Office, Hsin-Chu City, Taiwan, Republic of China.

Contributed by the Heat Transfer Division for publication in the JOURNAL OF HEAT TRANSFER. Manuscript received by the Heat Transfer Division February 19, 1996; revision received November 14, 1996; Keywords: Fire/Flames, Radiation, Thermophysical Properties. Associate Technical Editor: S. H. Chan.

fractions, and in situ measurements of soot extinction and scattering properties. Then, after checking that RDG-PFA theory was acceptable, this theory was used to find the fractal dimensions, refractive indices, and dimensionless extinction coefficients of the soot. Present measurements were carried out at visible wavelengths (350–800 nm) because this wavelength range is important for nonintrusive (optional) measurements of soot properties and is accessible for in situ optical techniques due to reasonably large soot scattering levels.

The paper begins with descriptions of experimental and theoretical methods. Results are then considered treating soot scattering properties, fractal dimensions, and optical properties in turn.

Experimental Methods

Apparatus. The apparatus is described by Köylü and Faeth (1994a). Combustion was in still air within a large enclosure to control room disturbances. A 50 mm diameter watercooled burner, injecting fuel gases vertically upward, was used to yield strongly buoyant turbulent diffusion flames. Soot properties were measured by collecting the combustion products in a hood and in a 152 mm diameter sampling duct (both of which were heated to prevent thermophoretic deposition of soot on their surfaces) that discharged into the main exhaust hood of the flame apparatus. Measurements showed that mixing within the collection system was sufficient to yield uniform properties (soot concentrations, gas concentrations, and temperatures) across the exit of the sampling duct where measurements were made. Note: using a collection system in this way does not affect soot structure and optical properties because soot properties are relatively independent of position in the overfire region and residence time within the long residence time regime (Köylü and Faeth, 1994a).

Sampling Measurements. Aside from routine sampling measurements of gas temperatures and compositions at the measuring location, sampling measurements included soot structure, density, composition, and gravimetric volume fractions. Soot structure was found by thermophoretic sampling and analysis using transmission electron microscopy (TEM), following Köylü and Faeth (1992). The sampling surfaces were the carbon-supported copper grids used to hold TEM specimens (3 mm diameter 200 mesh copper grids supported by a 20 nm thick elemental carbon film: SPI Supplies, Philadelphia, PA, Part No. 3520C). When sampling, the grids were parallel to the flow direction (vertical) at the flow axis. The grids were mounted on a double-acting pneumatic probe with sampling times measured using a pair of light-intercepting sensors and controlled so that soot aggregates covered less than 10 percent of the grid surface in order to avoid overlapping aggregates on the grid. Effects of aggregate size on sampling bias for the present soot aggregates are discussed by Köylü and Faeth (1992) and Köylü et al. (1995); approximating aggregates by equivalent spheres suggests sampling velocity variations less than 20 percent over the size range of 95 percent of the aggregates. Similarly, allowing for the branched structure of the aggregates, following Rosner et al. (1991), also suggests sampling velocity variations less than 20 percent over the aggregate size range. The samples were observed using a JEOL 2000 FX analytical electron microscope system with a 1 nm edge-to-edge resolution. Latex spheres having a diameter of 91 nm (5.8 nm standard deviation) were used to calibrate the TEM measurements. Samples of 400 primary particles selected from more than 50 aggregates were used to find the mean value of d_p with an experimental uncertainty less than 2 percent (95 percent confidence). These measurements also established that primary particles were reasonably monodisperse, i.e., standard deviations were typically 17–21 percent of mean values of d_p. Finally, the values of $\bar{N}$, due to Köylü and Faeth (1992), for the same soot were confirmed within experimental uncertainties.

Soot densities were found by thermophoretic sampling at the axis of the measuring location using a finned water-cooled metal plate. Soot was periodically scraped from the plate until a sample weighing roughly 500 mg was obtained. The samples were then compressed into pellets to facilitate density measurements using helium pycnometry with a 1000 mm^3 cell (Micrometrics Inc., Norcross, GA). Experimental uncertainties (95 percent confidence) of density measurements were estimated to be less than one percent. The composition of a portion of the overfire soot was known from Köylü (1992); therefore, these measurements were not repeated.

Gravimetric soot volume fractions were measured at the axis of the measuring location following Choi et al. (1995). This involved sampling the flow and determining the volumes of soot and gas collected. A 13 mm inside diameter water-cooled probe, aligned with the flow direction, was used for sampling. The probe was connected to a modified filter holder that could accommodate a 47 mm diameter filter (Gelman Product 2220, in-line). The filter was connected to a vacuum pump through a flowmeter and valve. The flowmeter had a manometer at its inlet and was calibrated over the required range of inlet pressures and flow rates using a wet test meter. Soot samples were collected for a timed period using two filters (Gelman Part No. 66143, 200 nm, TF200, PTFE membrane filter). One filter was

Nomenclature

C = optical cross section
d_p = primary particle diameter
D_f = mass fractal dimension
$E(m)$ = refractive index function = $Im((m^2 - 1)/(m^2 + 2))$
f_v = soot volume fraction
$F(m)$ = refractive index function = $|(m^2 - 1)/(m^2 + 2)|^2$
$i = (-1)^{1/2}$
I = light intensity
k = wave number = $2\pi/\lambda$
k_e = dimensionless extinction coefficient
k_{eR} = dimensionless extinction coefficient including scattering, Eq. (8)
k_f = fractal prefactor
L = light path length
m = soot refractive index = $n + i\kappa$
n = real part of soot refractive index
n_p = mean number of primary particles per unit volume
N = number of primary particles in an aggregate
q = modulus of scattering vector = $2k \sin(\theta/2)$
Q = volumetric optical cross section
R_g = radius of gyration of an aggregate
x_p = primary particle size parameter = $\pi d_p/\lambda$
θ = angle of scattering from forward direction
κ = imaginary part of soot refractive index
λ = wavelength of radiation
ρ_s = density of soot
ρ_{sa} = ratio of scattering to absorption cross sections
ρ_v = polarization ratio

Subscripts

a = absorption
e = extinction
h = horizontal polarization
ij = incident (i) and scattered (j) polarization directions
s = total scattering
v = vertical polarization

Superscripts

a = aggregate property
p = primary particle property
$(\bar{\ })$ = mean value over a polydisperse aggregate population

in the filter holder, and the second filter mechanically collected soot from the sampling line and filter assembly. The mass of sampled soot was found by weighing the filters before and after sampling using an electronic balance. Then, given the density of the soot, the mass of soot collected, the volume of gas collected, and gas temperatures at the sampling and volume measuring conditions, the gravimetric soot volume fraction can be calculated in a straightforward manner. Times of sampling for these measurements were adjusted to achieve experimental uncertainties less than 6 percent (95 percent confidence). The exhaust flow was nearly uniform so that sampling rates varying 4:1 around estimated isokinetic sampling rates had negligible effect on the measurements.

Optical Measurements. Scattering and extinction properties of the soot aggregates were found using the same general arrangement as Köylü and Faeth (1994a, b). The light sources used for measurements at various wave lengths were as follows: 351.2, 488.0, and 514.5 nm using an argon-ion laser (4 W Coherent Innova model 90-4); 405.0 nm using a mercury lamp and a 10 nm bandwidth filter (100 W, Oriel model 6333); 632.8 nm using a He-Ne laser (28 mW, Jodon Model HN10G1R); and 800.0 nm using a laser diode (700 mW, SDL-2360-P3). The incident beams were passed through a polarization rotator and a mechanical chopper before being focused on the axis of the sampling duct using a 1000 mm focal length lens. The collecting optics for scattering measurements were mounted on a turntable surrounding the exhaust duct so that scattering angles of 5–160 deg could be considered. The collecting optics consisted of an 85 mm focal length lens (having a collection angle of 0.7 msr), dichroic sheet polarizer filters (1 nm bandwidth for the laser sources and 10 nm bandwidth for the lamp source), neutral density filters (to control the dynamic range), and a photodetector. The extinction measurements employed similar, but rigidly mounted, collecting optics. As noted earlier, concentrations of soot were nearly constant along the optical path for extinction measurements; nevertheless, gravimetric measurements along the optical path allowed correction of the extinction measurements to conditions at the axis where all other measurements were made. An optical system housing and darkroom conditions in the laboratory were used to control optical noise from ambient lighting. The output of the photodetectors was passed through lock-in amplifiers, prior to sampling and storage using a laboratory computer.

The angular light scattering system was calibrated by measuring Rayleigh scattering from propane gas, except at 800 nm where an alternative approach was used, as discussed later. After correcting for the reciprocal sin θ effect caused by the geometry of the measuring volume, the vv and hh differential cross sections agreed with Rayleigh scattering predictions within 5 percent for $20 \leq \theta \leq 160$ deg. Then, absolute volumetric differential scattering cross sections of soot were found from ratios of the detector signal for soot and propane, after accounting for signal attenuation in the optical path, based on the Rayleigh scattering properties of propane from Rudder and Bach (1968) and Dyer (1979). Total volumetric scattering cross sections were found by integrating volumetric differential scattering cross sections over the whole spherical surface; this required extrapolation to reach $\theta = 0$ and 180 deg, but the effect of these extrapolations was small due to the relatively small solid angles involved. The optical arrangement for the extinction measurements was designed as discussed by Manickavasagam and Mengüc (1993) so that uncertainties due to forward scattering were less than one percent over the present test range. The experimental uncertainties (95 percent confidence) of the angular and total light scattering measurements were comparable and are estimated to be less than 10 percent (they are dominated by calibration uncertainties, finite sampling times, the finite aperture of the collection system, and the angular uncertainty of the collecting optics). The corresponding uncertainties of total extinction and absorption cross sections are smaller, less than 5 percent, due to reduced effects of calibration uncertainties.

Theoretical Methods

Analysis of the scattering measurements to find soot optical properties was based on RDG-PFA theory. The main assumptions of RDG-PFA theory are as follows: individual primary particles satisfy the Rayleigh scattering approximation, soot aggregates satisfy the Rayleigh-Debye-Gans (RDG) scattering approximation, primary particles are spherical and monodisperse, primary particles just touch one another, the number of primary particles per aggregate satisfies a log-normal probability distribution function, and the aggregates are mass fractal-like objects that satisfy the following relationship (Jullien and Botet, 1987):

$$N = k_f(R_g/d_p)^{D_f}. \tag{1}$$

These approximations have proven to be satisfactory during past evaluations for a variety of conditions (Köylü and Faeth, 1992, 1994a, b, 1996); nevertheless, they still were evaluated using present measurements before the theory was used to find soot optical properties.

The first step of the present calculations involve the determination of the mean number of primary particles per unit volume at the measurement location from the gravimetric measurement of soot volume fraction and the TEM measurement of primary particle diameter:

$$n_p = 6f_v/(\pi d_p^3). \tag{2}$$

Then, noting that $\bar{Q}_a^a = \bar{Q}_e^a - \bar{Q}_s^a$, so that $\bar{Q}_a^a$ can be found from present measurements of $\bar{Q}_e^a$ and $\bar{Q}_s^a$, the refractive index functions, $E(m)$ and $F(m)$ can be computed as follows:

$$E(m) = k^2\bar{Q}_a^a/(4\pi x_p^3 n_p) \tag{3}$$

$$F(m) = k^2(qd_p)^{D_f}\bar{Q}_{vv}^a(qd_p)/(k_f x_p^6 n_p) \tag{4}$$

where qd_p must be large enough so that scattering is in the large-angle (power-law) regime where Eq. (4) is appropriate. This requirement was established by noting the behavior of RDG-PFA scattering at the limiting conditions of small-angle (Guinier) and large-angle (power-law) scattering, as follows:

$$\bar{Q}_{vv}^a(qd_p)/Q_{vv}^p = (\bar{N}^2/\bar{N})\exp(-q^2\bar{R}_g^2/3), \text{ Guinier regime} \tag{5}$$

$$\bar{Q}_{vv}^a(qd_p)/Q_{vv}^p = k_f(qd_p)^{-D_f}, \text{ power-law regime} \tag{6}$$

where the expression for $\bar{R}_g^2$ in the Guinier regime can be found in Köylü and Faeth (1994a) while the value of $k_f = 8.5$ was adopted from the recent determination of Köylü et al. (1995). The volumetric primary particle Rayleigh scattering cross section used to normalize Eqs. (5) and (6) is given by

$$Q_{vv}^p = n_p x_p^6 F(m)/k^2. \tag{7}$$

From Eqs. (5) and (6) it can be seen that $\bar{Q}_{vv}^a(qd_p)/Q_{vv}^p$ approaches the aggregate size moment, $\bar{N}^2/\bar{N}$, as qd_p approaches zero in the Guinier regime. It is also evident that $\bar{Q}_{vv}^a(qd_p)/Q_{vv}^p$ provides a simple determination of soot fractal dimensions because D_f is the slope of this function in the power-law regime. Finally, $E(m)$ and $F(m)$ provide two nonlinear algebraic equations that can be solved to find the real and imaginary parts of the soot refractive indices.

The dimensionless extinction coefficient is a useful optical property that provides a simple relationship between extinction and soot volume fractions (Dobbins et al., 1994; Choi et al., 1995). This parameter was found for present test conditions by noting that properties were constant along the optical path used for extinction measurements which implies (Choi et al., 1995)

$$k_{eR} = k_e(1 + \rho_{sa}) = -\lambda \ln(I/I_o)/(L f_v). \quad (8)$$

Results and Discussion

Test Conditions. Flame and soot properties at the test conditions are summarized in Table 1. The flames involved heat release rates in the range 5100–7400 W. The flames are ordered in the table in terms of decreasing propensity to soot, as indicated by progressively decreasing primary particle diameters. Present measurements of soot densities are in the range 1850–1930 kg/m^3, which is typical of earlier measurements in the literature (Jullien and Botet, 1987; Köylü and Faeth, 1992). Primary particle diameters are in the range 30–47 nm and the mean number of primary particles per aggregate is in the range 364–467, both of which are in good agreement with the earlier measurements of Köylü and Faeth (1992) for the same soot. These values of d_p and $\bar{N}$ yield typical aggregate dimensions on the order of 1000–10,000 nm, which is somewhat larger than the visible wavelength range; therefore, present measurements involve significant effects of scattering. Finally, the compositions of this soot, measured earlier by Köylü (1992), exhibit significant variations over the test range, with C/H, C/O, and C/N atomic ratios in the ranges 12–17, 57–107, and 295–411, respectively.

Extinction and Scattering Properties. Measured volumetric extinction and scattering cross sections for the four fuels are plotted in Fig. 1. The values of $\bar{Q}^a_e$ and $\bar{Q}^a_s$ progressively increase with increasing propensity to soot. This effect is caused by both increasing concentrations of soot and increased scattering due to larger primary particle diameters and aggregate sizes as the propensity to soot increases, see Table 1. The values of $\bar{Q}^a_e$ and $\bar{Q}^a_s$ are relatively independent of wavelength over the present test range. It will be seen later that this behavior is caused by increasing refractive indices with increasing wavelength that nearly compensate, fortuitously, for decreasing scattering and extinction cross sections that are expected with increasing wavelength for RDG scattering if refractive indices are constant. The ratio of scattering to absorption cross sections, ρ_{sa}, also remains relatively constant for a particular fuel over the present test range; therefore, single values of ρ_{sa} are given for each fuel in Table 1, while the standard deviations of these values are less than five percent. This effect also follows from the variation of refractive indices which compensates for the greater sensitivity of scattering than absorption to wavelength variations for RDG scattering. Mean values of ρ_{sa} are in the range 0.25–0.43 and tend to increase with increasing propensity to soot. These values of ρ_{sa} are sufficiently large to yield significant effects of aggregate scattering for present conditions; for example, ignoring the contribution of scattering to extinction would overestimate optically-determined soot volume fractions by 25–50 percent. Finally, present values of ρ_{sa} for wavelengths of 350–800 nm agree with the results of Köylü and Faeth (1994a) at 514.5 nm for the same soot within 12 percent, which is well within experimental uncertainties.

Table 1 Test conditions[a]

Fuel	C_2H_2	C_3H_6	C_2H_4	C_3H_8
Heat release rate (W)	6160	6580	5140	7400
f_v (ppm)	0.476	0.247	0.0446	0.0278
n_p (million-part./mm^3)	8.76	6.84	2.60	1.97
Gas temperature (K)	370	420	420	450
ρ_p (kg/m^3)	1870	1850	1930	1900
d_p (mm)	47	41	32	30
$\bar{N}$(-)[b]	417	400	467	364
ρ_{sa}(-)[c]	0.43	0.41	0.32	0.25
D(-)[c]	1.74	1.79	1.78	1.78
Atomic ratios:[a]				
C/H	16.8	17.0	---	12.1
C/O	107	57.6	---	---
C/N	295	411	---	331

[a]Soot in overfire region of buoyant turbulent diffusion flames in long residence time regime.
[b]Measured by Köylü (1992) and Köylü and Faeth (1994a).
[c]Effect of wavelength is small compared to experimental uncertainties.

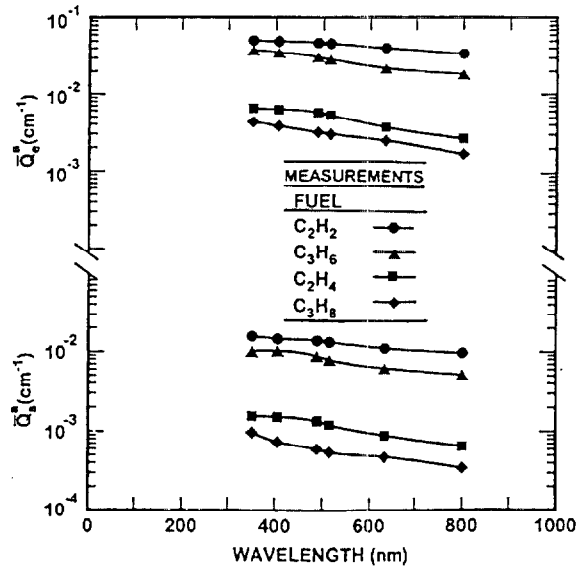

Fig. 1 Measured volumetric extinction and scattering cross sections as a function of wavelength

Scattering Patterns. RDG-PFA scattering theory was evaluated in order to justify the present approach to find soot refractive indices. The smallest wavelengths of the test range were a particular concern because values of x_p become large at these conditions, which raises questions about the RDG scattering approximations (Faeth and Köylü, 1995). Thus, measured and predicted scattering patterns at the worst-case condition for the present test range (acetylene soot at 351.2 nm which yields x_p = 0.42) are illustrated in Fig. 2. Similar to past findings at longer wavelength (Köylü and Faeth, 1994b), there is excellent agreement between measurements and predictions, justifying use of RDG-PFA scattering theory over the present test range. The scattering patterns in Fig. 2 exhibit strong scattering at small values of θ in the Guinier regime which is not typical of Rayleigh scattering where $\bar{Q}^a_{vv}$ would be relatively independent of θ. This highlights the importance of considering RDG-PFA scattering theory when interpreting present measurements to find soot optical properties.

The results illustrated in Fig. 2 indicate relatively strong effects of depolarization which must be handled empirically when using RDG-PFA theory. This was done similar to Köylü and Faeth (1994a) by defining a depolarization ratio, ρ_v, as follows:

$$\bar{Q}^a_{hv} = \bar{Q}^a_{vh} = \bar{Q}^a_{hh}(90 \text{ deg}) = \rho_v \bar{Q}^a_{vv}(90 \text{ deg}). \quad (9)$$

This parameter is then used analogous to Rayleigh scattering theory, see Rudder and Bach (1968), to find values of $\bar{Q}^a_{hh}(\theta)$ as follows:

$$\bar{Q}^a_{hh}(\theta) = [(1 - \rho_v)\cos^2\theta + \rho_v]\bar{Q}^a_{vv}(\theta). \quad (10)$$

Present values of ρ_v are summarized as a function of fuel type and wavelength in Table 2, except for C_3H_6, C_2H_4, and C_3H_8 at 800 nm where scattering levels were too small for an accurate determination of ρ_v. Predictions illustrated in Fig. 2 show that the resulting correlation of $\bar{Q}^a_{hh}(\theta)$ is excellent, similar to the

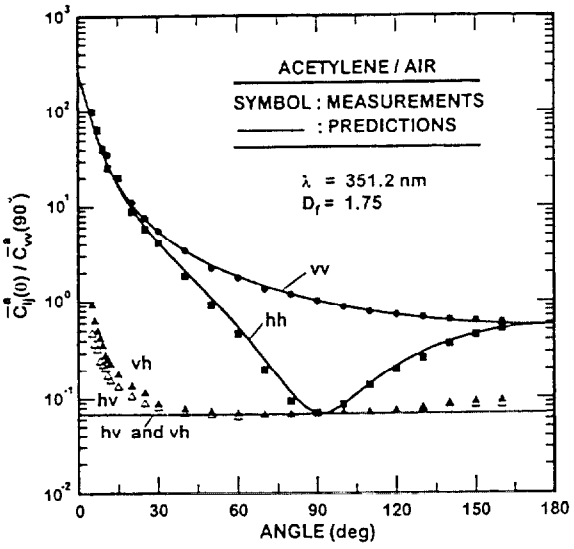

Fig. 2 Measured and predicted angular scattering patterns at 351.2 nm for overfire soot aggregates in buoyant turbulent acetylene/air diffusion flames

predictions of $\bar{Q}^a_{vv}(\theta)$. The values of $\bar{Q}^a_{hv}(\theta)$ and $\bar{Q}^a_{vh}(\theta)$ also are in good agreement with the correlation of Eq. (9), except near the forward scattering direction where measured values increase and the *vh* and *hv* components are no longer equal. Experimental difficulties in the small angle region are thought to be responsible for this behavior because problems of alignment and cross polarization leakage are severe in the forward scattering direction where scattering levels are very high. Scattering behavior at other test conditions was similar to Fig. 2.

The values of ρ_v, summarized in Table 2, are roughly an order of magnitude larger than typical values for Rayleigh scattering from gases, see Rudder and Bach (1968). This behavior is not unexpected because scattering is much stronger for RDG-PFA scattering from soot aggregates than for Rayleigh scattering from gases. Additionally, such trends are supported by the progressive increases of ρ_v with decreasing wavelength and increasing propensity to soot, which also corresponds to changes that increase the effects of scattering. Finally, present values of ρ_v at 514.5 nm agree with the earlier measurements of Köylü and Faeth (1994a) for the same soot within 20 percent, which is well within experimental uncertainties for this variable.

Fractal Properties. Evaluating whether present measurements properly reach the power-law regime, so that Eq. (4) can be used to find refractive indices, and exploiting these conditions to find fractal dimensions, can best be done by plotting $\bar{Q}^a_{vv}(qd_p)/Q^p_{vv}$ as a function of the modulus of the scattering vector, qd_p, as suggested by Eq. (6). These results are illustrated for all four fuels at a wavelength of 632.8 nm in Fig. 3, however, behavior at other wavelengths is similar. The results shown in the figure include the measurements and predictions over the available ranges of qd_p, as well as the extrapolation of power-law behavior based on Eq. (6). As before, the substantial departure of scattering properties from Rayleigh scattering behavior (where $\bar{Q}^a_{vv}(qd_p)/Q^p_{vv}$ would be independent of qd_p) is evident, with forward scattering 100–1000 times larger than back scattering for the present large soot aggregates. The measurements also clearly provide the extended power-law regime where scattering properties are represented by Eq. (6), e.g., roughly, $qd_p > 0.1$ is needed for the current in situ method to find soot refractive indices.

The measurements of $\bar{Q}^a_{vv}(qd_p)/Q^p_{vv}$ in the power-law regime were used to compute fractal dimensions as discussed earlier. It was found that effects of wavelength were small, which is reasonable because fractal properties should only depend on the morphology of the soot aggregates. Thus, only mean values of D_f over the present wavelength range are summarized for each fuel in Table 1. Clearly, the variation of D_f with fuel type is not very significant either, yielding a mean value of $D_f = 1.77$ with a standard deviation of 0.04. These results are in good agreement with earlier determinations of fractal dimensions due to Köylü and Faeth (1994a) for the same soot and with measurements of other soot in flame environments (see Köylü and Faeth

Table 2 Polarization ratios*

Wavelength (nm)	Fuel C_2H_2	C_3H_6	C_2H_4	C_3H_8
351.2	0.070	0.065	0.056	0.044
405.0	0.055	0.042	0.041	0.038
488.0	0.042	0.033	0.026	0.022
514.5	0.041	0.030	0.023	0.020
632.8	0.038	0.028	0.022	0.019
800.0	0.032	—	—	—

*For overfire soot in buoyant turbulent diffusion flames in the long residence time regime, as summarized in Table 1.

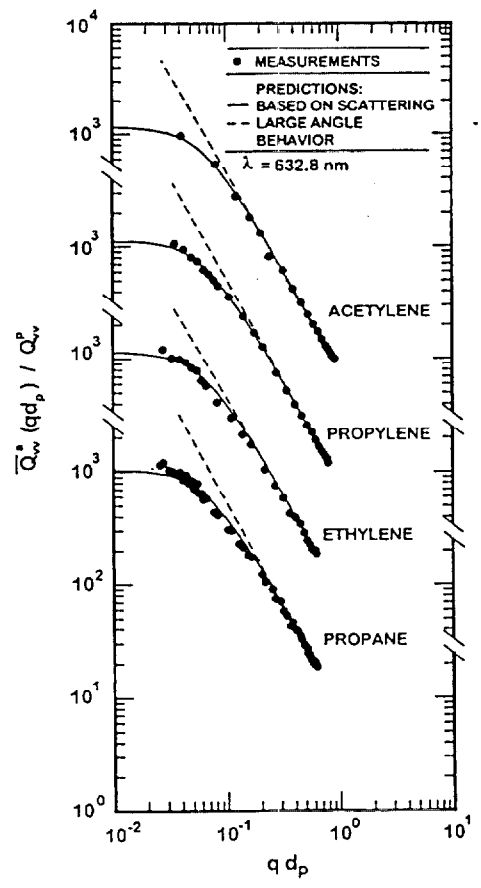

Fig. 3 Measured and predicted volumetric vv cross sections at 632.8 nm as functions of the modulus of the scattering vector

(1994a); Faeth and Köylü (1995); references cited therein). This universality of soot fractal dimensions in flames is very helpful for exploiting RDG-PFA scattering theory to find soot properties from scattering measurements and to estimate continuum radiation properties.

Optical Properties. Results, thus far, have shown that RDG-PFA theory performs reasonably well for present conditions, that present scattering measurements are consistent with earlier measurements for the same soot, that present fractal dimensions are in good agreement with earlier work, and that present scattering measurements at large angles ($qd_p > 0.1$) are within the power-law regime. Based on these findings, Eqs. (2)–(8) were used to compute soot optical properties from the present measurements after adopting $k_f = 8.5$ from Köylü et al. (1995), as mentioned earlier. Results at 800.0 nm, however, were analyzed somewhat differently from the rest because signal-to-noise ratios at this wavelength were too low to provide adequate absolute calibrations of scattering levels based on Rayleigh scattering from propane. Thus, since ρ_{sa} was nearly independent of wavelength for each fuel it was exploited, the values summarized in Table 1 were used to define absolute scattering levels at 800 nm from the extinction measurements for each fuel.

The resulting real and imaginary parts of the refractive indices of soot from the present measurements are plotted as a function of wavelength, with fuel type as a parameter, in Fig. 4. Combining all factors, the experimental uncertainties of the real and imaginary parts of the refractive indices of soot (95 percent confidence) are estimated to be less than 20 percent. Refractive index measurements exhibit relatively small effects of fuel type for present test conditions, with standard deviations of n and κ at each wavelength due to variations of fuel type only averaging three and 11 percent of their respective mean values. Thus, no effect of fuel type on refractive indices can be

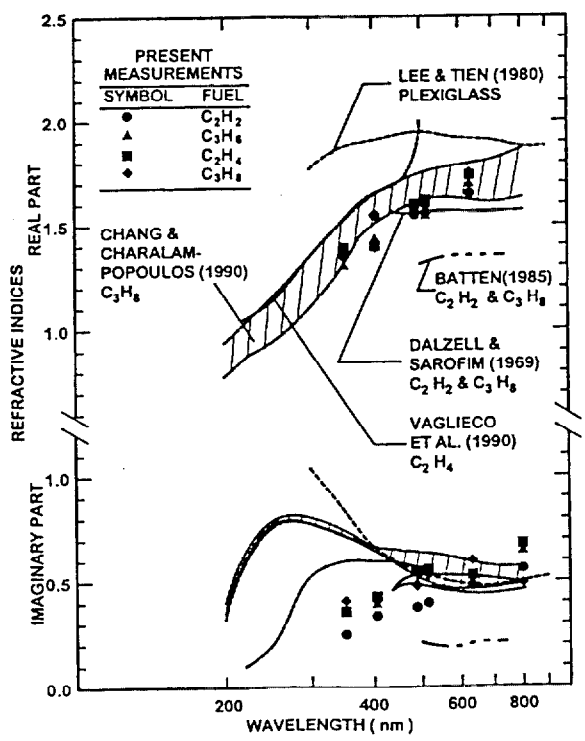

Fig. 4 Measured refractive indices of soot in the ultra-violet and visible portions of the spectrum

Table 3 Soot optical properties*

Wavelength (nm)	E(m)	F(m)	n	κ	k_{eR}
351.2	0.19	0.10	1.36	0.35	4.6
405.0	0.21	0.13	1.45	0.40	5.0
488.0	0.22	0.19	1.58	0.48	5.4
514.5	0.24	0.20	1.58	0.51	5.3
632.8	0.22	0.24	1.71	0.53	5.4
800.0†	0.23	0.36	----	0.65	5.1

*Average values for overfire soot within buoyant turbulent diffusion flames in the long residence time regime. Measurements consider flames fueled with acetylene, propylene, ethylene and propane burning in still air as summarized in Table 1.

†Results at this wavelength were found from extrapolated values of ρ_{sa}.

established for these results within present experimental uncertainties. This behavior generally agrees with past observations of soot refractive indices in diffusion flames (see Köylü and Faeth (1996); Faeth and Köylü (1995); Dalzell and Sarofim (1969); references cited therein). Naturally, functions of n and κ, such as $E(m)$ and $F(m)$, are relatively independent of fuel type as well; therefore, the values of $E(m)$, $F(m)$, n, κ, and k_{eR} (to be discussed later) are summarized as a function of wavelength in Table 3. The experimental uncertainties of $E(m)$ and $F(m)$ (95 percent confidence) are estimated to be less than 19 and 23 percent, respectively. The relatively close agreement between present measurements and the widely-quoted refractive index values of $n = 1.56$ and $\kappa = 0.57$ at 514.5 nm from Dalzell and Sarofim (1969) is quite evident, as discussed next.

Several earlier measurements of soot refractive indices are illustrated in Fig. 4 for comparison with the present results. These measurements include: the classical ex situ reflectometry measurements for soot in the fuel-lean region of acetylene/air and propane/air diffusion flames due to Dalzell and Sarofim (1969); the ex situ measurements for soot in the fuel-lean region of acetylene/air and propane/air diffusion flames due to Batten (1985); the in situ measurements for soot in the fuel-lean region of plexiglass/air diffusion flames due to Lee and Tien (1980); the in situ measurements for soot in the post-flame region of fuel-rich premixed propane/air flames due to Chang and Charalampopoulos (1990); and the in situ measurements for soot in the post-flame region of fuel-rich premixed ethylene/air flames due to Vaglieco et al. (1990). It should be noted that the ex situ measurements of Dalzell and Sarofim (1969) have been criticized by Lee and Tien (1980) for potential problems of soot property changes due to soot collection and sample preparation, and by Felske et al. (1984) for potential problems of diffuse scattering for reflectometry measurements due to surface roughness. On the other hand, the measurements of Lee and Tien (1980), Batten (1985), Chang and Charalampopoulos (1990), and Vaglieco et al. (1990) can be criticized, as noted earlier, because: they all involve questionable models for the optical properties of soot; some involve questionable soot transport properties in cases where dynamic scattering measurements are used to estimate soot aggregate properties; and some involve questionable approximations associated with either Drude-Lorentz dispersion models or Kramers-Krönig causality relationships used to close the procedure to find soot refractive indices. Finally, Chang and Charalampopoulos (1990) observe variations of soot refractive indices with increasing residence time in the post-flame region of premixed flames. This is attributed to an effect of soot aging (or annealing) in a high temperature environment, so that their results are indicated by a band.

The present measurements of soot refractive indices illustrated in Fig. 4 agree best with the findings of Dalzell and Sarofim (1969), as noted earlier, and are similar to the findings of Köylü and Faeth (1994a, 1996) in spite of past criticism of the methodology. Nevertheless, reasons for this behavior and

for the discrepancies among various investigators, as well as adequate definition of effects of fuel type, wavelength, flame conditions, and residence time, clearly merit additional study. Present refractive indices are seen to progressively increase as wavelength is increased. This behavior acts to reduce the variation of extinction, absorption, and scattering cross sections with wavelength, as discussed earlier. Finally, present measurements of soot refractive indices do not exhibit an effect of resonance in the near ultra-violet range of the spectrum that is seen for graphite; instead, the present soot refractive indices progressively decrease as the near ultra-violet is approached, which tends to agree with recent observations of Vaglieco et al. (1990) who observed only a slight effect of resonance near the uv. Naturally, this behavior suggests problems for some past determinations of soot refractive indices where the presence of resonance conditions is assumed, by analogy with graphite, when either Drude-Lorentz dispersion relations or Kramers-Krönig causality relationships were developed.

Present determinations of the dimensionless extinction coefficient, k_{eR}, are plotted as a function of wavelength, with fuel type as a parameter (Fig. 5). The experimental uncertainties of k_{eR} (95 percent confidence) are estimated to be less than 20 percent. Present values of k_{eR} are in the range 4.0–6.2 and really do not exhibit significant variations with wavelength and fuel type. This behavior comes about due to fortuitous cancellation of the effects of scattering, wavelength, and refractive index variations similar to the behavior of $\bar{Q}_e^a$ and $\bar{Q}_s^a$. Values of k_{eR} averaged over the four fuels are summarized as a function of wavelength in Table 3. Averaging over all the present data yields $k_{eR} = 5.1$ with a standard deviation of 0.5; this correlation is also illustrated in Fig. 5.

Other measurements of k_{eR} are plotted in Fig. 5 for comparison with the present measurements. This includes measurements for soot in the fuel-lean region of crude-oil/air diffusion flames, due to Dobbins et al. (1994), and measurements for soot in the post-flame region of premixed fuel-rich acetylene/air flames, due to Choi et al. (1995). These measurements are significantly larger than present measurements with values of k_{eR} in the range 8.1–9.4 reported by Dobbins et al. (1994), and a mean value of $k_{eR} = 8.6$ with a standard deviation of 0.5 reported by Choi et al. (1995). Because present results show that effects of fuel type (and thus degree of aggregation) and wavelength on k_{eR} were not very large, the reasons for this discrepancy are not obvious and clearly merit further study.

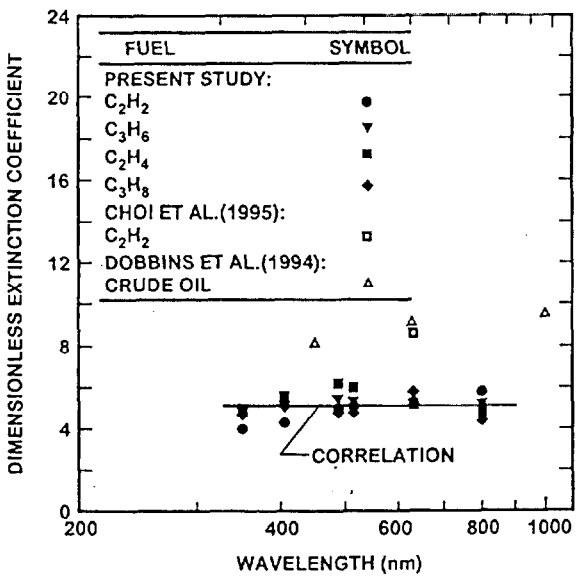

Fig. 5 Measured dimensionless extinction coefficients of soot in the visible and near-infrared portions of the spectrum

Conclusions

The fractal and optical properties of soot were studied experimentally considering soot within the overfire region of buoyant turbulent diffusion flames in the long residence time regime where soot properties are independent of position in the overfire region, and residence time, for a particular fuel. The investigation was limited to soot in flames fueled by acetylene, propylene, ethylene, and propane and burning in still air. They yielded soot having atomic C/H, C/O, and C/N ratios in the ranges 12–17, 57–107, and 295–411, respectively. The investigation was also limited to wavelengths in the visible (350–800 nm). The main conclusions of the study are as follows:

1 Present soot refractive indices did not vary significantly with fuel type and were in reasonably good agreement with earlier measurements for similar conditions due to Dalzell and Sarofim (1969).
2 Present soot refractive indices did not exhibit an approach to a resonance condition in the near uv that is observed for graphite; instead, refractive indices declined continuously as the near uv was approached, similar to the observations of Vaglieco et al. (1990) for amorphous carbon and soot.
3 Present dimensionless extinction coefficients were relatively independent of fuel type and wavelength yielding an average value of 5.1 and a standard deviation of 0.5; however, this value is significantly lower than values in the range 8.1–9.4 reported by Dobbins et al. (1994) and Choi et al. (1995) for reasons that still must be explained.
4 Present fractal dimensions were relatively independent of fuel type and wavelength yielding an average value of 1.77 and a standard deviation of 0.04, which is in reasonably good agreement with the measurements of Köylü and Faeth (1994a) for the same soot at a wavelength of 514.5 nm.
5 The approximate RDG-PFA scattering theory agreed with present measurements within experimental uncertainties; this represents a severe test of the approximate theory because primary particle optical diameters reached values up to 0.42, which represent the largest values considered thus far.

Acknowledgments

This research was supported by the Laboratory for Building and Fire Research of the National Institute of Standards and Technology, Grant Nos. 60NANB1D1175 and 60NANB4D1699, with H. R. Baum and K. C. Smyth serving as scientific officers. The authors also acknowledge the assistance of Ü. Ö. Köylü during the early phases of the work.

References

Batten, C. E., 1985, "Spectral Optical Constants of Soots From Polarized Angular Reflectance Measurements," *Appl. Optics*, Vol. 24, pp. 1193–1199.

Chang, H. Y., and Charalampopoulos, T. T., 1990, "Determination of the Wavelength Dependence of Refractive Indices of Flame Soot," *Proc. R. Soc. London A*, Vol. 430, pp. 577–591.

Charalampopoulis, T. T., 1992, "Morphology and Dynamics of Agglomerated Particulates in Combustion Systems Using Light Scattering Techniques," *Prog. Energy Combust. Sci.* Vol. 18, pp. 13–45.

Choi, M. Y., Mulholland, G. W., Hamins, A., and Kashiwagi, T., 1995, "Comparisons of the Soot Volume Fraction Using Gravimetric and Light Extinction Techniques," *Combust. Flame*, Vol. 102, pp. 161–169.

Dalzell, W. H., and Sarofim, A. F., 1969, "Optical Constants of Soot and Their Application to Heat Flux Calculations," ASME JOURNAL OF HEAT TRANSFER, Vol. 91, pp. 100–104.

Dobbins, R. A., and Megaridis, C. M., 1991, "Absorption and Scattering of Light by Polydisperse Aggregates," *Appl. Optics*, Vol. 30, pp. 4747–4754.

Dobbins, R. A., Mulholland, G. W., and Bryner, N. P., 1994, "Comparison of a Fractal Smoke Optics Model with Light Extinction Measurements," *Atmospheric Environment*, Vol. 28, pp. 889–897.

Dyer, T. M., 1979, "Rayleigh Scattering Measurements of Time-Resolved Concentration in a Turbulent Propane Jet," *AIAA J.*, Vol. 17, pp. 912–914.

Faeth, G. M., and Köylü, Ü. Ö., 1995, "Soot Morphology and Optical Properties in Nonpremixed Turbulent Flame Environments," *Combust. Sci. Tech.*, Vol. 108, pp. 207–229.

Farias, T., Carvalho, M. G., Köylü, Ü. Ö., and Faeth, G. M., 1995, "Computational Evaluation of Approximate Rayleigh-Debye-Gans/Fractal-Aggregate Theory for the Absorption and Scattering Properties of Soot," ASME JOURNAL OF HEAT TRANSFER, Vol. 117, pp. 152–159.

Felske, J. D., Charalampopoulos, T. T., and Hura, H., 1984, "Determination of the Refractive Indices of Soot Particles From the Reflectivities of Compressed Soot Pellets," *Combust. Sci. Tech.*, Vol. 37, pp. 263–284.

Habib, Z. G., and Vervisch, P., 1988, "On the Refractive Index of Soot at Flame Temperature," *Combust. Sci. Tech.*, Vol. 59, pp. 261–274.

Jullien, R., and Botet, R., 1987, *Aggregation and Fractal Aggregates*, World Scientific Publishing Co., Singapore, pp. 45–60.

Köylü, Ü. Ö., 1992, "Emission, Structure and Optical Properties of Overfire Soot From Buoyant Turbulent Diffusion Flames," Ph.D. Thesis, The University of Michigan, Ann Arbor, Michigan.

Köylü, Ü. Ö., and Faeth, G. M., 1992, "Structure of Overfire Soot in Buoyant Turbulent Diffusion Flames at Long Residence Times," *Combust. Flame*, Vol. 89, pp. 140–156.

Köylü, Ü. Ö., and Faeth, G. M., 1994a, "Optical Properties of Overfire Soot in Buoyant Turbulent Diffusion Flames at Long Residence Times," ASME JOURNAL OF HEAT TRANSFER, Vol. 116, pp. 152–159.

Köylü, Ü. Ö., and Faeth, G. M., 1994b, "Optical Properties of Soot in Buoyant Laminar Diffusion Flames," ASME JOURNAL OF HEAT TRANSFER, Vol. 116, pp. 971–979.

Köylü, Ü. Ö., and Faeth, G. M., 1996, "Spectral Extinction Coefficients of Soot Aggregates from Turbulent Diffusion Flames," ASME JOURNAL OF HEAT TRANSFER, Vol. 118, pp. 415–421.

Köylü, Ü. Ö., Faeth, G. M., Farias, T. L., and Carvalho, M. G., 1995, "Fractal and Projected Structure Properties of Soot Aggregates," *Combust. Flame*, Vol. 100, pp. 621–635.

Lee, S. C., and Tien, C. L., 1980, "Optical Constants of Soot in Hydrocarbon Flames," *Eighteenth Symposium (International) on Combustion*, The Combustion Institute, Pittsburgh, PA, pp. 1159–1166.

Manickavasagam, S., and Mengüc, M. P., 1993, "Effective Optical Properties of Coal/Char Particles Determined from FT-IR Spectroscopy Experiments," *Energy and Fuel*, Vol. 7, pp. 860–869.

Martin, J. E., and Hurd, A. J., 1987, "Scattering from Fractals," *J. Appl. Cryst.*, Vol. 20, pp. 61–78.

Medalia, A. I., and Heckman, F. A., 1969, "Morphology of Aggregates—II. Size and Shape Factors of Carbon Black Aggregates from Electron Microscopy," *Carbon*, Vol. 7, pp. 567–582.

Rosner, D. E., Mackowski, D. W., and Garcia-Ybarra, P., 1991, "Size- and Structure-Insensitivity of the Thermophoretic Transport of Aggregated 'Soot' Particles in Gases," *Combust. Sci. Tech.*, Vol. 80, pp. 87–101.

Rudder, R. R., and Bach, D. R., 1968, "Rayleigh Scattering of Ruby-Laser Light by Neutral Gases," *J. Opt. Soc. Amer.*, Vol. 58, pp. 1260–1266.

Tien, C. L., and Lee, S. C., 1982, "Flame Radiation," *Prog. Energy Combust. Sci.*, Vol. 8, pp. 41–59.

Vaglieco, B. M., Beretta, F., and D'Alessio, A., 1990, "In-Situ Evaluation of the Soot Refractive Index in the uv-Visible from the Measurements of Scattering and Extinction Coefficients in Rich Flames," *Combust. Flame*, Vol. 79, pp. 259–271.

Viskanta, R., and Mengüc, M. P., 1987, "Radiation Heat Transfer in Combustion Systems," *Prog. Energy Combust. Sci.*, Vol. 13, pp. 97–160.

NIST-114
(REV. 11-94)
ADMAN 4.09

U.S. DEPARTMENT OF COMMERCE
NATIONAL INSTITUTE OF STANDARDS AND TECHNOLOGY

MANUSCRIPT REVIEW AND APPROVAL

INSTRUCTIONS: ATTACH ORIGINAL OF THIS FORM TO ONE (1) COPY OF MANUSCRIPT AND SEND TO THE SECRETARY, APPROPRIATE EDITORIAL REVIEW BOARD.

(ERB USE ONLY)

ERB CONTROL NUMBER	DIVISION
PUBLICATION REPORT NUMBER	CATEGORY CODE
NIST GCR 99-769	
PUBLICATION DATE	NUMBER PRINTED PAGES
March 1999	

TITLE AND SUBTITLE (CITE IN FULL)
Mixing and Radiation Properties of Buoyant Luminous Flame Environments: II. Structure and Optical Properties of Soot

CONTRACT OR GRANT NUMBER
60NANB4D1696

TYPE OF REPORT AND/OR PERIOD COVERED
Final Report

AUTHOR(S) (LAST NAME, FIRST INITIAL, SECOND INITIAL)
S.S. Krishnan, T.L. Farias, J.-S. Wu, U.O. Koylu and G.M. Faeth

PERFORMING ORGANIZATION (CHECK (X) ONE BLOCK)
- [x] NIST/GAITHERSBURG
- [ ] NIST/BOULDER
- [ ] JILA/BOULDER

LABORATORY AND DIVISION NAMES (FIRST NIST AUTHOR ONLY)
Building & Fire Research Laboratory, Fire Safety Engineering Division

SPONSORING ORGANIZATION NAME AND COMPLETE ADDRESS (STREET, CITY, STATE, ZIP)
U.S. Department of Commerce
National Institute of Standards and Technology
Gaithersburg, MD 20899

PROPOSED FOR NIST PUBLICATION
- [ ] JOURNAL OF RESEARCH (NIST JRES)
- [ ] J. PHYS. & CHEM. REF. DATA (JPCRD)
- [ ] HANDBOOK (NIST HB)
- [ ] SPECIAL PUBLICATION (NIST SP)
- [ ] TECHNICAL NOTE (NIST TN)
- [ ] MONOGRAPH (NIST MN)
- [ ] NATL. STD. REF. DATA SERIES (NIST NSRDS)
- [ ] FEDERAL INF. PROCESS. STDS. (NIST FIPS)
- [ ] LIST OF PUBLICATIONS (NIST LP)
- [ ] NIST INTERAGENCY/INTERNAL REPORT (NISTIR)
- [ ] LETTER CIRCULAR
- [ ] BUILDING SCIENCE SERIES
- [ ] PRODUCT STANDARDS
- [x] OTHER NIST GCR

PROPOSED FOR NON-NIST PUBLICATION (CITE FULLY) [x] U.S. [ ] FOREIGN

PUBLISHING MEDIUM
- [ ] PAPER
- [ ] CD-ROM
- [ ] DISKETTE (SPECIFY)
- [ ] OTHER (SPECIFY)

SUPPLEMENTARY NOTES

ABSTRACT (A 2000-CHARACTER OR LESS FACTUAL SUMMARY OF MOST SIGNIFICANT INFORMATION. IF DOCUMENT INCLUDES A SIGNIFICANT BIBLIOGRAPHY OR LITERATURE SURVEY, CITE IT HERE. SPELL OUT ACRONYMS ON FIRST REFERENCE.) (CONTINUE ON SEPARATE PAGE, IF NECESSARY.)

An investigation of the structure and optical properties of soot is described, motivated by the need to develop nonintrusive methods for measuring soot properties and to estimate the continuum radiation properties of soot for flame environments. The study included evaluation of Rayleigh-Debye-Gans/polydisperse-fractal-aggregate (RDG-PFA) approximate scattering theory for the optical properties of soot aggregates, the determination of the structure and fractal properties of soot that are needed to make predictions with RDG-PFA theory, and the use of RDG-PFA theory to measure the refractive index and related optical properties of soot. Measured soot optical properties were in good agreement with the predictions of RDG-PFA theory over a broad test range, as follows: soot from both the fuel-rich and fuel-lean regions of buoyant diffusion flames, wavelenghts of 350-800 nm, primary particle size parameters as large as 0.46, and soot formed in diffusion flames burning in air for a variety of gaseous and liqud hydrocarbon fuels (acetylene, ethylene, propylene, butadiene, benzene, cyclohexane, toluene and n-heptane).

KEY WORDS (MAXIMUM OF 9; 28 CHARACTERS AND SPACES EACH; SEPARATE WITH SEMICOLONS; ALPHABETIC ORDER; CAPITALIZE ONLY PROPER NAMES)

fire research; flame research, flame structure; optical properties, refractive index; soot; soot aggregates

AVAILABILITY
- [x] UNLIMITED
- [ ] FOR OFFICIAL DISTRIBUTION - DO NOT RELEASE TO NTIS
- [ ] ORDER FROM SUPERINTENDENT OF DOCUMENTS, U.S. GPO, WASHINGTON, DC 20402
- [x] ORDER FROM NTIS, SPRINGFIELD, VA 22161

NOTE TO AUTHOR(S): IF YOU DO NOT WISH THIS MANUSCRIPT ANNOUNCED BEFORE PUBLICATION, PLEASE CHECK HERE. [ ]

ELECTRONIC INFORMS